

STUDYING THE INFLUENCE OF THE CONJUGATE TECHNOLOGICAL STAGES ON THE PERFORMANCE OF LINEAR BENZENES SYNTHESIS UNIT VIA THE MATHEMATICAL MODEL

Irena O. Dolganova^{1*}, Emilia D. Ivanchina¹, Elena N. Ivashkina¹, Anatoli Borissov²

¹ Chemical Engineering Department, Tomsk Polytechnic University, Russia

² General Vortex Energy Inc., Missouri City, USA

Received October 5, 2017; Accepted December 15, 2017

Abstract

Optimization of the operation of the chemical-technological system as a whole is possible only if the efficiency of each of the associated processes of all stages of production is increased, taking into account their interrelationship. These problems are successfully solved using the methods of mathematical modeling and computer modeling systems that take into account the volatility of the raw material composition, the change in catalyst activity and a large number of control parameters. This approach was used for benzene alkylation process and allowed us to reveal regularities of alkylation reactor depending on the technological conditions in the conjugate apparatuses. Thus, optimal HF-catalyst activity depends significantly both on the dehydrogenation feedstock composition and its flow rate.

Keywords: mathematical modeling; alkylation; catalyst activity; optimal technological mode.

1. Introduction

The increasing demand for detergents with stable foaming and biodegradability necessitates the development of new ways to increase the efficiency and operational safety of potentially hazardous production of linear alkylbenzenes (LAB) with a predominance of 2-phenylalkanes that can be converted to surfactants by sulfonation.

A multistage technology for LAB production consists in the sequential dehydrogenation of n-paraffins to olefins, followed by alkylation of benzene in the presence of a hydrogen fluoride catalyst [1-5]. The resulting LAB is subjected to sulfonation - the addition of a sulfuric anhydride SO₃ molecule, resulting in the formation of alkylbenzene sulfonic acid (ASA) [6-10].

The present study is devoted to the identification of optimal parameters for the alkylation process, depending on the performance of the equipment in the previous stages of production. The study was carried out using a specially developed mathematical model of the alkylation process, which sensitive to the composition of the feedstock and the change in the activity of the catalyst. This approach showed the efficiency in different technological processes [11-14].

The change in the HF catalyst activity is mainly affected by the concentration of heavy alkylaromatics (HAR) in the alkylation reactor, as well as the acid consumption in the regenerator, since HAR is capable of dissolving in the acid and being removed in its stream from the reactor. The increase in the value of the catalyst activity is due to an increase in the flow rate of acid withdrawn to the regenerator column should lead to an increase in the production of all products [15-18]. On the other hand, the increase in the HAR concentration leads to a decrease in HF activity [19-20].

Thus, it is necessary to establish such a flow of HF for regeneration, which will ensure optimum catalyst activity and high production of the desired product of the required quality. The peculiarity of the LAB production process as any multistage process is that the operating modes of the conjugate stages are interrelated, therefore, it is possible to recommend the

optimal parameters of the alkylation process only taking into account the operation modes of the apparatuses at the previous stages of the technology [21-25].

The concentration of HAR formed in the alkylation reactor is determined by the content of diolefins in the feed [26]. Therefore, it is necessary to consider the dependence of the optimal activity of the HF catalyst on the composition and rate of the feed flow, the type and activity of the dehydrogenation catalyst, the hydrogen/feed ratio in the dehydrogenation reactor [27].

2. Experimental

To describe the sulfonation reactor, the standard plug-flow reactor model was adopted to describe the reactor process. After that it was modified in the following way. Under unstable load conditions on the raw material we use the term "reduced time", or the total amount of recycled raw materials $Z=G \cdot t$. Then $\partial t = \frac{\partial Z}{G}$ and, subsequently,

$$G \frac{\partial C_i}{\partial Z} + G \frac{\partial C_i}{\partial V} = \sum_j W_j \cdot a_j$$

$$G \frac{\partial T}{\partial Z} + G \frac{\partial T}{\partial V} = \frac{1}{C_p} \sum_j W_j \cdot \Delta H_j \cdot a_j$$

$V=0, C_i=C_i^{in}, T=T^{in}.$

The Z parameter was calculated according to the values of the raw material flow rates. Replacing of t by Z reflects the process non-stationarity due to deactivating substances accumulation (coke for dehydrogenation, heavy aromatics for alkylation, high viscosity component for sulfonation) with the changing values of G . For dehydrogenation process, the a_j value for desired reaction varies from 1 to 0.57 along with Z increasing from 0 to 650000 m³. For alkylation process, the a_j value for desired reaction varies from 0.7 to 0.4 along with Z increasing from 0 to 750 m³.

3. Results and discussion

3.1. Dependence of the optimal parameters of the alkylation process on the composition of the dehydrogenation reactor feed stock

It is known that C₁₂-C₁₃ paraffinic hydrocarbons have a greater reactivity in dehydrogenation reactions than C₁₀-C₁₁ hydrocarbons. Isoparaffin hydrocarbons have a high reactivity in dehydrogenation and dehydrocyclization reactions. Due to the presence of heavy hydrocarbons in the feed stock, during the dehydrogenation on the platinum-containing catalyst, coke-based structures are formed. This leads to a drop in its activity. Thus, the recommended feedstock composition for a dehydrogenation reactor is a feedstock with a minimum content of isoparaffins and aromatic hydrocarbons, but with a sufficiently high content of C₁₂-C₁₃ paraffins having high reactivity with respect to target reactions.

To study the effect of the dehydrogenation feedstock composition on the optimal operating conditions of the alkylation reactor, the process indices for the feedstock compositions that differed as much as possible from the ratio of light and heavy hydrocarbons to the feedstock of the dehydrogenation reactor were computed (tab. 1).

Model calculation results are presented in tab. 2. As presented in tab. 2, the use of lighter feedstocks in the dehydrogenation process (with a higher ratio of (C₁₀ + C₁₁)/(C₁₂ + C₁₃)) results in a smaller amount of olefins being the raw material of the alkylation reactor, due to the low reactivity of the light paraffin components.

Fig. 1 shows the dependence of the LAB yield on the activity of the HF catalyst for various types of the dehydrogenation reactor feedstock.

Tab. 3 shows the optimal activity of HF and the ratio of acid to the reactor and for the types of raw materials characterized by different contents of light and heavy hydrocarbons: (C₁₀ + C₁₁)/(C₁₂ + C₁₃).

Table 1. Compositions of the dehydrogenation feed stock samples

Component	Content in the feedstock, wt. %		
	06.04.2013	02.04.2012	22.10.2012
C ₉	0.00	0.00	0.00
C ₁₀	11.58	14.22	12.70
C ₁₁	27.57	30.90	36.73
C ₁₂	34.23	30.72	28.97
C ₁₃	23.67	21.25	18.74
C ₁₄	0.18	0.38	0.95
Circulating LAB	0.18	1.03	1.87
Isoparaffins (C ₁₀ +C ₁₁)/(C ₁₂ +C ₁₃), rel. units.	0.676	0.861	1.033

Table 2. Dehydrogenation process calculation results

(C ₁₀ +C ₁₁)/(C ₁₂ +C ₁₃) in the dehydrogenation feedstock, rel. units	(C ₁₀ +C ₁₁)/(C ₁₂ +C ₁₃) olefines in the dehydrogenation products, rel. units	Olefines yield, kg/hour
0.676	0.565	4843.25
0.861	0.476	4854.75
1.033	0.599	4775.25

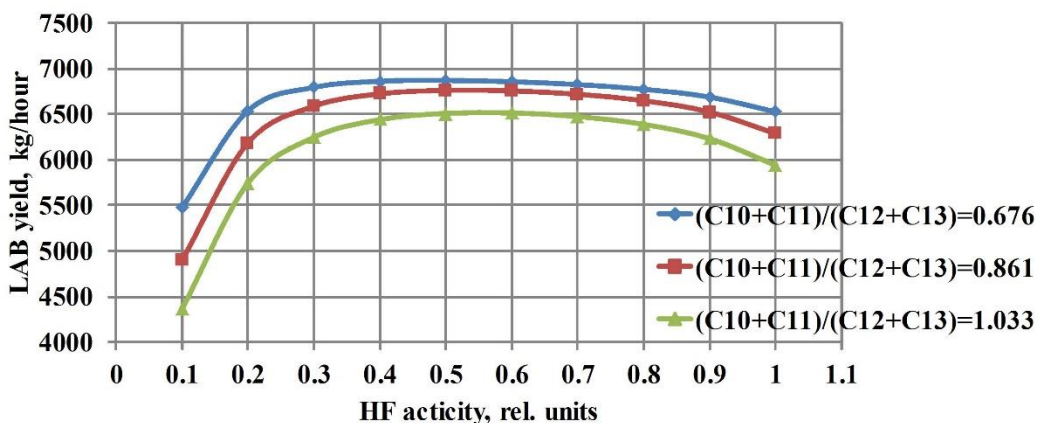


Figure 1. Dependence of the LAB yield on the activity of the HF catalyst for various types of the dehydrogenation reactor feedstock

Table 3. Optimal alkylation process parameters depending on the dehydrogenation feedstock composition

(C ₁₀ +C ₁₁)/(C ₁₂ +C ₁₃) in dehydrogenation feedstock, rel. units	Optimal HF catalyst activity, rel. units	HAr, kg/hour	Optimal HF flow rate to regeneration, m ³ /hour	LAB, kg/hour		ΔLAB, t/days
				Optimal mode	Current mode	
0.676	0.44	20	3.59	6610	6522	2.1
0.861	0.50	23	4.13	6693	6606	2.0
1.033	0.60	26	4.67	6592	6504	2.1

From the table 3 it follows that in order to ensure maximum LAB yield when feeding light feedstock to the reactor, it is required to maintain a higher HF activity and, consequently, a higher consumption of acid in the regenerator column. This is explained by the need to

compensate for the low reactivity of light hydrocarbons with a high activity of the HF catalyst. Thus, the smaller the ratio $(C_{10} + C_{11})/(C_{12} + C_{13})$, the less "tough" conditions are required for the dehydrogenation reaction in the first stage of production. This leads to a decrease in the content of diolefins in the feedstock of the alkylation process and, accordingly, to a decrease in the rate of HAR accumulation in the reactor.

Thus, from the point of view of LAB yield, it is advisable to use heavier raw materials in the paraffin dehydrogenation stage. All other things being equal, such raw materials make it possible to obtain the maximum LAB yield due to the high reactivity of hydrocarbons with a longer chain length. At the same time, each value of the feedstock of the dehydrogenation process corresponds to a certain value of the optimal activity of the HF catalyst, which makes it possible to increase the production of LAB in the alkylation stage. Thus, for example, for a feedstock with a composition $(C_{10} + C_{11})/(C_{12} + C_{13})$ of 0.676, the optimum activity of HF is 0.44 rel. units, and for raw materials with the composition $(C_{10} + C_{11})/(C_{12} + C_{13})$ of 1.033 the HF optimum activity is 0.6 rel. units.

3.2. Dependence of the alkylation process optimal parameters on the feedstock flow rate to dehydrogenation

Despite the fact that in the olefin production plant the raw material consumption was maintained at a level of 75 m³/hour for a long time, sometimes the load is reduced from 70 m³/hour. The reduction in the load on the raw material affects the contact time of the reagents in the dehydrogenation process and, accordingly, at the output and composition of the product.

With the use of a computer simulation system, the parameters of the dehydrogenation of olefins and the hydrogenation of diolefins were calculated at various feedstock flow rates to the dehydrogenation reactor. The results of calculations are shown in tab. 4.

Table 4. Calculation results for dehydrogenation reactor

Raw materials flow rate to dehydrogenation, m ³ /hour	$(C_{10}+C_{11})/(C_{12}+C_{13})$ in the hydrogenation products, rel. units	Diolefins in the dehydrogenation product flow, wt. %	Olefins yield, kg/hour
70	0.550	0.54	5096
75	0.549	0.52	4871

Calculations showed that when the feed flow rate to dehydrogenation reactor is 75 m³/hour, less olefins are formed than at 70 m³/hour (this is explained by the shorter contact time of the reactants), and the products of the dehydrogenation process are more heavy (this is due to the fact, that at a lower value of the contact time, more reactive olefins with a longer chain length can enter the dehydrogenation reaction). The low content of diolefins in the products of the dehydrogenation reactor at a higher consumption of raw materials is also due to a lower contact time.

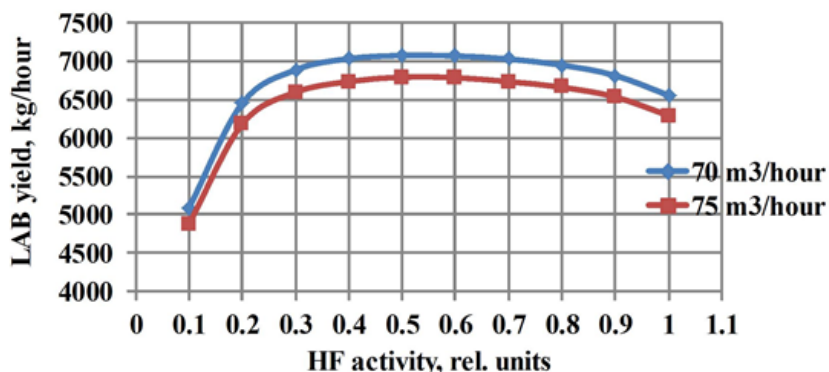


Figure 2. Dependence of the LAB yield on the current HF catalyst activity at various feedrates to the dehydrogenation reactor

Fig. 2 shows the dependence of the LAB yield on the current HF catalyst activity at various feedrates to the dehydrogenation reactor for a feed composition characterized by a ratio of $(C_{10} + C_{11})/(C_{12} + C_{13}) = 0.861$.

Tab. 5 presents the optimal parameters of the alkylation process and the regenerator at various feedstock flow rates to dehydrogenation reactor.

Table 5 Optimal alkylation process parameters depending on the dehydrogenation feedstock flow rate

Dehydrogenation feed flow rate, m ³ /hour	Diolefines in hydrogenation products	$((C_{10} + C_{11})/(C_{12} + C_{13}))$ in hydrogenation reactor products	HAR, kg/hour	Optimal HF flow rate to regenerator m ³ /hour	HF activity, rel. units	LAB, kg/hour		Δ LAB, t/day
						Optimal mode	Current mode	
70	0.54	0.550	0.50	24.0	4.3	6963	6878	2.03
75	0.52	0.549	0.52	23.0	4.1	6668	6578	2.16

With an increase in the feed rate to the dehydrogenation reactor from 70 to 75 m³/hour, the olefin consumption is reduced from 5096 to 4871 kg/hour, the content of diolefines in the dehydrogenation reactor products is also reduced from 0.54 to 0.52 wt. %, which is associated with a decrease in time contact. When dehydrogenation and hydrogenation products enter the alkylation reactor, a decrease in the amount of HAR is observed, leading to a reduction in the recommended flow rate of HF to the regenerator from 4.3 to 4.1 m³/hour. Maintaining HF activity at the required level allows to increase the production of LAB by about 2 tons/day.

4. Conclusion

Thus, the theoretical and numerical studies carried out, as well as the analysis of available experimental data, allowed us to establish the following patterns of change in the optimal activity of the HF catalyst in the alkylation stage, depending on the operating conditions of the dehydrogenation reactor.

1. When using light feedstocks (with the ratio $(C_{10} + C_{11})/(C_{12} + C_{13}) = 1.033$), the dehydrogenation stage requires the maintenance of a higher activity of HF catalysts to provide the required LAB production (0.6 rel. units) and more high flow rate HF in the regenerator (4.67 m³/hour).
2. With an increase in the feed rate to the dehydrogenation reactor and also with an increase in the hydrogen / feed ratio, the optimum flow rate of HF to the HF regeneration column is reduced by reducing the content of diolefines in the dehydrogenation process products and therefore in the feedstock of the alkylation reactor.

Acknowledgements

This research was supported by the Grant of the President of Russia № MD-5019.2016. The experimental calculations were carried out at Tomsk Polytechnic University within the framework of Tomsk Polytechnic University Competitiveness Enhancement Program grant.

List of symbols

C_i	concentration of the i -th component (mol m ⁻³)
C_p	heat capacity of reaction mixture (J m ⁻³ K ⁻¹)
G	feed flow (m ³ hour ⁻¹)
T	temperature (K)
T^0	initial temperature (K)
V	reaction volume (m ³)
W_j	reaction rate (mol m ⁻³ hour ⁻¹)
Z	the total volume of the recycled raw materials (m ³)
a_j	a change in the j -th reaction rate due to viscous component or coke accumulation
ΔH_j	change in the enthalpy of the j -th reaction (J mol ⁻¹)

References

- [1] Corma A, Martínez-Soria V, Schnoefeld E. Alkylation of Benzene with Short-Chain Olefins over MCM-22 Zeolite: Catalytic Behaviour and Kinetic Mechanism. *J Catal.*, 2000; 192(1):163–73.
- [2] Odedairo T, Al-Khattaf S. Comparative study of zeolite catalyzed alkylation of benzene with alcohols of different chain length: H-ZSM-5 versus mordenite. *Catal Today.* 2013; 204:73–84.
- [3] Laredo GC, Castillo JJ, Navarrete-Bolaños J, Perez-Romo P, Lagos FA. Benzene reduction in gasoline by alkylation with olefins: Comparison of Beta and MCM-22 catalysts. *Appl Catal A Gen.* 2012; 413–414:140–8.
- [4] Namuangruk S, Pantu P, Limtrakul J. Alkylation of benzene with ethylene over faujasite zeolite investigated by the ONIOM method. *J Catal.* 2004;
- [5] Alotaibi A, Bayahia H, Kozhevnikova EF, Kozhevnikov I V. Selective Alkylation of Benzene with Propane over Bifunctional Pt-Heteropoly Acid Catalyst. *ACS Catal.* 2015; 5(9):5512–8.
- [6] Zaid TA, Benmaza K, Chitour CE. Sulfonation of linear alkyl benzene (LAB) in a corrugated wall falling film reactor. *Chem. Eng. J.*, 2000; 76(2):99–102.
- [7] Molever K. Monitoring the linear alkylbenzene sulfonation process using high-temperature gas chromatography. *J Surfactants Deterg.* 2005; 8(2):199–202.
- [8] Strott CA. Sulfonation and molecular action. *Endocr Rev.* 2002; 23(5):703–32.
- [9] Foster NC. Sulfonation and Sulfation Processes. *Chemithon.* 1997; (206).
- [10] Gilbert EE, Jones EP. Sulfonation and Sulfation. *Ind Eng Chem.* 1960; 52(7):629–35.
- [11] Kirgina MV, Ivanchina ED, Dolganov IM, Chekantsev NV, Kravtsov AV, Fu F. Computer program for optimizing compounding of high-octane gasoline. *Chem Technol Fuels Oils.* 2014; 50(1).
- [12] Dmitriev VM, Gandga T V., Dolganov IM, Pisarev MO, Dolganova IO, Sizova EN, et al. Structure of network simulator for training and retraining of operators of controlled technological objects of oil and gas industry. *Pet Coal.* 2015; 57(6):691–5.
- [13] Belinskaya NS, Frantsina EV, Ivanchina ED, Popova NV, Belozertseva NE. Determination of optimal temperature of catalytic dewaxing process for diesel fuel production. *Pet Coal.* 2016; 58(7):695–699.
- [14] Belinskaya NS, Ivanchina ED, Ivashkina EN, Sejtenova G. Studying patterns of synthesis of low freezing distillates from atmospheric gasoil by means of mathematical modelling. *Curr Org Synth.* 2017; 14(3): 365–371.
- [15] Aguilar-Garnica E, Paredes-Casillas M, Herrera-Larrasilla TE, Rodríguez-Palomera F, Ramírez-Arreola DE. Analysis of recycled poly (styrene-co-butadiene) sulfonation: a new approach in solid catalysts for biodiesel production. *Springerplus.* 2013; 2(1):475. DOI: 10.1186/2193-1801-2-475.
- [16] Weng Z, Zhang PY, Chu GW, Zou HK, Wang W, Yun J, et al. Sulfonation of linear alkylbenzene in rotating packed bed with dilute liquid sulfur trioxide. *J Chem Eng Japan.* 2015; 48(2):127–32.
- [17] Kucera F, Jancar J. Preliminary Study of Sulfonation of Polystyrene by Homogeneous and Heterogeneous Reaction. *Chem Pap.*, 1996; 50(4):224–7.
- [18] Kučera F, Jancá J. Homogeneous and Heterogeneous Sulfonation of Polymer: A Review. *Polym Eng Sci.* 1998; 38(5):783–92.
- [19] Furimsky E. Deactivation of hydroprocessing catalysts. *Catal Today.* 1999; 52(4):381–495.
- [20] Cerqueira HS, Caeiro G, Costa L, Ramôa Ribeiro F. Deactivation of FCC catalysts. Vol. 292, *Journal of Molecular Catalysis A: Chemical.* 2008. p. 1–13.
- [21] Dealmeida JLG, Defaux M, Taarit YB, Naccache C. Linear Alkylbenzene. *J Am Oil Chem Soc.* 1994; 71(7):675–94.
- [22] Peressutti SR, Olivera NL, Babay PA, Costagliola M, Alvarez HM. Degradation of linear alkylbenzene sulfonate by a bacterial consortium isolated from the aquatic environment of Argentina. *J Appl Microbiol.* 2008; 105(2):476–84.
- [23] Mungray AK, Kumar P. Fate of linear alkylbenzene sulfonates in the environment: A review. Vol. 63, *International Biodeterioration and Biodegradation.* 2009. p. 981–7.
- [24] Albright LF, Shreve RN. Alkylation. *Ind Eng Chem.* 1956; 48(9):1551–62.
- [25] Konishi H. Alkylation process. *Petrotech (Tokyo, Japan).* 1987; 10(8):712–6.
- [26] Dolganova IO, Dolganov IM, Ivashkina EN, Ivanchina ED. development of approach to simulation of oil refining processes on example of benzene alkylation with ethylene. *Pet Coal.* 2012; 54(3): 213–9.
- [27] Arbuzov AB, Drozdov VA, Kazakov MO, Lavrenov AV, Trenikhin MV, Likhobov VA. Liquid-phase isobutane alkylation with butenes over aluminum chloride complexes synthesized in situ from activated aluminum and tert-butyl chloride. *Kinet Catal.* 2012; 53(3): 357–362.

To whom correspondence should be addressed: Dr. Irena O. Dolganova, Chemical Engineering Department, Tomsk Polytechnic University, Russia, dolganovaio@tpu.ru

ESTIMATION OF TECHNOLOGICAL PARAMETERS INFLUENCE ON THE COLD FLOW PROPERTIES AND YIELD OF DIESEL FUEL IN THE PROCESS OF CATALYTIC DEWAXING

Nataliya S. Belinskaya^{1}, Evgeniya V. Frantsina¹, Emilia D. Ivanchina¹, Ekaterina K. Bedareva¹, Anatoli Borissov²*

¹ Tomsk Polytechnic University, Russia

² General Vortex Energy Inc., Missouri City, USA

Received October 6, 2017; Accepted December 23, 2017

Abstract

The aim of this work is to study the process of catalytic dewaxing by the method of mathematical modelling. The influence of temperature and feedstock flow rate on the cold flow properties and yield of the product (diesel fuel) was studied depending on the feedstock composition. The temperature mode of the process was optimized depending on the composition and feedstock flow rate.

Keywords: : catalytic dewaxing; diesel fuel, cold flow properties; cold filter plugging point; the method of mathematical modelling.

1. Introduction

Diesel fuel is one of the most demanded product of oil refining industry. The demand for diesel fuel is constantly increasing all over the world [1-5]. Currently, the tendency towards increasing the demand for diesel fuel of winter and arctic grades, meeting EURO standards, is observed [6-8]. This is mostly due to exploration of the North territories, including Arctic regions [9-10]. The main quality indicators of diesel fuel of winter and arctic grades are cold flow properties, such as cloud point, cold filter plugging point, freezing point, which depend on the content of normal paraffins [11-13].

Under the conditions of decreasing the resource of "light" oil and domination of "heavy" paraffinic oil within oil extraction [14-16], hydroconversion processes assume greater and greater importance in oil refining industry [17-21], including the process of catalytic dewaxing of diesel fuels [22-24]. The studies on oil refining processes using the method of mathematical modelling are relevant these days. The models, developed based on the thermodynamic and kinetic regularities of the processes, allows making recommendations for control of the technological parameters of industrial processes, which ensures meeting specifications for product quality and achieving optimal yield of the product in the conditions of constantly changing composition of the feedstock [25-29]. The aim of this work is to study the process of catalytic dewaxing by the method of mathematical modelling.

2. Object and method of research

The object of the current research is the industrial process of catalytic dewaxing, which is aimed to produce diesel fuel of summer, winter and arctic grades.

The feedstock for the process of catalytic dewaxing is the mixture of the following components in different ratios: straight run diesel fraction, atmospheric gasoil and gasoline from visbreaking. Table 1 shows group composition and density of the components of catalytic dewaxing feedstock.

Table 1. Composition and density of the components of catalytic dewaxing feeds

Hydrocarbon group	Straight run diesel fraction	Atmospheric gasoil %wt.	Gasoline from visbreaking
N-paraffins C ₁₀ -C ₂₇	19.98	15.99	21.60
Olefins	3.75	6.52	19.20
Naphthenes	18.85	16.58	12.80
I-paraffins	32.02	29.01	27.40
Monoaromatics	17.30	19.10	19.00
Polyaromatics	8.10	12.80	0.00
Density, kg/m ³	845	870	727

Depending on the type of feedstock the firm-developer provides two variants of operation of catalytic dewaxing unit (Fig. 1).

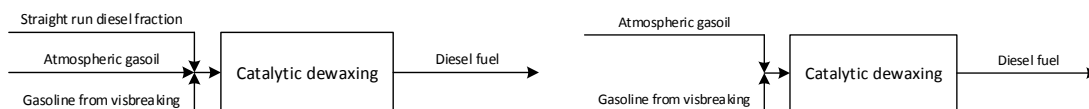


Fig. 1. Variants of catalytic dewaxing unit operation in terms of feedstock

Table 2 presents the ratios of fractions in the mixture of feedstock of the catalytic dewaxing process for the two variants of the unit operation.

Table 2. The ratios of fractions in the mixture of feedstock of the catalytic dewaxing process

Component of feedstock	Designed variants of the catalytic dewaxing unit operation	
	Variant 1	Variant 2
	%	
Straight run diesel fraction	75	0
Atmospheric gasoil	21	93
Gasoline from visbreaking	4	7

On the basis of compositions of feedstock components and their proportions in the feedstock mixture, the compositions and density of the mixed feedstock were calculated for the two variants of the dewaxing unit operation, presented in Table 3.

Table 3. Compositions of feedstock of catalytic dewaxing unit

Hydrocarbon group	Variant 1	Variant 2
	%wt.	
N-paraffins C ₁₀ -C ₂₇	19.21	16.38
Olefins	4.95	7.41
Naphthenes	18.31	16.32
I-paraffins	31.20	28.90
Monoaromatics	17.75	19.09
Polyaromatics	8.76	11.90
Density, kg/m ³	846	860

Thus, when the compositions and ratios of feedstock component change, the composition of the feedstock of catalytic dewaxing unit changes significantly. In such a way, the content of n-paraffins, which influence the cold flow properties of diesel fuel the most, changes by 3 %wt. The content of monoaromatics, which influences the cold flow properties of diesel fuels being the solvent of n-paraffins, changes by 2 %wt.

Such change in the feedstock composition requires constant correction of the mode of the dewaxing reactor operation, determination and maintenance of optimal technological parameters for the exact feedstock composition in order to obtain maximum yield of the product meeting required quality in terms of cold flow properties. In this work, the influence of tempe-

perature and feedstock flow rate on the yield and cold filter plugging point of the product was studied, as well as technological mode for the two variants of unit operation was optimized using the developed mathematical model [30].

The model is written as a system of material and heat balances as follows:

$$\begin{cases} G \cdot \frac{\partial C_i}{\partial z} + G \cdot \frac{\partial C_i}{\partial V} = \sum_{j=1}^m a_j \cdot W_j \\ G \cdot \frac{\partial T}{\partial z} + G \cdot \frac{\partial T}{\partial V} = \frac{1}{\rho \cdot C_p} \sum_{j=1}^m Q_j \cdot a_j \cdot W_j \end{cases} \quad (1)$$

Initial and boundary conditions are as follows: $z=0: C_i=C_{i,0}; T=T_0; V=0: C_i=C_{i,0}; T=T_0$, where z is the volume of refined feedstock from the moment of fresh catalyst load, m^3 ; G is the feedstock flow rate, m^3/h ; $z = G \cdot t$ (t is the catalyst operating time from the moment of fresh catalyst load, h); C_i is the content of i^{th} component, mol/l; V is the catalyst bed volume, m^3 ; a_j is the catalyst activity in j^{th} reaction; ρ is the density of mixture, kg/m^3 ; C_p^{mix} is the specific heat capacity of the mixture, $J/(kg \cdot K)$; Q_j is the heat effect of j^{th} reaction, J/mol ; T is the temperature, K ; W_j is the rate of j^{th} reaction, $mol/(l \cdot s)$; m is the number of reactions.

3. Experimental

3.1. Studying the influence of temperature on the dewaxing process

The influence of temperature on the content of n-paraffins in the product (diesel fuel), product cold filter plugging point and product yield in the process of catalytic dewaxing was studied in the range from 320°C to 360°C. Feedstock flow rate is equal to 320 m^3/h , hydrogen-containing gas flow rate is equal 15000 m^3/h , pressure is equal to 6.9 MPa. The calculation results are presented in Fig. 2-4.

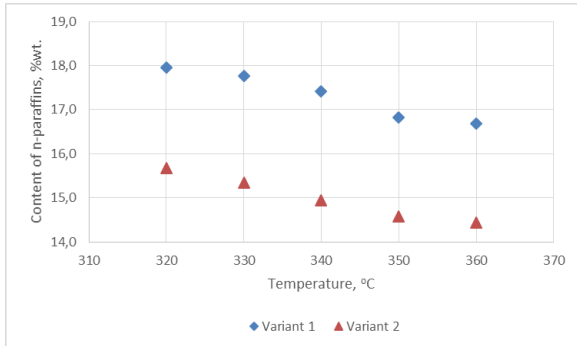


Fig. 2. Dependence of n-paraffins content in the product on the process temperature

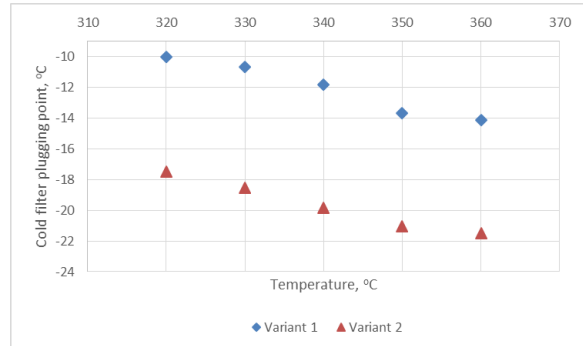


Fig. 3. Dependence of cold filter plugging point of the product on the process temperature

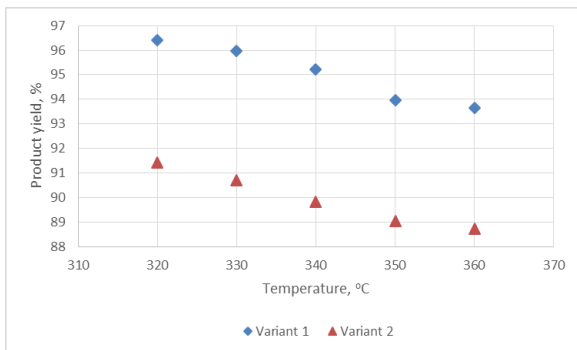


Fig. 4. Dependence of the product yield on the process temperature

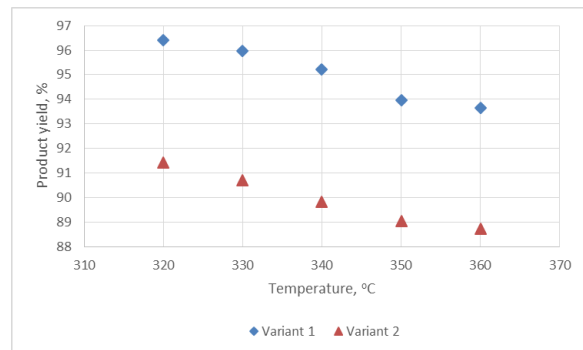


Fig. 5. Dependence of n-paraffins content in the product on the feedstock flow rate

As it can be seen in Fig. 2, the increase in process temperature by 40°C (from 320°C to 360°C) the content of n-paraffins in the product decreases by 7.2 % (from 18.0 %wt. to 16.7 %wt.) when the unit operates according to "Variant 1", and by 7.9 % (from 15.7 %wt. to 14.4 %wt.) when the unit operates according to "Variant 2". This is due to intensification of the target reaction of hydrocracking, which leads to the higher conversion of n-paraffins in this reaction during the time of contact of feedstock with catalyst. Due to the decrease in the content of n-paraffins the cold filter plugging point of the product decreases by 41 % (from -10°C to -14°C) when the unit operates according to "Variant 1", and by 23 % (from -17°C to -21°C) when the unit operates according to "Variant 2" (Fig. 3). The yield of the product decreases by 2.8 % (from 96.4 % to 93.6 %) when the unit operates according to "Variant 1", and by 2.7 % (from 91.4 % to 88.7 %) when the unit operates according to "Variant 2" (Fig. 4).

3.2. Studying the influence of feedstock flow rate on the dewaxing process

The influence of feedstock flow rate on the content of n-paraffins in the product (diesel fuel), product cold filter plugging point and product yield in the process of catalytic dewaxing was studied in the range from 290 m³/h to 320 m³/h. Temperature is equal to 350°C, hydrogen-containing gas flow rate is equal 15000 m³/h, pressure is equal to 6.9 MPa. The calculation results are presented in Fig. 5-7.

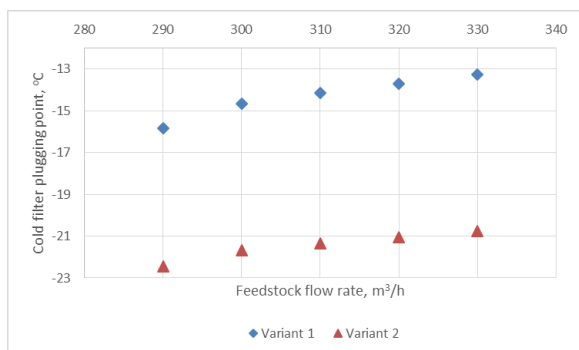


Fig. 6. Dependence of cold filter plugging point of the product on the feedstock flow rate

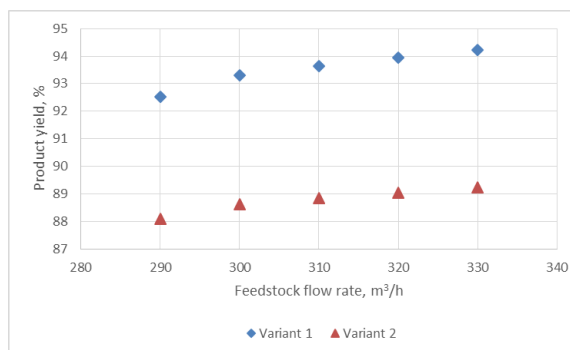


Fig. 7. Dependence of cold filter plugging point of the product on the feedstock flow rate

Increase in the feedstock flow rate by 40 m³/h (from 290 m³/h to 330 m³/h) leads to insignificant increase in the content of n-paraffins in the product by 4.9 % (from 16.2 %wt. to 17 %wt.) when the unit operates according to "Variant 1", and by 3.7 % (from 14.1 %wt. to 14.7 %wt.) when the unit operates according to "Variant 2" (Fig. 5). Due to this the cold filter plugging point increases by 16 % (from -16°C to -13°C) when the unit operates according to "Variant 1", and by 8 % (from -22°C to -21°C) when the unit operates according to "Variant 2" (Fig. 6). Meanwhile, the product yield increases by 1.7 % (from 92.5 % to 94.2 %) when the unit operates according to "Variant 1", and by 1.1 % (from 88.1 % to 89.2 %) when the unit operates according to "Variant 2" (Fig. 7).

In spite of the fact that lower feedstock flow rate ensures higher conversion of the feedstock and improving the cold filter plugging point, the yield of the product is the lowest along with the lowest unit productivity.

3.3. Optimization of temperature mode in the reactor depending on the feedstock composition and flow rate

Studying of the influence of temperature and feedstock flow rate on the dewaxing process, allowed revealing that increase in temperature and decrease in feedstock flow rate provides improving cold flow properties of diesel fuel. However, the yield of diesel fuel decreases. Hence, the aim of optimization is to determine the process temperature, which ensure meeting the product specifications at the maximum yield.

Optimization of temperature mode in the dewaxing reactor was carried out for feedstock flow rates of 280 m³/h, 300 m³/h and 320 m³/h. Flow rate of hydrogen-containing gas is equal to 15000 m³/h, pressure is equal to 6.9 MPa.

For the first variant of unit operation the temperature of the process was optimized in order to obtain diesel fuel EURO interseasonal (grade E) [31] with cold filter plugging point equal to -15 °C. The results of optimal temperature determination are presented in Table 4.

Table 4. The results of optimization for the feedstock

Feedstock flow rate, m ³ /h	Optimal temperature, °C	Content of n-paraffins in the product, % wt.	Cold filter plugging point of the product, °C	Diesel fuel yield, %wt.
280	342	16,76	-14	93
	347	16,38	-15	92
	352	16,06	-16	91
300	348	16,65	-14	93
	353	16,40	-15	92
	358	16,33	-15	92
320	352	16,75	-14	93
	357	16,67	-15	93
	362	16,71	-15	93

For the second variant of unit operation the temperature of the process was optimized in order to obtain diesel fuel EURO winter (grade 0) [31] with cold filter plugging point equal to -21°C. The results of optimal temperature determination are presented in Table 5.

Table 5. The results of optimization for the feedstock composition corresponding to operation of the dewaxing unit according to "Variant 2"

Feedstock flow rate, m ³ /h	Optimal temperature, °C	Content of n-paraffins in the product, % wt.	Cold filter plugging point of the product, °C	Diesel fuel yield, %wt.
280	330	15,1	-19	90
	335	14,85	-20	89
	340	14,59	-21	88
300	333	15,1	-19	90
	338	14,88	-20	89
	343	14,64	-21	88
320	337	15,07	-19	90
	342	14,85	-20	89
	347	14,66	-21	88

According to the results of optimization the following conclusions were made:

1. When increasing the feedstock flow rate in the dewaxing process the maintaining optimal temperature allows obtaining diesel fuel with required cold flow properties (cold filter plugging point of -15°C and -20°C respectively for interseasonal and winter diesel fuel) while ensuring high product yield (93 % and 89 % respectively for interseasonal and winter diesel fuel).
2. In the range of feedstock flow rate from 280 m³/h to 320 m³/h the optimal temperature in the dewaxing reactor lies in the range from 347°C to 357°C for the feedstock, consisting of straight run diesel fraction, atmospheric gasoil and gasoline from visbreaking ("Variant 1"), and from 335°C to 342°C for the feedstock, consisting of atmospheric gasoil and gasoline from visbreaking ("Variant 2").

4. Conclusions

The influence of temperature and feedstock flow rate in the ranges 320–360°C and 290–330 m³/h respectively on the cold flow properties and yield of the product (diesel fuel) was

studied depending on the feedstock composition. The temperature mode of the process was optimized depending on the composition and feedstock flow rate.

Acknowledgements

Ministry of Education and Science of the Russian Federation (10.8306.2017/6.7) supported the research. The research is carried out at National Research Tomsk Polytechnic University and within the framework of National Research Tomsk Polytechnic University Competitiveness Enhancement Program grant.

References

- [1] Hegab A, La Rocca A, Shayler P. Towards keeping diesel fuel supply and demand in balance: Dual-fuelling of diesel engines with natural gas. *Renewable Sustainable Energy Rev.* 2017; 70: 666-697.
- [2] Kholod N, Evans M. Reducing black carbon emissions from diesel vehicles in Russia: An assessment and policy recommendations. *Environ. Sci. Policy.* 2016; 56: 1-8.
- [3] Wadud Z. Diesel demand in the road freight sector in the UK: Estimates for different vehicle types. *Appl. Energy.* 2016; 165: 849-857.
- [4] Barla P, Gilbert-Gonthier M, Kuela JT. The demand for road diesel in Canada. *Energy Economics.* 2014; 43: 316-322.
- [5] Melikoglu M. Demand forecast for road transportation fuels including gasoline, diesel, LPG, bioethanol and biodiesel for Turkey between 2013 and 2023 // *Renewable Energy.* 2014; 64: 164-171.
- [6] Boldushevskii RE, Kapustin VM, Chernysheva EA, Gulyaeva LA, Grudanova AI, Stolonogova TI. Studying of the efficiency of a catalytic dewaxing process utilizing zeolite-based catalyst with an iron additive. *Catal. Ind.* 2015; 7(4): 301-306.
- [7] Grudanova AI, Gulyaeva LA, Krasil'nikova LA, Chernysheva EA. A catalyst for producing diesel fuels with improved cold flow characteristics. *Catal. Ind.* 2016; 8(1): 40-47.
- [8] Zhao Z, Xue Y, Xu G, Zhou J, Lian X, Liu P, Chen D, Han S, Lin H. Effect of the nano-hybrid pour point depressants on the cold flow properties of diesel fuel. *Fuel.* 2017; 193: 65-71.
- [9] Andreassen N. Arctic energy development in Russia – How “sustainability” can fit? *Energy Research & Social Science.* 2016; 16: 78-88.
- [10] Hintsala H, Niemela S, Tervonen P. Arctic potential – Could more structured view improve the understanding of Arctic business opportunities? *Polar Sci.* 2016; 10: 450-457.
- [11] Feng L, Zhang Z, Wang F, Wang T, Yang S. Synthesis and evaluation of alkyl acrylate-vinyl acetate-maleic anhydride terpolymers as cold flow improvers for diesel fuel. *Fuel Process. Technol.* 2014; 118: 42-48.
- [12] Sharafutdinov I, Stratiev D, Shishkova I, Dinkov R, Batchvarov A, Petkov P, Rudnev N. Cold flow properties and oxidation stability of blends of near zero sulfur diesel from Ural crude oil and FAME from different origin. *Fuel.* 2012; 96: 556-567.
- [13] Gerasimov DN, Fadeev VV, Loginova AN, Lysenko SV. Catalysts Based on Zeolite ZSM23 for Isodewaxing of a Lubricant Stock. *Catal. Ind.* 2013; 5(2): 123-132.
- [14] Hein F.J. Geology of bitumen and heavy oil: An overview. *J. Pet. Sci. Eng.* 2017; 154: 551-563.
- [15] Alaei M, Bazmi M, Rashidi A, Rahimi A. Heavy crude oil upgrading using homogenous nanocatalyst. *J. Pet. Sci. Eng.* 2017; 158: 47-55.
- [16] Coskuner G, Naderi K, Babadagli T. An enhanced oil recovery technology as a follow up to cold heavy oil production with sand. *J. Pet. Sci. Eng.* 2015; 133: 475-482.
- [17] Becker PJ, Celse B, Guillaume D, Costa V, Bertier L, Guillon E, Pirngruber G. A continuous lumping model for hydrocracking on a zeolite catalysts: model development and parameter identification. *Fuel.* 2016; 164: 73-82.
- [18] Dik PP, Klimov OV, Danilova IG, Leonova KA, Pereyma VY, Budukva SV, Uvarkina DD, Kazakov MO, Noskov AS. Hydroprocessing of hydrocracker bottom on Pd containing bifunctional catalysts. *Catal. Today.* 2016; 271: 154-162.
- [19] Becker PJ, Serrand N, Celse B, Guillaume D, Dulot H. A single events microkinetic model for hydrocracking of vacuum gas Oil. *Comput. Chem. Eng.* 2017; 98: 70-79.
- [20] Browning B, Afanasiev P, Pitault I, Couenne F, Tayakout-Fayolle M. Detailed kinetic modelling of vacuum gas oil hydrocracking using bifunctional catalyst: A distribution approach. *Chem. Eng. J.* 2016; 284: 270-284.

- [21] Penga C, Fanga X, Zeng R, Guo R, Hao W. Commercial analysis of catalytic hydroprocessing technologies in producing diesel and gasoline by light cycle oil. *Catal. Today*. 2016; 276: 11-18.
- [22] Kondrashev DO, Kleimenov AV, Gulyaeva LA, Khavkin VA, Krasil'nikova LA, Grudanova AI, Khrapov DV, Panov AV. Studying the efficiency of the diesel fuel isodewaxing process on a zeolite-containing nickel-molybdenum catalyst. *Catal. Ind.* 2017; 9(2): 128-135.
- [23] Grudanova AI, Gulyaeva LA, Krasilnikova LA, Shmelkova OI, Boldushevskii RE Jet fuel and arctic diesel fuel production by isodewaxing of waxy middle distillate fractions. *Fuel*. 2017; 193: 485-487.
- [24] Frantsina EV, Belinskaya NS, Lutsenko AS, Popova NV. Monitoring and Quality Control of Diesel Fraction Production Process. *IOP Conf. Ser.: Mater. Sci. Eng.* 2017; 189(1): Article number 012002.
- [25] Zagoruiko AN, Belyi AS, Smolikov MD, Noskov AS. Unsteady-state kinetic simulation of naphtha reforming and coke combustion processes in the fixed and moving catalyst beds. *Catal. Today*. 2014; 220-222: 168-177.
- [26] Khlebnikova ES, Dolganova IO, Ivashkina EN., Koshkin SA. Modeling of Benzene with Ethylene Alkylolation. *MATEC Web Conf.* 2016; 49: 1-5.
- [27] Khlebnikova E, Ivashkina E, Dolganova I. Benzene alkylation with ethylene: The way to increase the process efficiency. *Chem. Eng. Process. Process Intensification*. 2017; 120: 234-240.
- [28] Belinskaya NS, Ivanchina ED, Ivashkina EN, Sejtenova G. Studying patterns of synthesis of low freezing distillates from atmospheric gasoil by means of mathematical modelling. *Curr. Org. Synth.* 2017; 14(3): 365-371.
- [29] Ivanchina ED, Ivashkina EN, Frantsina EV, Dolganova IO, Ivanov SY Increasing the selectivity of synthesis stages for linear alkyl benzenes. *Curr. Org. Synth.* 2017; 14(3): 342-352.
- [30] Belinskaya NS, Frantsina EV, Ivanchina ED, Popova NV, Belozertseva NE. Determination of optimal temperature of catalytic dewaxing process for diesel fuel production. *Pet. Coal*. 2016; 58(7): 695-699.
- [31] Diesel Fuel EURO. Specifications. EN 590:2009.

To whom correspondence should be addressed: Dr. Nataliya S. Belinskaya, Department of Fuel Engineering and Chemical Cybernetics, Tomsk Polytechnic University, 30, Lenin Avenue, Tomsk, 6340

SIMULATION OF INDUSTRIAL MTBE PRODUCTION IN REACTIVE DISTILLATION COLUMN USING ASPEN HYSYS

Olga E. Mityanina^{1*}, *Kristina E. Sukhacheva*¹, *Veronika A. Kolmogorova*²

¹ *Division for Chemical Engineering, School of Earth Sciences & Engineering, Tomsk Polytechnic University, Russia*

² *Tomsk Oil and Gas Research and Design Institute, Russia*

Received October 6, 2017; Accepted December 23, 2017

Abstract

Simulation of reactive distillation by using special engineering software is promising way to its design, research and optimization. In this work we considered the industrial-scale facility of Western Siberia, which includes a line of methyl tert-butyl ether production in a reactive distillation unit. Aspen HYSYS® was used as an instrument of simulation and further optimization studies. The calculation error of the model does not exceed 5%. Simulation of the feedstock composition changes showed that more preferable hydrocarbon fraction for the process is isobutene-isobutylene fraction. After the optimization study we obtained values of optimal reflux ratio for isobutene-isobutylene fraction to be 0.75 and for butylene-isobutylene fraction – 0.80; optimal methanol flowrate for isobutene-isobutylene fraction is 6.500 ton/h, for butylene-isobutylene fraction – 6.000 ton/h.

Keywords: : reactive distillation; MTBE; simulation; industrial process; Aspen HYSYS®.

1. Introduction

Oxygenated additives are widely used in gasoline blending as alternative to tetra ethyl lead and aromatics. These additives improve the octane and combustion quality of gasoline and reduce greenhouse gas emissions [1]. The most popular oxygenated chemicals for liquid fuels are methyl tert-butyl ether (MTBE), ethyl tert-butyl ether (ETBE), methyl tert-amyl ether (TAME).

Operating experience of lab-scale and industry-scale MTBE production showed that maximum output of MTBE can be achieved using reactive distillation (RD) process, which is combination of chemical reaction and separation in one unit [2-4].

Despite all economic advantages of the process, [5-6] for most liquid-phase reversible reactions, design, simulation and control of RD are complicated due to interaction between chemical reaction and separation [7], heat integration [8-9], azeotropic mixtures [10]. In addition, many researchers draw attention to input and output multiplicities during production of MTBE in RD columns [11-14]. Experimental studies of proper column configuration and optimal operating conditions are expensive and sometimes infeasible within the conditions of industrial process. Therefore, mathematical simulation and developing a reliable model of the MTBE reactive distillation is an issue of current scientific interest.

There are many approaches to modeling and pre-analysis of reactive distillation, such as disjunctive programming [15], mixed integer nonlinear programming (MINLP) [16], graphical method [17], methods, based on wave propagation theory [18], stochastic methods [19-20]. Nowadays, design, optimization and research of many popular chemical engineering processes, including RD, can be implemented by means of special software. Most simulation studies and further analyses of RD etherification processes are conducted using engineering software like Aspen HYSYS®, Simulink etc.

A lot of recent research papers are devoted to simulation of RD problems by means of Aspen HYSYS® [11, 21-23], some of them consider MTBE production [11-12] but mostly on a pilot or laboratory scale.

In this work we aimed to develop a steady state model of industrial-scale MTBE synthesis implemented in production on one of the largest oil refineries of Western Siberia. The model became a basis for control parameter study and research of the influence of hydrocarbon feedstock on product yield.

2. Experimental

We implemented mathematical modeling as the main method. All the models used are based on physical and chemical fundamentals of reactive distillation. To verify the model we compared the calculation results with the data of industrial facility provided for January 2016. Software used: Aspen HYSYS® v.7.3, Microsoft Excel 2010.

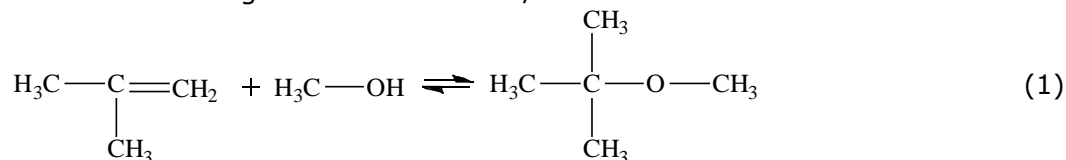
2.1 Initial data

The subject of research is industrial plant of RD MTBE production within the large-scale refinery of Russia located at Western Siberia. The plant capacity is 239,000 tons of MTBE per year. The facility under consideration consists of two parallel production lines including removal of nitrogen-containing impurities from feedstock, MTBE production, methanol removal from waste fraction and two units of methanol and nitrogen-containing compounds separation from flush water.

MTBE is produced by reactive distillation from methanol and isobutylene over ion-exchange catalyst with further separation of the end-products.

Mechanism of MTBE synthesis

The mechanism of MTBE synthesis reaction (1) involves formation of carbonium cations with heat releasing at the rate of 66 kJ/mole.



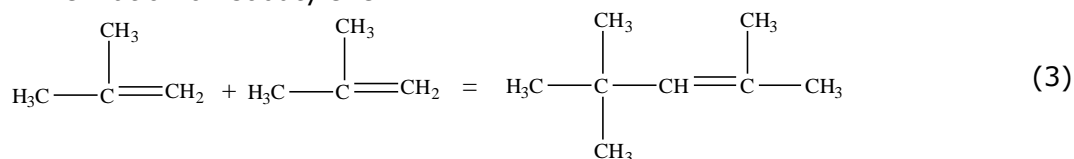
Kinetic parameters of the reaction (1) have been considered in the article [12], according to which reaction rate of MTBE forming can be express as:

$$r = k_f \cdot \left(\frac{\alpha_{IB}}{\alpha_{MeOH}} - \frac{\alpha_{MTBE}}{K_{eq} \alpha_{MeOH}^2} \right) \quad (2)$$

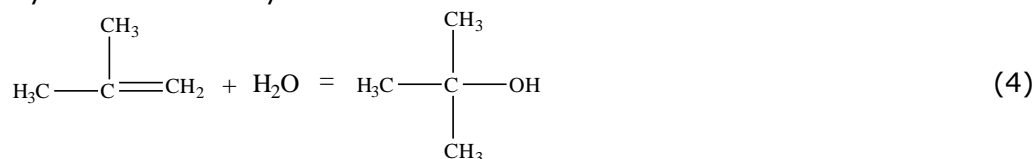
where $k_f = 3.67 \cdot 10^{12} \cdot e^{\frac{-11110}{T}}$ - forward reaction constant [12]; $K_{eq} = e^{\frac{(-16.3 + \frac{6820}{T})}{T}}$ - chemical equilibrium constant [12]; $\alpha_{IB}, \alpha_{MeOH}, \alpha_{MTBE}$ - activity coefficients of isobutylene, methanol and MTBE respectively.

The main reaction (1) is frequently followed by side reactions:

Dimerization of isobutylene:



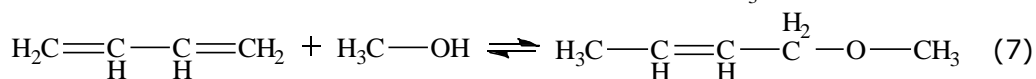
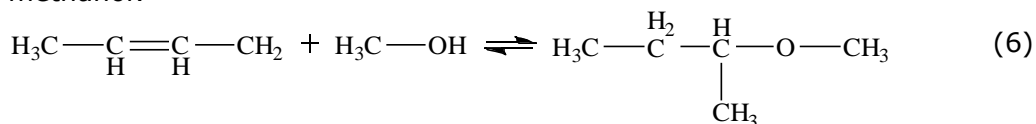
Hydration of isobutylene:



Intermolecular dehydration of methanol with formation of dimethyl ether and water:

$$2 \text{H}_3\text{C}-\text{OH} \rightleftharpoons \text{H}_3\text{C}-\text{O}-\text{CH}_3 + \text{H}_2\text{O} \quad (5)$$

The main feature of the process is usage of hydrocarbon feedstock of various composition – IIF (isobutene-isobutylene fraction) and BIF (butylene-isobutylene fraction). Thus, side products form due to reaction between hydrocarbons C₄ – C₅ from initial fraction and methanol:



In order to reduce side ethers yield, diolefins concentration in the feedstock is limited by special requirements [24].

The flowsheet of one production line of MTBE synthesis is presented in Figure 1 [24].

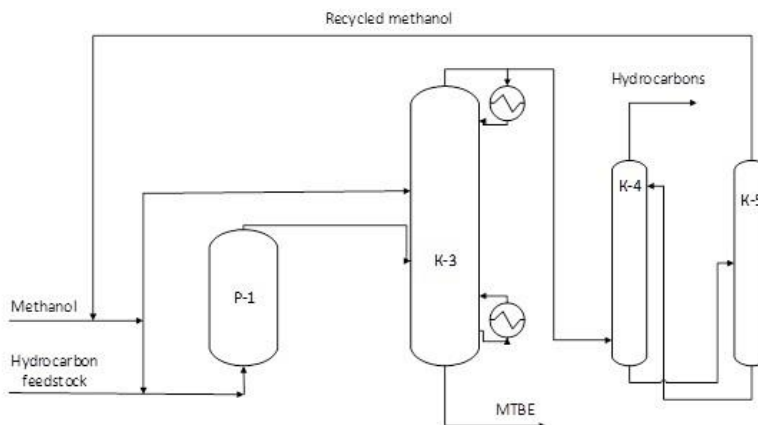


Figure 1. MTBE production flowsheet proposed by Research Institute "Yarsintez"

P-1 – reactor of evaporative-adiabatic type; *K-3* – reactive distillation column; *K-4* – water washing column; *K-5* – column of methanol recovery.

The feedstock streams are: IIF (composition is given in Table 1); BIF (composition is given in Table 1); methanol [25]. High product yield is provided by catalysts KU-2FPP or KIF-T.

KU-2FPP is combustible solid, chemical composition of which involves polypropylene and sulfonated styrene copolymer with divinylbenzene. KIF-T is also combustible solid and it consists of a composition of polypropylene and sulfonated styrene copolymer with divinylbenzene, acrylonitrile and sulfonated polyethylene.

Table 1. Feedstock composition

	IIF, %mass	BIF, % mass		IIF, %mass	BIF, % mass
Propane	0.18	0.10	Isobutylene	41.48	35.73
Isobutane	57.21	8.64	Butadiene	0.04	0.28
N-butane	0.63	19.55	Σ of butylenes	0.46	35.69

The operating parameters of the feedstock are shown in Table 2.

Table 2. Feedstock operating conditions

	Hydrocarbon feedstock	Methanol
Flow-rate, ton/h	0.027	0.006
Temperature, °C	79.5	33
Pressure, kPa	759.938	911.925

Material balance for MTBE production is made for 239,636 tones output per 2016 year and given in Table 3. The Table 3 shows that productive capacity of the unit is 28.29 tones per hour with conversion of isobutylene 98%.

Table 3. Material balance

Input				Output			
	Components	% mass	tones per hour		Components	% mass	tones per hour
	Isobutene-isobutylene fraction				<u>1.MTBE</u>	100.00	28.29
1	Propane, propylene	0.20	0.08		<u>2.Wasted hydrocarbon fraction</u>		
2	Iso-butane	56.10	21.46	1	Propane, propylene	0.33	0.09
3	Isobutylene	41.20	15.76	2	Iso-butane	79.78	22.07
4	N-butane	1.40	0.54	3	Isobutylene	6.50	1.84
5	N-butylenes	1.10	0.42	4	N-butane	11.88	3.36
	Total	100.00	38.25	5	N-butylenes	1.51	0.43
	<u>Butylene-isobutylene fraction</u>				Total	100.00	28.26
1	Propane, propylene	0.21	0.02		<u>3.Losses</u>	100.00	0.05
2	Iso-butane	7.61	0.61				56.60
3	Isobutylene	39.20	3.14		Total	100.00	8.00
4	N-butane	16.28	1.30		Methanol	100.00	10.35
5	N-butylenes	36.70	2.94		Total feedstock		56.60

According to the scheme in the Figure 1, the main units for the synthesis are the reactor P-1 and the RD column K-3. Therefore, proper simulation of kinetic, mass transfer, hydrodynamic features of these units, which are to be specified as nearly as possible to industrial conditions, provides successful modeling on the whole.

2.2 Selecting fluid package and modeling of kinetics

The first important step is chemical reaction modeling. After defining all the substances involved in the main and side chemical reactions, we need to choose the most suitable fluid package. The researchers of Tomsk polytechnic university have studied vapor-liquid equilibrium in the system "isobutylene – n-butene – MTBE – methanol" and arrived at the conclusion that the most appropriate fluid package for thermodynamic calculations of simple ethers is package *Wilson* [26].

Kinetic simulation of MTBE synthesis in Aspen HYSYS® requires selecting type of chemical reaction. The main reaction described by kinetic equation (2) can be defined in HYSYS® in a suitable manner using type *kinetic*. Kinetic type allows specifying forward and backward reaction rates and does not enable to describe catalyst parameters, which is obvious disadvantage for a heterogenic process simulation.

The forward and backward reaction rate constants are represented as temperature functions, generally expressed as:

$$k = A \cdot e^{\frac{-E}{RT}} \cdot T^{\beta}, \quad (8)$$

where A – pre-exponential factor; k – reaction rate constant; E – activation energy, J/mole; β – constant of the extended Arrhenius equation; R – universal gas constant, J/(mole·K); T – absolute temperature, K.

For the forward and backward reactions β is assumed to be 0. To bring the kinetic equation nearer to heterogenic process, we expressed the pre-exponential factors for forward and backward reactions with regard to catalyst mass parameter M_c [12]:

$$A^* = AM_c, \tag{9}$$

where A^* – pre-exponential factor in HYSYS®.

The Table 4 shows kinetic parameters of the main MTBE synthesis reaction specified in HYSYS®.

Table 4. Kinetic parameters of the reaction (1)

Parameter	Value	Parameter	Value
Type	kinetic	Phase of reaction	Liquid
Base component	Isobutylene		
Forward reaction		Backward reaction	
A	$7.34 \cdot 10^{20}$	A`	$7.88 \cdot 10^{15}$
E, J/mole	92324	E`, J/mole	149000

As the product yield is sufficiently high, side reactions (3) – (7) do not influence on the process significantly. At the same time, without necessary kinetic data of reaction behavior on the catalyst, it is appropriate to use equilibrium type for side reaction simulation.

2.3. Simulation of the main units

The main units for the MTBE synthesis are the reactor and the RD column. The reactor is a hollow cylindrical vessel with fixed-bed catalyst (P-1 in Figure 1). The screenshot of the reactor modeling is given in Figure 2.

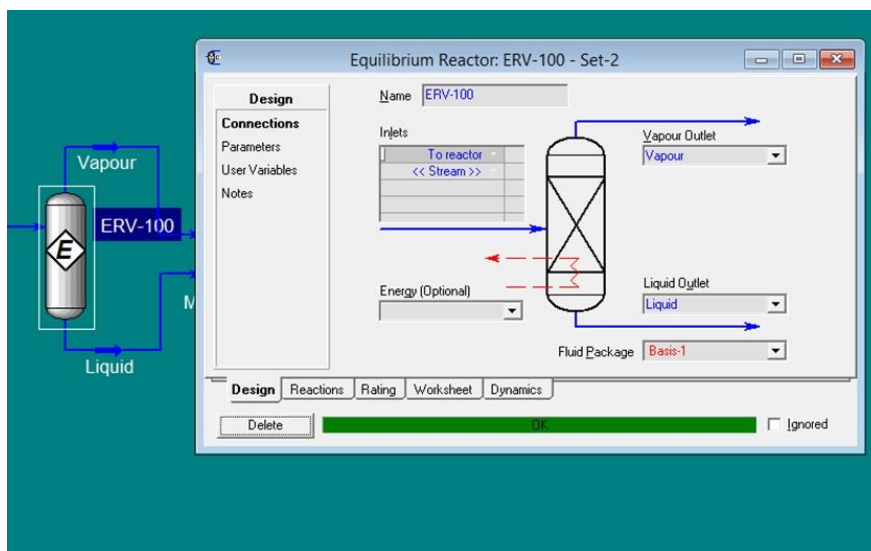


Figure 2. The MTBE synthesis reactor modeling in Aspen HYSYS®

Specifications of the reactor according to production documents are given in Table 5.

Table 5. Specifications of the MTBE synthesis reactor

Parameter	Value	Parameter	Value
Volume	75.6 m ³	Pressure	1300 kPa
Diameter	3000 mm	Temperature	100°C
Length	16680 mm		

The reactive distillation column includes three sections (see Figure 3): rectifying section, reactive section and stripping section.

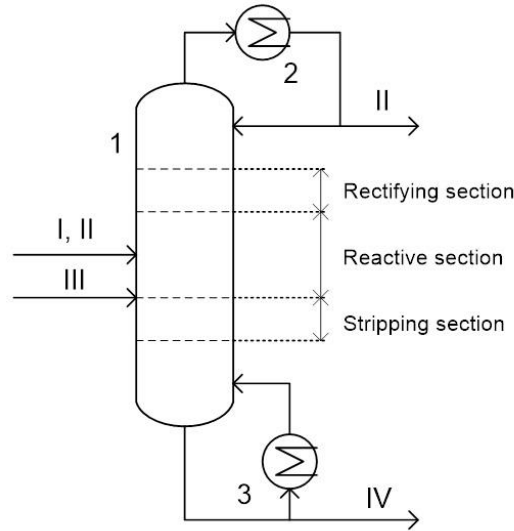


Figure 3. The reactive distillation column (I – isobutylene; II – n-butylenes; III – methanol; IV – MTBE; 1 - reactive distillation column; 2 - total condenser; 3 – reboiler)

Specifications of the reactive distillation column are given in Table 7.

Table 7. Specifications of the reactive distillation column

Parameter	Value	Parameter	Value
Pressure	1000 kPa	Overhead temperature	42 °C
Diameter	2200 mm	Number of trays	80
Height	58650 mm	Feed tray	29
Bottom temperature	135 °C		

The reactive distillation column was simulated in Aspen HYSYS® (see Figure 4).

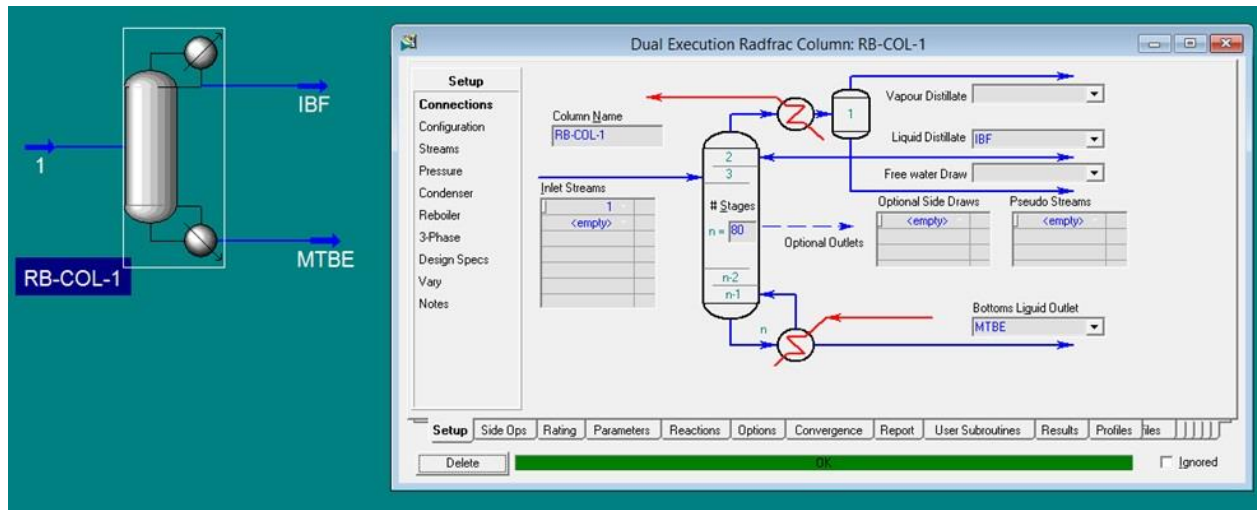


Figure 4. The reactive distillation column in Aspen HYSYS®

The last versions of Aspen HYSYS® make possible to use equilibrium models as well as non-equilibrium models for simulation of the reactive distillation columns. The main assumption of the equilibrium models is phase equilibrium, in this case calculation of the heat- and mass-transfer coefficients is not required. Due to its clearness equilibrium models are successfully

used in designing, research and control of the reactive distillation columns. It is believed that this type of models is suitable for description of the azeotropic polystable systems in reactive distillation columns, but according to some research papers [27] careful calculations of the heat- and mass-transfer could be very important for this kind of simulation.

Non-equilibrium (Rate-based) model was used for the reactive distillation column modeling because it allows taking into account kinetic parameters (Table 4).

The aggregate scheme of MTBE synthesis is presented in Figure 5. The developed model was verified, and then we made some prediction and optimization calculations.

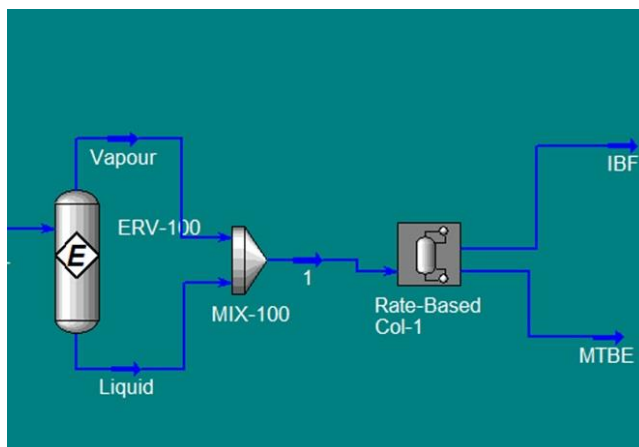


Figure 5. HYSYS® scheme of the MTBE production unit

2.4. Model verification

The model was verified by comparing the calculation results with the data of industrial facility of MTBE synthesis provided for January 2016. For that period of time hydrocarbon feedstock included IIF (isobutene-isobutylene fraction, composition is given in Table 1) and methanol.

The composition of the MTBE flow from the RD column bottom is given in Table 8. The composition of the wasted hydrocarbon fraction is presented in Table 9. Calculated values are shown in comparison with the same real values.

Table 8. Composition of the MTBE flow from the RD column bottom

	MTBE	Methanol	Isobutylene	MsBE	Water	Butylenes	Isobutane
Plant data, % mass	98.70	0.06	0.37	0.01	0.00	0.76	0.10
Calculation result, % mass	94.51	0.11	0.58	0.00	0.00	0.57	4.23

MsBE-methyl-sec-buthyl ether

As shown in Table 8, the error of MTBE content calculation is 4.2 %. Total calculated content of the by-products does not exceed 1 %, excepting isobutane. Considerable error of the isobutane content estimation is connected with imperfect calculation of the distillation process.

Table 9. Composition of the wasted hydrocarbon fraction

	Isobutane	N-butane	Isobutylene	Butadiene	Methanol	Butylenes	Propane
Plant data, % mass	96.85	1.12	0.76	0.07	0.00	0.88	0.32
Calculation result, % mass	94.45	0.78	3.91	0.05	0.00	0.50	0.31

According to Table 9, the error of isobutane content calculation is 2.5 %. Therefore, the developed model provides good accuracy of calculation and could be used for the MTBE synthesis process optimization.

2.5. Optimization of the MTBE synthesis process

The hydrocarbon feedstock of the MTBE synthesis process can be changed from IIF to BIF and back, so the influence of feedstock composition is significant for the process efficiency. For that reason optimization calculations should take into account both types of hydrocarbon feedstock, IIF and BIF (see Table 1).

We investigated how reflux ratio (R) and methanol flowrate influence MTBE concentration in the main product flow. Reflux ratio was varied from 0.6 to 1.0 and methanol flowrate – from 5.000 ton/h to 6.800 ton/h.

The MTBE content as a function of reflux ratio is presented in Figure 6. According to Figure 6, the MTBE content increases with reflux ratio growth, optimal R is 0.75 for IIF hydrocarbon feedstock and 0.8 for BIF hydrocarbon feedstock. The MTBE content as a function of methanol flowrate is presented in Figure 7.

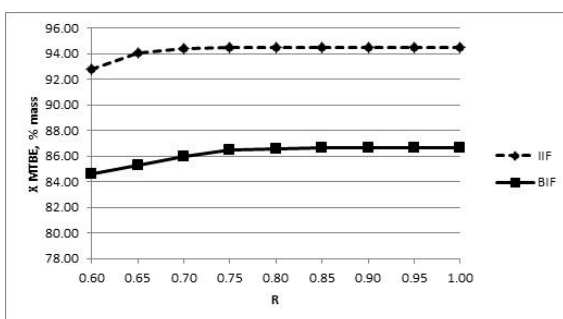


Figure 6. MTBE content as a function of reflux ratio

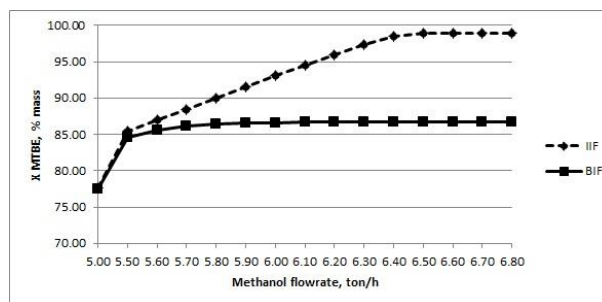


Figure 7. MTBE content as a function of methanol flowrate

As represented in Figure 7, the MTBE content increases with methanol flowrate growth, optimal flowrate is 6.500 ton/h for IIF hydrocarbon feedstock and 6.000 ton/h for BIF hydrocarbon feedstock. The optimal values of reflux ratio and methanol flowrate for the different types of hydrocarbon feedstock are given in Table 10. The calculated optimal values are shown in comparison with the same real values.

Table 10. The optimal values of reflux and methanol flowrate

Hydrocarbon feedstock type	Reflux ratio	Methanol flowrate, ton/h	MTBE content, % mass	
IIF	Plant data	0.90	6.100	94.51
	Optimal value	0.75	6.500	98.86
BIF	Plant data	0.90	6.100	86.66
	Optimal value	0.80	6.000	86.61

As shown in Table 10, the MTBE content is greater in case of IIF usage because content of isobutylene is 5 % higher in IIF then in BIF. In this respect, operating parameters for BIF as hydrocarbon feedstock should be corrected in order to provide decrease of thermal charge and feedstock flowrate.

Summary

1. Modern approaches to reactive distillation modeling are based on complicated mathematical models and require special software. Aspen HYSYS® enables to create stable and dynamic models of equilibrium and rate-based processes. At the same time, there are some limitations in specification of a catalyst of heterogeneous reaction.

2. The product line of MTBE synthesis within the industrial plant was simulated in Aspen HYSYS®. Calculation error does not exceed 5 % for the main product concentration, thus we considered the model as adequate and used it for further studies.
3. The main feature of industry-scale MTBE production is changes in hydrocarbon feedstock composition. The feedstock composition study showed that usage of IIF is more preferable than BIF as MTBE content in the main product stream is 12 % higher for IIF in comparison to BIF. Optimization calculations of the reflux ratio and the methanol flowrate lead us to the conclusion that: for IIF feedstock – optimal reflux ratio is 0.75, methanol flowrate – 6.500 ton/h; for BIF feedstock – optimal reflux ratio is 0.80, methanol flowrate – 6.000 ton/h.

Acknowledgements

The research is carried out at Tomsk Polytechnic University within the framework of Tomsk Polytechnic University Competitiveness Enhancement Program grant.

References

- [1] Norkobilov A. Comparative study of conventional, reactive-distillation and pervaporation integrated hybrid process for ethyl tert-butyl ether production. *Chemical Engineering & Processing: Process Intensification* 2017, <http://dx.doi.org/10.1016/j.cep.2017.07.003>.
- [2] Jithin Prakash KJ, Jana AK. Process Simulation and Design of Reactive Distillation Column. *Chemical Product and Process Modeling* 2009; 4(1): 783–792.
- [3] Sharma N, Singh K. Control of Reactive Distillation Column: A Review. *Int. J. Chemical Reactor Eng.* 2010; 8 (1), R5.
- [4] Sudibyo, Murat MN, Aziz N. Simulation Studies and Sensitivity Analysis of Methyl Tert-butyl Ether Reactive Distillation. *Proceedings of the 11th International Symposium on Process Systems Engineering*, 15-19 July 2012, Singapore.
- [5] Chadda N, Malone MF, Doherty MF. Feasibility and synthesis of hybrid reactive distillation systems. *AIChE Journal* 2002; 48 (12): 2754.
- [6] Taylor R, Krishna R. Review: Modelling reactive distillation. *Chem. Eng. Science.* 2000; 55(22): 5183-5229.
- [7] Chen FR, Huss RS, Doherty MF, Malone MF. Multiple steady states in reactive distillation: Kinetic effects. *Comput. Chem. Eng.* 2002; 26: 81-93.
- [8] Gadewar SB, Tao L, Malone MF, Doherty MF. Process alternatives for coupling reaction and distillation. *Trans IChemE, Part A, Chemical Engineering Research and Design* 2004; 82(A2): 140–147.
- [9] Huang K, Nakaiwa M. Reactive distillation design with considerations of heats of reaction. *AIChE Journal* 2006; 52(7): 2518-2534.
- [10] Chua WJ, Rangaiah GP, Hidajat K. Design and optimization of isopropanol process based on two alternatives for reactive distillation. *Chemical Engineering and Processing: Process Intensification* 2017; 118: 108–116.
- [11] Hauan S, Hertzberg T. Why methyl tert-butyl ether production by reactive distillation may yield multiple solutions. *Industrial & Engineering Chemistry Research* 1995; 34(3): 987 – 991.
- [12] Singh BP. Steady state analysis of reactive distillation using homotopy continuation. *Chemical Engineering Research and Design* 2005; 83(A8): 959 – 968.
- [13] Jacobs R, Krishna R. Multiple solutions in reactive distillation for methyl tert-butyl ether synthesis. *Eng. Chem. Res.* 1993; (32): 1706-1709.
- [14] Sneesby MG, Tadó MO, Smith TN. Multiplicity and pseudo-multiplicity in MTBE and ETBE reactive distillation. *Chemical Engineering Research and Design* 1998; 76 (4): 25–531.
- [15] Jackson JR, Grossman IE. A disjunctive approach for the optimal design of reactive distillation columns. *Comput Chem Eng.* 2001; 25: 1661–1673.
- [16] Babu BV, Muzaffar K. Optimization of reactive distillation processes using differential evolution strategies. *Asia-Pac. J. Chem. Eng.* 2007; 2:322–335.
- [17] Lee JW, Westerberg AW. Graphical design applied to MTBE and methyl acetate reactive distillation processes. *AIChE J.* 2001; 47: 1333–1345.
- [18] Kienle, A. Nonlinear model reduction for nonreactive and reactive distillation processes using nonlinear wave propagation theory. In: *SPC-2000, Third Symposium on Process Control*, Ploiesti, Romania. 2000. 72–78.

- [19] Segovia-Hernández JG, Hernández S, Petriciolet AB. Reactive distillation: A review of optimal design using deterministic and stochastic techniques. *Chemical Engineering and Processing* 2015; 97: 134–143.
- [20] Lima RM, Salcedo RL, Barbosa D. SIMOP: efficient reactive distillation optimization using stochastic optimizers. *Chem. Eng. Sci.* 2006; 61: 1718–1739.
- [21] Smejkal Q, Soos M. Comparison of computer simulation of reactive distillation using ASPEN PLUS and HYSYS software. *Chemical Engineering and Processing* 2002; 41: 413–418.
- [22] Giwa A, Karacan S. Simulation and optimization of ethyl acetate reactive packed distillation process using ASPEN HYSYS. *TOJSAT: The Online Journal of Science and Technology* 2012; 2(2): 57–63.
- [23] Karacan S, Karacan F. Simulation of reactive distillation column for biodiesel production at optimum conditions. *Chemical Engineering Transactions* 2014; 39: 1705–1710.
- [24] http://yarsintez.ru/media/MTBE_21.pdf (in Russian)
- [25] ГОСТ 2222-95. Метанол технический (Industry standard 2222-95. Methanol) (in Russian).
- [26] Mityanina OE, Samborskaya MA, Kravtsov AV. Modelirovanie parozhidkostonogo ravnovesija v sisteme «Izobutilen – n-buten – metanol - MTBE» (Modeling of vapor-liquid equilibrium in the system 'Isobutylene–n-buten–methanol–MTBE'). *Neftepererabotka i neftehimija (Refining and petrochemistry)*. 2009; 8: 11–14. (in Russian).
- [27] Lee JH, Dudukovic MP. A comparison of equilibrium and nonequilibrium models for multicomponent reactive distillation. *Comp. Chem. Eng.* 1998; 23: 159–172.

To whom correspondence should be addressed: Olga E. Mityanina, Division for Chemical Engineering, School of Earth Sciences & Engineering, Tomsk Polytechnic University, Russia; oem@tpu.ru

NUMERICAL STUDY OF ETHYLENE BUBBLE RISING IN BENZENE FLOW

Elena Khlebnikova^{1}, Anatoliy Vorobev², Elena Ivashkina¹, Tatyana Lubimova³*

¹ Tomsk Polytechnic University, Tomsk, Russia

² Southampton University, Southampton, UK

³ Perm State University, Perm, Russia

Received October 5, 2017; Accepted December 23, 2017

Abstract

The bubble rising in viscous liquids is enough common in many industrial processes and an important fundamental problem in fluid dynamics. In the current work, we deal with the numerical modeling of a single gaseous bubble that rises in liquid. In particular, we are interested in benzene alkylation that is conducted by the chemical interaction of ethylene and benzene in the presence of the Lewis catalyst. Thus, the rate of absorption is the main focus of this work.

Keywords: : bubble rising; ethylbenzene; numerical approach; modeling; multiphase flow.

1. Introduction

The reactants mixing modeling is needed in various processes of chemical engineering [1-4]. The understanding of the system flow dynamics is a great importance in engineering applications. Rising bubbles in liquid have been enough studied theoretically [5-6] and experimentally [7-8]. In such systems slow and limited miscibility of gaseous species in liquids frequently limits reaction rates, so reactants are supplied in excessive quantities in order to obtain the desired amounts of the products. The mixing rate would strongly depend on the contact area of the phases, and, typically, to increase the contact between the phases, the gaseous phase is fed into a liquid-filled reactor at in the form of small bubbles.

In particular we are interested in alkylation of benzene with ethylene for ethylbenzene production. This technology is the large-capacity commercial process in terms of benzene consumption and processing: 75% of produced in the world benzene is used in production of ethylbenzene and isopropylbenzene. Market of ethylbenzene is closely linked to the production of styrene.

In the present work, the gas/liquid mixture is represented as a heterogeneous binary system with the mass transfer through phase boundaries. The evolution of the gas/liquid mixture using the phase field approach was examined.

2. Experimental

The interface separating gas/liquid mixture was represented as a transitional boundary of finite thickness. The concentration field C , defined as the mass fraction of one liquid in the mixture, is used to trace the evolution of the interfacial boundary. The specific free energy function is defined as a concentration function and gradient of concentration [9]

$$f(C, \nabla C) = f_0(C) + \frac{\epsilon}{2} (\nabla C)^2 \quad (1)$$

In this expression, the second term, proposed by Cahn and Hilliard, takes into account the surface tension effects. The capillary constant ϵ is assumed sufficiently small so to be able to neglect this term everywhere except at the places of large concentration gradients, where the interface is located. The double-well potential is frequently used for the classical part of the

free energy function, f_0 , especially, when the primary interest is tracing the evolution of the immiscible interface.

The free energy function (1) can be used to re-derive the Navier-Stokes equations for the mixture. The so-obtained full Cahn-Hilliard-Navier-Stokes equations are however very complex for numerical treatment because of quasi-compressibility that forces to use the full continuity equation even for description of two incompressible liquids. The Boussinesq approximation [10] of the full equations was used to define the evolution of the gas bubble rising in benzene.

The governing equations reflect the conservation of momentum, species, and mass:

$$(1+\rho)\frac{\partial \vec{u}}{\partial t}+(\vec{u}\cdot\nabla)\vec{u}=-\nabla\pi+\frac{1}{Re}\nabla^2\vec{u}-Ca\nabla^2\mu+2GrC, \quad (2)$$

$$\frac{\partial C}{\partial t}+(\vec{u}\cdot\nabla)C=\frac{1}{Pe}\nabla^2\mu, \quad (3)$$

$$\nabla\cdot\vec{u}=0, \quad (4)$$

$$\mu=Gr(\vec{r}\cdot\vec{\gamma})+2AC+4C^2-Ca\nabla^2C \quad (5)$$

Here, the common notations are used for the variables. These equations are applied to the whole multiphase system, including the interface. One sees that the Navier-Stokes equation contains an addition force that defines morphology of the interface. The diffusion is defined the generalised Ficks law, i.e. through the gradient of the chemical potential μ . The diffusion term includes in addition to the usual concentration diffusion, the barodiffusion terms.

$\vec{\gamma}$ is the unit vector directed upward.

The equations are written in non-dimensional form and include the following non-dimensional parameters;

the Grashof number: $Gr = \varphi \frac{gL^*}{\mu^*}, \quad (6)$

the Reynolds number: $Re = \frac{\rho^*\mu^{*1/2}L^*}{\eta^*}, \quad (7)$

the Peclet number: $Pe = \frac{\rho^*L^*}{\alpha\mu^{*1/2}}, \quad (8)$

the capillary number: $Ca = \frac{\epsilon}{\mu^*L^*}, \quad (9)$

where L^* - typical size; ρ^* - the density scale; μ^* - the unit of the chemical potential; η_1 - the viscosity scale; α - the mobility constant; and $\varphi = (\rho_2 - \rho_1)/\rho_1$ is the density contrast, with ρ_2 and ρ_1 being the densities of the pure components of the binary mixture.

The rise of an isolated single bubble was examined. The computational domain is represented by a vertical cylinder with circular cross section. The cylinder's radius is taken as the length scale. The radial and axial coordinates are denoted by r and z , respectively. The cylinder is closed at the bottom and top ends. It is assumed that the size of the bubble is sufficiently less than 1 (the radius of the computational domain), so the influence of the boundary conditions imposed on the cylinder's walls can be neglected. For the same reason, the initial position of the bubble is chosen at $z = 0.5$ (sufficiently far from the lower end), and the height of the cylinder, $H = 6$, is also chosen so large to observe a sufficiently long rise of the bubble before it reaches the upper end. The axisymmetric symmetry is assumed, and owing to the symmetry only a half of cylinder was considered.

The governing equations are supplemented with the boundary conditions below.

At the lower end: $z = 0 : u_r = u_z = 0, \partial C/\partial z = 0, \partial\mu/\partial z = 0 \quad (10)$

At the upper end: $z = H : u_r = u_z = 0, \partial C/\partial z = 0, \partial\mu/\partial z = 0 \quad (11)$

At the centreline: $r = 0 : u_r = u_z = 0, \partial C/\partial r = 0, \partial\mu/\partial r = 0 \quad (12)$

At the tube's wall: $r = 1 : u_r = 0, \partial u_z/\partial r = 0, \partial C/\partial r = 0, \partial\mu/\partial r = 0 \quad (13)$

Thus, all walls are assumed to be impermeable. The no-slip boundary conditions are used for the velocity field. For the chemical potential, we impose the absence of the diffusive flux through the walls. The conditions for the concentration should reflect the wetting conditions. We however consider the simplest case when the molecules of the mixture components interact with the wall equally, so the contact angle is 90° . In fact, we are interested in the evolution of the bubble far from the boundary conditions, so the wetting properties are not important

for the current study. The boundary conditions at the centerline are written to reflect the axial symmetry.

The typical shapes of the rising bubbles for four different Reynolds numbers and for two different capillary numbers are shown in Fig. 1. The actual time moments and the actual sizes of the bubbles are shown as well.

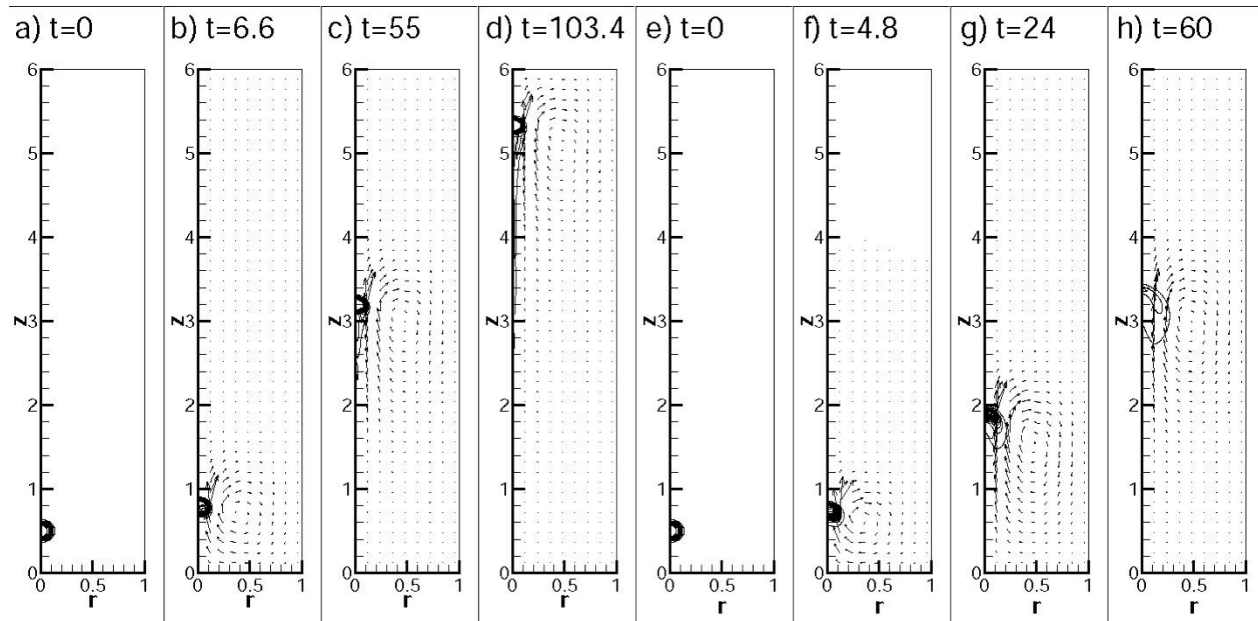


Figure 1. Bubbles at the middle of their rise for $H = 6$, $r_0 = 0.2$, $A = -0.5$, $Pe = 105$, $Gr = 0.1$, (a-d) $Ca = 8 \cdot 10^{-4}$; (e-h) $Ca = 2 \cdot 10^{-4}$; (a,e) $Re = 10$, (b,f) $Re = 25$, (c,g) $Re = 50$, and (d,h) $Re = 100$

Obviously, the interface becomes thinner if the capillary number is lower. Deformation of the bubble is stronger at lower capillary numbers, which is explained by smaller surface tension coefficient at such numbers. In this case, at sufficiently higher Reynolds numbers, the bubble can even break. The moment of the break up is depicted in Fig. 1d. At $Ca = 2 \cdot 10^{-4}$, the bubble breaks up at $Re > 50$. At $Ca = 8 \cdot 10^{-4}$, the bubble breaks up at $Re > 100$.

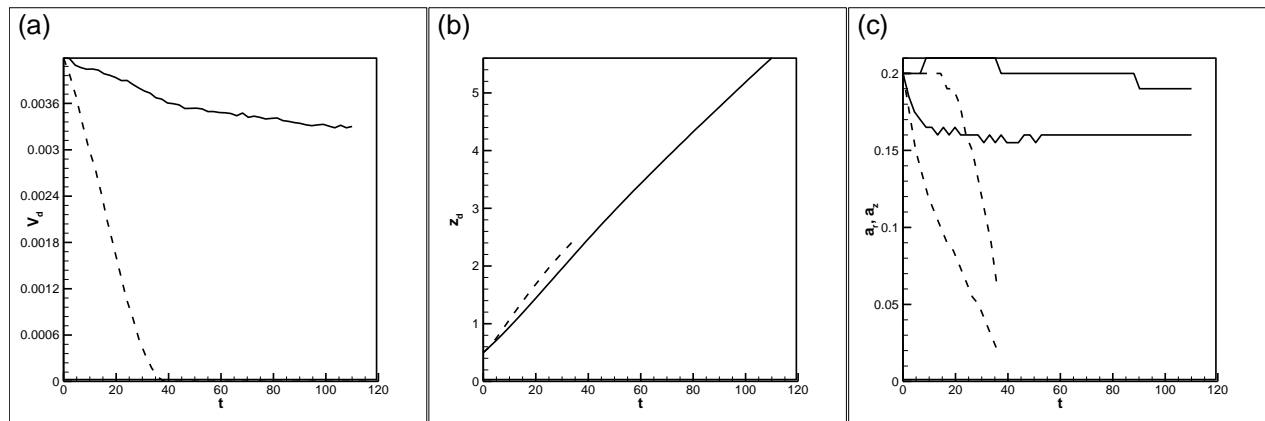


Figure 2. (a) The droplet's volume vs. time; (b) the vertical position vs. time; and (c) the size of the droplet in the radial and vertical directions vs. time. The curves are plotted for two Peclet number ($Pe=10^7$ – solid lines and $Pe=10^5$ – dashed lines) and for the other parameters as in Figure 1

The speed of the bubble rising is high at high Reynolds number. All bubbles in Fig. 1 started to rise from the same point and are shown at the similar positions, but at the different time moments, as the rise time is smaller if the Reynolds number is increased. The dissolution of

the bubble is accompanied by the convective motion near the bubble. The intensity of this motion is also increased at higher Reynolds numbers.

The results in Fig. 1 are shown for $Pe = 10^5$. At such Peclet numbers the diffusion through the interface is small, but it is different from zero. The actual sizes of the bubbles are indicated in Fig. 1. One sees that the diffusion is strongly intensified by convective flows, so that at higher Reynolds numbers the bubbles rise faster, but they decrease in size also much faster.

Fig. 2 shows the time evolution of the bubble's volume, position and shape.

An unexpected result is an impact of the Peclet number on the speed of rise. For the cases with higher Peclet numbers (weaker diffusion) the time of the initial acceleration is much lower and the attached speed of rise is also lower. The agreement between the Stokes prediction and the numerical results are getting better at higher Peclet numbers, which is expectable.

3. Conclusions

Currently, we have investigated the evolution of the bubble in the case of weaker interfacial diffusion. We have compared the obtained results with the data available for immiscible systems, and found that all classical formulae earlier obtained on the bases of other theoretical and experimental approaches can be successfully reproduced with the help of the phase-field approach. In future work, we aim to focus on the effect of absorption, the rate of absorption of bubbles of different sizes, and the influence of the absorption on the speed of bubble rise and on the evolution of the bubble shape.

Acknowledgements

The study was financially supported by RFBR as part a research project № 16-51-10079 "Mixing dynamics in diffusion-limited reactions

References

- [1] Meyers RA. Handbook Of Petrochemicals Production Processes. McGraw – Hill Professional. 2005.
- [2] Lee S. Encyclopedia of Chemical Processing. CRC Press. 2005. P. 3291.
- [3] Khlebnikova E, Bekker A, Ivashkina E, Dolganova I, Yurev E. Procedia Chemistry. 2015, 15: 42-48.
- [4] Belinskaya NS, Frantsina EV, Ivanchina ED, Popova NV, Zyryanova IV, Averyanova EV. IOP Conference Series: Earth and Environmental Science. 2016; 43: 1-6.
- [5] Davies RM, and Taylor FI. The Mechanics of Large Bubbles Rising through Extended Liquids and through Liquids in Tubes. Proc. R. Soc. Lond. 1950; A 200(1016):375-390.
- [6] Moore DW. The rise of a gas bubble in a viscous liquid, J. Fluid Mech. 1959; 6(1):113-130.
- [7] Ryskin G and Leal LG. Numerical solution of free-boundary problems in fluid mechanics. Part 2. Buoyancy-driven motion of a gas bubble through a quiescent liquid. J. Fluid Mech. 1984; 148:19-35.
- [8] Bhaga D and Weber ME. Bubbles in viscous liquids: shapes, wakes and velocities. J. Fluid Mech. 1981; 105:61-85.
- [9] Vorobev A. Boussinesq approximation of the Cahn-Hilliard-Navier-Stokes equations. J. Physical Review E 82, 2010; 056312.
- [10] Lowengrub J, Truskinovsky L. Quasi-incompressible Cahn-Hilliard fluids and topological transitions. R. Soc. Lond. Proc. Ser. A Math. Phys. Eng. Sci. 1998; 454(1978): 2617–2654.

To whom correspondence should be addressed: Dr. Elena Khlebnikova, Chemical Engineering Department, Tomsk Polytechnic University, 30, Lenin Avenue, Tomsk, 634050, Russia; tel.: (+7-3822) 563443; fax: (+7-3822) 563-435; e-mail: elena.khle@gmail.com

COMPARISON OF VARIOUS REFORMER TYPES BY USING EXERGY ANALYSIS METHOD

A. Garmroodi Asil¹, A. Behroozsarand², A. Nakhaeipour³

¹ Chemical Engineering Department, Faculty of Engineering, University of Bojnord, Bojnord, Iran

² Faculty of Chemical Engineering, Urmia University of Technology, Urmia, Iran

³ Chemistry Department, Faculty of Science, Ferdowsi University of Mashhad, Mashhad, Iran

Received October 18, 2017; Accepted December 23, 2017

Abstract

Exergical analysis of four reforming processes comprising two stand-alone autothermal reformers (ATR) and top fired reformers (TFR) plus their combination forms as a parallel and series arrangements have been investigated in the present article. The coupled mathematical code in the Visual Basic program and Aspen HYSYS process simulator linked together in order to calculate physical and chemical exergies of industrial plants streams. Four distinct key parameters including dry productivity, exergy loss to dry productivity ratio, fuel consumption, and CO₂ emission have been considered to compare all the reformers arrangements together. The maximum and minimum dry productivity among all reformers belongs to TFR (86058 kg/hr) and parallel mode (73220 kg/hr), respectively. The exergy loss to dry productivity ratio for TFR, ATR, series and parallel modes is 1.88, 0.46, 0.73 and 0.57, respectively. It was shown that, although single ATR has minimum exergy loss to dry productivity ratio, no undesirable CO₂ emission and does not consume fuel, but it utilizes high cost O₂ as an oxidant agent which demand separate oxygen plant. Also, parallel reformer arrangement has consumed around 57% more fuel than series arrangement. Furthermore, it was concluded that high consumption of steam rate in processes would increase the possibility of exergy loss.

Keywords: : Synthesis gas; Aspen HYSYS; Exergy analysis; Reformer arrangement; ATR.

1. Introduction

Nowadays, environmental pollution and public health problem caused by fossil-fuel burning challenge scientist to find alternative environmentally friendly fuel resources. No pollution emissions, production from diverse primary energy sources, such as hydrocarbons, biomass, water or solar energy have introduced hydrogen as an attractive alternative energy source in recent decades [1]. Petroleum refining and petrochemical industries especially ammonia and methanol production plants are the largest sectors that consume hydrogen as a feedstock. Various processes such as coal and biomass gasification, water electrolysis, photo-electrolysis, photo-dissociation and biological operation can produce hydrogen. Among these procedures, steam methane reforming (SMR) is one of the most promising and commonly used processes for large hydrogen production with more than 80 years of history [2]. At the steam reforming unit synthesis gas, i.e., mixture hydrogen and carbon monoxide, is produced. Generally, the process scheme comprises reforming, water-gas shift, CO₂ removal by amine solution and methanation units. The synthesis gas production from hydrocarbon resources is accomplished by two well-known primary and secondary reformers. Steam methane reforming (SMR) and autothermal reforming (ATR) are two industrial examples of primary and secondary reformers, respectively [3]. Generally, the different routes of producing syngas are: autothermal reforming (ATR), steam methane reforming (SMR), a combination of ATR and SMR which is called combined reforming, and heat exchange reforming involving series and parallel arrangements. It is obvious that combination of both primary and secondary reformers enjoys the benefits of an individual reformer as it is commercialized in ammonia manufacturing plants. Combination

of these reformers has been installed for synthesis gas production in facilities such as Mossel Bay (South Africa), Bintulu (Malaysia), Oryx (Qatar), Pearl GTL (Qatar), and Escravos (Nigeria) [31]. The high initial investment cost is the problem of combination process. High productivity, low energy uses or consumed fuel, and minimum release of a component such as carbon dioxide are the important factors which should be considered in synthesis gas production units. Progress and optimization in synthesis gas production processes are essential for large scale production of these valuable materials as a feed for gas to liquid (GTL), ammonia or methanol production plants [4].

Thermodynamic analysis, particularly exergy analysis, appears to be an efficient tool to evaluate the sustainability of a process, system design, analysis and optimization of industrial systems. Totally, exergy analysis is used to recognize the location, magnitude, and sources of thermodynamic deficiencies, and to optimize the usage of energy resources regard to economic and environmental aspects [5].

There are relatively few studies focused on the syngas units comprising of ATR and SMR in series and parallel arrangements. Bakkerud investigates the combination of HTER (Haldor-Topose exchanger reformer) and ATR reformer in series and parallel arrangement for GTL application by changing steam to carbon (S/C) ratio [6]. Since in the series arrangement, all gas passes through the steam reforming unit, and then through ATR, steam reforming catalyst may set for lower S/C ratio. Independent feeding of two reformers in parallel arrangements giving freedom to optimize S/C ratio individually. Rafiee et al. studied the S/C ratio, purge ratio, amount of tail gas recycled to Fisher-Tropsch (F-T) synthesis units and reactor volume in a GTL plant for configurations of SMR-ATR plus ATR-GHR (gas-heated reformers) series arrangement [7]. The optimization results indicate that installing a steam methane reformer in the syngas production unit will reduce the total oxygen consumption and make the oxygen plant smaller. Ebrahimi et al. simulated four cases of a single SMR, a single ATR, combined series and parallel arrangements for industrial case study and optimization issue is applied to the systems for choosing the optimum conditions [8]. It was shown that the important stream is one that connects SMR to the ATR for the optimized production of syngas. Moreover, the series configuration consumes lower fuel and releases lower amount of CO₂ emission compared to the parallel arrangement.

Up to best of our knowledge, an exergetic comparison of various reformer types for production of synthesis gaseous has not been considered in the previous researches. In the present study, a straightforward method for calculating physical and chemical exergy of various streams inside the industrial plant for a different arrangement of primary and secondary reformers (single autothermal (ATR), single top fired reformer (TFR), parallel (ATR-TFR), series (ATR-TFR)) was performed. The mathematical code in Visual Basic programming was linked to Aspen HYSYS process simulator to evaluate exergy analysis for all streams inside flowsheet. Exergy balance is resulting in more insight into the nature of irreversibilities and exergy loss points associated with specific processes. It was shown that the ATR case is preferable reformer due to the low exergy loss object.

2. Exergy-definitions

Exergy is defined as the maximum obtainable amount of work from the mass of fluid which can be obtained as a process is changed reversibly from the given (existing) state to a state of equilibrium (zero) with the environment, or the maximum work that can be obtained from any quantity of energy [9]. Exergy balance relies on the decomposition of input and output streams in material, work, and heat streams. In addition, output streams can be classified into waste and useful streams [10]. The waste stream includes all streams pushed to the environment without recycling or reusing, while useful streams are heat or material used in the downstream process. A General Grassmann representation of a process or generic system studied through exergy balances is illustrated in Figure 1.

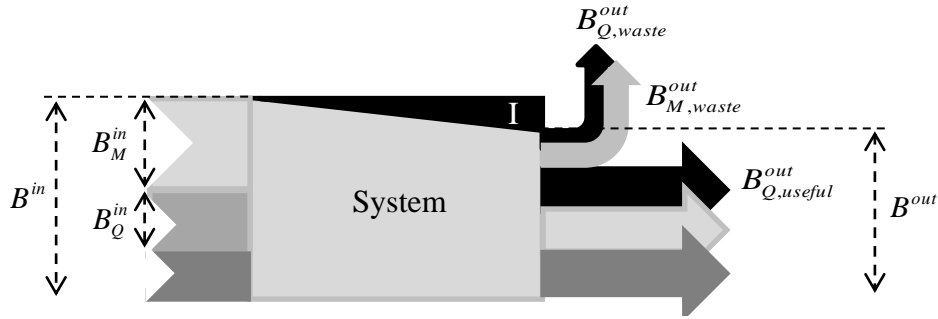


Fig. 1. Overview Grossman diagrams for process or system

In this system that can be either considered as a single unit operation, an energy balance can be written as follows [10]:

$$H_M^{in} + Q^{in} + W^{in} = H_M^{out} + Q^{out} + W^{out} \quad (1)$$

In the above equation, "H," "Q," and "W" are enthalpy, heat, and work respectively. In exergy balance, there is "internal exergy loss" which was shown in Figure 1 by the term I, corresponding to the exergy destroyed inside the system because of irreversibilities of the process:

$$B^{in} = B^{out} + I \quad (2)$$

In the above equation, total exergy input (B^{in}) and total exergy output (B^{out}) are respectively given by the sum of input and output exergies associated with material (NS_M streams), work (NS_W streams) and heat streams (NS_Q streams):

$$B^{in} = \sum_{i=1}^{NS_M^{in}} B_{M,i}^{in} + \sum_{i=1}^{NS_Q^{in}} B_{Q,i}^{in} + \sum_{i=1}^{NS_W^{in}} B_{W,i}^{in} \quad (3)$$

$$B^{out} = \sum_{i=1}^{NS_M^{out}} B_{M,i}^{out} + \sum_{i=1}^{NS_Q^{out}} B_{Q,i}^{out} + \sum_{i=1}^{NS_W^{out}} B_{W,i}^{out} \quad (4)$$

Regarding the "useful-waste" concept, the equation (2) can be expressed in the following form:

$$B^{in} = B_{useful}^{out} + \underline{B_{waste}^{out}} + I \quad (5)$$

where the underlined term is called "external exergy loss." Assuming that the exergy flow corresponding to work output is always useful exergy, the exergy balance can finally be expressed as follows:

$$\sum_{i=1}^{NS_M^{in}} B_{M,i}^{in} + \sum_{i=1}^{NS_Q^{in}} B_{Q,i}^{in} + \sum_{i=1}^{NS_W^{in}} B_{W,i}^{in} = \sum_{i=1}^{NS_M^{out,useful}} B_{M,useful,i}^{out} + \sum_{i=1}^{NS_M^{out,waste}} B_{M,waste,i}^{out} + \sum_{i=1}^{NS_Q^{out,useful}} B_{Q,useful,i}^{out} + \sum_{i=1}^{NS_Q^{out,waste}} B_{Q,waste,i}^{out} + \sum_{i=1}^{NS_W^{out}} B_{W,i}^{out} + I \quad (6)$$

Establishment of exergy balances on a given system needs to evaluate all the terms of above equation precisely. Classification of useful stream from waste ones is an important factor which depends on the recognition of the whole process accurately [10].

2.1. Exergy calculation methodology

Exergy similar to energy can be divided into physical, chemical, potential, and kinetic exergies. In the absence of electrical, magnetic, surface tension and nuclear effects, total exergy of a given system is the summation of four distinct elements [9]:

$$E_{sys} = E_{sys}^{Ph} + E_{sys}^{Ch} + E_{sys}^{Kn} + E_{sys}^{Pt} \quad (7)$$

In the above equation, E^{Ph} , E^{Ch} , E^{Kn} and E^{Pt} are physical exergy, chemical exergy, kinetic exergy and potential exergy respectively. Each of these exergies defined as follows:

$$E_{sys}^{Kn} = \frac{1}{2} m \vec{V}^2 \quad (8)$$

$$E_{sys}^{Pt} = mgz \quad (9)$$

$$E_{sys}^{Ph} = (H - H_0) - T_0(S - S_0) \quad (10)$$

$$E_{sys}^{Ch} = \sum_i x_i \varepsilon_i + \int RT_0 \sum_i x_i \ln x_i \quad (11)$$

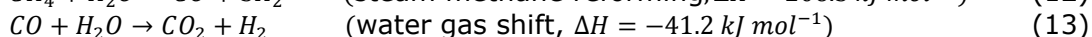
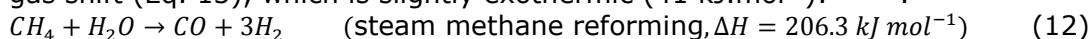
In the equations of (8) and (9), parameters V and z is the velocity of the stream relative to the surface of the earth and altitude of the stream above the sea level respectively [9]. Generally, the share of these two components from total exergy is normally negligible. Hence they can be disregarded. In the Equation (10), parameters h and S are the enthalpy and entropy of the substance at actual conditions, and h_0 and S_0 are the enthalpy and entropy of the substance at reference conditions, respectively. In the present work, the reference temperature and pressure are defined as $T_0 = 298.15$ K and $P_0 = 1.013$ bar. Chemical exergy originates from the difference between the chemical potentials when a substance is changed from reference conditions to the chemical equilibrium state. In the equation (11), x_i is the fraction of species i in the mixture of gases, ϵ_i is the standard chemical exergy of the same species, and R is the universal gas constant. A comprehensive discussion on various types of exergy calculation is given by Sato [11] and Hinderink *et al.* [12]. In the present article, two types of physical and chemical exergies were considered for each species in the inlet and outlet streams.

Exergy analysis in the field of reforming units has been studied by different researchers. For instance, Atsonios *et al.* [13] studied exergy analysis of a hydrogen-fired combined cycle with pre-combustion carbon capture. Chen *et al.* [14] investigated hydrogen production through SMR from both exergy efficiency and CO₂ emission points of view. Their sensitivity analysis shows a reverse relationship between CO₂ emission and system efficiency. Hajjaji and *et al.* [5] have been used exergy analysis to calculate the energy consumption of an SMR process. Based on the exergetic results and identifying the thermodynamic imperfections of the process, they have proposed a more efficient process by incorporating a third economizer (heat exchanger) to the original process for waste heat recovery. In others work by Simpson and Lutz [15], the performance of hydrogen production via SMR was evaluated using exergy analysis with emphasis on exergy flows, destruction, waste, and efficiencies. Their investigation shows the majority of the exergy destruction occurs due to the high irreversibility of chemical reactions and heat transfer. A brief review on hydrocarbon reforming will be presented in the following section.

3. Hydrocarbon reforming

3.1. Primary reformers

As it was emphasized before, SMR is considered as an industrial example of primary reformers [2]. Reforming process produces syngas with an H₂/CO ratio in the range of about 2.2 to 4.848 depending on the feed composition, CO₂ recycle and operating conditions such as pressure and temperature. Generally, steam Methane Reforming proceeds in two steps, the reforming reaction (Eq. 12), which is strongly endothermic (206 kJ.mol⁻¹), and the water gas shift (Eq. 13), which is slightly exothermic (41 kJ.mol⁻¹): [4b,8].



The comparison of the heat of reaction values indicates that the net reaction is endothermic. For this reason, additional energy has to be provided by external heating. It means that the tubular catalytic reactor needs a heat source, generated by a furnace. Mostly, industrial furnaces that were used for reforming process were classified into four groups: top-fired, terraced-wall, bottom-fired and side-fired. Usually, the top-fired primary reformer is used for methanol and ammonia plants with large single train capacity containing up to 1000 catalyst tubes. Nickel and cobalt in the form of thick-walled raschig rings with several holes are the best catalysts for SMR, and the overall rate in steam reforming is limited by the heat transfer, at high temperatures. The product of SMR is sent to the product line or enters to the secondary reformer. In the present paper, the primary reformer is presumed SMR with a top-fired furnace.

3.2. Secondary reformers

Generally, the conversion of hydrocarbon feed in primary reformers is not complete, specially, for heavy feed stock such as gasoil or naphtha. Conventionally, the product of pri-

many reformers was sent to other reformers entitled "secondary reformer." Industrial ATR used in the present work consist of two sections: 1) Partial oxidation chamber (POX); 2) fixed bed catalytic reformer. The main reaction occurred in the POX chamber stated below (Eq. 15) [3b]:

$$CH_4 + 0.5O_2 \rightarrow CO + 2H_2O \quad (\text{Partial Oxidation, } \Delta H = -520 \text{ kJ mol}^{-1}) \quad (15)$$

Preheated natural gas and oxygen (separated from the air) are fed to the reactor and mixed by a burner and finally react in a turbulent diffusion flame. Due to fast exothermic combustion reactions, all oxygen is consumed with methane completely. In contrast to ATR, SMR has a bulky installation, due to the large SMR furnace with catalyst tubes and large flue gas heat recovery section. However, SMR process is preferred for the production of hydrogen, as a result of the high H_2/CO molar ratio (3-5) compared to ATR (1.6-2.65).

3.3. Combined configuration with different reformer arrangement

Poor economy of scale, large input heat requirement and production of syngas with at least 3:1 hydrogen to carbon monoxide ratio prevent utilizing standalone SMR for large scale industrial application such as GTL [7] Also, high cost feature of the ATR process is not preferable. Adding secondary reformer to primary one could convert the probable un-reacted methane remained from SMR and adjusted the H_2/CO ratio based on the suitable application such as methanol, F-T, and ammonia synthesis. Figure 4 and 5 depict the parallel and series arrangements of SMR and ATR reformers, respectively [7-8,16]. In the parallel type, the hydrocarbon feed such as natural gas is divided into two distinct parts: one part is conducted into primary reformer (TFR) directly, another portion is sent to secondary one (ATR), and finally the output products of two reformers are connected together. In the series form, the output product of TFR and fresh hydrocarbon mix together with relevant ratio and convey to the secondary reformer. In the present paper, exergy analysis of both series and parallel schemes are compared together.

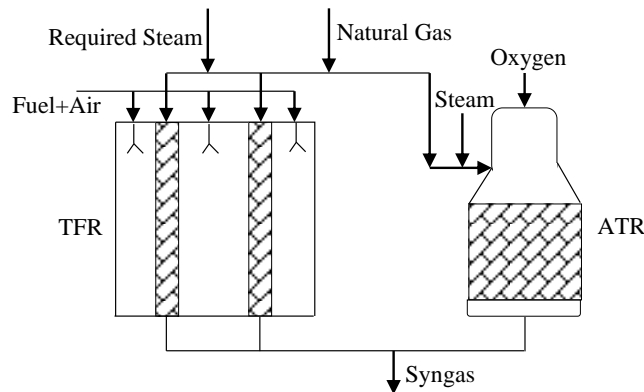


Fig. 2. Schematic diagram of parallel reformers arrangement

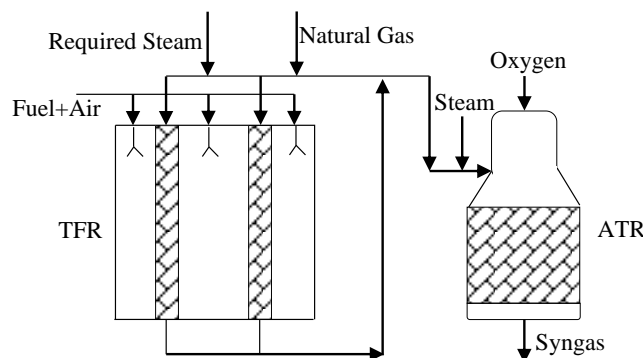


Fig. 3. Schematic diagram of series reformers arrangement

4. Exergy as New User Property in Aspen HYSYS

Process simulator software such as Aspen HYSYS does not calculate any form of exergy in the main stream flowsheet, hence, the mathematical code in visual basic programming provided and linked to Aspen HYSYS as a new user variable worksheet [17].

Figure 4 and 5 shows the overview of visual basic codes environment related to the user variables entitled "Chemical Exergy," "Physical Exergy," Kinetic Exergy" and "Potential Exergy." Neglecting the kinetic and potential exergies, total exergy of the specific stream would be the sum of the physical and chemical exergies.

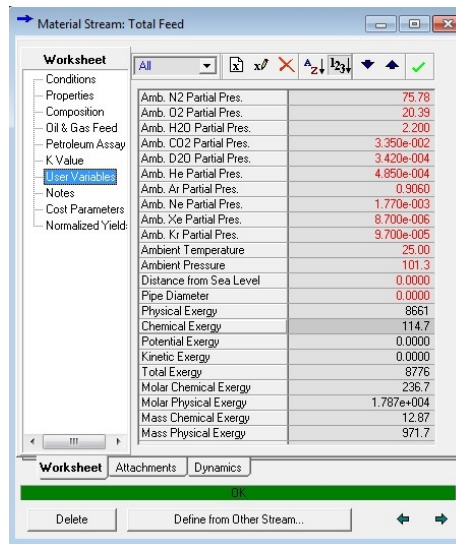
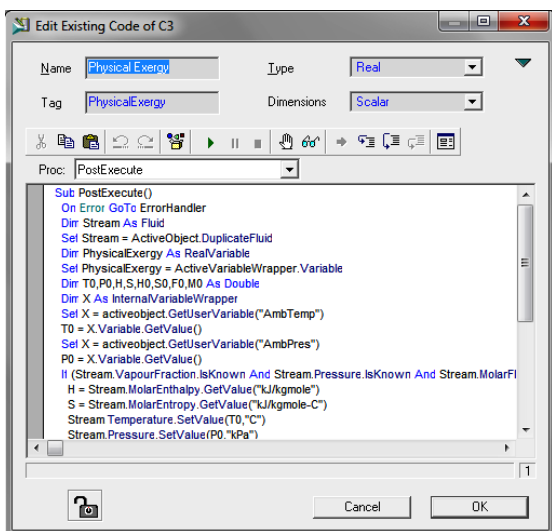


Fig. 4. Overview of User Variable coding environment Fig. 5. Overview of User Variable results page

5. Simulation procedure

In this study, the information of industrial ethylene plant feed stream was simulated by Aspen HYSYS software under steady state condition. The component list was completed by available constituents restricted to Table 1. The thermodynamic data (Fluid package) and phase behavior predictions of the material streams were obtained using the Soave–Redlich–Kwong equation of state. The primary reformer, SMR, was simulated by a library model equilibrium reactor with the three main reactions of (Eq. 12-14). Furthermore, first, Gibbs free energy minimization concept was used for partial oxidation reaction (POX) section of ATR and similar to SMR reformer, the catalytic bed section was simulated by an equilibrium reactor. Also, operational facilities such as heat exchangers, pumps, compressors and other equipment's were included in exergy analysis.

Table 1. Feed characteristics of simulation cases

Parameter name	Value (Unit)	Composition	Mole(%)
Temperature	500 (°C)	Ethane	3.2
Pressure	20 (bar)	Propane	1.9
Mass flow	39 086.46 (kg/hr)	i-Butane	0.0
Molar flow	1 745 (kmol/hr)	n-Butane	0.6
Composition	Mole (%)	i-Pentane	0.0
Hydrogen	0.0	n-Pentane	0.1
CO	0.0	n-Hexane	0.0
CO ₂	25.1	H ₂ O	0.0
Nitrogen	4.2	Oxygen	0.0
Methane	65.0		

6. Results and discussion

Exergical analysis of four primary and secondary reformers arrangements including single SMR, single ATR, combined SMR and ATR in series and parallel forms in order to produce synthesis gas with an H₂/CO molar ratio of 1 has been performed in the present article. All the feed streams conditions such as temperature, pressure, composition, and flow rate are kept constant for all simulated cases.

Comparison of exergy loss for different reformers arrangements is presented in Table 2. According to this table, although TFR has the highest productivity rate (86058 kg.hr⁻¹), it consumes higher amount of fuel (1740 kmol.hr⁻¹) and release large quantity of anthropogenic greenhouse carbon dioxide (1809 kmol.hr⁻¹) into the atmosphere. On the other hand, ATR reformer has no undesirable CO₂ emission and does not consume fuel, but it utilizes high cost O₂ as an oxidant agent which demand separate oxygen plant. These findings are in a good agreement with earlier studies (10).

Table 2. Comparison of exergy loss for different arrangement of synthesis gas production

Parameter/arrangement	TFR	ATR	Series TFR-ATR	Parallel TFR-ATR	Min. /Max.
Productivity* (kg.hr ⁻¹)	86 058	80 542	74 796	73 220	Parallel/TFR
Feed molar flow (kmol.hr ⁻¹)	1 745	1 745	1 745	1 745	-
Consumed fuel(kmol.h ⁻¹)	1 740	0	522	820	ATR/TFR
Released CO ₂ (kmol.h ⁻¹)	1 809	0	148	375	ATR/TFR
H ₂ /CO ratio (mol/mol)	1.05	1.1	0.99	1.02	ATR/TFR
Physical exergy loss (W)	-162 113	-37 060	-54 758	-41 958	ATR/TFR
Chemical exergy loss (W)	148	93	105	86	TFR/Parallel
Total exergy loss (W)	-161 965	-36 968	-54 653	-41 872	ATR/TFR
Exergy Loss/Productivity (W.kg ⁻¹ .s)	1.88	0.46	0.73	0.57	ATR/TFR

Productivity has been reported on dry basis

The third row of Table 2 shows that parallel reformers arrangement has consumed around 57% more fuel than series arrangement. Although, physical exergy of series reformers are 31% more than parallel arrangement, however, the chemical exergy of parallel is 22% more than series ones. Investigation of total exergy loss which is the summation of physical and chemical exergies reveals that alone ATR and TFR have the minimum (-36968 W) and maximum (-161965 W) amount of total exergies respectively. The series and parallel arrangements lie between these two amounts. The last row of Table 2 represents the total exergy loss divided to dry productivity rate. Again, the ATR and TFR have assigned to the minimum (0.46) and maximum (1.88) amounts, and series (0.73) and parallel (0.57) arrangement are in the next ranks, respectively. Detailed exergy loss calculation data for studied cases have been presented in Tables 3-6. These tables have been classified into five columns. The first column shows the name of input and output of material and energy streams which have been connected to each arrangement mode. Second and third columns represent the values of physical and chemical exergies of related streams. Moreover, the fourth column corresponds to the summation of physical and chemical exergies of each stream, and finally, fifth ones are the fraction of total exergy of each stream to total input or output exergy. The exergy loss indicates the difference between input and output exergies. Table 3 present results of exergy analysis for single TFR. As it is obvious, required steam stream in TFR reformers has the highest fraction of total exergy around 76.81% (67441/87806) and air stream has the lowest existence exegy with 0.02% from input streams. Since the TFR reformer does not consume pure oxygen, the related exergy will be set to zero. Table 4 shows the exergy analysis of single ATR. No gas fuel is involved in ATR process, so the amount of gas fuel exergy will be zero. Again, input steam stream to ATR reformer has the highest value of total exergy about 56.98% and O₂ assigned to the minimum value around 3.99%. Comparison of Table 3 and 4 proves that alone ATR reformer has lower exergy loss (-36968 W) compared to TFR reformer (-161965 W). Also, it can be concluded that high consumption of steam rate in processes will increase the possibility of exergy loss. Perhaps, a sharp decrease in temperature and pressure

of steam in the process is the reason for such behavior. As it was mentioned before, the advantages of ATR process compared to TFR are a lower initial investment and relatively no carbon dioxide emission, but investment on distinct air separation unit to provide expensive oxygen is accounts disadvantages. Moreover, it can be concluded that the alone TFR is preferable in accordance with high productivity object, but it has high exergy loss.

Table 3. Exergy analysis results for top fired reformer

	Physical Exergy	Chemical Exergy	Total Exergy	% of Total
Total Feed	8 775	115	8 890	10.12%
Refinery-CO ₂	11 330	4	11 334	12.91%
Air	11	10	20	0.02%
Gas Fuel	4	116	120	0.14%
Steam	0	0	0	0.00%
Required Steam	67 424	17	67 441	76.81%
O ₂	0	0	0	0.00%
Input Exergy	87 544	262	87 806	100%
Total Product	136 517	51	136 568	54.68%
Fuel gas	113 140	62	113 202	45.32%
Output Exergy	249 657	114	249 771	100%
Exergy loss	-162 113	148	-161 965	

Table 4. Exergy analysis results for autothermal reactor

	Physical Exergy	Chemical Exergy	Total Exergy	% of Total
Total Feed	8 661	115	8 776	15.82%
Refinery-CO ₂	11 290	4	11 295	20.36%
Air	2	2	4	0.01%
Gas Fuel	1	23	24	0.04%
Steam	0	0	0	0.00%
Required Steam	33 712	8	33 721	60.77%
O ₂	1 667	1	1 667	3.00%
Input Exergy	55 333	153	55 486	100%
Total Product	85 805	34	85 839	77.94%
Fuel gas	24 287	13	24 300	22.06%
Output Exergy	110 092	47	110 139	100%
Exergy loss	-54 758	105	-54 653	

Table 5 and 6 represent the detailed exergy analysis of series and parallel reformers arrangement respectively. Similar to previous single reformers, the highest fraction of total exergies attributed to the steam (and required steam) stream in both series and parallel arrangements with a percentage more than 60%. The values of total exergies for series and parallel reformers are between two single reformers. Additionally, comparison of Table 3, 5 and 6 shows that the total exergy of exit streams such as total product and gas fuel in TFR reformer are close to each other, but in series and the parallel arrangement has reverse behavior. Comparison of four key parameters for single TFR, single ATR, combined TFR and ATR in series and parallel arrangements depicts in figure 8. It is clear that all the parameters should be minimized except dry productivity. It can be inferred that TFR has highest productivity rate which is considered as a pros. However, exergy loss to dry productivity ratio consumed fuel and release CO₂ parameters are also in maximum values which are considered as cons. Overall view of figure 6 reveals that single ATR has a better position from series and parallel arrangements in all four key parameters. Although exergy loss to dry productivity ratio is slightly in favor of parallel arrangement, but series mode has higher productivity rate and lowers consumed fuel and released CO₂. So it seems that series arrangement which feeds of ATR is supplied by a mixture of both SMR product and the fresh, natural gas is a better choice than the parallel mode.

Table 5. Exergy analysis results for top fired with autothermal reactor in series arrangement

	Physical Exergy	Chemical Exergy	Total Exergy	% of Total
Total Feed	8 661	115	8 776	12.73%
Refinery-CO ₂	11 290	4	11 295	16.38%
Air	2	2	4	0.01%
Gas Fuel	1	23	24	0.03%
Steam	14 047	4	14 050	20.37%
Required Steam	33 712	8	33 721	48.90%
O ₂	1 092	0	1 092	1.58%
Input Exergy	68 805	156	68 961	100%
Total Product	87 222	57	87 279	78.75%
Fuel gas	23 541	13	23 554	21.25%
Output Exergy	110 763	70	110 833	100%
Exergy loss	-41 958	86	-41 872	

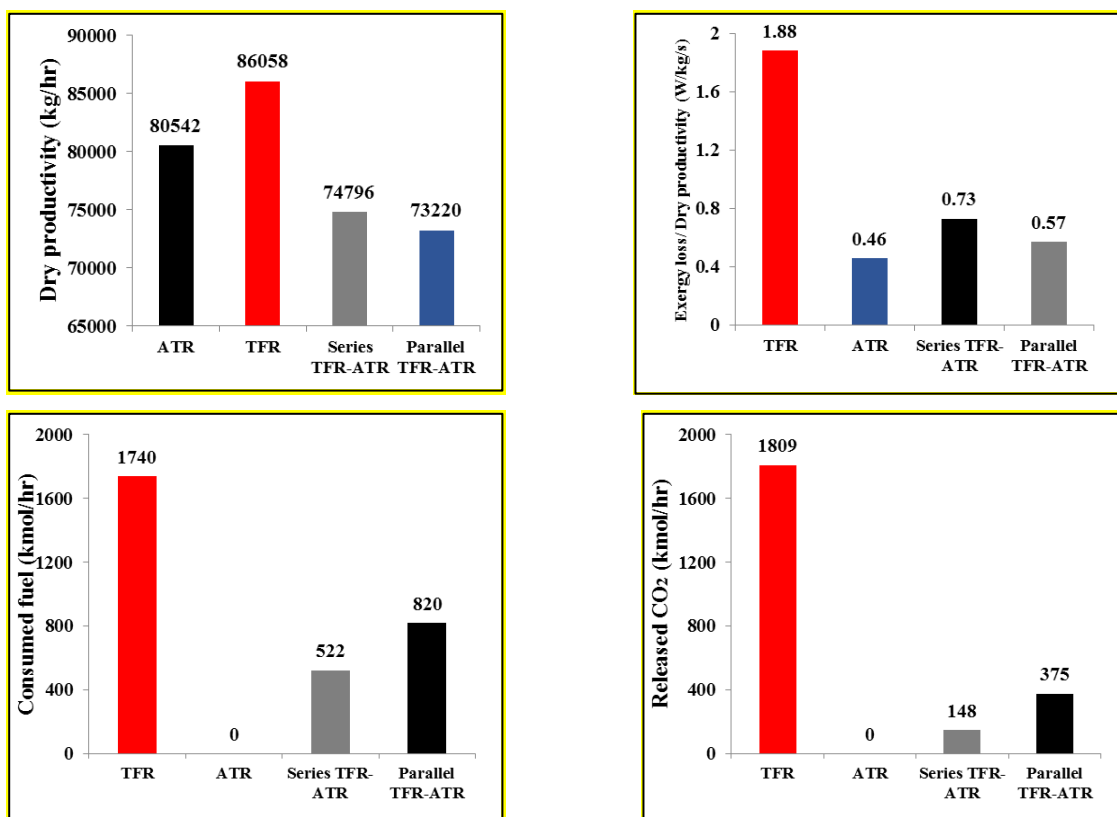


Fig. 6. Comparison of four key parameters in different studied cases: (a) Dry productivity; (b) Ratio of exergy loss to dry productivity; (c) Consumed fuel; (d). Released CO₂

Table 6. Exergy analysis results for top fired with autothermal reactor in parallel arrangement

	Physical Exergy	Chemical Exergy	Total Exergy	% of Total
Total Feed	8 661	115	8 776	12.73%
Refinery-CO ₂	11 290	4	11 295	16.38%
Air	2	2	4	0.01%
Gas Fuel	1	23	24	0.03%
Steam	14 047	4	14 050	20.37%
Required Steam	33 712	8	33 721	48.90%
O ₂	1 092	0	1 092	1.58%
Input Exergy	68 805	156	68 961	100%
Total Product	87 222	57	87 279	78.75%
Fuel gas	23 541	13	23 554	21.25%
Output Exergy	110 763	70	110 833	100%
Exergy loss	-41 958	86	-41 872	

7. Conclusion

In the present article, industrial synthesis gas production by some commercialized reformers such as SMR, as a primary reformer, ATR, as a secondary and their combination form in series and parallel arrangements were investigated. Several parameters such as productivity rate, fuel consumption, oxygen consumption, CO₂ released to atmosphere and exergy loss has been considered for selecting best case of syngas production. The exergy analysis regards as a powerful tool for analysis, evaluation, and improvement of thermal processes was applied to identify the magnitude and sources of thermodynamic inefficiencies of reformers arrangements which are not received proper attentions in previous studies. The mathematical code provided in the Visual Basic environment and linked to the Aspen-HYSYS as a user variable subroutine in order to calculate physical and chemical exergies of single TFR, a single ATR, combined series and parallel arrangements. Obtained conclusions revealed that single TFR is a preferable choice in accordance with productivity rate. Also, TFR has a maximum exergy loss per dry productivity ratio, fuel consumption and CO₂ emission to atmosphere among all other reformer arrangements which are not preferable to the point of process irreversibility and environmental conditions. No fuel consumption and CO₂ emission to the atmosphere in addition to minimum exergy loss to dry productivity ratio lead single ATR reformer seems to be the best choice for syngas production. From an economical point of view, ATR reformer requires expensive pure oxygen supplied from air separation unit. The dry productivity of series and parallel arrangements are lower than single reformers. In addition, the exergy loss to dry productivity ratio, fuel consumption, and CO₂ emission is between single TFR and single ATR. Finally, it was concluded that high consumption of steam in the processes would increase the possibility of exergy loss. It should be noted that among these reformers arrangements, single ATR uses the lowest amount of steam.

Nomenclature

ATR	Autothermal	W	Work
SMR	Steam methane reforming	B	Energy Flow
TFR	Top fired reformer	E	Energy
GTL	Gas to Liquid	Ph	Physical
S/C	Steam to carbon ratio	Sys	System
F-T	Fisher-Tropsch	Kn	Kinetic
In	Input	Pt	Potential
Out	Output	E	Standard chemical exergy
H	Enthalpy	X	Mole fraction
Q	Heat	WGS	Water gas shift

References

- [1] Kumar S, Tondwal N, Kumar S and Kumar S., Chemical Product and Process Modeling, 2016; 11: 125-140.
- [2] Karimipourfard D, Kabiri S and Rahimpour M., Journal of Natural Gas Science and Engineering, 2014; 21: 134-146.
- [3a] Maqbool W, Park SJ and Lee ES., Industrial & Engineering Chemistry Research, 2014; 53: 9454-9463;
- [3b] Ayodele BV and Cheng CK., Chemical Product and Process Modeling, 2015; 10: 211-220.
- [4a] Pour AN, Housaindokht MR, Irani M and Shahri SMK. Fuel, 2014; 116: 787-793.
- [4b] Pour AN, Housaindokht MR, Tayyari SF, Zarkesh J and Shahri SMK. Chemical Engineering Research and Design, 2011; 89: 262-269.
- [4c] Zamani Y., Pet Coal, 2015; 57: 71-75.
- [4d] Popok EV, Levashova AI, Gladchenko TM, Burlutskiy NP and Juravkov SP. Pet Coal, 2016; 58.
- [4e] Hasanpour F, Karimi S, Anahid S, Tavasoli A and Zamani Y., Pet Coal, 2016; 58.
- [5] Hajjaji N, Pons M-N, Houas A and Renaudin V., Energy policy, 2012; 42: 392-399.
- [6] Bakkerud PK., Catalysis Today, 2005; 106: 30-33.
- [7] A Rafiee and M. Hillestad, Chemical Engineering & Technology, 2012; 35: 870-876.
- [8] Ebrahimi H, Behroozsarand A and Zamaniyan A., Chemical Engineering Research and Design, 2010; 88: 1342-1350.

- [9] Kotas T.J., The exergy method of thermal plant analysis, Elsevier, 2013.
- [10] Ghannadzadeh A. in Exergetic balances and analysis in a Process Simulator: A way to enhance, Process Energy Integration, Vol. INPT, 2013.
- [11] Sato N., Chemical energy, and exergy: an introduction to chemical thermodynamics for engineers, Elsevier, 2004.
- [12] Hinderink A, Kerkhof F, Lie A, Arons JDS and van der Kooi H., Chemical Engineering Science, 1996; 51: 4693-4700.
- [13] Atsonios K, Panopoulos KD, Doukelis A, Koumanakos A and Kakaras E., Energy Conversion and Management, 2012; 60: 196-203.
- [14] Chen B, Liao Z, Wang J, Yu H and Yang Y., International Journal of Hydrogen Energy, 2012; 37: 3191-3200.
- [15] Simpson AP and Lutz AE., International Journal of Hydrogen Energy, 2007; 32: 4811-4820.
- [16] Dybkjaer I., Hydrocarbon processing, 2005; 84:63-67.
- [17] Abdollahi-Demneh F, Moosavian MA, Omidkhah MR and Bahmanyar H., Energy; 2011, 36: 5320-5327.

To whom correspondence should be addressed: Dr. A. Garmroodi Asil, Chemical Engineering Department, Faculty of Engineering, University of Bojnord, Bojnord, Iran, A.garmroodi@ub.ac.ir

DEVELOPMENT OF GASOLINE BLENDING RECIPES TAKING INTO ACCOUNT VOLUME AND COMPOSITION OF THE INVOLVED FEEDSTOCK

Maria V. Kirgina, Elizaveta V. Sviridova, Bogdan V. Sakhnevich, Nikita V. Chekancev, Yury A. Chursin*

Department of Fuel Engineering and Chemical Cybernetics, Tomsk Polytechnic University, Russia

Received October 12, 2017; Accepted December 23, 2017

Abstract

The process of gasoline blending is a sophisticated multistage industrial technology. In this paper, blending recipes of different gasoline brands were developed using computer modeling system "Compounding" considering the volume and changing composition of the involved feedstock. The developed modeling system allows increasing the efficiency of the gasoline production using only internal resources of the refinery with no additional investments and expenses.

Keywords: gasoline; mathematical modeling; blending recipes; octane number.

1. Introduction

Automobile fuels, primarily, gasoline and diesel fuel are the most significant part of petroleum products which play a crucial role in the economics of Russian Federation. On a modern refinery, the most part of the crude oil is being refined into motor fuels, primarily in gasoline. This makes gasoline blending an important process for petroleum industry with the main goal to mix products of refinery processes in specific proportions and obtain a final blend that complies all quality requirements [1-2].

This multi-staged process is one of the most sophisticated technologies from the standpoint of economic efficiency. The key point lies in the complexity of feedstock mixtures which consist of large quantities of individual hydrocarbons, in conditions of ever-changing feedstock composition. In addition, detonation resistance does not follow the law of additivity (octane number is a non-linear characteristic), so this makes it more difficult to optimize the process.

Considering all above-mentioned factors, it appears to be impossible to formulate a universal blending recipe; existent recipes need to be revised in real time to correspond the changing conditions of blending.

Thus, optimization of trade gasoline blending process is an urgent industrial-oriented research direction in terms of the modern trends of annual increase in demand for high-octane gasoline. There is a large number of research works of domestic and foreign scientists dedicated to the study of aspects of this problem [3-5].

However, the most efficient way of optimization and of gasoline blending process and prediction of operational properties of blended gasoline is to apply modeling systems which use physico-chemical properties of hydrocarbons as a basis for calculations.

The main role of such systems is to formulate economically feasible recipes of gasoline blending considering the composition of the involved feedstock.

2. Complex modeling system for optimization of gasoline blending

During the research, complex system for optimization of gasoline production was developed. The following interconnected modules are presented in the system: Module of chromat-

graphic data systematization; Module of detonation and physic-chemical characteristics calculation; The module of optimal gasoline blends.

The developed modeling system provides the user with calculations of detonation properties and a wide range of physical and chemical characteristics of gasoline and gasoline components including octane number, vapor pressure, density and viscosity of mixtures and precise hydrocarbon composition of each stream based on chromatographic analysis data. On the basis of this data, the system calculates an economically optimal gasoline recipe for different brands of gasoline.

A detailed description of modules is provided in the following sub-chapters.

2.1. Module of chromatographic data systematization

In this modeling system, chromatography data of feedstock streams serve as an input data for calculations of detonation characteristics.

In view of the fact that hydrocarbon composition gasoline component streams vary significantly in set and number of hydrocarbons, the module of chromatographic data systematization "UniChrom" has been introduced into the system for unification and standardization of experimental chromatography data.

Systematization of the chromatography is an automatic process constituting the reclassification of hydrocarbons in the initial mixture to the set of 110 key components. This set serves as a baseline for high accuracy calculations of octane numbers of blending gasoline. This set includes both individual hydrocarbons and pseudo-components [6].

2.2. Module of detonation and physic-chemical characteristics calculation

The module of detonation and physic-chemical characteristics calculation provides calculations for the following detonation characteristics of gasoline:

1. Octane numbers (RON, MON) of hydrocarbon stream involved in the blending process taking into account their non-additivity;
2. Mixture density, by the Mendeleev formula;
3. Mixture viscosity, by the Orrick and Erbar formula;
4. Saturated vapor pressure (SVP) by the Antoine equation;
5. Aromatics, olefins hydrocarbons, and benzene percentage.

The main module is developed in Borland "Delphi 7" workspace combining a user-friendly interface, coordination, integrity of sub-components and stable functioning of the system in general. It is possible to manually change flow rates of input streams [7-8].

2.3. Module of optimal gasoline blends

From the standpoint of economic profitability of the refinery, optimal blend of gasoline must ensure the biggest economic effect: Refinery has to use the cheapest raw materials for blending of gasoline with low market value (low-octane brands) and the cheapest raw streams, and high-octane raw streams for the most commercially demanded brands, respectively. Refinery tends to produce the maximum possible volume of gasoline, using available stocks of the raw stream; the product must comply with the demands of the Russian Technical Regulations and State Standard R 51866-2002.

In the research, a logical algorithm was compiled on purpose to formulate optimal blending recipes. In this algorithm, 12 typical hydrocarbon streams are involved in the blending process:

1. Hydrotreated catalytic cracking gasoline (HYT FCC);
2. Catalytic cracking gasoline (FCC);
3. Reformate from catalytic gasoline reforming unit with continuous catalyst regeneration (Reformate (moving-bed));
4. Reformate from catalytic gasoline reforming unit with periodic catalyst regeneration (Reformate (fixed-bed));
5. Toluene concentrate on the complex production of aromatic hydrocarbons (Toluene);

6. Isomerate from the isomerization unit of light gasoline fractions (Isomerate);
7. The fraction of the isopentane from the isomerization unit of light gasoline fractions (Isopentane);
8. Alkyl gasoline with the unit of the sulfuric acid alkylation (Alkylate);
9. Methyl tertiary butyl ether (MTBE);
10. Straight-run gasoline fraction from atmospheric and vacuum pipe stills (Straight-run gasoline);
11. Gasoline fraction from complex production of aromatics hydrocarbons (Feedstock for aromatics production);
12. Gasoline- raffinate from the complex production of aromatic hydrocarbons (Raffinate of aromatics production).

Limiting conditions in recipes formulation are strictly regulated characteristics as RON, MON, SVP and content of benzene, aromatic and olefin hydrocarbons, sulphur and MTBE in trade gasoline of a specific brand.

The module of optimal gasoline blends formulation was developed in the workspace Borland "Delphi 7" on the basis of the algorithm flowchart of the logical algorithm is presented in Figure 1.

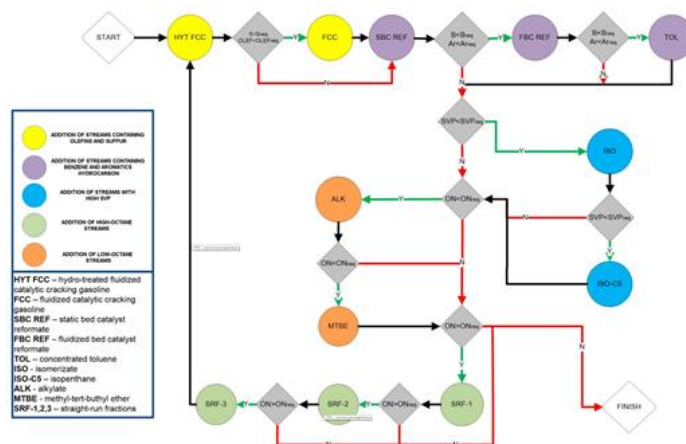


Fig. 1. Flowchart of the logical algorithm for optimal gasoline blends formulation

The developed algorithm automatically optimal gasoline blends on the basis of a formalized hydrocarbon composition of involved streams and predict all detonation characteristics of blended gasoline. Gasoline blending is carried out step-by-step as well as a recalculation of required quality characteristics.

Priority of using streams is chosen to the way of the biggest resource saving production. So first use the lowest-quality (and therefore least expensive) components, and then, when that streams are consumed, or used as much as possible, involve more expensive components.

The proposed approach has several advantages: first of all, it becomes possible to respond to changes in the composition of raw materials, develop "flexible" blending recipes and formulate recommendations for the involvement of streams with different composition when the blended to different gasoline brands.

Secondly, the algorithm is aimed to the efficient solution of several technological situations: production of the certain volume of gasoline, maximization of the particular brand yield, and the combination of several gasoline brands with an ability to set "the priorities of the sequence."

Thirdly, the algorithm reflects the concept of resource-saving blending, which allows to saving the most expensive components, involving unspent reserves only into the production of high quality fuels and reducing of unwanted quality giveaways and production of off-grade gasoline. These measures are able to increase the economic efficiency of blending, using only internal resources of the refinery without additional investments.

3. Formulation of gasoline blending recipes considering the volume of involved feedstock

For this research, blending recipes of different gasoline brands were developed using computer modeling system "Compounding." The recipes were formulated on the basis of data on configuration and composition of feedstock for one of the largest refineries in Russian Federation.

Here, we demonstrate calculated blending recipes for gasoline of Premium-95 brand corresponding to the Euro-5 quality standard of yield rate: 100, 500, 1000 and 2000 tons, respectively. In each case, the volume of each feedstock component equals 200 tons (hereafter refers to gasoline pool). Calculated recipes of Premium-95 gasoline for 100 (I), 500 (II), 1000 (III) and 2000 (VI) tons are shown in Figure 2 and in Table 1.

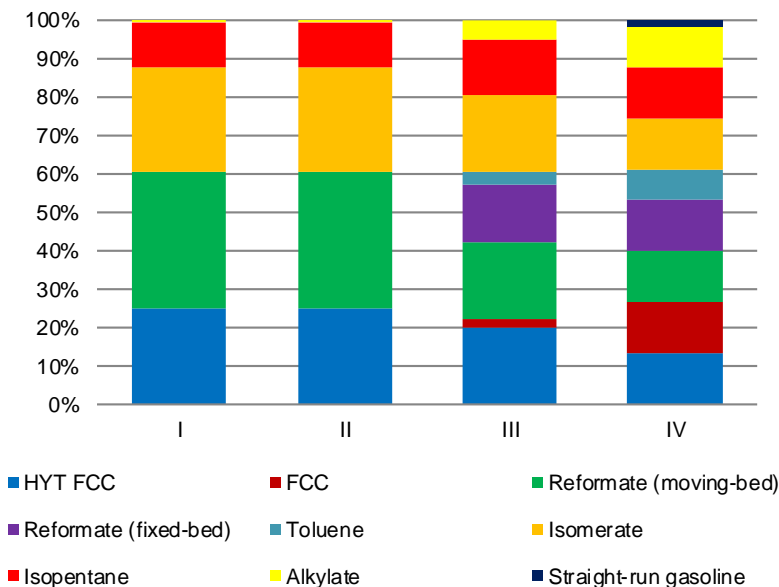


Fig. 2. The recipes of Premium-95 brand gasoline blending (Euro-5 quality standard)

Table 1. The main properties of gasoline of Premium-95 brand (Euro-5 quality standard)

Characteristics	Weight, tons			
	100	500	1000	2000
RON	95.0	95.0	95.0	95.2
MON	88.7	87.3	88.5	88.5
SVP, kPa	50.2	50.1	51.7	50.1
Density, kg/m ³	727.9	726.3	720.0	724.8
Benzene, wt. %	0.89	0.74	0.98	0.83
Aromatic hydrocarbons, wt. %	34.98	34.98	34.98	34.98
Olefins, wt. %	6.72	12.35	5.80	6.25

As it can be seen from Figure 2 and Table 1, calculation of blending recipes was conducted in such way that the values of benzene, aromatic hydrocarbons contents, as well as the SVP values, were maximized most closely to the values regulated by Russian Technical Regulations, but not exceeding them. The logic of algorithm is a multi-step mixing of available feedstock components in the order of the increased value. Such an approach tends to formulate gasoline blending recipes for required volume and quality of the product in a resource-efficient way.

On the basis of obtained results, it can be concluded that the structure of blending recipes depends on the required volume of product: in case of small volumes, the constraining factors

are quality requirements for certain gasoline characteristics, and in case of large volumes availability of feedstock plays the crucial role in the structure of blend.

Consider another practical task which consists in the production of several gasoline brands from a limited volume of feedstock in a certain time period of scheduling horizon and specific sequence of blending. The developed logical algorithm of complex modeling system is able to formulate blending recipes for simultaneous production of gasoline brands from the total available gasoline pool.

In this case, the task is to produce trade gasoline brands from gasoline pool volume of 200 tons in the following order and quantity: Regular-92, Euro-5 – 500 tons; Premium-95, Euro-5 – 500 tons; Super-98, Euro-5 – 500 tons.

All calculations for this case including the actual volume of gasoline blended by this algorithm are provided in Figure 3 and in Table 2.

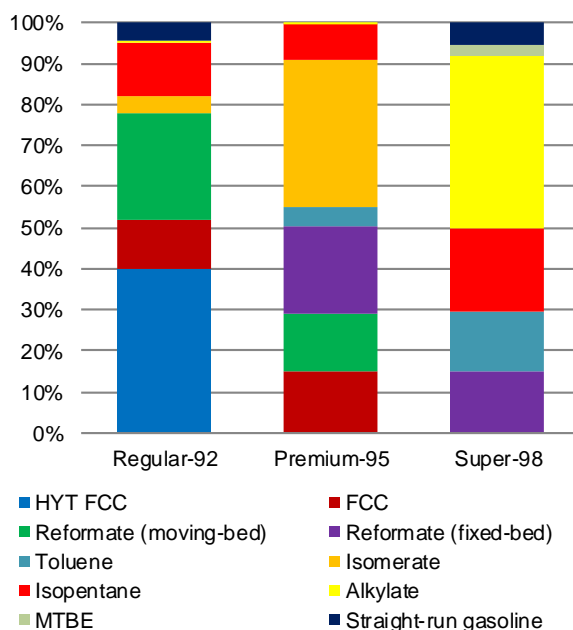


Fig. 3. The recipes of gasoline of Regular-92, Premium-95 and Super-98 brand gasoline blending in case of joint production

Table 2. The main properties of gasoline of Regular-92, Premium-95 and Super-98 brand gasoline blending in case of joint production

Characteristics	Regular-92	Premium-95	Super-98
RON	92.0	95.0	98.0
MON	84.2	89.4	93.1
SVP, kPa	50.2	50.1	58.4
Density, kg/m ³	731.3	723.1	720.3
Actual product amount, tons	500	500	460
Benzene, wt. %	0.89	0.74	0.98
Aromatic hydrocarbons, wt. %	34.98	34.98	34.98
Olefins, wt. %	6.72	12.35	5.80

As it can be seen from in Table 2, all quality properties of blended gasoline comply with the requirements of Russian Technical Peculations and State Standard R 51866-2002. During the recipes formulation, the involvement of basic refinery products such as reformate, catalytic cracking gasoline, and straight-run gasoline fraction is maximized that ensures the economy of expensive components such as MTBE (188 tons), toluene (111 tons).

Such an approach in the formulation of gasoline recipes reflects the strategy of economically-efficient blending. It tends to obtain gasoline brands with the maximum possible involvement of the less valuable and surplus components while minimizing percent of the most valuable, scarce ones. The latter components are added after all the other in order to comply with the requirements or can be saved for the next blending operations.

4. Formulation of gasoline blending recipes considering the composition of the involved feedstock

During the production cycle, hydrocarbon composition of refinery products is ever-changing; in its turn, it leads to changes in detonation characteristics of the obtained gasoline. Thus, resource-efficient gasoline production requires continuous real-time correction of blending recipes. In this section, calculations of optimal blending recipes depending on the composition of the involved feedstock are presented.

The main properties of feedstock components involved in gasoline production are shown in Table 3. For components demonstrating the most significant deviations of the detonation characteristics (Reformate m/b, Reformate f/b, Isomerate, and Isopentane), additional samples of the worst (I) and the best (II) quality are provided.

Table 3. The main properties of feedstock gasoline streams

Stream	RON	SVP, kPa	Characteristics Density, kg/m ³	Summary content, wt. %	
				Benzene	Aromatic hydrocarbons
HYT FCC	89.1	43.2	722.4	0.70	23.76
FCC	91.0	53.6	741.4	0.80	34.49
Reformate m/b	105.4	14.0	820.8	2.00	81.40
Reformate m/b I	102.6	20.5	812.7	2.50	78.68
Reformate m/b II	106.3	16.5	826.0	1.50	81.85
Reformate f/b	95.7	21.6	790.2	2.70	65.40
Reformate f/b I	90.7	27.7	780.3	1.20	58.57
Reformate f/b II	97.5	24.0	791.7	1.30	66.57
Toluene	117.0	7.2	854.7	0.00	100.00
Isomerate	90.0	62.0	636.8	0.00	0.00
Isomerate I	89.5	61.2	638.5	0.00	0.00
Isomerate II	93.6	67.4	637.3	0.00	0.00
Isopentane	92.4	146.3	600.9	0.00	0.00
Isopentane I	92.0	143.7	601.4	0.00	0.00
Isopentane II	93.0	141.4	601.8	0.00	0.00
Alkylate	96.6	34.7	678.6	0.00	0.00
MTBE	125.0	40.3	717.5	0.00	0.00
Straight-run gasoline	59.3	26.1	716.3	0.30	5.05

In the previous calculations, it was accepted that gasoline pool is constant; however, often in a real production situation, the volumes of available components are unequal due to different capacities of refinery units and volumes of product tanks.

The trends of feedstock availability were calculated for one production cycle (1 week) with a focus on the quantitative data from refineries. The average index of availability of feedstock for gasoline blending is shown in Table 4.

In this way, unequal amounts of feedstock were used for calculations of gasoline blending recipes depending on the composition of feedstock. The total gasoline pool is set to 2 400 tons; such situation (Table 4) reflects the average real situation of production of refinery products in the refinery.

Table 4. The average index of availability of feedstock for gasoline blending

Streams	The average index of availability of feedstock	Streams	The average index of availability of feedstock
HYT FCC	0.2763	Isomerate	0.0759
FCC	0.1220	Isopentane	0.0897
Reformate m/b	0.2215	Alkylate	0.0695
Reformate f/b	0.0631	MTBE	0.0119
Toluene	0.0163	Straight-run gasoline	0.0256
Total			1.0

Blending recipes for Premium-95 gasoline corresponding to the Euro-5 quality standard with a total yield of 1000 tons and various compositions of the involved feedstock (I – worse, II – medium, III – best feedstock) are shown in Table 5 and Figure 4.

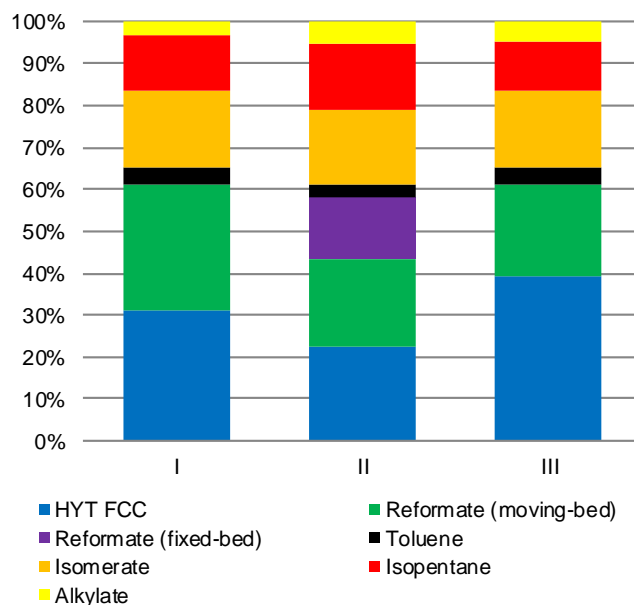


Fig. 4. The recipes of gasoline of Premium-95 brand gasoline blending considering various compositions the involved feedstock

Table 5. The main properties of gasoline of Premium-95 brand (Euro-5 quality standard) blending considering various compositions the involved feedstock

Characteristics	I	II	III
RON	95.0	95.0	95.0
MON	87.9	87.6	88.0
SVP, kPa	51.2	51.6	51.6
Density, kg/m ³	721.8	720.2	720.6
Actual product amount, tons	1000	1000	1000
Benzene, wt. %	0.98	0.98	0.61
Aromatic hydrocarbons, wt. %	34.94	34.98	31.34
Olefins, wt. %	8.52	6.03	10.61

As it can be seen from Tables 4 and 5, changes in hydrocarbon composition influence the detonation characteristics of streams; in its turn, it leads to a reformulation of blending recipes. For ensuring of the efficient gasoline blending refinery has to respond to changes in feedstock composition and adjust blending recipes to produce trade gasoline avoiding extra quality giveaways, as well as overruns of expensive high-quality hydrocarbon streams and production off grade gasoline batches.

In this case, at the beginning of the production cycle, Premium-95 gasoline brand (Euro-5) was produced using feedstock with average quality (Feedstock No. II, Table 5). As the composition of feedstock has been changing continuously within the certain limits during refinery operations, that influenced the quality of the obtained product. Calculations of detonation characteristics of produced gasoline in conditions of changes in composition are shown in Table 6. Feedstock No. I represent changes to the worst quality of components and Feedstock No. II, to the best quality, respectively.

Table 6. The main properties of gasoline considering various compositions the involved feedstock

Characteristics	Feedstock I	Feedstock II
RON	93.9	95.9
MON	87.3	89.2
SVP, kPa	53.6	52.9
Density, kg/m ³	717.3	721.7
Benzene, wt. %	0.90	0.70
Aromatic hydrocarbons, wt. %	33.40	35.24
Olefins, wt. %	6.10	6.08

As it can be seen from Table 6, production of gasoline by averaged ("universal") recipes is not economically profitable because there are unwanted deviations of operational characteristics of gasoline brands are observed throughout the changes in hydrocarbon composition.

Thus, in case of a decline in the feedstock quality (Feedstock I) gasoline, produced by the averaged recipes demonstrates drop in octane number down to 93.93 points as well as a decrease in density. Such deviations are not allowable for product certification, so the quality of gasoline needs to be additionally raised up to requirements Russian Technical Regulations demands and State Standard R 51866-2002. In case of an increase in the feedstock quality, unwanted RON giveaway (95.85) is observed, which is evidence of an overrun of high-quality components.

In order to avoid these issues, correction of gasoline blending recipes was automatically performed by the use of developed integrated modeling system (Table 5). In every single case, formulated blending recipes reflect the concept of the most resource-efficient distribution of available gasoline pool of certain quality and volume.

Considering the revealed data above we can suggest that using the modeling system for correction of gasoline blending in respect to changes in feedstock composition leads to positive results, such as:

1. In case of the worst feedstock, correction of recipes allows avoiding off-grade gasoline production; however, it becomes impossible to use Reformate F/B due to high contents of benzene and aromatic hydrocarbons. The necessity to compensate the shortage of octane number forces to involve 88 additional tons of the Reformate M/B.
2. In case of the best feedstock, correction of recipes allows saving scarce, high-quality components: 6 tons of Alkylate and 37 tons of Isopentane. Also, the involvement of 170 tons of FCC gasoline is an effective decision due to its low detonation characteristics and availability at refinery tanks.

5. Conclusion

1. It was established that for resource-efficient maintenance of gasoline blending process it is necessary to correct blending recipes considering the hydrocarbon composition of involved feedstock and non-linear nature octane numbers throughout blending operations.
2. For this research, the logical algorithm for the formulation of the optimal gasoline blending recipes was created. It ensures economically efficient blending as well as obtaining of the required amount of gasoline which meets contemporary environmental and technical standards.

3. In this work, optimal blending recipes for Premium-95 gasoline brand (Euro-5 quality) were formulated using the developed complex modeling system. Joint and separate production regimes are simulated.
4. Influence of changes in hydrocarbon composition of feedstock on detonation characteristics of gasoline is shown. In case of a change to the worst-quality feedstock, correction of recipes allows avoiding production of off-grade gasoline; it is also possible to save high-quality components in case of a change to the best-quality feedstock.
5. The developed modeling system allows increasing the efficiency of the gasoline production using only internal resources of the refinery with no additional investments and expenses. Corrections of gasoline blending recipes considering changes in the composition of the involved feedstock allow avoiding undesirable quality giveaways trade gasoline and overruns of expensive components. The results show the concept of the resource-efficient gasoline production which makes a large economic effect for the refinery.

Acknowledgements

The study is supported by the Ministry of Education and Science of the Russian Federation, project 2.3649.2017 / 4.6.

References

- [1] Braginsky OB. Prediction of the Russian automotive fuels market. Open seminar Economic problems of energy comple" (seminar of A.S. Nekrasov). One hundred and twenty-ninth meeting of 24 April 2012.
- [2] Smolikov MD. The production trade gasoline at domestic refineries. Problems and solutions. Chemistry under the SIGMA sign: investigations, innovations, technologies: all-Russian youth school-conference, Omsk, 2010, pp. 251-252.
- [3] Kulkarni-Thaker S, Mahalec V. Multiple optima in gasoline blend planning. Industrial and Engineering Chemistry Research, 2013; 52(31): 10707-10719.
- [4] Pasadakis N, Gaganis V, Foteinopoulos C. Octane number prediction for gasoline blends", Fuel Processing Technology, 2006; 87: 505-509.
- [5] Caixia G, Jinbiao G, Lei Z. Application of mathematical programming in off-line formulation optimization of gasoline blending. Petroleum Refinery Engineering, 2013; 43(3): 61-64.
- [6] Sakhnevich BV, Kirgina MV, Chekantsev NV, Ivanchina ED. Development module of chromatographic data systematization to improve the efficiency of the process compounding trade gasoline. Izvestia of the Tomsk Polytechnic University, 2014; 324(3): 127-136.
- [7] Maylin MV, Kirgina MV, Sviridova EV, Sakhnevich BV, Ivanchina ED. Calculation of gasoline octane numbers taking into account the reaction interaction of blend components. Procedia Chemistry, 2014; 10: 477-484.
- [8] Ivanchina ED, Kirgina MV, Chekantsev NV, Sakhnevich BV, Sviridova EV, Romanovsky RV. Complex modeling system for optimization of compounding process in gasoline pool to produce high-octane finished gasoline fuel. Chemical Engineering Journal, 2015; 282: 1-12.

To whom correspondence should be addressed: Nikita V. Chekancev, Department of Fuel Engineering and Chemical Cybernetics, Tomsk Polytechnic University, 30, Lenin Avenue, Tomsk, 634050, Russia; e-mail: Chekancev@tpu.ru

SIMULATION AND OPTIMIZATION OF AMINE SWEETENING PROCESS

Rami Hameidi, C. Srinivasakannan

Khalifa University of Science and Technology, The Petroleum Institute, Chemical Engineering Department, Abu Dhabi, UAE

Received November 11, 2017; Accepted December 23, 2017

Abstract

Amine sweetening is the most vital segment of the gas processing plant, which contributes to the removal of H₂S, CO₂ and other minor contaminants such as COS and mercaptans. The work attempts to improve the efficiency of the gas processing process through a process simulation exercise towards which ProMax was utilized. A base case simulation mimicking a real operational amine sweetening plant was developed using process parameters and flow rates currently being in practice. Based on a thorough literature search, it was understood that parameters such as the pH, heat stable salts, regenerator pressure, and absorption column intercooling were found to influence the plant efficiency. The present work attempts to assess the effect of the above said parameters on the base case simulation and identify optimal conditions to enhance the overall efficiency. A decrease in the pH was attempted through the addition of different acids, and it was not found to improve the efficiency of the operation as stated in the literature pertaining to MEA solvent. In other words, the regenerator energy consumption was found to increase with the increase in the acid concentration. An increase in the regenerator pressure was found to decrease the regenerator energy requirement contributing to better energy efficiency, with the optimal operating pressure being 2.5 bar. An increase in the heat stable salts at a controlled concentration was found to improve the absorption efficiency of the H₂S while had no significant effect on CO₂ absorption. The application of intercooler improved the absorption efficiency of both H₂S and CO₂ as well as reduced the reboiler heat duty. The combination of optimal conditions revealed that the plant processing capacity could be increased to about 4.2 % with an energy reduction of 81,000 tons of steam per year.

Keywords: gas sweetening; amine solvent; acid gases, simulation; ProMax; MDEA; gas processing; Heat stable salts.

1. Introduction

Natural gas that comes from an underground reservoir is predominantly a mixture of hydrocarbons mainly methane along with other hydrocarbons like ethane, propane, and butane. The gas can also carry an appreciable amount of non-hydrocarbons such as hydrogen sulfide, nitrogen, carbon dioxide and other minor contaminants such as mercury, water, and other inorganic compounds. They are widely utilized for industrial, commercial and residential purposes as it is the most preferred fuel for the generation of heat and electricity. Natural gas accounts for 23.7% of the global primary energy consumption (BP Statistical Review of World Energy, 2015). The growth is expected to be 1.9% per annum mainly due to the demand from the power and other industrial sectors [1-2].

The natural gas processing plants typically include a number of stages to remove the contaminants such as dusting stage, acid gases removal, dehydration and Hg removal, nitrogen rejection, so as to meet the product specification. The dusting stage is a gas filtration stage to remove small solid particles. In the acid gas removal, operation separates acid gases hydrogen sulfide (H₂S) and carbon dioxide (CO₂) from the natural gas directing it to the sulfur recovery process [3]. In dehydration stage, water is removed, while in the mercury removal stage separates extremely toxic mercury. The nitrogen rejection stage separates nitrogen so as to improve the heating value methane [4-5].

Sour gas contains different concentrations of H_2S and CO_2 ; these gases have certain threshold values and a specific standard for their concentration as products of a sweetening process. The selection of the appropriate sweetening process to achieve certain gas specification is dependent on many factors like the limits of concentration of both the sour and the sweet gas, the maximum design flowrate, the pressure of the inlet gas, the requirements for sulfur recovery and propose an acceptable method to dispose of waste products [6].

There are many different processes for sour gas sweetening, but one of the most popular and the one that is discussed in this work is the liquid-phase absorption by chemical solvents. In chemical solvent processes, absorption of the acid gases is achieved mainly by use of alkanol amines that can absorb H_2S , CO_2 , and to some extent COS. Chemical solvents are specifically suitable when contaminants at relatively low partial pressure have to be removed to very low concentrations [7]. In natural gas sweetening industry, the removal of carbon dioxide and hydrogen sulfide by alkanol amines is essential and maybe the most popular. This technology depends mainly on absorption/desorption reactions between the acid gases and alkanol amines. This treatment step is critical in any gas processing industry because the presence of such contaminants can cause corrosion to pipelines and equipment, can also affect the human health and deteriorate the surrounding environment [8].

2. Methodology

2.1. Base case simulation

The base case simulation model involving absorption and desorption columns mimicking the operation conditions of a typical gas processing plant was built using ProMax simulation tool. The details of the process parameters utilized in developing the simulation are provided in Table 1. The process simulator utilized Peng-Robinson Amine Sweetening property method to perform the simulations. The process flow diagram adopted for simulation is shown in Fig. 1.

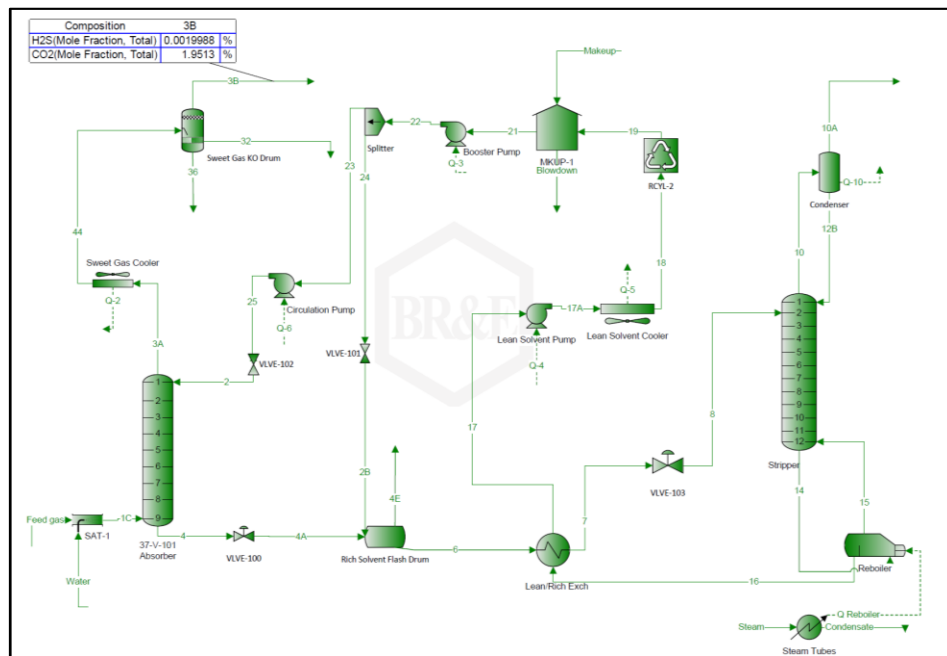


Figure 1. Base Case Process Flow Diagram

Since the design data and process flow for each stream were available, it was much easier to build the model block by block with the correct state of phases, compositions, and flowrates. The feed stream contains mostly hydrocarbons ($C_1 - C_3$) along with Hydrogen Sulfide (H_2S) at 4.8% and Carbon Dioxide (CO_2) at 5.5%. The feed stream saturated with water will enter a 9 stages absorber, while the solvent is flowing downward the column noted as rich amine stream

goes to a flash drum that flashes any gases still in the vapor phase out from the loop. Then the stream exchange heat with the lean amine wherein the temperature increase to 104 °C, and enters a stripping section wherein all the dissolved acid gases were stripped out and sent to sulfur recovery units. The stripper is operated by a steam driven reboiler that provides enough energy for stripping and recovery of the solvent that is recycled back to the absorber.

Table 1. The Base Case Specifications along with simulation results

Specification	Value	Specification	Value
Plant capacity (MMSCFD)	379	Solvent rate (m ³ /hr)	790
Acid H ₂ S (mol. %)	4.8	Solvent concentration (wt. %)	45
Acid CO ₂ (mol. %)	5.5	Regenerator pressure (bar)	2
Sweet H ₂ S (ppm)	19.98	HSS content (mol. %)	0.041
Sweet CO ₂ (mol. %)	1.95	Rich amine loading	0.568
Steam rate (Kg/min)	2060	Lean amine loading	0.003
Steam pressure (bar)	5	Property method	PR-Amine Sweetening

2.2. Acid injection case (pH swing)

The effect of acid injection for an MDEA sweetening plant has not been reported in the open literature, and hence an attempt has been made to assess its effect. Three weak acids were tested with the model to lower the pH. Adipic, phthalic and suberic acids were added to the MDEA solvent at 1-5 wt. %

2.3. Regenerator pressure elevation

In the base case model, the regenerator operating pressure was 2 bars; with the corresponding reboiler temperature of 127°C. The effect of regenerator pressure was assessed covering the pressure in the range of 2 to 3 bars, while all the other parameters were held constant corresponding to the base case. These reboiler temperatures were acceptable as they were lower than the amine degradation temperature. The effect of regenerator pressure on the energy consumption was assessed along with a check on the reboiler temperature.

2.4. Inter-cooled absorber (ICA)

The effect of the addition of an inter cooler to the MDEA process has not been reported in the open literature and hence attempt to assess its effect was made [9]. Towards this the hot MDEA solution was withdrawn from stage 5 and was cooled using an air-cooled heat exchanger and reinjected back. From the total volumetric flowrate 20% was withdrawn from stage 5, cooled by -4°C, before being injected back to the column in stage 6. All other parameters were held constant at the base case level

2.5. Heat stable salts (HSS)

The presence of HSS in the amine system is well established. In order to quantify their presence, a weak acid like Phosphoric Acid (H₃PO₄) was added to the amine solvent by very small percentages in the range 0.1-0.5 mol. %. This range was acceptable because small addition of acid showed a significant effect on the sweet gas specification [10]. To follow up the concentration of the protonated form of the amine (MDEAH⁺) an ionic info analysis was used in the model to keep track of the concentration buildup of HSS.

3. Results and discussion

3.1. Addition of weak acids

Figures 2&3 show the simulation results on the effect of adipic, phthalic and suberic acid on the CO₂ as well as the H₂S mole % leaving the absorption column. The data clearly indicate an increase in the concentration of the CO₂ in the sweet gas with an increase in the acid concentration, while the concentration of the H₂S was almost constant. Among the three acids,

adipic acid seem to have a far higher effect on the CO₂ exit concentration compared to the other two acids. Considering the permissible sweet CO₂ specification of only 2 %, any increase in the pH.

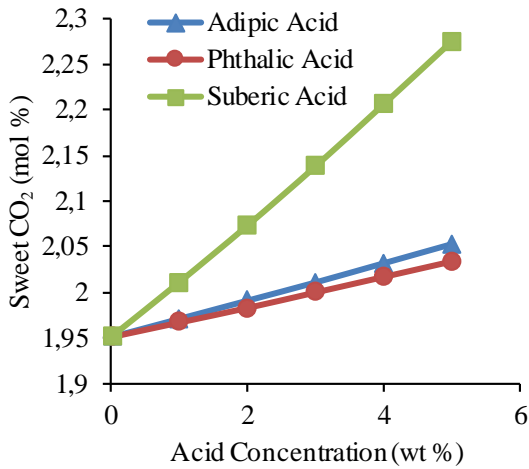


Figure 2. Effect of acids addition on sweet CO₂ concentration

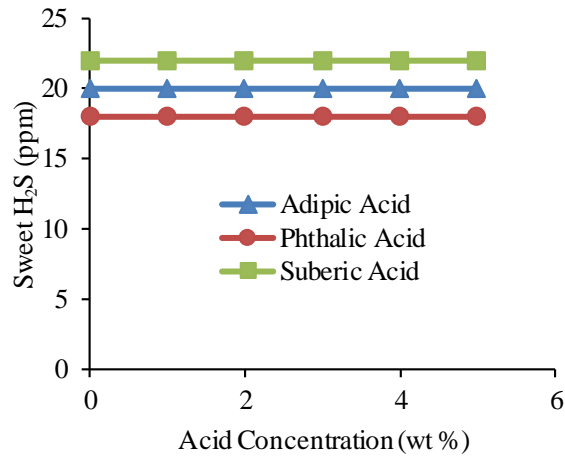


Figure 3. Effect of acids addition on H₂S concentration

Figure 4 shows that all acids had a negative effect on the regenerator performance. The reboiler duty increased with increase in the acid concentration. However, the effect of adipic & phthalic acids on the steamrate was marginal as compared to suberic acid. In the regeneration section, it was noticed that the increased percentage of acid had a negative effect on desorption energy requirement. As the percentage of acid is increased, the pH value decreased, and the steam supply to the regenerator increased in proportion.

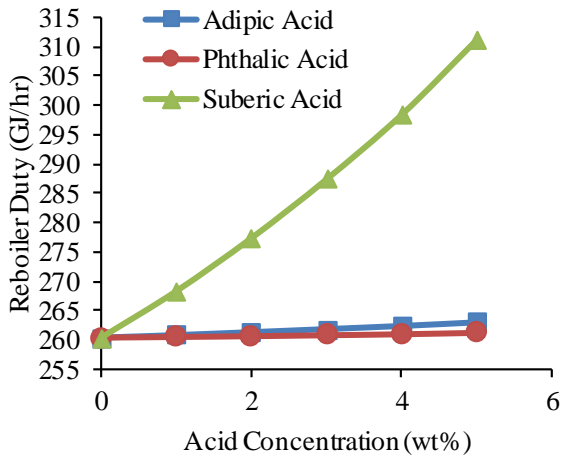


Figure 4. Effect of acids addition on reboiler duty

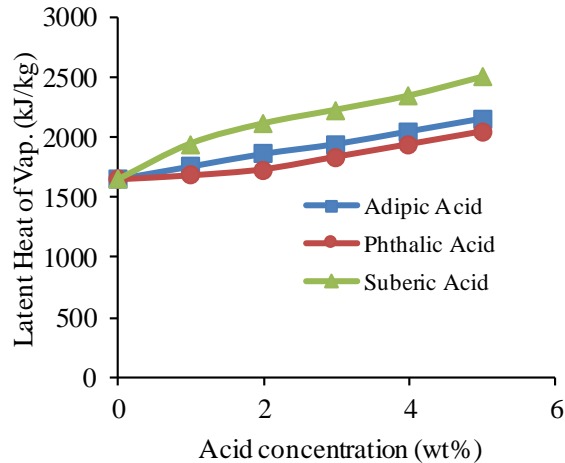


Figure 5 Effect of acids addition on the latent heat of vaporization

Since the steam supply is one of the key contributors to operating cost of the process, a detailed assessment of the regenerator was performed in order to understand the increase in regeneration energy. The below figure summarizes the effect of each acid based on the latent heat of vaporization of the solvent in the reboiler.

It can be seen that an increase in the percentage of acid, so as to lower the pH increases the latent heat of vaporization of the solvent entering the regeneration stage while maintaining other terms relatively constant. An increase in the acid concentration contributed to the increase in boiling point of the regenerator solvent which in turn demands higher desorbing energy to strip the acid gases.

The details of the various contributors affecting desorption energy can be summarized as follows:

$$Q_{reg} = Q_{des,CO_2} + Q_{sens} + Q_{vap,H_2O}$$

$$Q_{reg} = \Delta H_{abs,CO_2} + \frac{\rho_{solvent} V C_p (T_{reb} - T_{feed})}{\dot{m}_{CO_2}} + \frac{\dot{m}_{H_2O} \times \Delta H_{2O,vap}}{\dot{m}_{CO_2}}$$

where, $\Delta H_{abs,CO_2}$ is heat of reaction; C_p is the heat capacity of the rich solvent; T_{reb} & T_{feed} are reboiler temperature and feed solvent temperature, respectively; \dot{m}_{H_2O} is the mass flow rate of water vaporized from stripper and $\Delta H_{2O,vap}$ is the latent heat of vaporization.

The addition of acids was claimed to be beneficial for the gas sweetening process having MEA as the solvent [11]. Hence simulations were performed to cross verify the claims with the MEA solvent. The results of the simulation are presented in the section below.

3.1.1. Reboiler duty for absorber with MEA solvent

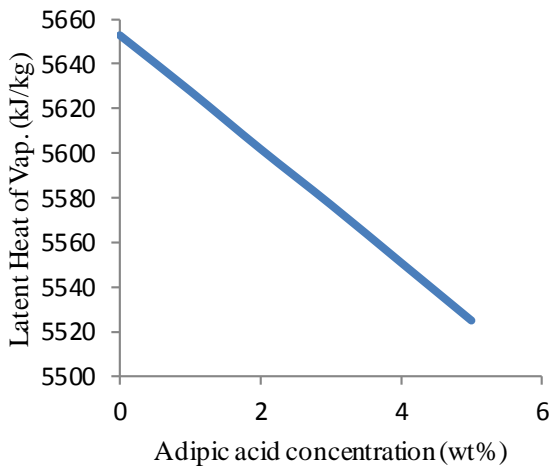


Figure 5 Effect of acid addition on MEA systems

Figure 6 presents the results of the simulation specific to Adipic acid addition for an absorber with MEA as a solvent. An increase in the acid concentration was found to decrease the reboiler due to the reduction in the latent heat of vaporization. The results clearly authenticate that the addition of acid to MEA solvent system is beneficial while with the MDEA solvent it contributes to an increase in the regenerator energy.

3.2. Effect of stripper operating pressure

Figure 7 shows the effect of regenerator operating pressure with the sweet gas specifications of H₂S and CO₂.

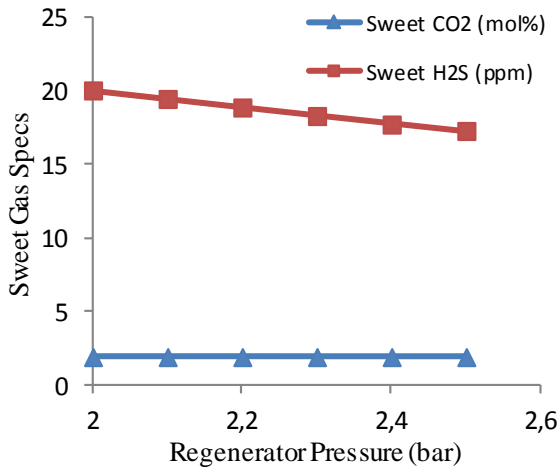


Figure 6. Effect of increased stripper pressure on sweet gas specs

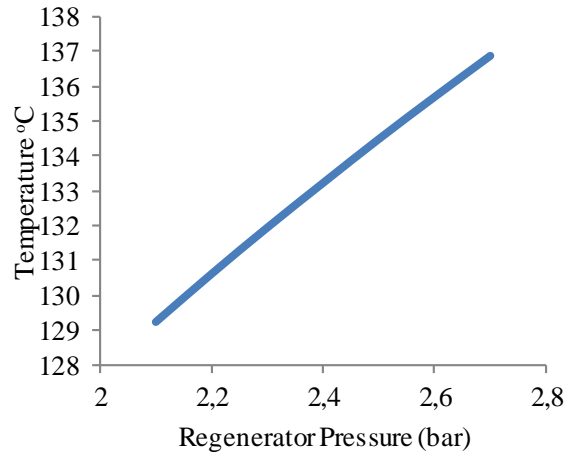


Figure 7. Regenerator pressure effect on temperature

An increase in the regenerator pressure is found to decrease the sweet gas H₂S concentration favorably while the concentration of CO₂ was not affected. This could be attributed to the better performance of regenerator due to decreased lean loadings. The effect of acid addition on the absorption section was not very much noticed.

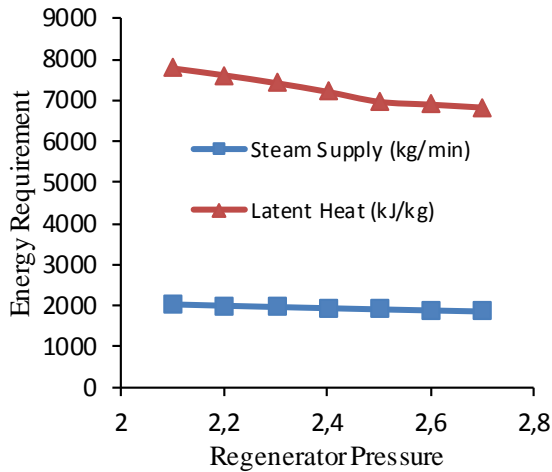


Figure 8 Increased regenerator pressure data with steam supply

Figure 8 captures the effect of stripper temperature with increase in the regenerator pressure. An increase in the regenerator pressure was found to increase the regenerator temperature thus rendering an effective stripping. Although the increase in pressure was found to be beneficial, the optimal pressure was chosen to be 2.5 bars based on the amine degradation temperature of 140°C. A temperature safety margin of 5°C was chosen to select the optimal regenerator pressure.

The major effect was observed in the steam supply with increased regenerator pressure. Elevating regenerator pressure helped in increasing regeneration temperature, which led to better performance and more efficient stripping of gases.

The figure 9. summarizes the effect of increased pressure on the regeneration energy requirement. It can be noticed that as the pressure is increased, the latent heat of vaporization of the solvent mixture decreases which eventually contributes to a reduction in the steam requirement for regeneration.

3.3. Effect of the addition of intercooler to the absorber

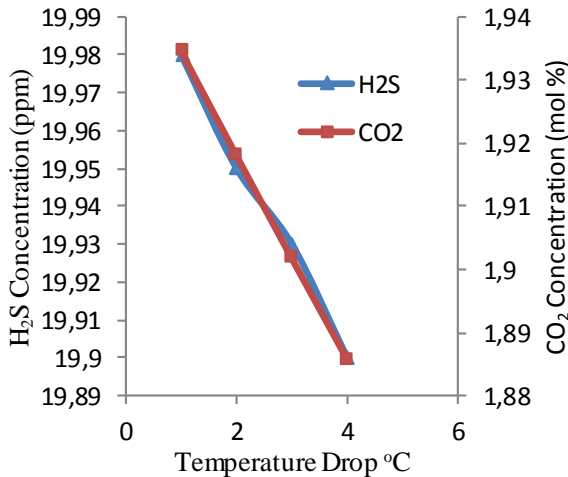
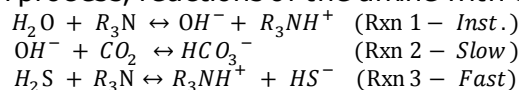


Figure 9. Effect of intercooling on sweet gas specs

The effect of the addition of an intercooler on the overall performance of the amine sweetening process is assessed by reducing the absorber temperature to a maximum of - 4°C. The simulation results are captured in Figure 9. It can be seen that an increase in the degree of cooling showed a positive impact on the sweet gas specs, especially for CO₂. A temperature reduction of 4°C has contributed to a reduction in the concentration of CO₂ from 1.95 % to 1.88 %, also evident from the increased rich loading of the absorber. In the regeneration section, intercooling helped in stripping more acid gases as with decreasing lean loadings of the amine.

In any amine absorption process, reactions of the amine with CO₂ and H₂S are as follows:



As the solubility increase with a decrease in temperature, provision of an intercooling would increase the mass transfer rate thus absorbing more CO₂ lowering its concentration in the sweet gas stream. From the above reaction between CO₂ and amine, it can be seen that as more absorption of CO₂ occurs, the reaction shifts toward consuming more CO₂ while decreasing the equilibrium concentration of OH⁻.

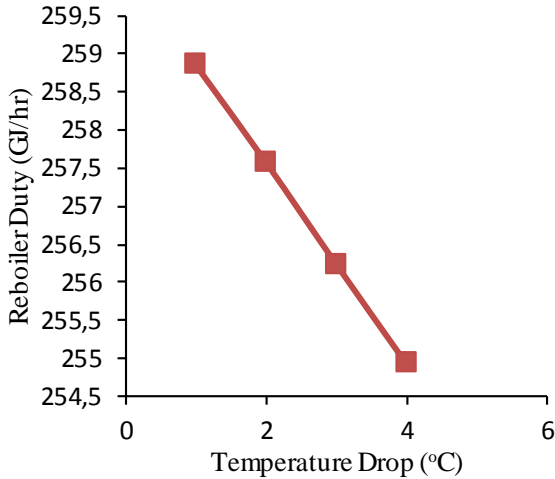


Figure 10 Effect of intercooling on regeneration energy

2% CO₂, it is possible to increase the processing capacity of the plant with the presence of side cooler or to reduce the steam supply to the reboiler.

3.4. Effect of heat stable salts (HSS)

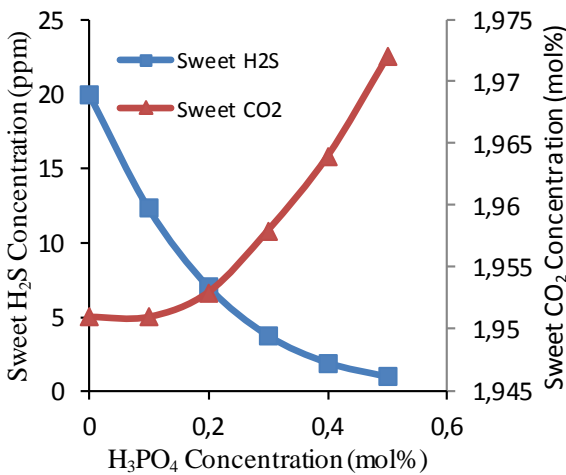
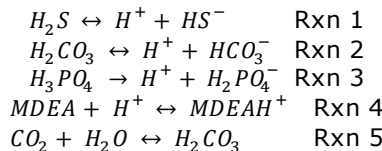


Figure 11. Effect of H₃PO₄ concentration on sweet gas specs

Reactions governing the absorption and desorption reactions with the presence of HSS are as follows:



It can be clearly seen that as the concentration of H₃PO₄ is increased, more H⁺ ions are present increasing the concentration of the heat stable salts. The concentration of H₂S is sharply decreased by the addition of the acid to very low values, and this can be explained from Rxn 1, as the concentration of H⁺ ions is increased from the acid, the equilibrium concentration of HS⁻ is decreased shifting the reaction towards consuming more H₂S. For CO₂ it can be seen from both Rxn 2 and Rxn 3 that as the amount of H⁺ is increased this shifts the Rxn towards producing more H₂CO₃ and from Rxn 5 as the concentration of H₂CO₃ is

This would shift the first reaction towards making more OH⁻ increasing absorption of CO₂. On the other hand, and for the absorption of H₂S, the instantaneous reaction of an amine with water will increase the equilibrium concentration of R₃NH⁺ rendering reaction (3) to proceed towards keeping H₂S concentration in the dissolved phase at the relatively constant magnitude.

It was also noted that an increase in cooling duty contributed to higher degrees Fig.10 re summarizes effects on regeneration energy with intercooling. It can be seen that as the cooling degree is increased, the reboiler demand less energy for stripping, reflecting less steam supply. Since the plant specs are at 20 ppm H₂S and

Figure 12 presents the effect an increase in H₃PO₄ concentration so as to capture the effect of an increase in the HSS concentration. It showed the significant positive effect on sweet gas H₂S concentration whereas the opposite effect for CO₂ but at the insignificant magnitude. In regeneration, the increased concentration of HSS helped in stripping more of H₂S but less CO₂ in comparison.

increased, this shifts the Rxn toward making more CO_2 , and that's why the effect is reversed from H_2S .

When H_3PO_4 is added to the mixture, it increases the amount of H^+ present. This shifts the amount of MDEA and MDEAH^+ present in this basic system of water, amine, and acid from that observed when just the water and amine are present. It is this additional amount of MDEAH^+ that can represent heat stable salts [11].

The effect and concentration of HSS were tracked in the absorber and in the regenerator as well as whenever there is a pressure or temperature variations in the process.

In the amine absorber, H_2S and CO_2 dissolve into the aqueous solution. These dissolved gases can then undergo Rxn 1 and Rxn 5. If the aqueous solution did not contain anything to react with the dissolved gases or the resulting ions, the capacity of the solvent would be very limited on the amount of acid gas that it can absorb [12]. To explain the opposite effect of adding acid, adding a base to the solvent increases its capacity. The increase in capacity is due to the removal of H^+ on the product side of Rxn 1, 2, and H_2CO_3 in Rxn 5. This can progress until Rxn 4 reaches equilibrium, at which point the solvent reaches maximum capacity [13].

In the regenerator, the temperature and pressure are drastically changed from the absorption column. The increased temperature and decreased pressure greatly reduce the amount of dissolved acid gas in the liquid solvent [14]. By reducing these, the reactions shift away from the ions and towards the production of dissolved gas. As the solvent travels down the column, more acid gas is removed resulting in less MDEAH^+ being present as the reactions shift.

Since the H_3PO_4 remains in solution, the amount of H^+ present is slightly higher than if it were not present. This increase in pH assists in stripping the acid gasses from the solvent. However, if more H_3PO_4 is added, eventually enough MDEA remains the MDEAH^+ state that the amine no longer picks up enough H^+ produced by the dissolved acid gas species and the capacity of the solvent diminishes. It is usually when this happens that reclamation is brought online so as to reduce the amount of MDEAH^+ that is in solution by removing the salts and freeing up the amine base.

As the temperature of an aqueous solution of H_2S , CO_2 , and MDEA is increased, the solubility of the dissolved gasses decreases. This results in H_2S and CO_2 leaving the solution [15]. This reduces the concentration of reactants for Rxn 1 and Rxn 5. Based on Le Chatelier's principle, Rxn 1 and Rxn 5 will shift in the direction of making dissolved gas molecules. This reduces the amount of H^+ , as directly observable in Rxn 1, and observable through a combination of Rxn 5 and Rxn 2. Reducing the amount of H^+ thus affects Rxn 4 such that less MDEAH^+ is present [16].

A decrease in temperature increases the solubility of the gasses in the liquid solvent. Assuming that equilibrium is reached, and reaction kinetics is ignored, the increase in the dissolved gasses will cause the Rxn 1 and reactions Rxn 5 and Rxn 2 to shift to creating a larger amount of H^+ . The increase in H^+ will increase the amount of MDEAH^+ in the system as Rxn 4 shows.

Changes in pressure have a similar effect on the system. As pressure is lowered, the solubility of the dissolved gasses is reduced. This causes Rxn 1 and Rxn 5 to shift to the reactant side, causing a decrease in H^+ and a resulting shift in Rxn 4 so that less MDEAH^+ is present in the system.

An increase in pressure increases the solubility of the gasses in the liquid solvent. The increase in dissolved gasses will again increase the amount of MDEAH^+ , as discussed for the case where the temperature was decreased.

3.5. Limits for the dominance of corrosion and fouling

The total amount of acceptable HSS depends on kinds of ions present, and its corrosion characteristics, its effect on the performance of the system [17]. The simulation results indicate complete consumption of free amine at 1.2% addition of H_3PO_4 , beyond which the H_2S concentration started to raise and present in its protonated form. It doesn't necessary mean that the acid can be added up to this point because the negative effects start to appear at

much lower concentrations. The solution to retrieve the free amine is either to flush fresh solvent to the system or by solvent reclamation techniques like Ion Exchange, Electro dialysis, etc. [18].

4. Conclusion

In summary, optimal conditions to enhance the overall efficiency of the sweetening process were discussed. Although the decrease in the pH was not found to improve the efficiency of the operation as stated in the literature pertaining to MEA solvent and the reason can be explained from kinetics point of view and reactions governing the desorption process. However, an increase in the regenerator pressure was found to decrease the regenerator energy requirement contributing to better energy efficiency, with the optimal operating pressure being 2.5 bar. An increase in the heat stable salts at a controlled concentration of 0.2 mol.% was found to improve the absorption efficiency of the H₂S while had no significant effect on CO₂ absorption. The application of intercooler improved the absorption efficiency of both H₂S and CO₂ as well as reduced the reboiler heat duty by achieving higher mass transfer driving force as the temperature is brought down. The combination of optimal conditions revealed that the plant capacity could be increased to about 4.2 % process capacity with an energy reduction of 81,000 tons of steam per year.

References

- [1] Mazyan W, Ahmadi A, Ahmed H, and Hoorfar M. Market and technology assessment of natural gas processing: A review. *J. Nat. Gas Sci. Eng.*, 2016; 30: 487–514.
- [2] Faramawy S, Zaki T, and Sakr AA-E. Natural gas origin, composition, and processing: A review. *J. Nat. Gas Sci. Eng.*, 2016; 34: 34–54.
- [3] Fouad WA and Berrouk AS. Using mixed tertiary amines for gas sweetening energy requirement reduction. *J. Nat. Gas Sci. Eng.*, 2013; 11: 12–17.
- [4] Aissaoui T, Al Nashef IM, and Benguerba Y. Dehydration of natural gas using choline chloride based deep eutectic solvents: COSMO-RS prediction. *J. Nat. Gas Sci. Eng.*, 2016; 30: 571–577.
- [5] Chang C, Ji Z, Liu C, and Zhao F. Permeability of filter cartridges used for natural gas filtration at high pressure. *J. Nat. Gas Sci. Eng.*, 2016; 34: 419–427.
- [6] Kazemi A, Kharaji AG, Mehrabani-Zeinabad A, Faizi V, Kazemi J, and Shariati A. Synergy between two natural gas sweetening processes. *J. Unconv. Oil Gas Resour.*, 2016; 14: 6–11.
- [7] Sarker NK. Theoretical effect of concentration, circulation rate, stages, pressure and temperature of single amine and amine mixture solvents on gas sweetening performance. *Egypt. J. Pet.*, 2016; 25(3): 343–354.
- [8] Jassim MS. Sensitivity analyses and optimization of a gas sweetening plant for hydrogen sulfide and carbon dioxide capture using methyldiethanolamine solutions. *J. Nat. Gas Sci. Eng.*, 2016; 36(part a): 175–183.
- [9] Bonalumi D, Ciavatta A, and Giuffrida A. Thermodynamic Assessment of Cooled and Chilled Ammonia-based CO₂ Capture in Air-Blown IGCC Plants. *Energy Procedia*, 2016; 86: 272–281.
- [10] Lim J, Scholes CA, Dumée LF, and Kentish SE. Nanofiltration for the concentration of heat stable salts prior to MEA reclamation. *Int. J. Greenh. Gas Control*, 2014; 30: 34–41.
- [11] Du M, Feng B, An H, Liu W, and Zhang L. Effect of addition of weak acids on CO₂ desorption from rich amine solvents. *Korean J Chem Eng*, 2012; 29(3): 362–368.
- [12] Makino T, Kanakubo M, Matsuki T, Kamio E, Takaba H, and Matsuyama H. High pressure CO₂ solubility and physical properties of tetrabutylphosphonium l-prolinate. *Fluid Phase Equilibria*, 2016; 420: 89–96.
- [13] Hadj-Kali MK, Mokraoui S, Baudouin O, Duval Q, and Richon D. Modeling of gaseous hydrocarbons solubility in aqueous-amine systems by VTPR model. *Fluid Phase Equilibria*, 2016; 427: 539–548.
- [14] Singto S, Supap T, Idem R, Benamor A. Synthesis of new amines for enhanced carbon dioxide (CO₂) capture performance: The effect of chemical structure on equilibrium solubility, cyclic capacity, kinetics of absorption and regeneration, and heats of absorption and regeneration. *Sep. Purif. Technol.*, 2016; 167: 97–107.
- [15] Singh P, (Wim) Brilman DWF, and Groeneveld MJ. Evaluation of CO₂ solubility in potential aqueous amine-based solvents at low CO₂ partial pressure. *Int. J. Greenh. Gas Control*, 2011; 5(1): 61–68.

- [16] Xu Q and Rochelle G. Total pressure and CO₂ solubility at high temperature in aqueous amines. *Energy Procedia*, 2011; 4: 117–124.
- [17] Li L and Rochelle G. CO₂ Mass Transfer and Solubility in Aqueous Primary and Secondary Amine. *Energy Procedia*, 2014; 63: 1487–1496.
- [18] Mesgarian R. Corrosion Management in Gas Treating Plants (GTP's): Comparison between Corrosion Rate of DEA and MDEA A Case Study in Sour Gas Refinery. in *International Conference on Industrial Engineering and Operations Management*, Bali, Indonesia, 2014.
- [19] Fisher KS, Searcy K, Rochelle GT, Ziaii S, Schubert C. Advanced Amine Solvent Formulations and Process Integration for Near-Term CO₂ Capture Success, Final Report for DOE Grant DE-FG02-06ER84625, June 2007.

To whom correspondence should be addressed: Prof. C. Srinivasakannan, Khalifa University of Science and Technology, The Petroleum Institute, Chemical Engineering Department, Abu Dhabi, UAE, csrivasakannan@pi.ac.ae

THE POTENTIAL OF COMPOSITE ANTHILL-WASTE CHICKEN EGGSHELL AS HETEROGENEOUS CATALYST IN BIODIESEL PRODUCTION

Adeyinka Sikiru Yusuff^{1, 2}, Olalekan David Adeniyi², Sarafa Oluwatosin Azeez², Moses Aderemi Olutoye² and Uduak George Akpan²

¹ Department of Chemical and Petroleum Engineering, Afe Babalola University, Ado-Ekiti, Nigeria

² Department of Chemical Engineering, School of Engineering and Engineering Technology, Federal University of Technology, Minna, Nigeria

Received November 22, 2017; Accepted December 23, 2017

Abstract

Biodiesel is an alternative fuel which provides a solution to two main problems associated with petroleum-based diesel. These problems include fossil fuel depletion and environmental degradation. It is commonly produced via transesterification reaction of vegetable oil or animal fat with alcohol in the presence of a catalyst. This catalyst required is either homogeneous or enzyme or heterogeneous. However, amongst these catalysts, heterogeneous catalyst is regarded as most suitable one for the biodiesel production because it discourages the generation of wastewater and also allows catalyst recovery after the reaction process. This present study provides a comprehensive review of different heterogeneous catalysts which have been explored in the past by different researchers in biodiesel production with emphasis on the potential use of mixed anthill clay-eggshell catalyst for biodiesel synthesis. Attention is focused on likely transformation of raw mixed anthill-eggshell sample to highly active metal oxides structure and how to create an environment friendly way of reusing waste eggshells and converting anthill which harbors dangerous animals into worth items. Following this, the mechanism of active phase (CaO) contained in this composite catalyst, the preparation method and characterization techniques for accurate estimation of the physicochemical properties of the solid catalyst are described.

Keywords: Anthill; eggshell; biodiesel; characterization; preparation.

1. Introduction

The use of solidly based catalysts in the field of renewable energy to produce renewable fuel has become a significant area of research. This is due to environmental concerns resulting from continual dependence on fossil fuel sources, current industrial energy demands, and upswing in the world population. To this end, current research is focusing on fuel derivable from renewable sources using heterogeneous catalyst and its utilization in the transportation industries and other industrial processes. Development of heterogeneous catalyst from waste and naturally occurring materials doped with metals for hydrocarbon (triglycerides) reactions are a particular area of interest that require more attention of researchers.

The global realization of the finite nature of fossil hydrocarbon and the deleterious effect arising from its consumption has triggered a worldwide search for alternative fuels. The utilization of diesel fuel from petroleum source continues to rise due to increase in population, energy consumption and rapid industrialization [1]. These have triggered a worldwide search for alternative fuels which include biodiesel, bio-alcohol, biogases and other biomass sources. Among the aforementioned renewable fuels, biodiesel has received considerable attention mainly because it provides a solution to problems associated with fossil fuel which include its depletion and environmental degradation [2]. Besides, it could be obtained from biomass [3]. Generally, biodiesel is prepared from vegetable oils and animal fat. However, it can be synthe-

sized from waste oil with same features and ability in minimizing gas emission from the engine without compromising quality [4].

Biodiesel is an alternative and biogenic fuel which comprises of different esters of fatty acid and has been accepted worldwide because of the problems associated with the petroleum derived fuel [5]. Biodiesel can be produced from any fat or oil through transesterification. A transesterification is a form of catalytic reaction whereby triglyceride contained in a vegetable oil or animal fat reacts with primary alcohol commonly methanol to produce esters and glycerol. In biodiesel production, oils and fats are transesterified with methanol in the presence of catalyst [6], to produce fatty acid methyl esters (FAME) and glycerol as a byproduct [7-8]. However, homogeneous catalyzed transesterification process has some disadvantages which include the formation of the unwanted product, corrosion problems, generation of wastewater, and difficult to recycle [3]. Enzymes are also employed in the production of biodiesel.

Enzymes are naturally occurring materials with impressive performance and resistant to compositional changes in a reaction medium. They can enhance biodiesel production via esterification or transesterification process [5]. Enzymatic-catalyzed reaction is carried out at mild and favourable conditions, so as not to denature the enzyme. Enzymatic transesterification has the advantage to provide high yields, but cannot be employed industrially as a result of the exorbitant cost of the enzyme. Another problem is that of deactivation usually caused by impurities contained in reaction feed. Therefore, heterogeneous catalysts are very important for biodiesel production as they possess many advantages over homogeneous catalysts and enzymes [5]. They are noncorrosive, environmentally benign and do not form soaps through free fatty acid neutralization or saponification of triglyceride. Besides, product purity and regeneration of the catalyst are achievable in heterogeneous catalysis [9-10].

Although there is an increasing interest in deriving solid catalysts from naturally occurring and waste materials, locally sourced anthill has not been explored as a catalyst to transesterify vegetable oil to fatty acid methyl esters. This also includes its modification by any of the metal oxides. Moreover, previous research has not provided detailed work on the catalytic performance of two or more of these materials in a combined (composite) form to synthesis fatty acid methyl esters. This present study, therefore, considers the possible development of composite heterogeneous catalyst from anthill and eggshell. Following this, the preparation methods and characterization techniques for accurate estimation of the physicochemical properties of the heterogeneous catalyst are described. Moreover, a possible way of improving the activity of the composite anthill-eggshell with the promoter is described.

2. Heterogeneous catalysis and its fundamental

Heterogeneous catalysis describes the process in which reactant(s) and required catalyst are differed in phase, however, in a heterogeneously catalyzed alcoholysis reaction, in which three-phase system exists, the catalyst is usually solid in nature while oil and alcohol act as reactants. The oil and alcohol are two immiscible liquid phases. Heterogeneous catalysis is of very importance in the field of renewable fuel [11-12]. Heterogeneous catalysts used for biodiesel production are either solid base or acid catalysts. The former is mostly used for biodiesel synthesis because of its better performance and faster rate of reaction as compared to the latter [13]. Meanwhile, the heterogeneous acid catalyst is usually employed, when the feedstock is highly rich in free fatty acid and moisture [14].

Heterogeneous acid catalyst, however, requires elevated reaction time and alcohol to oil molar ratio to enhance the product yield and rate of reaction [13,15]. Nevertheless, heterogeneous catalyzed transesterification process is known for mass transfer (diffusion) limitation, because two different phases (liquid and solid) are involved, and this reduces the reaction rate [12,16]. Hillion *et al.* [15] had identified a way of overcoming diffusion limitation in heterogeneous catalysis. The authors suggested the use of catalytic materials which include promoter and support. These materials provide large specific surface area and pores for active components of the catalyst, thus enhancing methanol adsorption onto active sites. Aluminum oxide (alumina) had been recognized as the suitable promoter for the transesterification reaction

without catalyst loss. It has also been widely employed as catalyst support due to its thermal stability [17].

Taufiq-Yap *et al.* [18] investigated the transesterification of palm oil with methanol over NaOH/Al₂O₃ catalyst. The catalyst preparation was optimized, and 99% conversion of palm oil to fatty acid methyl esters was achieved under the favourable reaction conditions. More so, Hak-Joo *et al.* [19] investigated the performance of different alumina supported catalysts (Na/γ-Al₂O₃, NaOH/γ-Al₂O₃, and Na/NaOH/γ-Al₂O₃) in the conversion of soybean oil to biodiesel. However, amongst the alumina supported catalysts, Na/NaOH/γ-Al₂O₃ showed good catalytic activity by providing highest biodiesel yield under optimum reaction conditions. Furthermore, Arzamendi *et al.* [20] compared the activity of raw and calcined NaOH/γ-Al₂O₃ in the transesterification of sunflower oil to biodiesel. However, under the same optimum conditions, raw catalyst achieved nearly 100% conversion, while calcined catalyst provided 86% biodiesel yield. From the aforementioned studies, the results obtained indicate that alumina supported heterogeneous catalysts have good catalytic activity and could be employed for the industrial production of biodiesel.

Many types of heterogeneous catalysts for biodiesel production have been reported ranging from the use of strong acid catalysts to strong base catalysts [21]. Findings have proven that rare earth metals are the most suitable heterogeneous catalyst in biodiesel production [22], but unfortunately, these catalysts are expensive, and their preparation is quite complex [23]. Therefore, to make biodiesel production sustainable, the use of low cost solid heterogeneous catalysts from waste and naturally occurring materials is suggested [24]. These are being investigated to replace the homogeneous catalysts and enzymes, and this research constitutes part of that investigation. These low-cost materials include chicken eggshell [25], Ostrich eggshell [26], Quail eggshell [27], *Pomacea sp.* shell [28], waste animal bone [29], solid waste coral fragment [30], alum [31], montmorillonite clay [32], modified- peanut husk ash [33] and many more. Most of these materials are cheap sources of calcium oxide (CaO) and other alkaline earth metal oxides and reduce the biodiesel production cost [7]. However, anthill which is siliceous fire clay has not been explored as a catalyst for the production of biodiesel. Research has revealed that anthill contains a higher percentage of silica (SiO₂), alumina (Al₂O₃) and iron oxide (Fe₂O₃) [34]. These metal oxides in anthill have high tendency to interact with CaO in eggshell after activation and form a new phase of more active mixed oxides with close interaction.

3. Anthill

Anthill is naturally occurring clay which can serve as a potential starting material for a catalyst in transesterification reaction process. According to Akinwekomi *et al.* [34], anthill sample contains several metal oxides in which some of them in their pure forms have been used as catalysts for biodiesel synthesis. An anthill is a form of siliceous or fire clay which is formed at the entrances of the subterranean dwelling of ant colonies [35]. An ant colony is an underground chamber where ants live and are being built and maintained by worker ants. According to Paton *et al.* [36], an anthill is classified into two categories, namely, type I and type II anthills. Type I nest is less noticeable in the ant territory because it is small in size and shape as shown in Figure 1. However, they are characterized by waste deposition and are easily influenced by erosion [37-38]. By comparison, type II mound as shown in Figure 2, is huge, often sticks together, sometimes surrounded by vegetation and persists for many years [35].

Research has proven that anthill sample has large silica content, followed by alumina and it was also found that chemical compositions of those components contained in anthill samples from different locations vary. The chemical compositions of two different anthills from two different locations in West Africa are presented in Table 1.

Anthill materials are important constituents of the landscape not only because they are readily available, but because of their industrial usefulness. For example, it has been used to make ceramic [35], cement, bricks and sand casting [39], refractories [34] and furnace [35]. More so, due to the presence of silica (SiO₂), alumina (Al₂O₃), iron oxide (Fe₂O₃) and calcium oxide (CaO), anthill has potential ability to be employed as industrial heterogeneous catalyst.

Besides, it is readily available and environmentally benign. However, the potential application of anthill as a catalyst for biodiesel production is attributed to the presence of CaO, Al₂O₃, and SiO₂ which can serve as an active ingredient, promoter and support, respectively.

Table 1. Compositional analysis of anthill from two different locations [34-35]

Constituent	Chemical composition (%)	
	Biadan Ghana Anthill	Akure Nigeria Anthill
SiO ₂	68.70	58.83
Al ₂ O ₃	18.43	22.69
Fe ₂ O ₃	2.36	2.42
MgO	0.44	0.84
CaO	0.41	0.01
Na ₂ O	0.20	0.06
K ₂ O	1.60	2.10
TiO ₂	1.30	0.72
Others	5.56	12.33



Figure 1. Type I Anthill Situated in Front of Owolabi Hall at Afe Babalola University, Ado-Ekiti, Nigeria



Figure 2. Type II Anthill Located at Afe Babalola University, Ado Ekiti, Nigeria on an Elevation of 1165 ft. above sea level, having latitude (N7°36.409) and longitude (E005°18.627)

4. Chicken eggshell

Chicken eggshells are parts of waste materials from hatcheries, poultry industries, homes, and eateries, which can be easily collected in large amount. Chicken eggs are consumable product worldwide because it is rich in amino acids, vitamin, and minerals [25]. In the past, egg consumption in Nigeria was primarily concentrated in the major urban areas. This is because people from urban areas are better informed about the nutritional value and the protein supply of eggs [40]. In addition, they earn a higher income than the average rural dwellers.

Nowadays, series of awareness on the importance of egg consumption being created by Poultry Association of Nigeria (PAN) and Nutrition Society of Nigeria has made everyone knows the nutritional value of eggs. However, waste chicken eggshells constitute a solid waste disposal problem. Dry chicken eggshell contains nearly 94% of calcium carbonate (CaCO₃) by mass, while remaining components are magnesium carbonate (MgCO₃), calcium phosphate (CaPO₄) and organic matter [41]. Roughly 40% of the poultry wastes are chicken eggshells which are generated as a result of broken eggs and incubation. However, the majority of these waste eggshells are disposed of without further and proper processing by taking to landfill at an exorbitant rate depending on where the landfill site is located [42]. Meanwhile, waste management by landfill method attracts rodents or vermin which in turn spread diseases. Therefore, it is necessary to find a way of converting the waste chicken eggshells into some valueble products [42], as it would help in overcoming the high cost of waste management and environmental concerns.

Several techniques are now being adopted to transform the waste chicken eggshells into valuable items; giving financial benefits to competitive egg processing industries [42]. The various applications in which chicken eggshell could be used include adsorbent for contaminant removal from wastewater [41], stabilizing material for soil properties improvement [43], ink-jet printing paper [44], as a catalyst for lactulose production from lactose [45], as an excipient for acetaminophen tablet production [42].

Waste bird eggshells have the great unrealized ability as solid heterogeneous catalysts for the synthesis of biodiesel [26]. Calcium trioxocarbonate (IV) constitutes the larger percentage in eggshells and when it is subjected to a thermal treatment; it decomposes into calcium oxide and carbon dioxide. The chemical composition of the thermally treated waste eggshell is shown in Table 2. However, research had proven that calcium oxide (CaO) based catalyst is most widely used catalytic material for the synthesis of fatty acid methyl esters [46-47]. This is attributed to the fact that it is cheap, readily available, low toxicity, slightly soluble in methanol, has the high basic strength and minimum environmental impact. Chicken eggshells as a source of CaO, in particular, had been widely reported in the literature. Meanwhile, CaO based catalysts do leach into the reaction media if they are not anchored by supporting particles [24]. This statement was corroborated by Umdu *et al.* [48], who found that supported CaO showed far more activity and stability than unsupported CaO. Therefore, the authors suggested the use of silica or alumina as a supporting particle, as the basic site density and basic strength which are the factors driving the catalytic activity, get improved [48]. In this present study, however, a possible way of synthesizing supported CaO base catalyst is proposed.

Table 2. Percentage composition of calcined waste eggshell at 900°C (wt %) [49]

Constituent	CaO	MgO	P ₂ O ₅	SO ₃	K ₂ O	SrO	Cl	Fe ₂ O ₃	CuO	Total
Composition	97.42	1.63	0.52	0.26	0.08	0.05	0.02	0.01	0.01	100

5. Composite anthill-eggshell as a supported catalyst

Composite heterogeneous catalyst derived from an anthill and chicken eggshell can be regarded as a supported catalyst. This is because anthill is made up of several metal oxides (Table 1) in which some of these oxides have been used as supports for the solid catalysts [10], besides there is little amount of K, Ca, Mg and Na oxides contained in anthill which have been regarded as super basicity and active species of supported catalysts for biodiesel production [16]. According to Sun *et al.* [50], apart from the specific surface area and pore volume of the catalyst, surface basicity remains the main determinant of catalyst activity. This indicates that anthills could serve as no cost source of super basicity and their supports; same could be said of the waste eggshells. Waste eggshells of chicken were found to be 94% calcium carbonate, 1% magnesium carbonate, 1% calcium phosphate (Ca₃(PO₄)₂) and 4% organic matter [51]. It is, therefore, possible to synthesis from eggshell an active phase of composite anthill-eggshell catalyst due to the high CaCO₃ composition, the intrinsic pore structure, and its availability in large amount. The successful experiments on the use of waste bird eggshells as cheap sources of CaO for use as low cost solid based catalysts has been reported [25, 46-47, 52-53].

However, when anthill is properly mixed with eggshell in best proportion and well prepared under favourable conditions, the composition of CaO would increase. The presence of the compounds which serve as an active ingredient, support, and promoter for the catalyst justifies the usage of mixed anthill-eggshell for biodiesel production, besides CaO and Al₂O₃ serve as basic and acidic components which make the catalyst to act like dual sites type. Furthermore, a sample containing CaO supported on high surface area materials is regarded as a most active catalyst, besides it minimizes problems of lixiviation. In contrast, non-supported CaO suffers from this disadvantage [54].

6. Preparation of composite anthill-eggshell catalyst

Its preparation is aimed to attach the active phase present in eggshell onto the support particles contained in anthill powder. Several catalyst preparation techniques such as impregnation, sol-gel, precipitation, just to mention but a few, had been described in the literature [55]. Some of these techniques have their own advantages and disadvantages [56]. In preparing supported catalysts, impregnation or precipitation technique is usually employed [57-58]. According to Rojas [58], impregnation is related to ion-exchange or adsorption process, and the interaction with support is prevalent. This method had been widely employed by a lot of researchers to prepare supported heterogeneous catalysts for biodiesel production. Lithium (Li) was impregnated on CaO to catalyze transesterification of high FFA content oil, and its activity was not significantly altered by the vegetable oil containing more than 3 wt. % FFA [59]. More so, Sirichai *et al.* [60] impregnated ZnO with an aqueous solution of $\text{Ca}(\text{NO}_3)_2 \cdot 4\text{H}_2\text{O}$. After pretreatment and calcination steps, CaO-ZnO was liberated and used for transesterification process. Impregnation technique is a simple and commonly used procedure for dispersing active phase over the desired support. Furthermore, it allows rapid deposition of high metal loading [56]. Its disadvantage is that it does not allow uniform deposition of active phase along the pores of the support [61].

Precipitation technique involves the use of the precipitating agent in order to obtain a solid material in a porous form. Sirichai *et al.* [60] made use of Na_2CO_3 as a precipitant to prepare CaO-ZnO catalyst using co-precipitation method and used it to speed up the rate of transesterification reaction between palm oil and methanol. Ammonia solution had also been used as a precipitant for the preparation of CaO-ZrO₂ catalyst using co-precipitation technique [62]. Furthermore, a mixture of Na_2CO_3 and NaOH was used as precipitants to prepare nanometer magnetic solid base catalysts by dispersing CaO on Fe_3O_4 [63]. Meanwhile, the use of single precipitant to precipitate metal ion in solution is not as effective as multi precipitants [64]. The authors proposed triple precipitants that are ammonia solution, carbon dioxide, and ethanol which are base precipitant, acid precipitant, and neutral precipitant respectively. This novel method was applied by same authors to prepare CaO-La₂O₃ and compare with those prepared by impregnation, physical mixing and co-precipitation techniques. The authors observed that there were synergies among the precipitants which provided a better specific BET surface area and a high catalytic activity during biodiesel production.

Based on a preliminary experiment carried out and available literature [60, 65-66], the impregnation by incipient wetness condition was found to be the appropriate and best technique to prepare mixed anthill-eggshell catalyst. This is because it is simple and can also be employed to prepare catalyst industrially the same way it is prepared in the laboratory [56]. More so, apart from being a good and precise method, it is the only method that can be applied to high porous silica where the other methods fail [61]. In preparing mixed anthill-eggshell catalyst by incipient wetness impregnation method, the anthill and eggshell powders have to be mixed in best proportion in such a way that eggshell would constitute larger percentage because the component that will serve as active phase (CaO) is contained in eggshell while supporting particles are present in an anthill. However, the pretreatment steps which include mixing solution or solid, aging, solid-liquid separation and drying have to be carefully and thoroughly carried out so as to obtain homogenize solid mixture at least [58]. More so, calcination which is the final stage during supported catalyst preparation has to be carried out at a very high temperature. Thermal treatment of dried mixed anthill-eggshell catalyst at high temperature would lead to complete removal of adsorbed gases such as CO₂, SO₂, and moisture and change the components into a new phase of more active mixed metal oxides with close interaction [10]. Therefore, thermogravimetric analysis/differential thermal analysis (TGA/DTA) is recommended to determine the thermal stability of the catalyst and also identify various chemical reactions that occur during the thermal treatment process.

7. Characterization of the heterogeneous catalyst

Generally, characterization of the catalyst is necessary so as to gain insight into its physical and chemical compositions. It also helps in correlating catalyst properties to its performance. Thus, different properties of the as-synthesized catalyst can be determined by the following characterization techniques:

8. Determination of physical properties of the catalyst

Catalytic material usually passes through series of stages during preparation, and each of these stages has an influence on its activity, basic strength, and structural stability. To ascertain the effect of these factors, it is pertinent to deduce the physical properties of the as-synthesized catalyst before subjecting it to activity test. However, these properties are often determined using Brunauer-Emmett-Teller (BET) method. This characterization technique helps in determining the distribution properties of the as-synthesized catalyst which include specific surface area, pore size, and pore volume.

The specific surface area is often evaluated by an automatic micrometric surface area machine based on N_2 adsorption and desorption isotherms at 77 K. It is required that the samples should be degassed in a vacuum and at elevated temperature in order to expose the pores and surface of the catalyst. The specific surface area is then calculated based on BET model and also use Barrett-Joyner-Halenda (BJH) method to obtain the pore size distribution. Many researchers had correlated surface area of heterogeneous catalyst to catalytic activity [26, 67-68].

Olutoye *et al.* [68] prepared four different samples of Bi-ZnO catalyst by co-precipitation method by varying ratio of Bi:Zn from 1:49 to 4:.49. After the determination of textural properties comprising of surface area, total pore volume and average pore diameter, the sample with the ratio 2:49 of bismuth loading on zinc has better textural properties with BET surface area of $30.76 \text{ m}^2/\text{g}$, and it was chosen amongst all other catalysts prepared for transesterification process. This indicates that surface area is a function of catalyst activity.

This statement was also corroborated by Lopez *et al.* [69] who compared the catalytic activity of two different superacid catalysts (sulfated zirconia and tungstated zirconia) in methanolysis process. Sulfated zirconia exhibited good performance as a result of higher BET surface area ($134 \text{ m}^2/\text{g}$) as compared to tungstated zirconia which has BET surface area of $89 \text{ m}^2/\text{g}$. It is therefore recommended that the preparation condition of a mixed anthill-eggshell catalyst should be optimized in order to identify the optimum conditions that will provide a catalyst with better textural properties.

Furthermore, Tan *et al.* [26] developed CaO based heterogeneous catalysts from ostrich and chicken eggshells and determined their BET surface areas to be $71.0 \text{ m}^3/\text{g}$ and $54.6 \text{ m}^3/\text{g}$, respectively. The FAME contents provided by ostrich and chicken eggshells catalyst were 96% and 94%, respectively. High biodiesel yield obtained was as a result of large surface area possessed by those two synthesized catalysts. However, the higher biodiesel yield provided by calcined ostrich eggshell catalyst was as a result of more active sites present on its surface which allowed better interaction between the CaO-based material and the methanol in the reaction mixture. This is attributed to better textural properties and strong basicity which are possessed by calcined ostrich eggshell compared to that of calcined chicken eggshell [26].

9. Determination of basicity of the catalyst

It is well known that not all catalyst sites participate in transesterification reaction, those that take part in it are referred to as base sites, and they are usually active centers for transesterification [2]. However, the activity of the solid base catalyst is normally evaluated based on its base strength and basicity. Basicity is defined as the number of exposed basic sites per unit weight of catalyst sample. It is linearly related to catalyst surface area [20].

The basic site of solid base catalyst usually alkaline earth metal oxides is oxygen which behaves as proton acceptor [70]. Sun *et al.* [50] in their work investigated the correlation between activity and surface basicity of $\text{La}_2\text{O}_3/\text{ZrO}_2$ catalyst and the authors concluded that catalytic activity displayed a linear relationship with the basicity towards FAME synthesis,

which indicates that high biodiesel yield could be achieved when the basic strength is stronger. However, the high yield in activity observed for the $\text{La}_2\text{O}_3/\text{ZrO}_2$ catalyst was due to the presence of ZrO_2 which is amphoteric in nature and makes the catalyst to act like dual site type. Therefore, owing to the presence of supports such as SiO_2 and Al_2O_3 in an anthill, it is expected that mixed anthill-eggshell catalyst would exhibit dual sites (acidic and basic centers) behaviour.

The basicity of solid catalyst could be determined by different methods such as Hammett indicator and temperature-programmed desorption (TPD) methods. However, the simplest among the aforementioned methods is the indicator method, according to this method, the colour of acid-base indicators are changed based on the strength of the surface site of the catalysts [70]. The catalyst basic strength is expressed by Hammett function (H) suggested by Paul and Long [71]. When Hammett function (H) of a heterogeneous solid base catalyst is more than 26, such catalyst is referred to as super solid base [2, 71]. Meanwhile, evaluation of basicity via indicator method is always accompanied by the interference of indicators reaction which is not related to acid-base chemistry. Besides, the evidence of reaction is many times provided by a colour change, which may not give an accurate result and also, selective in term of catalyst required [70].

Temperature programmed desorption (TPD) had also been employed by many researchers to measure catalyst basicity and also, evaluate the various number of sites on it. During a TPD operation, the elevated temperature is required in order to desorb strongly bound probes adsorbates. Besides, it is carried out under the same operating conditions so as to compare samples that are involved [70]. Temperature programmed desorption (TPD) technique is of three kinds namely; CO_2 -TPD, H_2 -TPD, and pyrolysis-TPD. However, temperature programmed of carbon dioxide (CO_2 -TPD) is widely used for probing of basic materials. For instance, super solid base catalysts synthesized from birds' (chicken and ostrich) eggshells have been analyzed using TPD of CO_2 . The two catalysts exhibited same desorption behaviour, that is, desorption peak at approximately 600°C . This peak value obtained herein is attributed to CO_2 interaction with strong basic sites. Generally, peak desorption of CO_2 occurs at an elevated temperature as revealed in the case of catalyst synthesized from ostrich eggshell which provided basicity of $595 \mu\text{mol/g}$ compared to that of catalyst from chicken eggshell which was calculated as $205 \mu\text{mol/g}$. However, the higher basic amount of $595 \mu\text{mol/g}$ obtained for calcined ostrich eggshell catalyst indicated that the more surface area available for CO_2 desorption was as a result of higher surface area possessed by the catalyst. Thus, the results suggested that the surface basicity was the reason for the high yield in activity observed for the catalyst derived from ostrich eggshell [26].

Furthermore, H_2 -TPD had been used majorly to characterize such catalysts prepared from γ -alumina supported bimetallic precursors or monometallic precursors. Sirichai *et al.* [60] had successfully used temperature programmed desorption of hydrogen spectroscopy to evaluate the surface basicity and a number of sites found on CaO-ZnO catalyst. Based on the results obtained from H_2 -TPD analysis, the authors suggested that the interaction between Ca and Zn at the favourable atomic mixing ratio has great influence on the catalytic activity. Also, the particle size of CaO is identified as one of the crucial factors that determine CaO-ZnO activity.

10. Chemical properties of the catalyst

These properties include composition, structure, and morphology. In catalytic reaction, these properties of the solid catalyst could be significantly altered with repeated experimental runs. The activity, stability and basic strength of the catalyst may change owing to enhanced metal support interactions, the prepared orientation of the active species, accessibility hindrance of the active component and particle size and shape transformation by agglomeration [56]. Consequently, the characterization of chemical properties of the supported catalyst helps to gain insights into the reaction mechanisms encountered in a transesterification process. The heterogeneous catalyst produced could be characterized by its chemical composition using the X-Ray Fluorescence (XRF) or Energy Dispersive X-ray (EDX) machines. The morphologic and

crystallographic structure of the catalyst could be examined using X-Ray Diffraction (XRD), Scanning Electron Microscope (SEM), and Transmission Electron Microscope (TEM) machine while the surface functional groups will be determined by the Fourier Transform Infrared (FTIR) machine.

11. Future research plan

The promotion of anthill-eggshell by mixed metal oxides has great fulfillment for biodiesel production from low grade feedstock. As discussed in the literature, the activity of bird eggshells increases with the impregnation of natural material or biomass on them [65-66]. Likewise, modification of eggshell with mixed metal oxide would also improve its performance. Most of the stearate metals (Ca, Ba, Mg, Zn, Co, Ni, Mn, Cd, and Pb) are divalent, and they tend to act as electron-acceptor via formation of a four-membered ring transition state [8, 72-74]. A maximum yield of biodiesel (96%) was reported by Di Serio *et al.* [8] during transesterification of soybean oil with methanol over different stearate metal oxides. Although, both anthill and eggshell do transform into several metal oxides after thermal treatment at elevated temperature, only two stearate metals (calcium and a small amount of magnesium) are present in those catalytic materials.

However, further research is required to get abundant results in using the anthill-eggshell promoted stearate metal oxides catalyst in biodiesel production. Another research which requires urgent attention involves mixed anthill clay (natural occurring item) and eggshell (waste) and its modifications for successful direct conversion of low-grade feedstock such as waste frying oil and other non-edible oils into FAME by one step transesterification method. Present two-step transesterification technique for producing biodiesel from high free fatty acid (FFA) feedstock still not guarantee 100% conversion of triglyceride and complete removal of fatty acid. Currently, research has not been geared towards this direction. But the gathered research findings had shown that the use of modified composite material like mixed anthill-eggshell materials and its modification as a heterogeneous catalyst for high FAME content yield is realistic [75-76].

12. Conclusion

Research nowadays has shown that application of supported heterogeneous catalysts derived from biomass source has unrealized potential to avoid the use of expensive commercial rare earth metal oxides in biodiesel production. Transformation of waste eggshell and anthill soil to calcium oxide (active phase) and other metal oxides which are to serve as catalyst support and promoter may solve the problem of environmental degradation and also reduce the production cost. The mixed anthill-eggshell catalyst is considered as biomass derived catalyst which is formed from abandoned materials. However, the thermally treated mixed anthill-eggshell might have the great potential to curb leaching of catalyst active species into the reaction media.

Composite anthill-eggshell is a heterogeneous base catalyst which is expected to be tolerant of high free fatty acid vegetable oil and moisture. However, optimization of catalyst preparation condition is necessary in order to obtain best preparation parameters that will give a catalyst with good activity for transesterification reaction and thus, should be improved and tested its performance with various oil types.

References

- [1] Lin L, Cunshan Z, Vittayapadung S, Xiangqian S, and Mingdong O. Opportunities and challenges for biodiesel fuel. *Applied Energy*, 2011; 88: 1020-1037.
- [2] Refaat AA. Biodiesel production using solid metal oxide catalysts. *International Journal of Environmental Science and Technology*, 2011; 8(1): 203-221.
- [3] Zabeti M, van Daud WMA, and Aroua K. Activity of solid catalysts for biodiesel production: A review. *Fuel Processing Technology*, 2009; 90(6): 770-777.
- [4] Refaat AA. Different techniques for the production of biodiesel from waste vegetable oil. *International Journal of Environmental. Science and Technology*, 2010; 7(1): 183-213.

- [5] Basumatary S. Transesterification with a heterogeneous catalyst in the production of biodiesel. A Review. *Journal of Chemical and Pharmaceutical Research*, 2013; 5(1): 1-7.
- [6] Aijaz B, and Flora TTN. A single step solid acid-catalyzed process for the production of biodiesel from the high free fatty acid feedstock. *Energy & Fuels*, 2010; 24(9): 4712-4720.
- [7] Shah B, Sulaimana S, Jamal P, and Alam MZ. Production of heterogeneous catalyst for biodiesel synthesis. *International Journal of Chemical and Environmental Engineering*, 2014; 5(2): 73-75.
- [8] di Serio M, Dimiccoli M, Cammarota F, Nastasi M, and Santacesaria E. Synthesis of biodiesel via homogeneous Lewis acid catalyst. *Journal of Molecular Catalysis A: Chemical*, 2005; 239(1): 111-115.
- [9] Alonso DM, Mariscal R, Granados ML, and Maireles-Torres P. Biodiesel preparation using Li/CaO catalysts: Activation process and homogeneous contribution. *Catalysis Today*, 2009; 143(1-2): 167-171.
- [10] Olutoye MA, and Hameed BH. A highly active clay-based catalyst for the synthesis of fatty acid methyl ester from waste cooking palm oil. *Applied Catalysis A: General*, 2013; 450: 57-62.
- [11] Kim HJ, Kang BS, Kim MJ, Park YM, Kim DK, Lee JS, and Lee KT. Transesterification of vegetable oil to biodiesel using a heterogeneous base catalyst. *Catalysis Today*, 2004; 93(95): 315-320.
- [12] Mbaraka IK, and Shanks BH. Conversion of oils and fats using advanced mesoporous heterogeneous catalysts. *Journal of the American Oil Chemists' Society*, 2006; 83: 79-91.
- [13] Yun JT, Dehkhoda AM, and Ellis N. Development of biochar-based catalyst for transesterification of canola oil. *Energy & Fuels*, 2011; 25: 337-344.
- [14] Boz N, and Kara M. Solid base catalyzed transesterification of canola oil. *Chemical Engineering Communications*, 2009; 196: 80-92.
- [15] Hillion G, Delfort B, le Pennee D, Bournay L, and Chodorge J. Biodiesel production by a continuous process using a heterogeneous catalyst. *Prepr. Pap. - American Chemical Society, Division of Fuel Chemistry*, 2003; 48(2): 636-638.
- [16] Sani YM, Daud WMAW, and Abdul Aziz AR. Biodiesel feedstock and production technologies, successes, challenges and prospects. *Intech*, 2013; 4: 77-101.
- [17] Furuta S, Matsuhashi H, and Arata K. Biodiesel fuel production with solid super acid catalysis in fixed bed reactor under atmospheric pressure". *Catalysis Communication*, 2004; 5(12): 712-723.
- [18] Taufiq-Yap YH, Abdullah NF and Basri M. Biodiesel production via transesterification of palm oil using NaOH/Al₂O₃ catalysts. *Sains Malaysiana*, 2011; 40(6): 587-594.
- [19] Hak-Joo K, Bo-Seung K, Min-Ju K, Young P, Deog-Keun K, Jin-Suk L and Kwan-Young L. Transesterification of vegetable oil to biodiesel using heterogeneous base catalyst. *Catalysis Today*, 2004; 93(95): 315-320.
- [20] Arzamendi G, Arguinarena E, Camp I, Zabala IS and Gandia LM. Alkaline and alkaline-earth metals compounds as catalysts for the methanolysis of sunflower oil. *Catalysis Today*, 2008; 133(135): 305-313.
- [21] Kondamudi N, Mohapatra S, and Misra M. Quintinite as a bifunctional heterogeneous catalyst for biodiesel synthesis. *Applied Catalysis A, General*, 2011; 393(1-2): 36-43.
- [22] Pinzi S, Gandia LM, Arzamendi G, Ruiz JJ, and Dorado MP. Influence of vegetable oils fatty acid composition on reaction temperature and glycerides conversion to biodiesel during transesterification. *Bioresource Technology*, 2011; 102: 1044-1050.
- [23] Leung DYC, Wu X, and Leung MKH. A review on biodiesel production using catalysed transesterification. *Applied Energy*, 2010; 87: 1083-1095.
- [24] Boey PL, Mariam G, Hamid SA, and Ali DMH. Utilization of waste cockle shell (*Anadara granosa*) in biodiesel production from palm olein optimization using response surface methodology. *Fuel*, 2011; 90: 2353-2358.
- [25] Sharma YC, Singh B and Korstad J. Application of an efficient nonconventional heterogeneous catalyst for biodiesel synthesis from *Pongamia pinnata* oil. *Energy & Fuels*, 2010; 24: 3223-3231.
- [26] Tan YH, Abdullah MO, Hipolito CN, and Taufiq-Yap YH. Waste ostrich and chicken-eggshells as heterogeneous base catalyst for biodiesel production from used cooking oil: catalyst characterization and biodiesel yield performance. *Applied Energy*, 2015; 2: 1-13.
- [27] Cho YB, and Seo G. High activity of acid treated of quail eggshell catalysts in the transesterification of palm oil with methanol. *Bioresource Technology*, 2010; 101: 8515 -8524.

- [28] Margaretha YH, Prastyo HS, Ayucitra A and Ismadji S. Calcium oxide from pomacea sp. shell as a catalyst for biodiesel production. *International Journal of Energy and Environmental Engineering*, 2012;3: 1-9.
- [29] Obadiah A, Swaroopa GA, Kumar SV, Jeganathan KR, and Ramasubbu A. Biodiesel production from Palm oil using calcined waste animal bone as catalyst. *Bioresource Technology*, 2012; 116(2): 5-16.
- [30] Roschat W, Kacha M, Yoosuk B, Sudyoaduk T, and Promarak V. Biodiesel production based on heterogeneous process catalyzed by solid waste coral fragment. *Fuel*, 2012; 2: 194-202.
- [31] Aderemi BO, and Hameed BH. Alum as a heterogeneous catalyst for the transesterification of palm oil. *Applied Catalysis. A General*, 2009; 370: 54-58.
- [32] Olutoye MA, Wong SW, Chin LH, Asif M, and Hameed BH. Synthesis of fatty acid methyl esters via transesterification of waste cooking oil by methanol with a barium-modified montmorillonite K10 catalyst. *Renewable Energy*, 2015; 86: 392-398.
- [33] Dai Y, Chen K, Wang Y, and Chen C. Application of peanut husk ash as a low-cost solid catalyst for biodiesel production. *International Journal of Chemical Engineering and Applications*, 2014; 5(3): 276-280.
- [34] Akinwekomi AD, Omotoyinbo JA, and Folorunso D. Effect of high alumina cement on selected foundry properties of anthill clay. *Leonardo Electronic Journal of Practices and Technology*, 2012; 1: 37-46.
- [35] Henne GA. Anthill as a resource for ceramics. Published PhD Thesis, Faculty of Fine Art, Kwame Nkrumah University of Science and Technology, Ghana, 2009.
- [36] Paton TR, Humphreys GS, and Mitchel PB. *Soils ± A Global View*: London: UCL Press, 1995.
- [37] Sharma V, and Sumbali G. An overview of the symbiotic interaction between ants, fungus and other living organisms in ant-hill soil. *International Journal of Environmental Science*, 4(3) (2013) 432-443.
- [38] Kristiansen SM, and Amelung W. Abandoned anthill in a temperate deciduous forest morphology and organic matter composition. *European Journal of Soil Science*. 52 (2001) 355– 363.
- [39] Olusegun HD, and Ajiboye TK. Design construction and testing of vibrator-compactor block making machine for rural application. *International Journal of Engineering*, 3(1) (2009) 1-14.
- [40] Elufisan MO. Determinants of household consumption-expenditure on egg in Ilorin east and west local Areas, Kwara State, Nigeria. Unpublished B. Agric Thesis, Department of Agricultural Economics and Farm Management, University of Ilorin, Nigeria. 1994: 1-168.
- [41] Tsai WT, Yang JM, Lai CW, Cheng YH, Lin CC and Yeh CW. Characterization and adsorption properties of eggshells and eggshell membrane. *Bioresource Technology*, 2006; 121: 167-173.
- [42] Than MM, Lawanprasert P, and Jateleela S. Utilization of eggshell powder as excipient in fast and sustained release of acetaminophen tablet. *Mahidol University Journal of Pharmaceutical Sciences*, 2012; 39(3-4): 32-38.
- [43] Amu OO, Fajobi AB and Oke BO. Effect of eggshell powder on the stabilizing potential of lime on expensive clay oil. *Research Journal of Agricultural and Biological Science*, 2005; 1: 80-84.
- [44] Yoo S, Hsieh JS and Zou P and Kokoszka J. Utilization of calcium carbonate particles from eggshell waste as coating pigments for ink-jet printing paper. *Bioresource Technology*, 2009; 100: 6416-6421.
- [45] Montilla A, del Castillo MD, Sanz ML and Olano A. Egg shell as catalyst of lactose isomerisation to lactulose. *Journal of Food Chemistry*, 2005; 90: 883-890.
- [46] Nakatani N, Takamori H, Takeda K, and Sakugawa H. Transesterification of soybean oil using combusted shell waste as a catalyst. *Bioresource Technology*, 2009; 100:1510-1513.
- [47] Wei Z, Xu C, and Li B. Application of waste eggshell as low-cost solid catalyst for biodiesel production. *Bioresource Technology*, 2009; 100: 2883-2885.
- [48] Umdu ES, Tuncer M, and Seker E. Transesterification of *Nannochloropsis aculata* microalga's lipid to biodiesel on Al₂O₃ supported CaO and MgO catalysts. *Bioresource. Technology*, 2009; 100: 2828-2831.
- [49] Witton T. Characterization of calcium oxide derived from waste eggshell and its application as CO₂ sorbent. *Ceramics International*, 2011; 37: 3291-3298.
- [50] Sun H, Ding Y, Duan J, Zhang Q, Wang Z, Lou H, and Zheng X. Transesterification of sunflower oil to biodiesel on ZrO₂ supported La₂O₃ catalyst. *Bioresource Technology*, 2010; 101:(2010) 953-958.
- [51] K. Chojnacka, Biosorption of Cr(III) ions by Eggshells. *Journal of Hazardous. Materials*. 121 (2005) 167-169.

- [52] R. Chakraborty, S. Bepari and A. Banerjee, Transesterification of soybean oil catalyzed by fly ash and egg shell derived solid catalysts. *Chemical Engineering Journal*, 165 (2012) 798–801.
- [53] N. Viriya-empikul, P. Krasae, W. Nualpaeng, B. Yoosuk, and K. Faungnawakij, Biodiesel production over Ca-based solid catalysts derived from industrial wastes. *Fuel*. 92 (2012) 239–344.
- [54] A. Sivasamy, K.Y. Cheah, P. Fornasiero, F. Kemausuor, S. Zinoviev and S. Miertus, Catalytic applications in the production of biodiesel from vegetable oils. *ChemSusChem*, 2 (2009) 278–300.
- [55] C.H. Bartholomew, and R.J. Farrauto, *Fundamentals of Industrial Catalytic Processes*. John Wiley & Sons Inc., Hoboken, New Jersey, (2006).
- [56] Q.M. Quddus, A novel mixed metallic oxygen carriers for chemical looping combustion: Preparation, characterization and kinetic modeling, published PhD thesis. Department of Chemical and Biochemical Engineering, University of Western Ontario London, Ontario Canada, 2013.
- [57] K. Koeler, *Modern methods in heterogeneous catalysis research*”, Fritz Haber Institute, TU Berlin & HU Berlin, p.1-35, 2006.
- [58] S. Rojas, *Preparation of Catalysts: Heterogeneous catalysts*, CSIC. 1-52, 2013.
- [59] A. D’Cruz, M.G. Kulkarni, L.C. Meher, and A.K. Dalai, Synthesis of biodiesel from canola oil using heterogeneous base catalyst. *Journal of American Oil Chemical Society*. 84 (2007) 937–943.
- [60] C.A. Sirichai, C.A. L. Apanee, and J. Samai, Biodiesel production from palm oil using heterogeneous base catalyst. *International Journal of Chemical and Biological Engineering*. 6 (2012) 230–235.
- [64] G. Leofanti, G. Tozzola, M. Padovan, G. Petrini, S. Bordiga, and A. Zecchina, 1997. Catalyst characterization: characterization techniques. *Catalysis Today*. 34 (1997) 307–327.
- [62] H. Wang, M. Wang, S. Liu, N. Zhao, W. Wei, and Y. Sun, Influence of preparation methods on the structure and performance of CaO–ZrO₂ catalyst for the synthesis of dimethylcarbonate via transesterification. *Journal of Molecular Catalysis A: Chemical*. 258 (1-2) (2006) 308–312.
- [63] K. Liu, H. He, Y. Wang, S. Zhu, and X. Ziao, Transesterification of Soybean Oil to Biodiesel Using CaO as A Solid Base Catalyst. *Fuel*. 87 (2008) 216–221.
- [64] S.L. Yan, S.O. Salley, and K.Y. Simon Ng, Simultaneous transesterification and esterification of unrefined or waste oils over ZnO–La₂O catalysts. *Applied Catalysts A: General*. 353(2) (2009) 203–212.
- [65] J.K. Lakhya, C. Singh, B. Jutika, K. Rupam, and D. Dhanapati, Biochar supported CaO as heterogeneous catalyst for biodiesel production. *International Journal of Innovative research & Development*. 1(7) (2012) 186–195.
- [66] M.A. Olutoye, O.D. Adeniyi, and A.S. Yusuff, Synthesis of biodiesel from palm kernel oil using mixed clay-eggshell heterogeneous catalyst. *Iranica Journal of Energy and Environment*. 7(3) (2016) 308–314.
- [67] D. Kumar, and A. Ali, Nanocrystalline KeCaO for the transesterification of a variety of feedstocks: structure, kinetics and catalytic properties. *Biomass Bioenergy*. 46 (2012) 459–468.
- [68] M.A. Olutoye, B. Sulaiman and A.S. Yusuff, Bi-ZnO heterogeneous catalyst for transesterification of crude jatropha oil to fatty acid methyl ester”. *Advances in Research* 7(1) (2016) 1–8.
- [69] D.E. Lopez, J.G. Godwin Jr., O.A. Bruce and E. Lotero, Transesterification of triacetin with alcohol on solid acid and base catalysts. *Applied Catalysis A: General*, 2 (2005) 97–105.
- [70] M. Alsawalha, Characterization of acidic and basic properties of heterogeneous catalysts by test reactions. PhD dissertation, University of Oldenberg Germany. 2004 1–121.
- [71] F. Audry, P.E. Hoggan, J. Saussey, J.C. Lavalley, H. Lauron-pernot, and A.M. Le Govic, 1997. Infrared study and quantum calculation of the conversion of methylbutynol into hydroxymethylbutanone on Zirconia. *Journal of Catalysis*. 168 (1997) 471–481.
- [72] Y. Li, F. Qiu., D. Yang, X. Li, and P. Sun, Preparation, characterization and application of heterogeneous solid base catalyst for biodiesel production from soybean oil. *Biomass Bioenergy*. 35 (2011) 2787–2795.
- [73] V. Kumar, and P. Kant, Biodiesel production from sorghum oil by transesterification using zinc oxide as catalyst. *Petroleum & Coal*. 56(1) (2014) 35–40.

- [74] G. Feng, and F. Zhen, 2011. Biodiesel production with solid catalysts, biodiesel- feedstocks and Processing Technologies, Dr. Margarita Stoytcheva (Ed.), ISBN: 978-953-307-713-0, InTech.
- [75] A.S. Yusuff, O.D. Adeniyi, M.A. Olutoye, and U.G. Akpan, A review on application of heterogeneous catalyst in the production of biodiesel from vegetable oil. *Journal of Applied Science and Process Engineering*. 4(2) (2017) 142-157.
- [76] A.S. Yusuff, O.D. Adeniyi, M.A. Olutoye, and U.G. Akpan, Performance and emission characteristics of diesel engine fuelled with waste frying oil biodiesel-petroleum diesel blend. *International Journal of Engineering Research in Africa*. 32 (2017) 100-111.

To whom correspondence should be addressed: Dr. Adeyinka Sikiru Yusuff, Department of Chemical and Petroleum Engineering, Afe Babalola University, Ado-Ekiti, Nigeria, yusuffas@abuad.edu.ng

PROCESS SIMULATION AND OPTIMIZATION OF CATALYTIC REACTORS OF SULFUR RECOVERY UNIT (SRU) VIA ASPEN PLUS

Sepehr Sadighi, Seyed Reza Seif Mohaddecy

Research Institute of Petroleum Industry (RIPI), Catalysis Technologies Development Division, P.O. Box 14665137, Tehran, Iran

Received November 13, 2017; Accepted December 23, 2017

Abstract

In this study, the solid package of Aspen plus is applied for simulating and optimizing temperatures of Claus convertors in an industrial scale sulfur recovery unit (SRU). At first, to prove the accuracy of the simulator developed for the target SRU, H₂S conversion and rate of sulfur production which are calculated by Aspen plus, are compared with design data. It is observed that Aspen plus can predict the total H₂S conversion of the process with the absolute average deviation (AAD%) of 1.59% at the average reaction temperature. Moreover, the total sulfur production rate of the plant can be simulated with the AAD% of 10.22%. From these results, it is concluded that the simulator is reliable to be applied for optimizing temperatures of Claus convertors in the target process. After performing the sensitivity analysis, it is shown that by decreasing the average temperatures of 2nd and 3rd convertors from 213.9°C and 199°C to 205°C and 190°C, respectively, the H₂S conversion increases about 1.2% which is significant to decrease the emission of this harmful compound.

Keywords: *Claus process; Simulation; Aspen plus; Optimization; Sulfur.*

1. Introduction

Hydrogen sulfide (H₂S) is a toxic gas, and it is so harmful to live issues; therefore, its present in the exhaust gas of oil and gas refineries are under strict environmental regulations. The modified sulfur recovery unit (SRU) is favorably used to transform H₂S into elemental sulfur [1-3]. This product is an extremely useful element, and its largest application is for the manufacture of fertilizers with other principal users including rubber industries, cosmetics, and pharmaceuticals [4]. Consequently, SRU is momentous from economic and environmental aspects.

Respect to the simulation of a catalytic section of the modified Claus process, there are scarce studies reported in the literature. Asadi *et al.* [5] have studied the effect of H₂S concentration on the reaction furnace temperature and sulfur recovery. First, the simulation of Claus process was considered using a process simulator called TSWEET, and then the effect of H₂S concentration and H₂S/CO₂ ratio in three different concentrations of oxygen (in input air into the unit) on the main burner temperature and sulfur recovery were studied and compared. Also, in this paper, it was shown that recovery rate of sulfur increases up to a maximum value, and then decreased as H₂S concentration and H₂S/CO₂ ratio (in all three concentrations of oxygen) increased. In the other work, Pahlavan *et al.* [6] simulated the reaction furnace of a Claus process using a kinetic based model. The predicted outlet temperature and concentrations by this model were compared with experimental data published in the literature, and also data obtained by PROMAX V2.0 simulator. The results demonstrated that the accuracy of the proposed kinetic model and its simulator were almost similar. Nabgan *et al.* [7] proposed a simulation for a Claus process plant via Aspen HYSYS V8.8 simulator. In this study, it was shown that only factors which could affect the conversion of H₂S were the feed composition and its molar flow rate. Eghbal Ahmadi [8] simulated the Claus process based on simultaneous data reconciliation and parameter estimation. The Claus process was characterized by several

problems for predicting the behavior of the reactors. In this paper, industrial plant was simulated using Hysys software based on simultaneous data reconciliation and parameter estimation using a Genetic algorithm (GA). Analysis of the results proved that the standard deviation of the reconciled data was reasonably reduced comparing with their raw measured values. Accordingly, measuring errors caused by various unfavorable problems in the plant such as instrumentation inaccuracy were reduced. Having developed simulation model with accurate values of process variables, the behavior of the plant was precisely monitored. Moreover, the developed simulation model could be used for process optimization and control purposes.

In the present study, the capability of Aspen plus to simulate the conversion of H₂S and carbon-sulfur compounds are studied. The results are validated versus the design data provided by the licensor of the target SRU. After validating the simulation, the temperature of the catalytic Claus reactors are optimized, and the effect of the recommended operating conditions on the conversion of H₂S is reported. Due to the importance of the SRU from the environmental view point, this research and the proposed methodology can be significant.

2. Process description

Sour Gas is routed through the sour gas separator D-101 to heat exchanger E-101. A schematic process flow diagram of Claus process unit is shown in Figure 1.

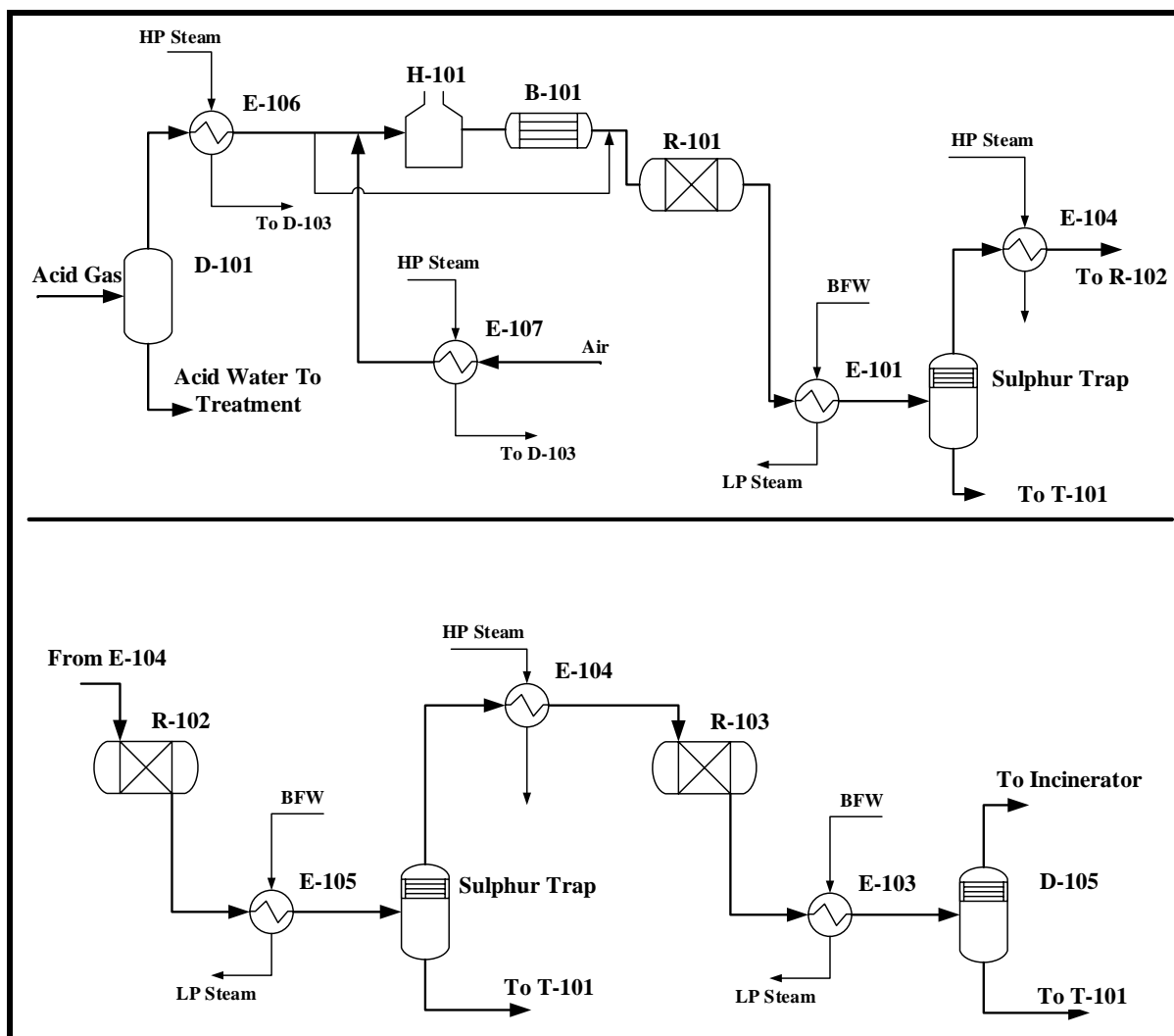


Figure 1. Process flow diagram of Claus process unit

If water precipitates in D-101, it will be routed to the slop drum by means of the sour water pump. The central muffle is used to combust fuel gas for heating purposes during start-up, shutdown or low-load. The size of the combustion chamber H-101 is selected so as to approximately reach the thermodynamic equilibrium in the off gases from the central muffle and the H₂S-burners. Many chemical reactions taking place in the combustion chamber H-101 transform part of the H₂S into sulfur vapor.

Directly connected to the combustion chamber, H-101 is the Claus process gas cooler B-101 with the steam drum, which serves to cool the process gas from about 1009°C to about 250°C and precipitate part of the sulfur vapor. To control the gas temperature to the first Claus reactor R-101, part of the process gas is sent directly through Claus process gas cooler B-101 via a central pipe to a Claus mixing valve, which mixes the cooled gas with the hot gas. After leaving the Claus mixing valve, the process gas is routed to the first Claus reactor R-101. Here the sulfur components are further converted into elemental sulfur over a catalytic bed. The extent of conversion depends on prevailing temperature in this reactor. The reactor has an outlet temperature of approximately 325°C. After leaving the first Claus reactor R-101, the process gas enters the first sulfur condenser E-101 with the steam drum, which serves to cool the process gas to about 175°C and precipitates part of the sulfur vapor. The gas leaving the first sulfur condenser E-101 has to be heated to the inlet temperature of the second Claus reactor (205°C). In the second Claus reactor, R-102 converts the remaining sulfur compounds to elemental sulfur. The process gas leaves the second Claus reactor with a temperature of approximately 229°C and is cooled to about 130°C in the downstream second sulfur condenser E-105 to precipitate most of the sulfur vapor. Before the process gas is routed to the section for further treatment, it passes the sulfur separator D-105 where entrained liquid sulfur is separated from the gas stream.

3. Simulation methodology

3.1. Feed specifications

The specifications of the feed introduced to the first reactor of the target SRU unit are presented in Table 1.

Table 1. Specifications of the feed entered into the first catalytic reactor

	Value		Value
Mole flow (kmol/h)	1.77	Pressure (bara)	1.38
Temperature (°C)	250		
Composition (mol%)			
H ₂ S	3.61	CO	1.77
SO ₂	2.86	CO ₂	24.30
H ₂ O	25.24	H ₂	1.03
COS	1.91	N ₂	38.97
CS ₂	0.17	S ₅ to S ₈	0.13

The feed of the catalytic bed and also produced sulfur exited from the SRU convertors mostly included sulfur with 8 atoms (Octa-sulfur, the common allotrope of sulfur). Therefore, to simplify the simulation, all allotrope of sulfur (i.e., S₂ to S₈) is lumped as the S₈ compound.

3.2. Simulation of SRU convertors

Aspen Plus (Aspen Tech, V7.2) can simulate the process in which solids are produced, or they should be handled. In this simulator, a wide range of unit operation models are provided for solid operations. In this study, to simulate catalytic reactors of SRU process, REquil model which is available in the model library of the Aspen Plus is applied. REquil models reactors when reactions meet the equilibrium. This module can calculate single phase chemical equilibrium, or simultaneous phase and chemical equilibria. Moreover, REquil is capable of calculating equilibrium by solving stoichiometric chemical and equilibrium state equations. To do this task, it is assumed that the following equations are carried out in the SRU convertors:



Since properties of sulfur and other phases cannot be estimated with the same type of models, produced sulfur is distributed over the other sub stream, and its properties are calculated by using Solid package. Additionally, the S8 product exited from each catalytic reactor is separated from the other components using a component separator (Sep module).

4. Results and discussions

4.1. Validation of SRU simulation

Based on the design data and the described methodology, the target sulfur recovery facility was simulated in the Aspen plus (see Fig.2).

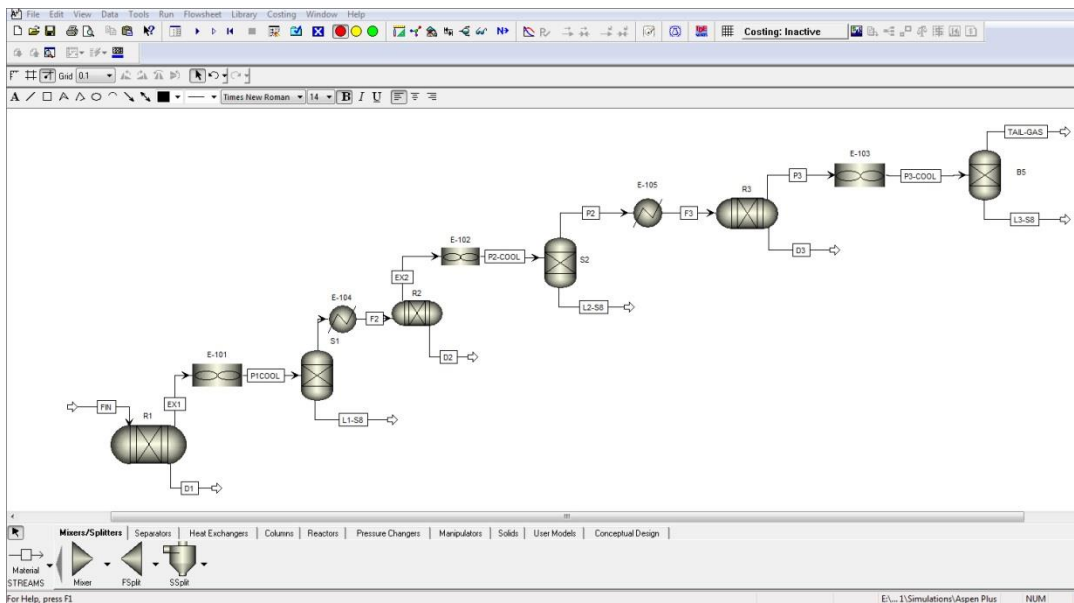


Figure 2. Process flowsheet for simulating SRU catalytic convertors in Aspen plus

The absolute average deviation (AAD%) of simulated data against the design data for total H₂S, CS₂, and COS conversions are shown in Table 2. These data confirm that the flowsheet simulation developed in Aspen plus for the target Claus process can satisfactorily calculate the main output variables of the process and it can be used for analyzing this process. As observed, such as the total conversions, Aspen model can appreciably predict these output variables with acceptable accuracy.

Table 2 Comparison of simulation results and design data for H₂S, COS, and CS₂ conversion

Conversion	Design	Simulation	AAD%
H ₂ S (mol%)	93.94	92.44	1.59
COS (mol%)	94.8	99.99	5.48
CS ₂ (mol%)	90.2	100.00	10.86

To have a better justification, comparisons between the simulated sulfur production versus design data are illustrated Figure 3. As observed, such as the total conversions, Aspen model can appreciably predict these output variables with an acceptable accuracy.

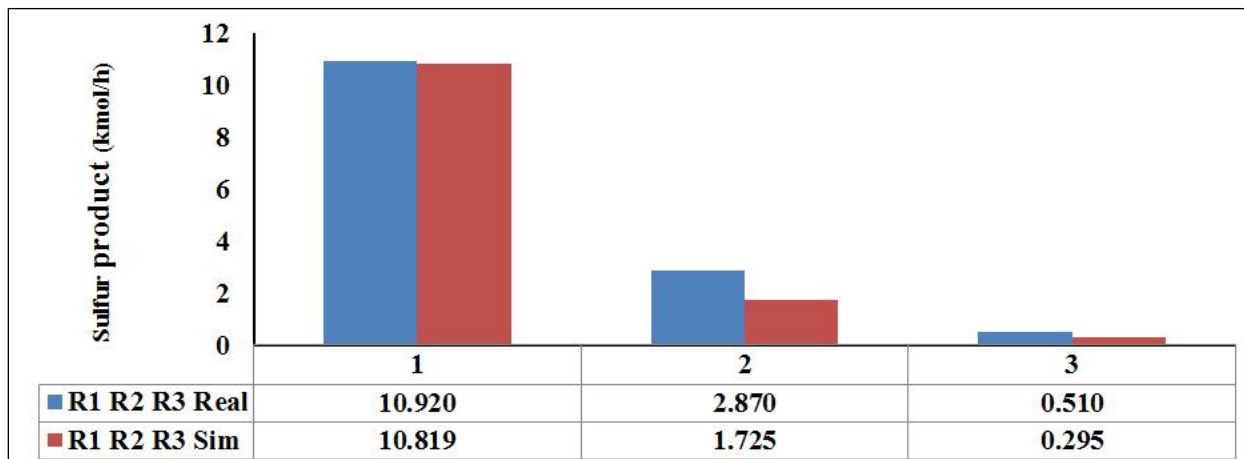


Figure 3. Comparison of simulation results and design data for sulfur production

4.2. Sensitivity analysis for SRU simulation

After validating the SRU simulator, the sensitivity analysis of the H₂S conversion to average bed temperature for 1st, 2nd, and 3rd catalytic convertors are presented in Figs 4 to 6, respectively. As seen from these figures, by increasing the average temperature of beds, the H₂S conversion decreases sharply. This phenomenon is expectable due to the exothermic nature of the Claus reactions; therefore, a cooler and condenser is provided between catalytic beds for decreasing the temperature and also removing the produced sulfur from the gas stream. If the partial pressure of sulfur increases through the catalytic beds, pore plugging due to the capillary condensation of sulfur will happen; consequently, the catalyst will be deactivated fast. Sulfur molecules formed during the Claus reactions can plug pores of catalyst even at a temperature higher than sulfur dew point temperature.

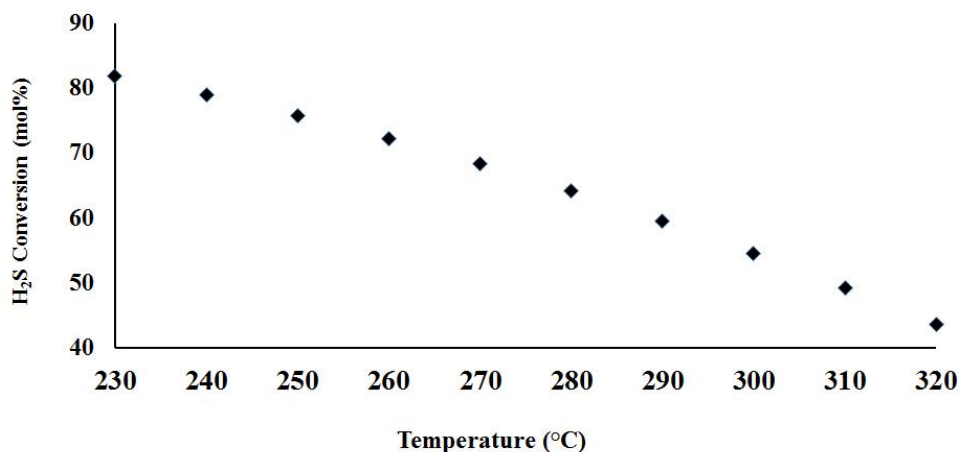


Figure 4. Total conversion of H₂S as a function of average temperature in the 1st catalytic convertor

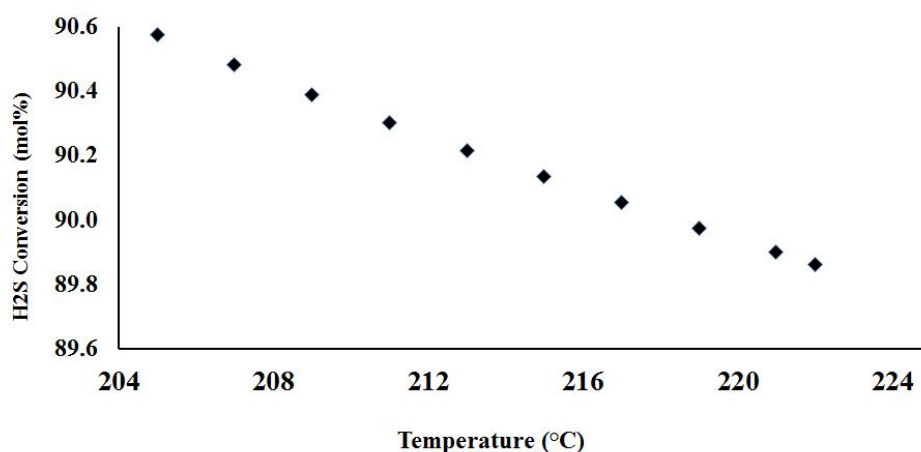


Figure 5. Total conversion of H₂S as a function of average temperature in the 2nd catalytic convertor

It should be noted that the first convertor is more sensitive to the temperature because of the high partial pressure of H₂S, and also higher operating temperature. In the 1st catalytic reactor, a layer of promoted pure titanium oxide (titania or TiO₂) sulfur recovery catalyst after the first layer (activated alumina catalyst) is provided. This catalytic bed is considered for total hydrolysis of COS and CS₂ compounds which their corresponding reactions promote at a temperature higher than 280°C, preferably 300°C.

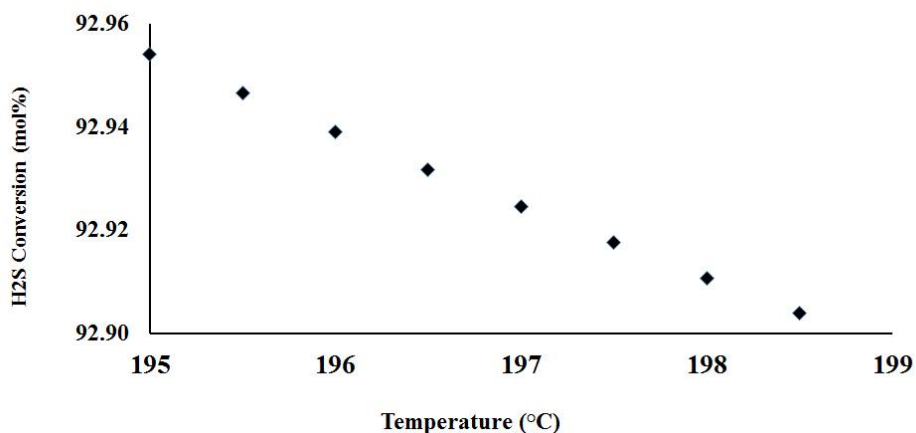


Figure 6. Total conversion of H₂S as a function of average temperature in the 3rd catalytic convertor

4.3. Optimizing temperatures of SRU catalytic reactors

For determining optimum operating conditions, it is recommended that the average temperatures of the 2nd and 3rd convertor can be meticulously decreased. Therefore, by reducing these temperatures, higher H₂S conversion and lower emission can be expected. Due to the importance of the hydrolysis reactions carried out in the second catalytic layer of the 1st reactor (as described before), the average temperature of the first convertor is not included in the optimization program.

If the target SRU currently operates at average bed temperatures of 214°C and 199°C, respectively, these temperatures can be slightly reduced. In Figure 7, variations of H₂S conversion versus temperature reduction in average bed temperature of 2nd and 3rd reactors are depicted. As seen, up to 2°C temperature reduction, no significant total H₂S conversion of the plant has been observed. After this point, for each degree centigrade reduction in bed tempe-

ratures, about 0.1 mol% increase in the H₂S conversion is expected. If the temperature can be reduced to 205°C and 190°C for 2nd and 3rd convertors, respectively, about 1% in H₂S conversion is accessible which is equal to 4% decrease in the H₂S emission.

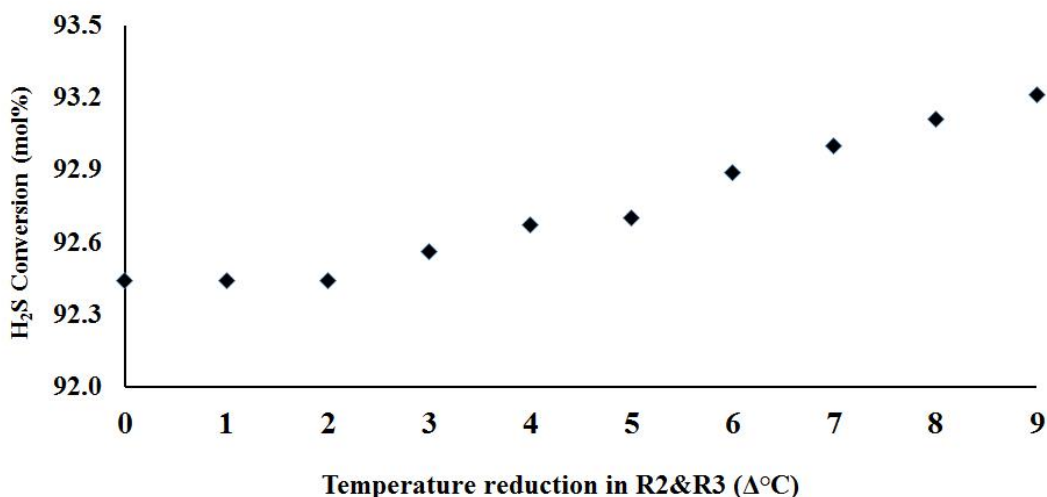


Figure 7. Variations in the total conversion of H₂S vs. temperature reduction of the 2nd and 3rd convertors

5. Conclusions

In this present research, it was demonstrated that Equilibrium reactor (REQUIL) and solid package provided in Aspen plus simulator could be successfully used to simulate Claus convertors of an SRU. In this industrial scale plant, three catalytic reactors were provided to convert H₂S and carbon sulfide compounds (i.e., COS and CS₂) to the sulfur (mainly 8-atomic). It was concluded that Aspen plus could calculate the H₂S conversion of the 1st, 2nd and 3rd catalytic reactors with the accuracy of 22.19%, 0.59%, and 1.59%, respectively. The higher deviation of the simulation for the first reactor was mainly due to the multi-layers of alumina and titania catalyst loaded in that for converting H₂S and hydrolysis of carbon sulfur compounds and, simultaneously. Additionally, based on the designed operating conditions, the rate of the sulfur product calculated by Aspen plus was 12.84 ton/h closed to the design value which was supposed to be 14.3 ton/h.

After validating the SRU simulator, results confirmed that 5°C decrement in the average temperatures of the 2nd and 3rd convertors could increase the total conversion of H₂S from 92.67 mol% to 93.21 mol% due to the exothermic nature of the Claus reactions. Because the 1st reactor was designed to hydrolysis COS and CS₂, and these reactions were substantially promoted at a temperature higher than 300°C, decreasing the temperature of this convertor was not recommended.

Acknowledgement

The author's thanks, Research Institute of Petroleum Industry (RIPI) and National Iranian Gas Company (NIGC) for supporting this project.

References

- [1] Laperdrix E, Justin I, Costenin G, Saur O, Lavalley JC, Aboulayt A, Ray JL, Nédez C. Comparative study of CS₂ hydrolysis catalyzed by alumina and titania. *Applied Catalysis B: Environmental*, 1998; 17, 167-173.
- [2] Abedini R, Koolivand Salooki M. A Simple Molar Flow Modeling and Simulation of Catalytic Beds in Claus Process. *Pet Coal*, 2010; 52(3): 173-178.

- [3] Mahdipoor HR, Kakavand M. The Effect of Amine Concentration on the Performance of TGT Absorber Column. *Pet Coal*, 2015; 57(1): 56-59.
- [4] <https://www.sulphurinstitute.org/learnmore/faq.cfm>.
- [5] Asadi S, Pakizeh M, Pourafshari Chenar M, Shanbedi M, Amiri A. Effect of H₂S concentration on the reaction furnace temperature and sulphur recovery. *International Journal of Applied Engineering Research*, 2011; 1(4): 961.
- [6] Pahlavan M, Fanaei MA. Modeling and Simulation of Claus Unit Reaction Furnace. *Iranian Journal of Oil & Gas Science and Technology*, 2015; 5(1): 42-52.
- [7] Nabgan W, Amran A, Nabgan B, Ripin A, Bin Kidam K, Moghadamian I. A Simulation of Claus Process Via Aspen Hysys for Sulfur Recover. *Chemical Product and Process Modeling*, 2016; 11(4): 273-278.
- [8] Eghbal Ahmadi MH, Rad A. Plant-Wide Simulation Model for Modified Claus Process Based on Simultaneous Data Reconciliation and Parameter Estimation. *Chemical Engineering Transactions*, 2017, 57: 997-1002.

To whom correspondence should be addressed: Dr. Sepehr Sadighi, Research Institute of Petroleum Industry (RIPI), Catalysis Technologies Development Division, P.O. Box 14665137, Tehran, Iran, Sadighis@ripi.ir

FLOW ASSURANCE OPERATIONAL PROBLEMS IN NATURAL GAS PIPELINE TRANSPORTATION NETWORKS IN NIGERIA AND ITS MODELING USING OLGA AND PVTsim SIMULATORS

Kevin C. Igwilo¹, Emeka Emmanuel Okoro¹, P.A.L Anawe¹, S.T.A. Okolie¹, and Onisobuana Cyril Aduma²

¹ School of Petroleum Engineering, Covenant University Ota, Ogun State, Nigeria

² Federal University of Technology Owerri, Imo State, Nigeria

Received September 18, 2017; Accepted December 1, 2017

Abstract

The challenges associated with natural gas Pipeline flow assurance is an increasingly important issue as the world supply for natural gas expands, and is expected to rise more strongly to match the global demand for a cleaner energy. Flow assurance challenges in pipelines include hydrate formation, paraffin wax deposition, asphaltene deposition, sand deposits, black powder, and on the wall of pipelines, all of which obstruct the flow of well fluids and associated produced hydrocarbons. This study addressed these flow assurance concerns from a technical view by quantifying the threats and establishing appropriate mitigation schemes, leading to designed solutions and operational procedures. Modeling and simulation approach was adopted to achieve the overall aim. The simulation software tools PVTsim and OLGA were used for both steady state and dynamic states. The phase envelope investigation indicates that the cricondentherm within the constraint of the delivery temperature. The slugging analysis, indicates that hydrodynamic slugging will not be predominant for the pipeline operations at the design flow rate of 30MMscfd along Alakiri – Obigbo, and at 70MMscfd along the Obigbo Tie-in - Intermediate scrap station; as the flow regimes are mainly stratified for both pipeline systems. From the hydrate analysis investigated, after a shutdown period (no-touch time); hydrate threat is envisaged during the shutdown period of the Intermediate scraper trap – ALSCON along pipeline system, since the temperature drops to the hydrate formation temperature.

Keywords: Flow Assurance; Pipeline; Natural Gas; Modeling.

1. Introduction

Global energy demand has rapidly increased as a result of increase in population and industrialization, with oil and natural gas constituting over 65% of the primary sources. Measured in financial indicators, 90% of chemical products in industrially developed countries are from organic sources whose 98% production are based on oil and natural gas as basic organic chemical feeds [1]. Since petroleum as an energy source is non-renewable, the crude reserves are fast declining due to long period of utilization while the global focus is now shifting towards natural gas as the major source of energy due to its abundance availability, economic viability and environmental friendliness. The increasing use of natural gas as a primary fuel source has led to its greater production and exportation in gaseous and liquid (Liquefied Natural Gas (LNG) forms from many countries that hold sufficient reserves. This has equally increased the global transboundary pipeline networks with minimal considerations to the impacts of its failure it could have on the environment [2]. Natural gas is a combustible gaseous mixture of light hydrocarbon compounds and other components. Its main components are methane (CH₄) and other non-reactive hydrocarbons in gaseous state at ambient temperature and atmospheric pressure. The gas with low energy density is either found in association with crude oil (either dissolved at high temperature and pressure or as gas cap in the same reser-

voir) or as a non-associated gas. This origin of formation, coupled with type, location of deposit, geological structure of the region and other factors determine its composition. The gas is colorless and odorless in its pure state and when burnt, it gives off a great deal of energy with low level of pollutants compared with other fossil fuels [2].

The oil industry is currently working under completely different circumstances than thirty years ago. The oil companies have a desire to develop marginal fields far from land, and at other nodes at greater water depths than before. Oil recovery can now be accomplished down to 9,843ft of water depth. At such extreme depths, the seawater is cold, which increases the risk of hydrate formation in pipelines [3]. Flow assurance challenges in pipelines include hydrate formation, paraffin wax deposition, asphaltene deposition, sand deposits, black powder, and on the wall of pipelines, all of which obstruct the flow of well fluids and associated produced hydrocarbons. Oil and gas pipeline flow assurance technology puts forward flow assurance measures through predicting the flow variation of oil and gas in the pipeline and evaluating the flow safety.

Flow assurance refers to ensuring successful and economical flow of hydrocarbon stream from reservoir to the point of sale and is closely linked to multiphase flow technology. Flow assurance developed because traditional approaches are inappropriate for deepwater production due to extreme distances, depths, temperatures or economic constraints. While flowing through a long pipeline, it is important to take an account of viscosity, acidity and salt content for field operations. All these factors can affect pipeline capacity. The process of ensuring a constant flow of oil despite different issues which can cause flow obstacles is known as flow assurance. Although flow assurance consists of a spectrum of issues, four main issues are: corrosion, salts, asphaltenes and waxes [4].

The challenges associated with natural gas pipeline flow assurance is an increasingly important issue as the world supply for natural gas expands, and is expected to rise more strongly to match the global demand for a cleaner energy. This study was tailored towards addressing these flow assurance concerns from a technical view by quantifying the threats and establishing appropriate mitigation schemes that will lead to designing solutions and operational procedures.

2. Flow assurance brief background

During flow through pipeline, wax may be deposited on pipe walls. A thermal gradient between the outside ambient conditions and the internal oil flow must exist for flow deposition. The internal wall temperature due to the gradient must be below the initial wax appearance temperature. In addition, internal shear forces in the flow must be low enough to allow crystal growth. Wax deposits, can grow and restrict flow. While it is rare for deposition to completely shut down a pipeline, the loss in production capacity is a major concern during waxy crude oil transportation through pipelines. Flow assurance is an important area for multiphase flow of oil, gas and water to minimize financial loss for the petroleum industry [5].

The term flow assurance was first used by Petrobras in the early 1990s in Portuguese as *Garantia do Escoamento* (pt.: *Garantia do Escoamento*), meaning literally "Guarantee of Flow", or Flow Assurance. Flow assurance is extremely diverse, encompassing many discrete and specialized subjects and embrace all kinds of engineering disciplines. Besides network modeling and transient multiphase simulation, flow assurance involves handling many solid deposits, such as, gas hydrates, asphaltene, wax, scale, and naphthenates. Flow assurance is a most critical task during deep water energy production because of the high pressures and low temperature involved. The financial loss from production interruption or asset damage due to flow assurance mishap can be astronomical.

What compounds the flow assurance task even further is that these solid deposits can interact with each other and can cause blockage formation in pipelines and result in flow assurance failure. Flow assurance is applied during all stages of system selection, detailed design, surveillance, troubleshooting operation problems, increased recovery in late life etc.,

to the petroleum flow path (well tubing, subsea equipment, flowlines, initial processing and export lines).

The gas is located thousands of meters below the earth surface with the fluid's pressure in the pores of the rocks ranging between 10MPa/km while in hydrostatic regime (only supporting the weight of the overlying fluid column) to 25MPa/km in geostatic regime (supporting all or part of the weight of the rock column) [6]. Various transportation options of natural gas from off-take include long pipelines transport, methanol, Liquefied Natural Gas (LNG) and compressed natural gas (CNG) of pressure between 3000 and 3600 psi [7]. From these options, only long pipelines and LNG are in common use. The unit cost of pipeline option is clearly superior to that of LNG due to the required high cost of refrigeration and liquefaction of boiled-off liquids and the high risk of over-pressurization for LNG. Pipelines are mainly divided into gas and oil pipelines depending on the nature of the cargo conveyed. Main components of a pipeline network are operational areas and the pipeline segments. Operational areas may be distribution centers, ports or refineries and are connected by pipeline segments. Gas and liquid hydrocarbon pipelines are essentially similar with the greatest operational difference resulting from the varying needs of transporting gas versus liquid. Oil pipelines require pumps to propel the liquid contents while gas lines rely on compressors to force the resource through the pipes.

From field processing facilities, the dried, cleaned natural gas enters the gas transmission pipeline system, analogous to the oil trunk line system [8]. Gas pipelines are usually buried underground about 3-7ft in lands or rights-of-way acquired by, or granted to the pipeline company. Whenever burying the pipe becomes less convenient, the strategy is to place the pipeline 5-6ft above the ground (under strict specifications to withstand environmental conditions) in order to allow for wildlife or any other factor that might damage the pipe. Surely, without pipeline we would not be able to satisfy the huge oil and gas demand of our planet. Pipelines have provided economic, reliable means to transport oil and natural gas from upstream production, often very remote regions, to downstream refineries, power stations, crossing nations, oceans, and continents.

3. Methodology

The system consists of network of pipelines connected in segments. The starting point is Alakiri field of Rivers State and the final receiving point is the ALSCON station at Ikot Abasi (Etetuk) of Akwa Ibom state. The primary fluid flowing is an associated gas from SPDC sources with the aim of supplying gas to the Aluminium Smelting Company of Nigeria (ALSCON).

To study the flow assurance challenges associated with the operations of the Nigeria Gas Company limited (NGC) gas supply pipeline from Alakiri to ALSCON station at Ikot Abasi of Akwa-Ibom state of Nigeria, hydraulic data was collected from NGC.

The pipeline network is about 114km which comprises of three major pipeline segments.

SEGMENT 1: The line diameter is 14" and the length of the segment is about 32km. The starting point is Alakiri launching scraper trap station. The end segment is at Obigbo North tie-in receiving trap station. The first 17km of the pipeline runs parallel to the existing Nigerian Gas Company Alakiri-Onne gas pipeline, traversing mainly swamp area and cross the Bonny River. The last 15.2km of the pipeline traverses mainly build-up area and crosses the following features; railway, express road, tarred roads, pipelines.

SEGMENT 2: The line diameter is 16" and the length is about 44.4km. Starting point is Obigbo North tie-in scraper station and the ends at Intermediate scraper trap station.

SEGMENT 3: The starting point is Intermediate scraper trap station and the end of the segment is at Aluminium Smelting Company of Nigeria (ALSCON) at Ikot Etetuk. The pipeline diameter is 24" and the length is about 37.7km. Currently, the flow assurance problems solved in the above pipeline network system were the hydraulic parameters verification (Pressure, temperature and flow rate).

This study developed flow assurance studies using OLGA software tool, this tool was used to define pipeline operating procedures and control schemes with the aim of ensuring smooth operation during the transportation of the produced gas fluid. OLGA version 7.0 transient

simulator was used to build and analyze models for the Alakiri-Obigbo-Ikot Abasi (ALSCON) pipeline network system. The fluid composition was made suitable for use by OLGA via the use of PVTsim to create table files, which transfers fluid thermodynamic properties into OLGA software format.

The model assume that inlet to the system is a closed node and a mass source that provides the specified flow rate is placed at the inlet node. Since the ALSCON conditions are known and specified at the outlet node of the model, the simulator is able to compute the required parameters along the pipeline length down to the inlet node, such that the entire process from the inlet to the receiving facilities are fully defined.

PVTsim was used to characterised the fluid and predict the hydrocarbon phase envelope characteristics at the Alakiri gas source composition and Obigbo source gas composition.

4. Development of the simulation models with available data

Operating conditions: The information gathered from the acquired data shows that the gas will be delivered to ALSCON pipeline at the delivery points at a maximum pressure of 60 bar. Gas temperature at delivery points: Alakiri gas source: 37.5°C; Obigbo gas source: 46.7°C

Gas operating conditions at the ALSCON Terminal station downstream of the metering system at the NGC battery limit are:

Temperature: Maximum: +35°C; Minimum: +20°C.

Pressure: Maximum: 40bar; Normal: 30bar; Minimum: 25bar.

Gas flow rate: Alakiri-Obigbo: 30MMSCFD; Obigbo-Ikot Etetuk: 100MMSCFD.

For the hydraulic calculation the following pipe characteristics have been assumed: 14" OD wall thickness: 6.4mm; 16"OD wall thickness: 6.4mm; 24" OD wall thickness: 11.9mm.

4.1. Modeling of the pipeline network using OLGA simulator

Based on the available data, the pipeline network system was built using OLGA software tool. The pipeline wall is defined by the steel thickness and the insulation thickness is an unknown parameter, which is calculated based on the minimum required arrival temperature at the ALSCON terminal. The flow path is simulated using two major nodes, which are the upstream node which is defined as a closed node (no flow across the node) and the downstream node is modelled as a pressure node (flow across the node) in which the arrival pressure is 60 bar. The models in OLGA are as shown in Figure 1.

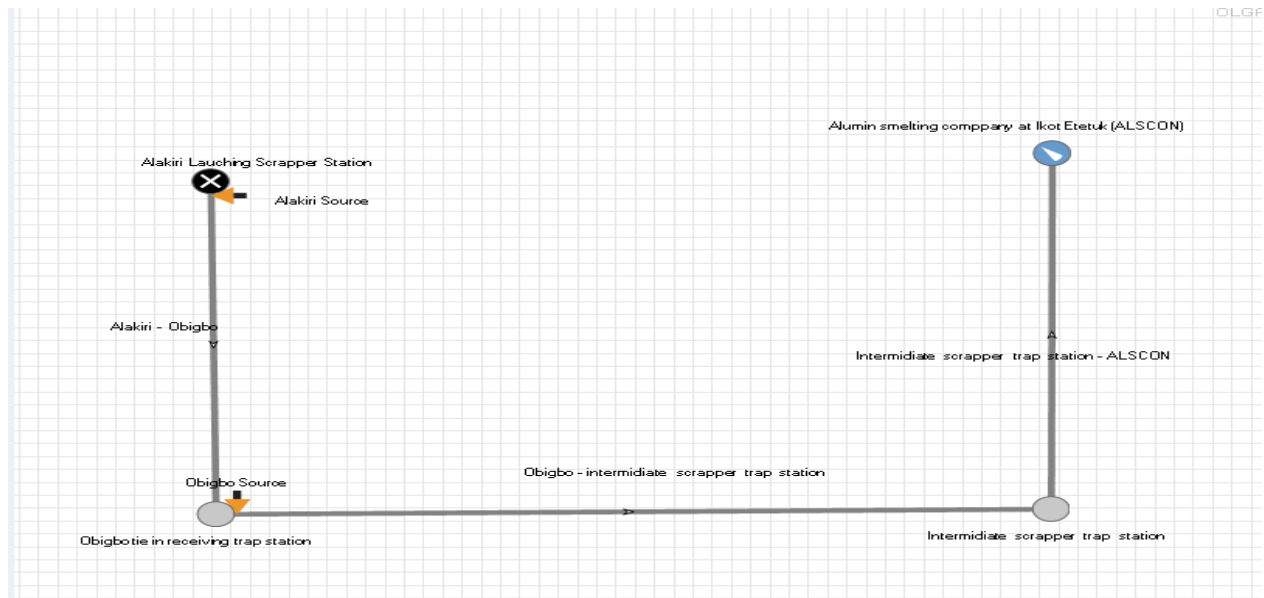


Figure 1. Schematic diagram of OLGA models with nodes and source inlet

From the figures 2 and 3, we have two sources, four nodes, and three flow paths; these pipeline network system points are defined as stated below:

SOURCES: Source 1: Alakiri source; Source 2: Obigbo source

NODES: Node 1: Alakiri source; Node 2: ALSCON at Etetuk; Node 3: Intermediate scraper trap station; Node 4: Obigbo tie -in

FLOW PATHS: Flow path 1: Alakiri-Obigbo; Flow path 2: Obigbo-Intermediate scraper station; Flow path 3: Intermediate scraper station- ALSCON at Etetuk.

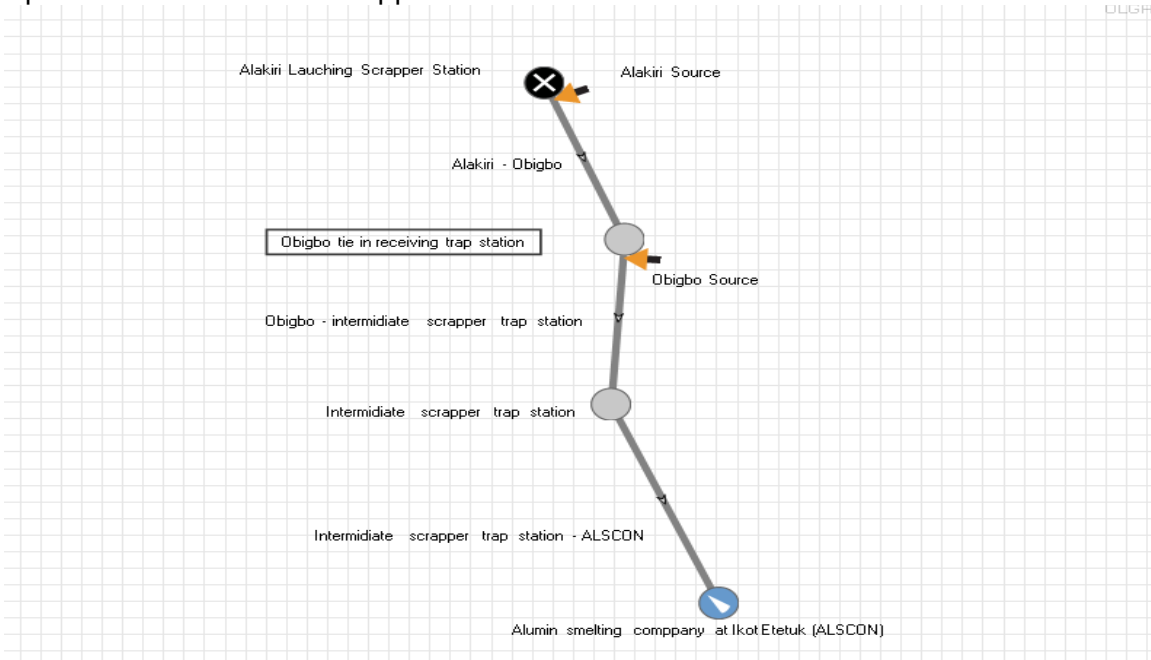


Figure 2. Schematic diagram of OLGA models with nodes and source inlet

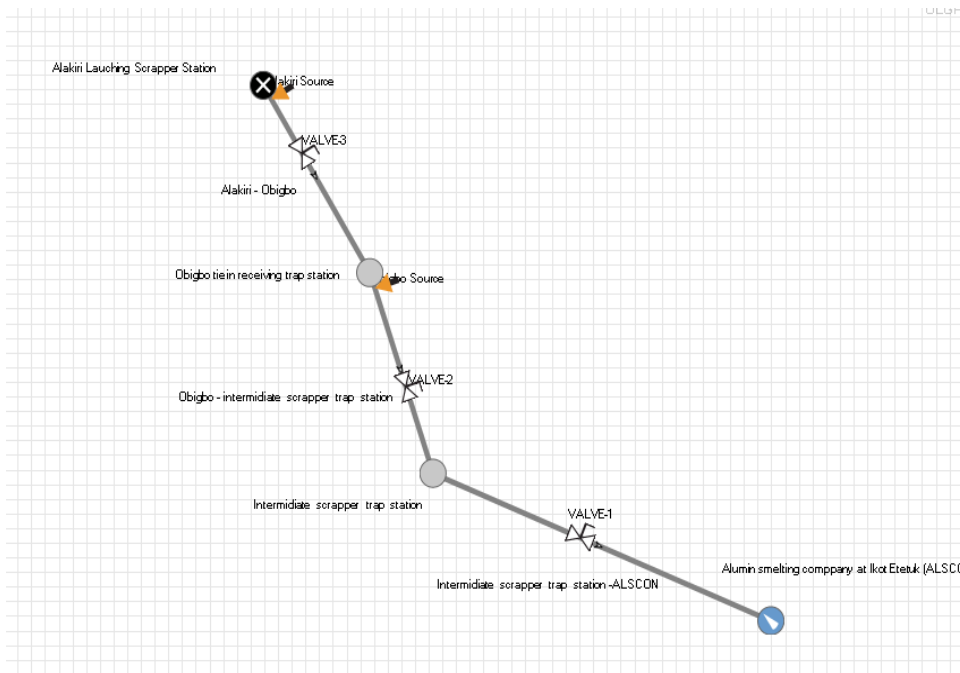


Figure 3. Schematic diagram of OLGA models with valves along the flow path with nodes and sources inlet

Geometry of the Pipeline

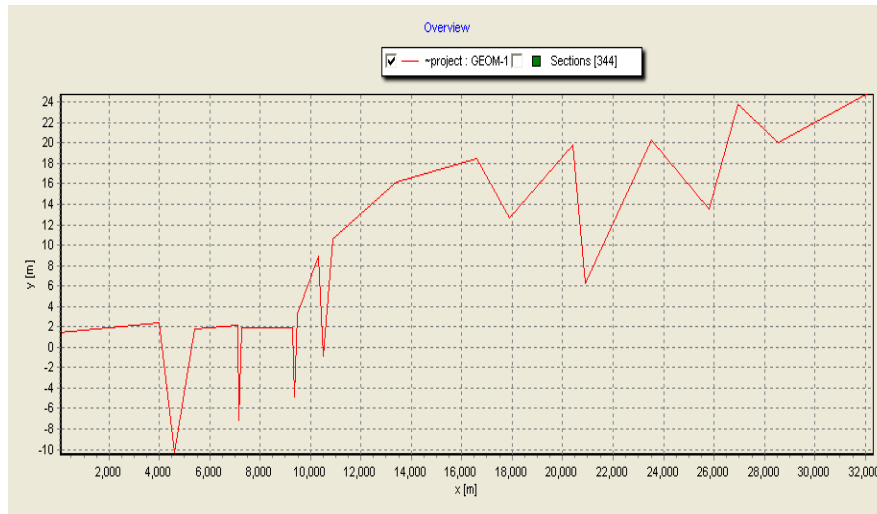


Figure 4. Alakiri - Obigbo Tie-in Profile Plots

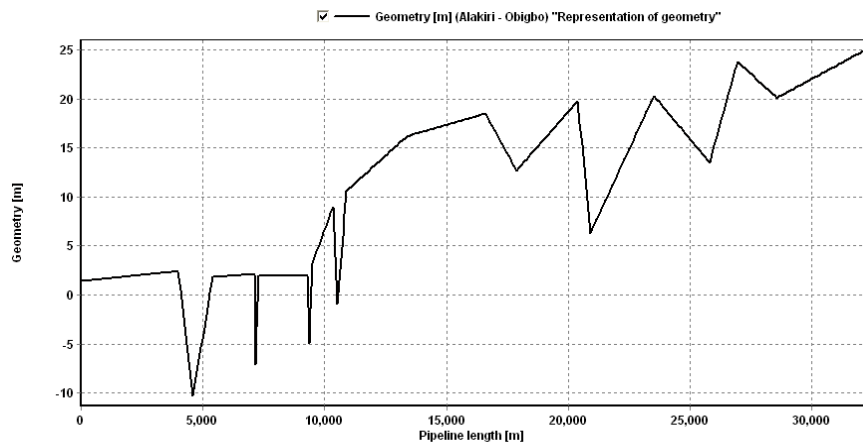


Figure 5. The Alakiri - Obigbo Trap Station Profile Plots



Figure 6. The Alakiri - Obigbo Profile Plots

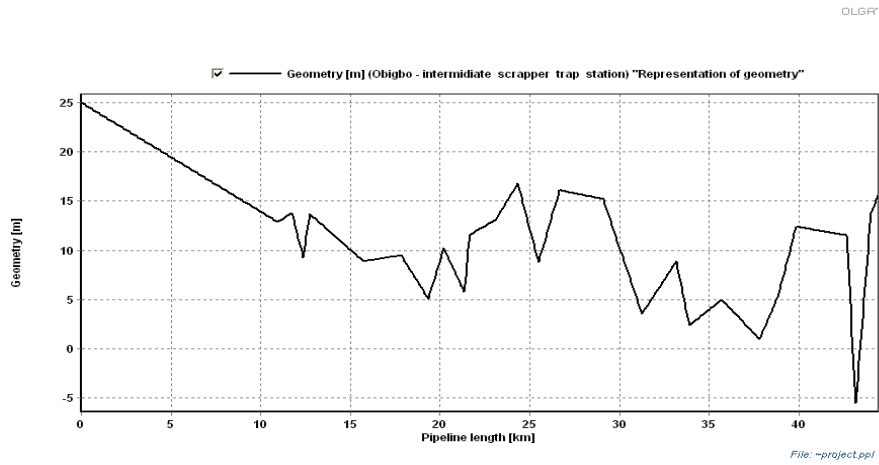


Figure 7. The Obigbo – Intermediate Scrapper Trap Station Profile Plots



Figure 8. The Obigbo – Intermediate Scrapper Trap Station Profile Plots

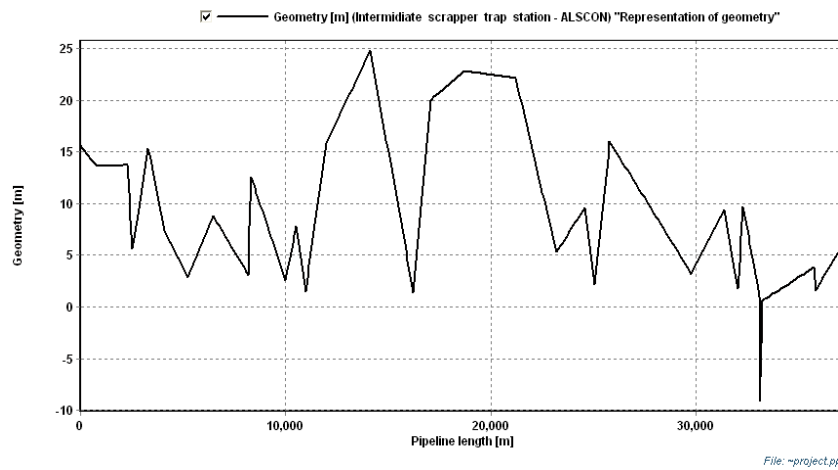


Figure 9. The Intermediate Scrapper Trap Station- ALSCON at Etetuk profile plots

5. Results and discussion

5.1. Phase envelope

From the phase envelope in Figures 10 and 11, the cricondentherm which is the maximum temperature above which liquid cannot be formed regardless of the pressure for Alakiri is -7.27°C and the corresponding cricondentherm pressure is 51.05bar. The cricondenbar which is the maximum pressure above which no gas can be formed regardless of the temperature is found to be 86.98bar and the corresponding cricondenbar temperature is -28.05°C ; while the critical temperature is -47.33°C and the critical pressure is 76.87bar.

Likewise, the cricondentherm for Obigbo is 18.184°C and the corresponding cricondentherm pressure is 43.97bar. The cricondenbar is found to be 100.44bar and the corresponding cricondenbar temperature is -17.17°C ; while the critical temperature is -52.56°C and the critical pressure is 75.15bar. From the available data, the gas will be delivered to the ALSCON pipeline at the delivery points at a maximum of 60bar. The gas temperature at the delivery points are:

- Alakiri gas source is 37.5°C
- Obigbo gas source is 46.7°C

This suggests that for optimum transmission of natural gas with the given composition and condition and to ensure that no liquid entrainment is present; the temperature of the gas should be above the cricondentherm temperatures and the pressure should be above the cricondenbar pressure values found for Alakiri and Obigbo source respectively.

However, the gas transmitted is at 37.5°C and 46.7°C for both Alakiri and Obigbo respectively, which implies that both sources are within the constraint of the temperature, which will not encourage the presence of a liquid phase in the gas. Conversely, liquid formation in the pipeline is still possible since the cricondenbar pressures are above the gas delivery pressure, this is expected because the gas is hydrocarbon wet which suggests the presence liquid hydrocarbon, hence two phase. So if there is a possibility of these undesired slugs of liquid, then a suction knock-out pots should be install as close as possible to the compressor, with drains, level detection and trip functions, in order to remove these liquid entrainment before it is allowed into a compressor.

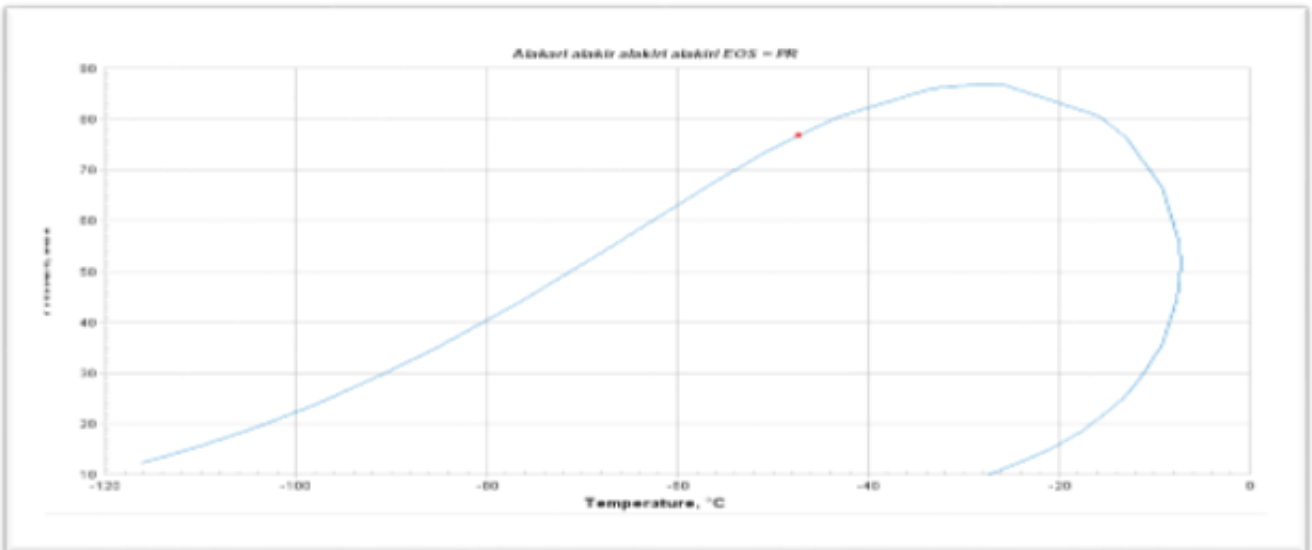


Figure 10. Alakiri Source Phase Diagram

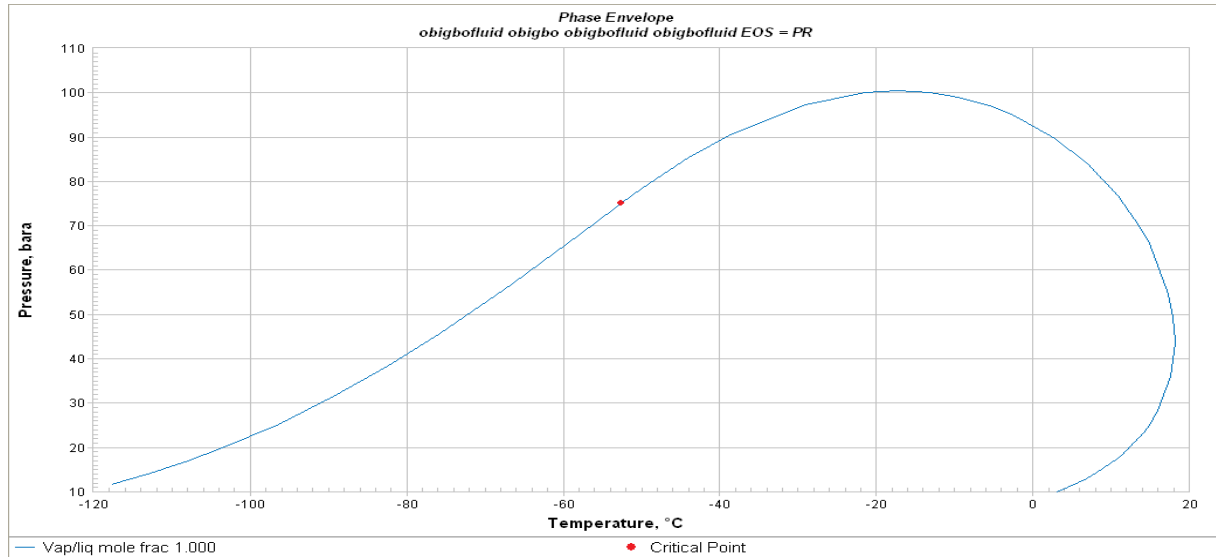


Figure 11. Obigbo source phase diagram

5.2. Steady state simulation model validation with reference to existing data

The steady state analysis was based on gas flow rate of 100MMscfd at the ALSCON terminal station. The system is designed for a maximum pressure and minimum inlet pressure of 40barg, and 25barg respectively, also, with a minimum temperature of 20°C at the ALSCON terminal. Other operating conditions are the Alakiri source temperature of 37.5°C and Obigbo source temperature of 46.7°C. The model built was compared with the existing data. Although there is no conversion from Barg (Gauge pressure) to (Absolute pressure) as atmospheric pressure changes from day to day. However, an approximate conversion can be made by simply adding 1000mBar to Barg to obtain a pressure value in Bar, with error difference of 50mBar.

After performing series of steady state simulations the figures 12 - 17 were obtained and presented below:

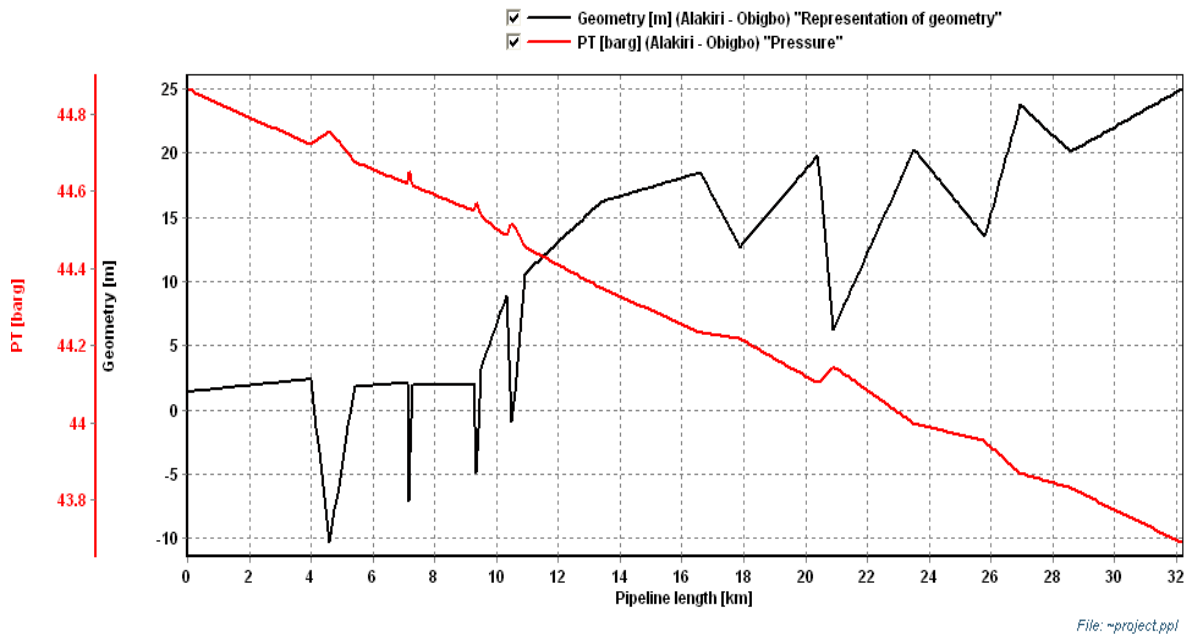


Figure 12. Pressure drop variation along Alakiri-Obigbo within the expected pressure

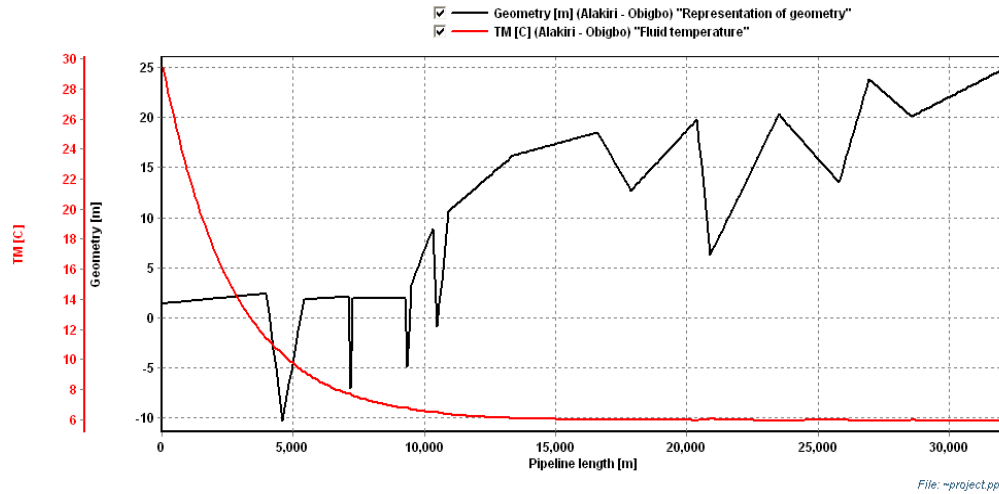


Figure 13. Temperature drop variation along Alakiri- Obigbo within the expected value

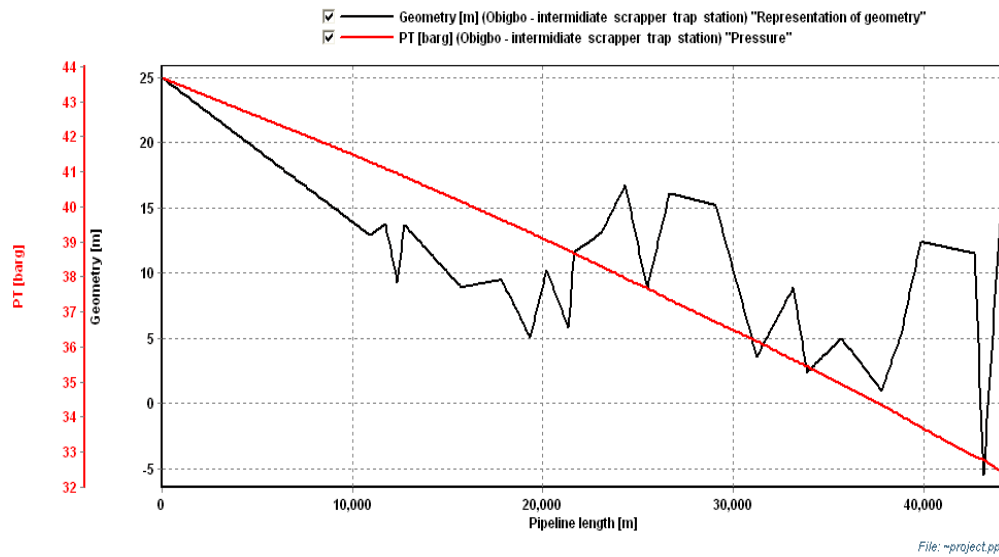


Figure 14. Pressure drop variation along Obigbo-intermediate scrapper trap station within expected value

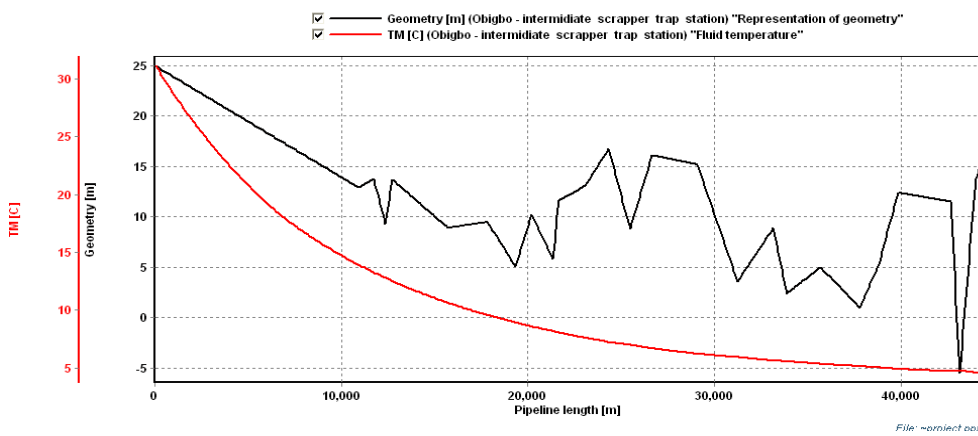


Figure 15. Temperature drop/variation along Obigbo-intermediate scrapper trap station within expected value

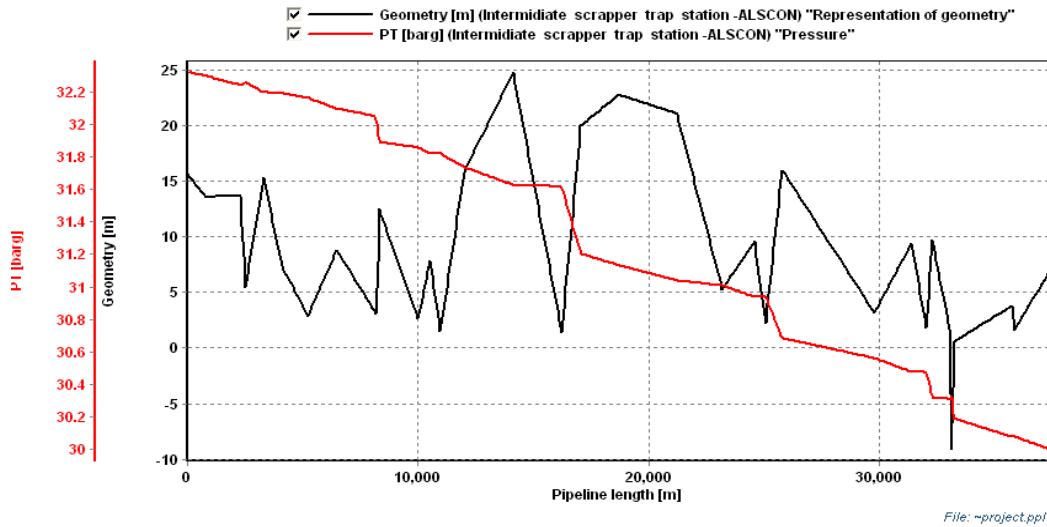


Figure 16. Pressure drop/variation along intermediate scrapper trap-ALSCON less than expected value

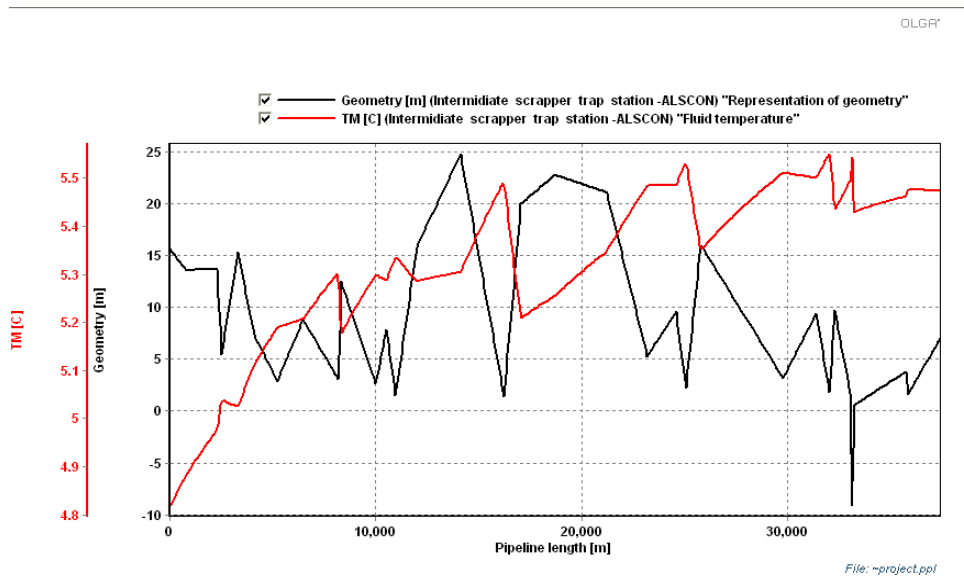


Figure 17. Temperature variation along intermediate scrapper trap-ALSCON less than expected value

Following the steady state analysis, based on gas flow rate of 100MMscfd at the ALSCON terminal. Also the system was designed for a minimum pressure of 25barg and minimum temperature of 20°C at the ALSCON terminal. Other operating conditions are that the sources, Alakiri has temperature of 37.5°C and Obigbo has temperature of 46.7°C.

The simulation results when compared with the existing data indicates that the production system is operating within the pressure and temperature constraints for each platform and the set delivery values.

5.3. Investigating hydrate risks and determining hydrate formation potential during "no touch" time of 24 hours after shutdown

After running the hydrate check simulation in OLGA, the results are presented below:

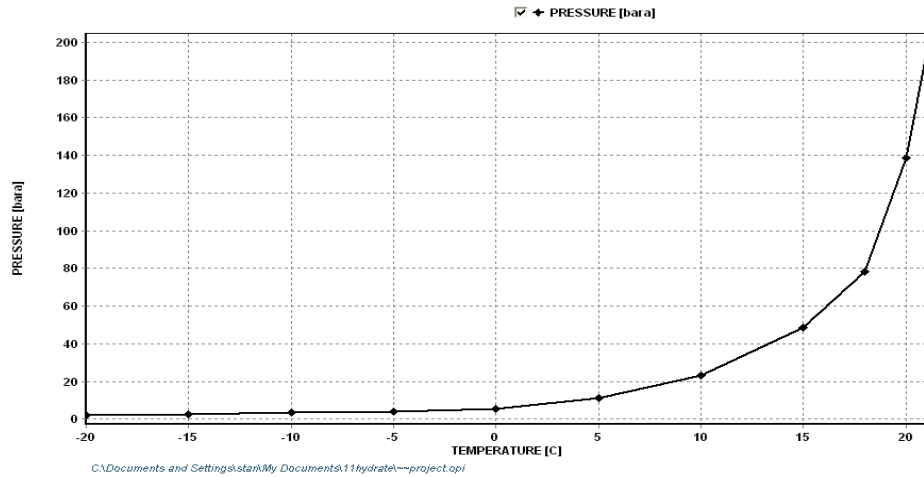


Figure 18. Hydrate curve

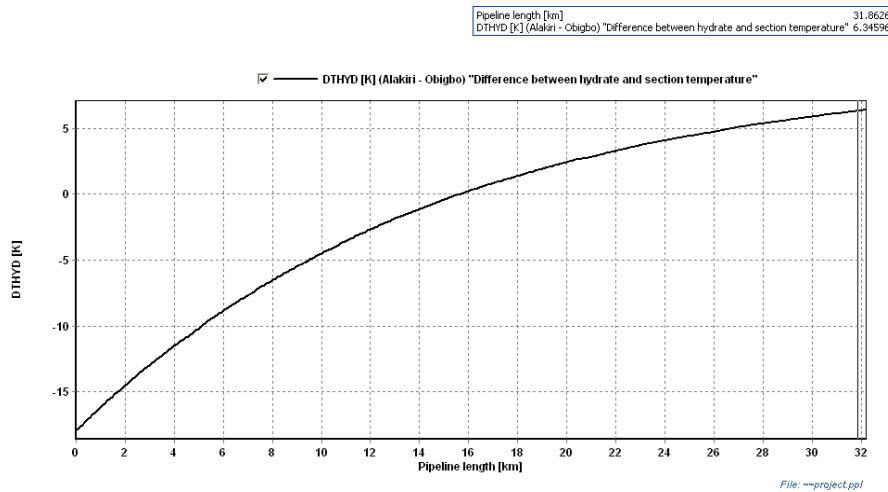


Figure 19. Alakiri – Obigbo different between Hydrate and section temperature

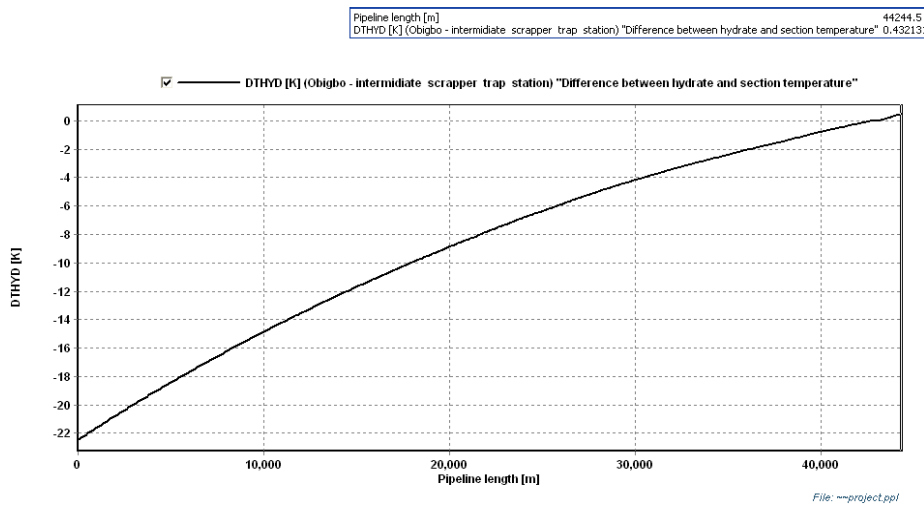


Figure 20. Obigbo - Intermediate scrapper Trapper station different between Hydrate and section temperature

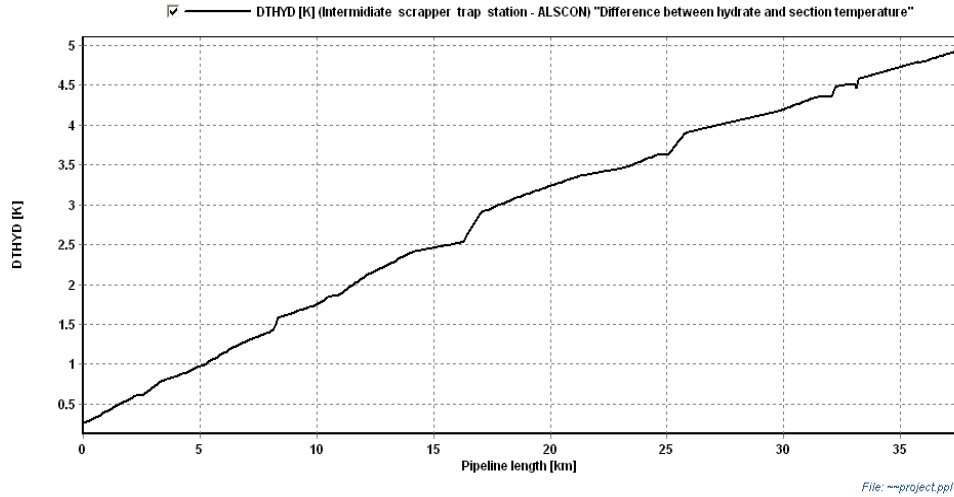


Figure 21. Intermediate scrapper trap station-ALSCON different between Hydrate and section temperature

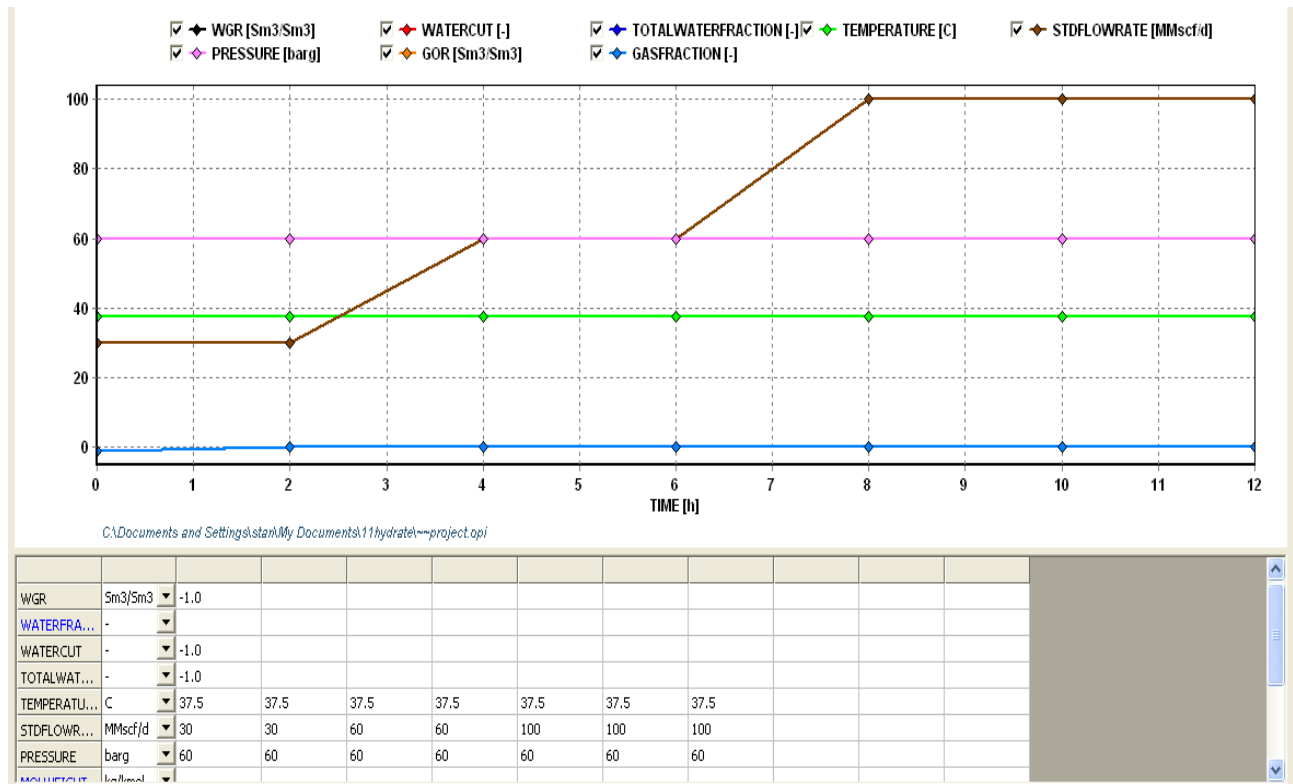


Figure 22. Alakiri Source Ramp-up

The entire pipeline segment from Alakiri - Obigbo-ALSCON was shut down after 12 hours. After a total shutdown period (no-touch time) of 24 hours. The fluid temperature for Alakiri - Obigbo pipeline segments as shown in Fig. 21 and that of Obigbo - Intermediate scrapper station pipeline segments shown in Fig. 22, indicates that they are above the hydrate formation (Difference between hydrate and section temperature is negative for these respective pipelines). Thus, the hydrate analysis before shutting down the plant indicates that no hydrate was formed along Alakiri and Intermediate scrapper station. Hence, there is no risk of hydrate formation during the operations and the shutdown period. However, Figure 23 which represent the pipeline Segment 3 indicates the possibility of hydrate formation along

Intermediate scrapper trap station – ALSCON; if the temperature drops to hydrate formation temperature more often than segment 1 and segment 2. Hence, hydrate threat is envisaged during this shutdown period.

Ramp-up simulation was done based on turndown results, in an effort to return the pipeline back to its peak flow rate. However, in this simulation analysis the flow rate will be ramped up from 30MMscfd to 100MMscfd at the Alakiri source, and then ramped up from 100MMscfd to 160MMscfd at the Obigbo source respectively for 12 hours. To have a basis for surge volume calculation different withdrawal rates were considered. The aim of this simulation is to determine the liquid rate and surge volume into the ALSCON receiving facility at different withdrawal rate.

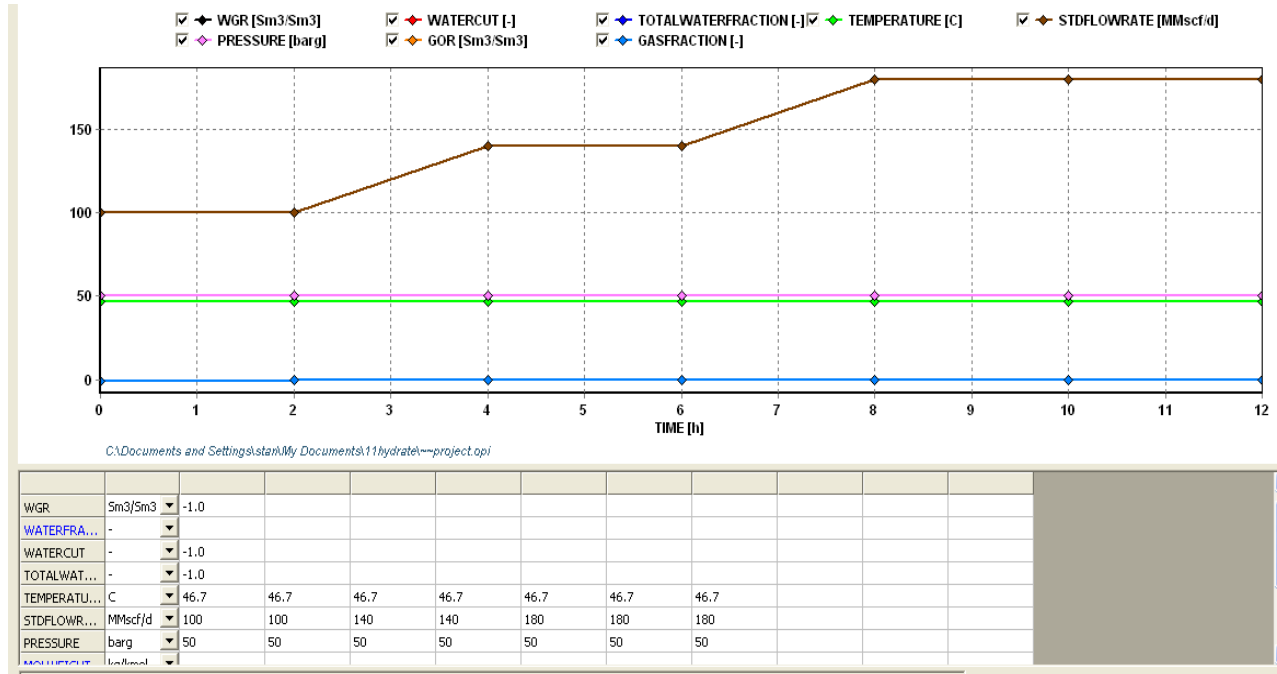


Figure 23. Obigbo Source Ramp-Up

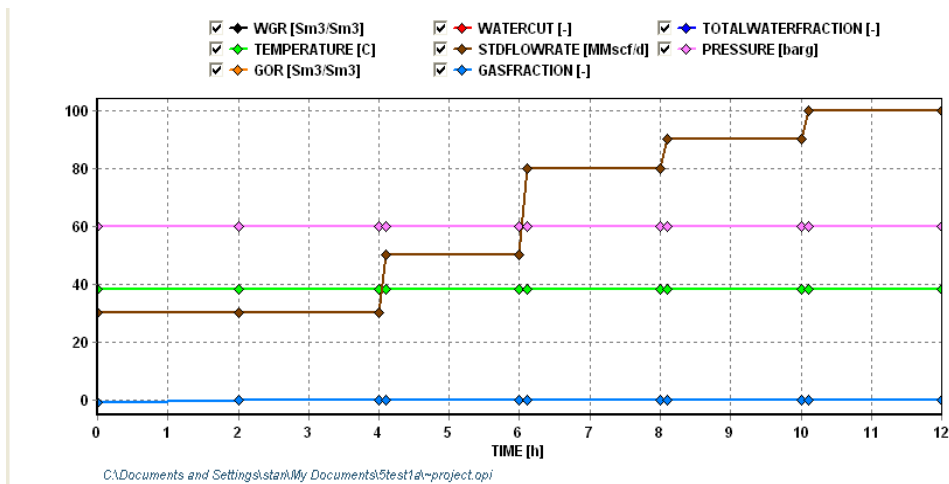


Figure 24. Ramp-up Alakiri Source

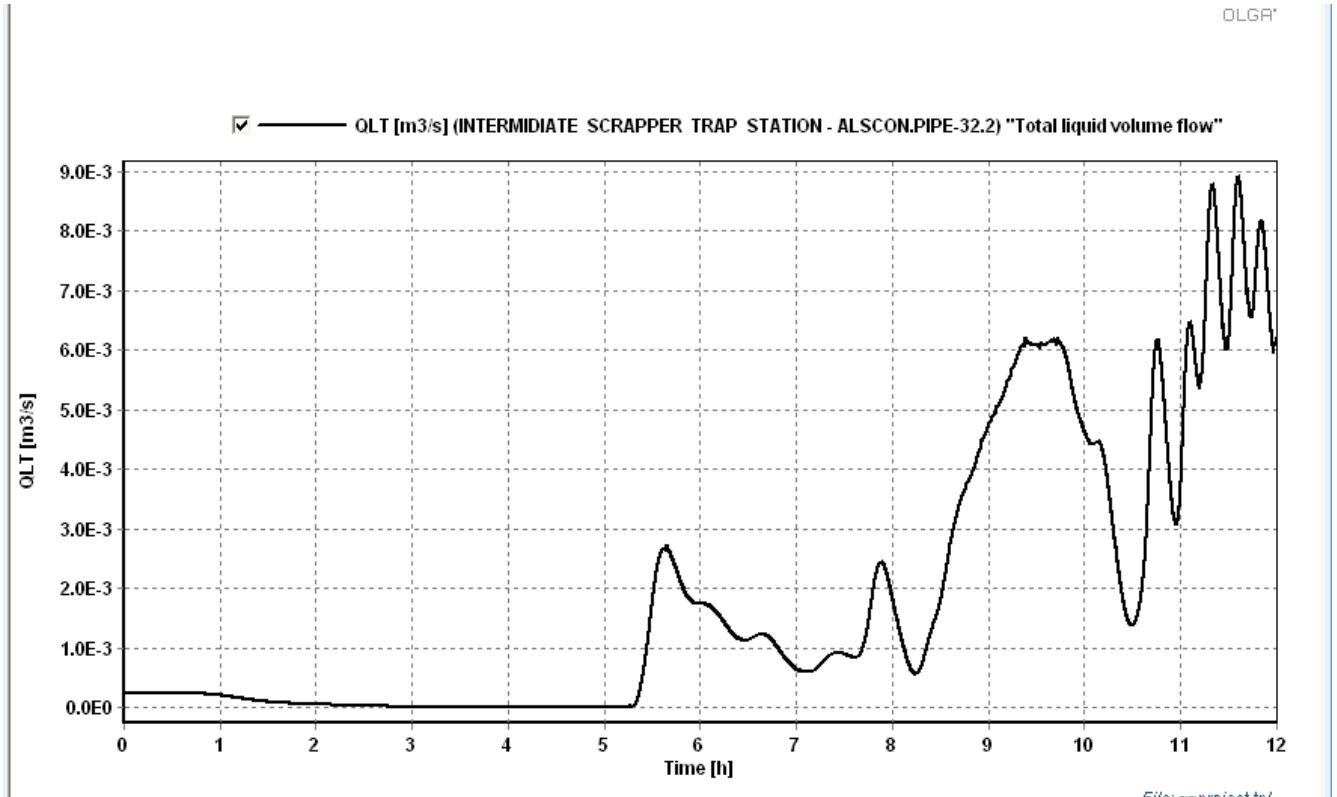


Figure 25. Total Liquid volume at ALSCON

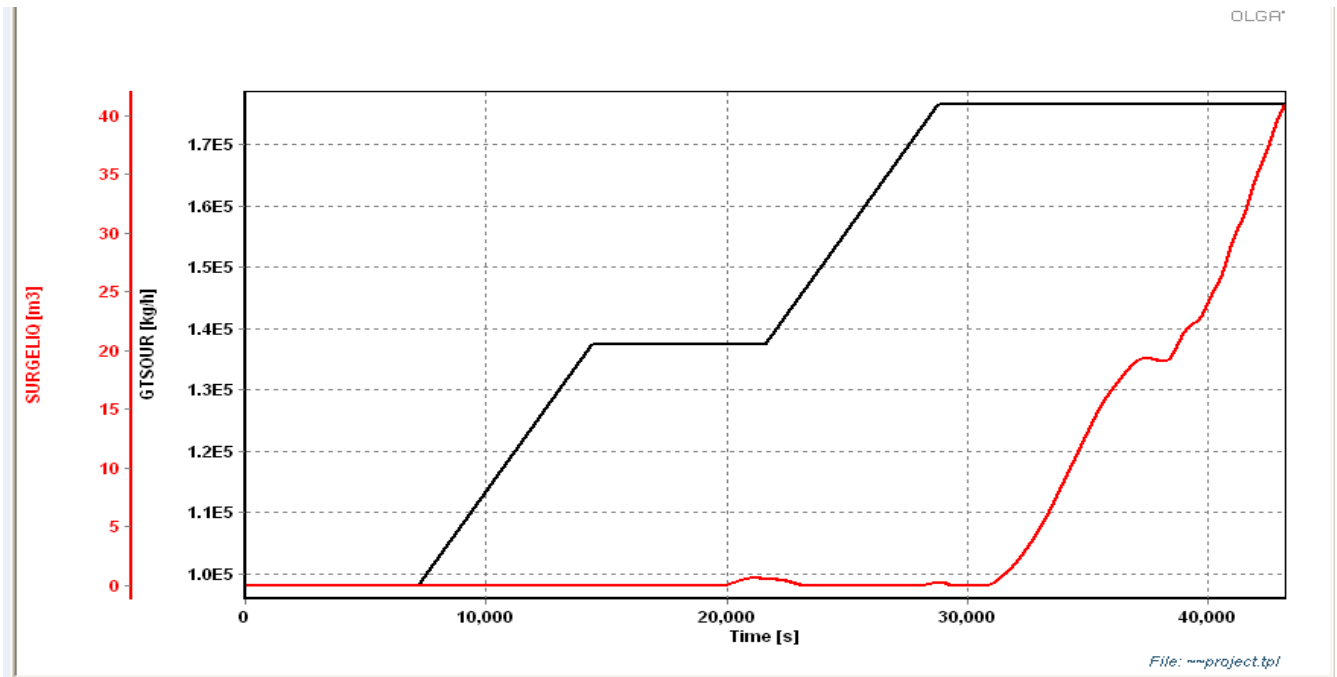


Figure 26. Obigbo Source mass rate and surge liquid volume for Intermediate scrapper trap - ALSCON

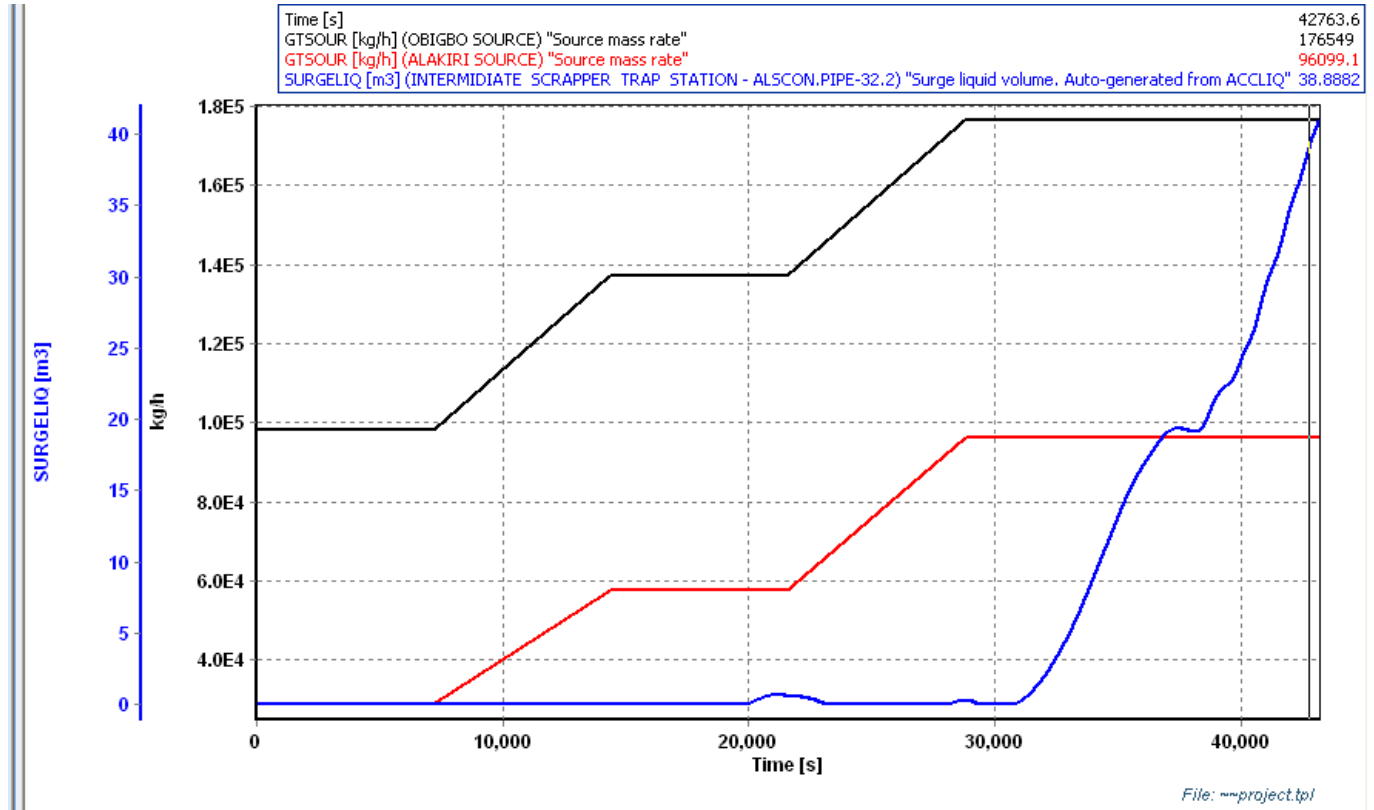


Figure 27. Alakiri Source and Obigbo mass rate and surge liquid volume for intermediate scrapper trap - ALSCON

From Figures 22 - 24, the flow rate was increase variably from 30MMSCFD to 100MMscfd at the Alakiri source while the Obigbo source was ramp up from 100MMscfd to 160MMscfd for 12 hours. Generally, lower ramp-up duration will result in rapid rate of liquid sweeping from the pipeline into the receiving facility to achieve the final flow rate of 160MMscfd. When the gas flow rate is increased, the higher gas velocity will sweep the lines for excess liquid contents. From Figures 28 and 29, we observed that the surge volume increases to 40m³ at the ALSCON terminal. The surge volume is still within the limit of the recommended slug catcher dimension size of 83m³.

Also, the pigging simulation using OLGA is intended to effectively remove condensate from the pipeline system and manage the liquid inventory associated with the maximum production rate. The aim of this pigging simulation is to determine the surge volume required at the ALSCON pipeline outlet to handle the liquid surge generated during the pigging operations. Pigging was performed on the ALSCON flow line. Prior to pigging, the ALSCON flow line has been flowing with gas from segment 1 and segment 2 at 100mmscfd. The pig was inserted at 90 minutes and the gas flow rate was kept steady at 100mmscfd.

The results are presented below:
 Where: UPIG is the Pig velocity as defined by OLGA; ZZPIG is the pig’s total distance travelled; SURGELIQ (liquid surge volume) is the required liquid surge capacity in the slug catcher.

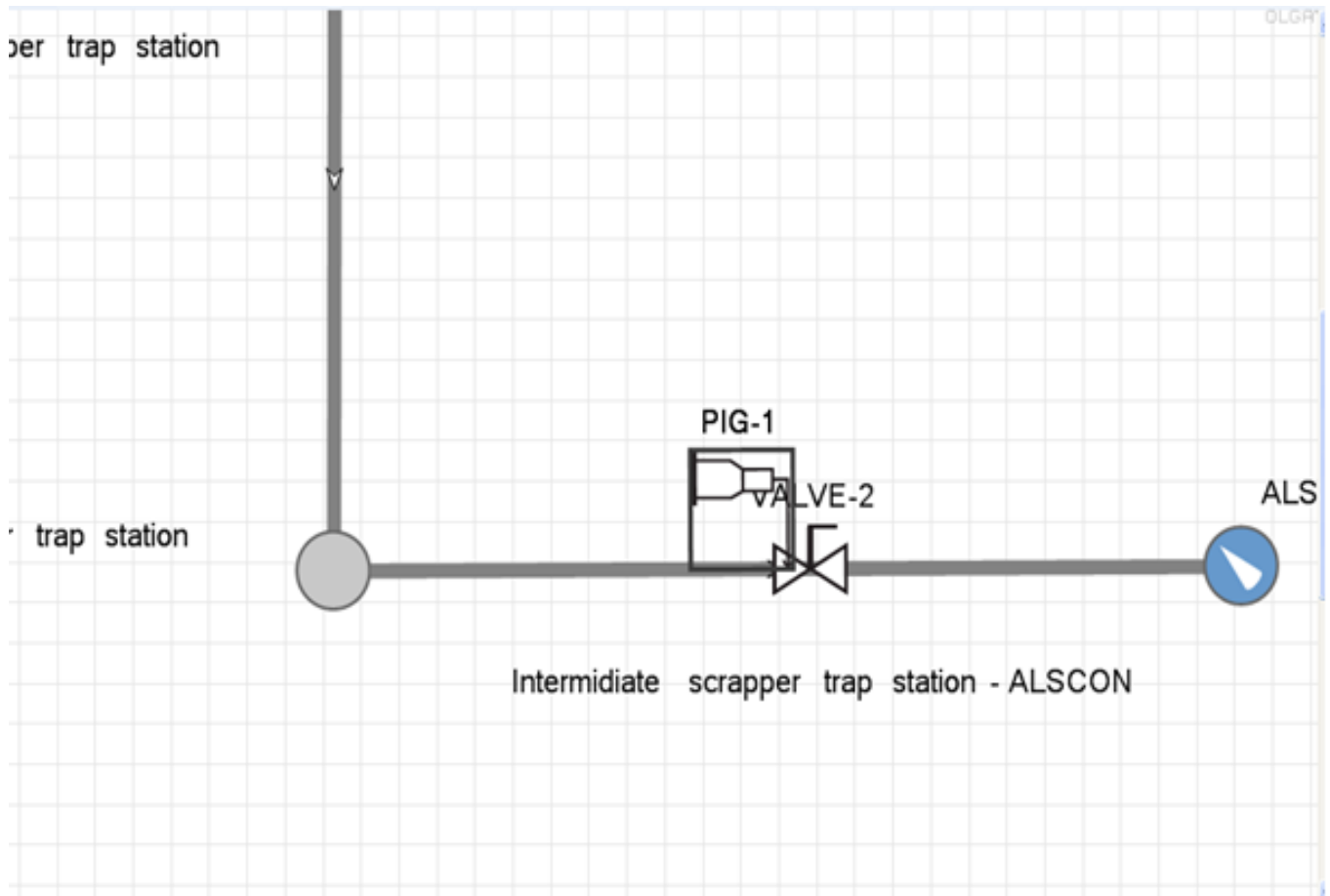


Figure 28. Pig model view 1

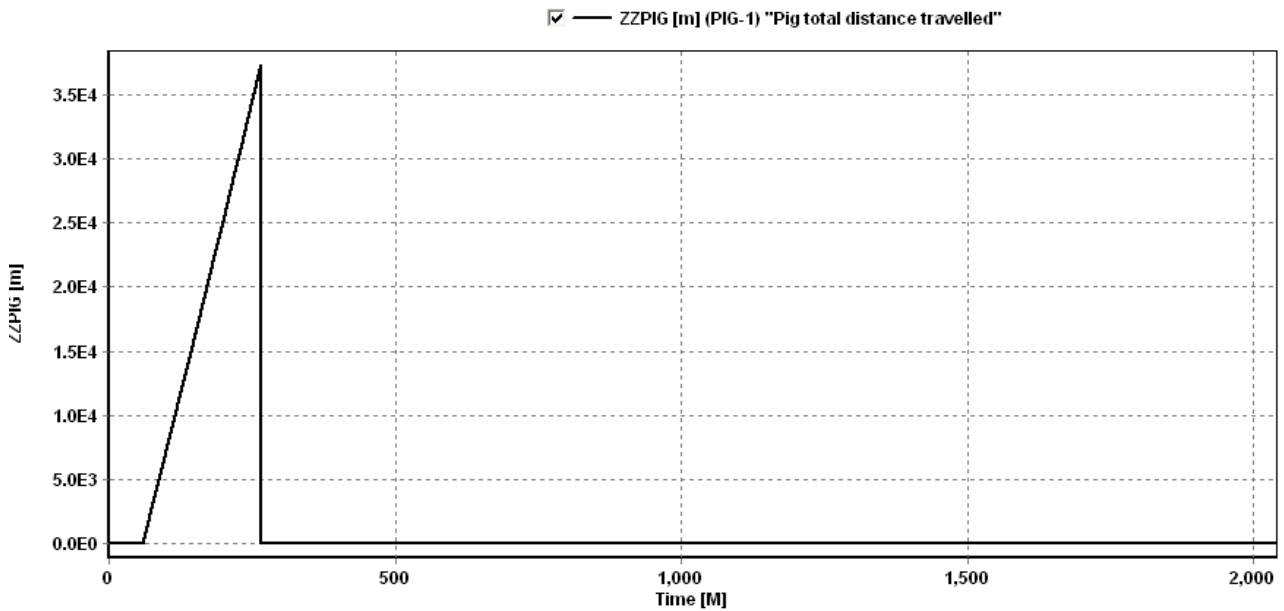


Figure 29. Pig trend plot of ZZPIG to determine when the pig reaches the trap

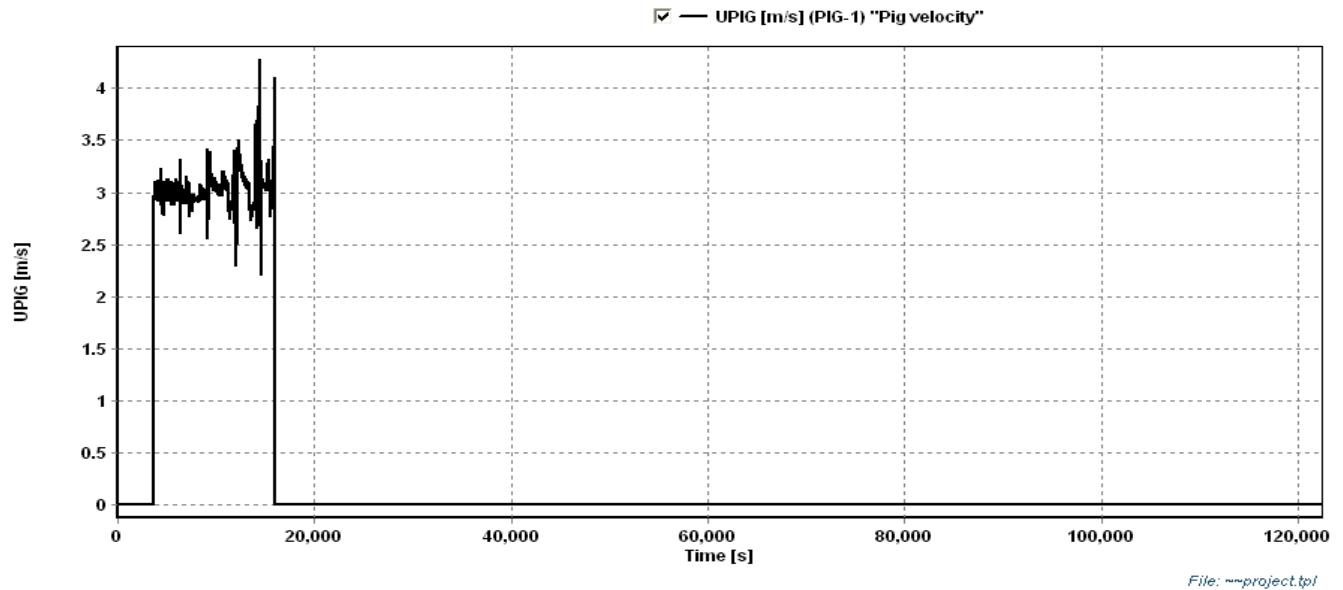


Figure 30. Pig velocity plot to determine the travelling velocity of the pig

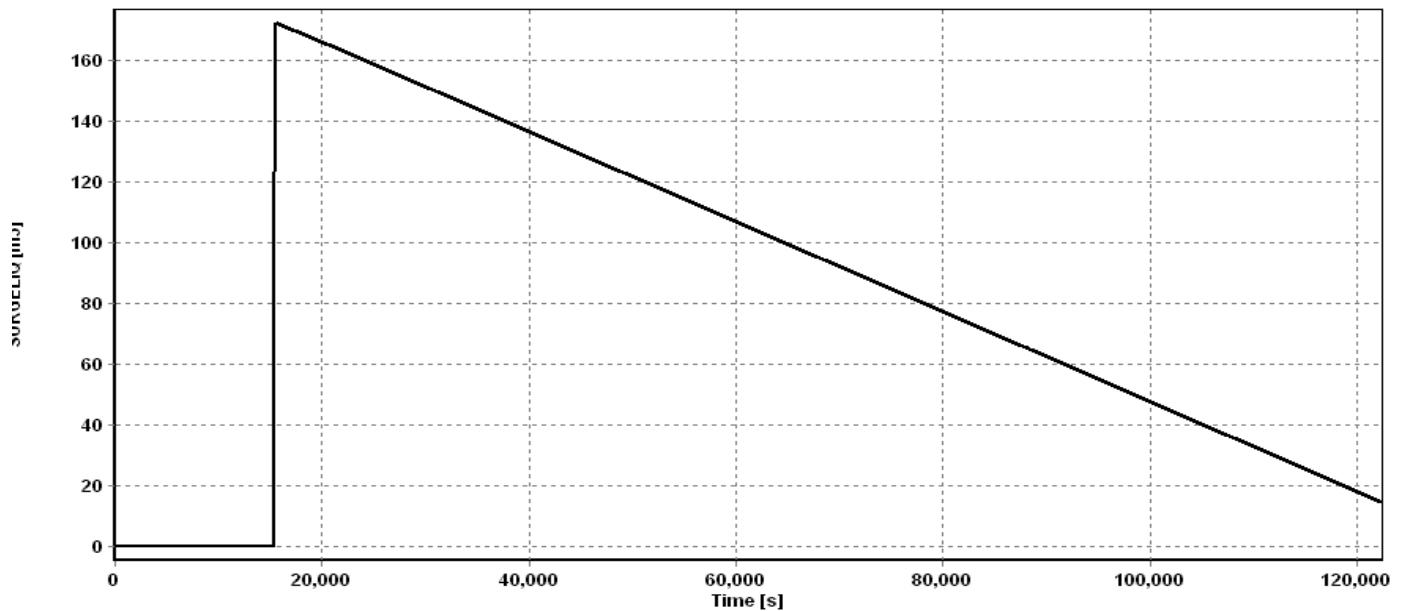


Figure 31. Plot of surge volume to determine the maximum pigging surge volume

From Figure 29, we observed that the pig reached the trap at approximately 266 minutes or 4.33 hours of simulation. The pig travelling time was verified by plotting the pig velocity as shown in Fig. 32. From the analysis shown in Figure 33, the maximum surge volume evaluated was 190m³ with a corresponding pig velocity of 4.1m/s. During the pigging operation the liquid contents in the flow line increase and expel to the slug catcher as shown in Figure 34.

From the foregoing analysis, it can be concluded that the maximum surge volume dimension of 100m³ and pig velocity of 4.1m/s values were not within the constraint for the slug catcher which was dimension for 83m³.

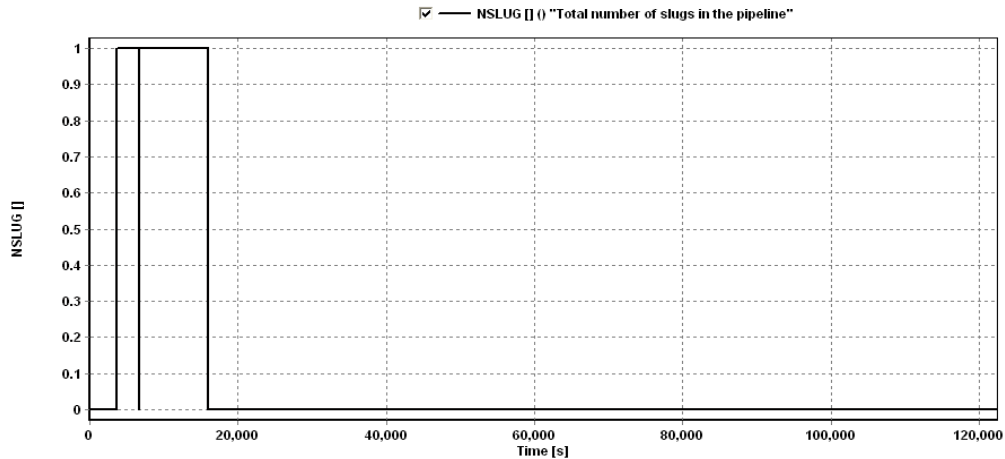


Figure 32. Plot of NSLUG to determine the total number of slugs in the pipeline

6. Conclusion

The research focus was on the Alakiri - Obigbo tie-in- Ikot Abasi, supplying gas to the Aluminum Smelter Plant (ALSCON) at Ikot Abasi. As designed, the pipeline network is about 114km which comprises of three pipeline segments.

From the phase envelope investigations, the natural gas composition used which is hydrocarbon wet suggesting two phase fluid. From the simulations the result indicates that the cricondentherm are within the constraint of the of the delivery temperature, since the cricondentherm is lower than the delivery temperatures for Alakiri and Obigbo. From the steady state analysis based on the gas flow rate of 100MMscfd at ALSCON receiving station, the production operating system is within the temperature and pressure constraints for each platform and the set delivery values, which is necessary to keep the pipeline insulation capable of preventing hydrate formation.

From the slugging analysis, hydrodynamic slugging will not be predominant for the pipeline operations at the design flow rate of 30MMscfd along Alakiri –Obigbo, and at 70MMscfd along the Obigbo Tie-in - Intermediate scrap station respectively, as the flow regimes are mainly stratified for both pipeline systems. However, slugging tendencies will be pronounced during turndown. Conversely, the Intermediate scraper trap-ALSCON pipeline segment with gas flow rate 100MMscfd is predominantly operating in the hydrodynamic slug flow regime. Therefore, this pipeline is operating under an unstable condition.

From the hydrate analysis investigated, after a shutdown period (no-touch time); hydrate threat is envisaged during the shutdown period of the Intermediate scraper trap – ALSCON along pipeline system, since the temperature drops to the hydrate formation temperature.

Acknowledgement

The authors wish to express their thanks to Department of Petroleum Engineering, Covenant University, and the entire Management of Covenant University Canaan Land Nigeria; for their support and enabling environment to embark on this study.

References

- [1] Janovic Z. Oil and Petrochemical Processes and Products II, Hrvatsko, drustvo za goriva I maziva, Zagreb, Croatia, 2005: 1-427.
- [2] Obanijesu E, Pareek V, Gubner R and Tade MO. (2011), –Hydrate Formation and its Influence on Natural Gas Pipeline Internal Corrosion RateII, NAFTA Journal, 2011; 62(5-6): 164-173.
- [3] Valmot OR. Fase to for flerfasestrøm», Teknisk Ukeblad, Published 18th March, 2013, Norway. Pp. 30-31.

- [4] Hussain M, Mansoori GA, and Ghotbi S. Phase behaviour prediction of petroleum fluids with minimum characterization data, *Journal of Petroleum Science & Engineering*, 1999; 22: 67-93.
- [5] Gupta A and Anirbid S. Need of Flow Assurance for Crude Oil Pipelines: A Review. *International Journal of Multidisciplinary Sciences and Engineering*, 2015; 6(2): 43-49.
- [6] Rojey A, Jaffret C, Cornot-Gandolphe S, Durand B, Jullian S and Valais M. *Natural Gas: Production, Processing, Transport*, Imprimerie Nouvelle, SaintJean-de-Braye, 1997, France.
- [7] Imperial Venture Corp. *Natural Gas Utilization Study: Offshore Newfoundland*, A Report Prepared for Atlantic Canada Opportunity Agencies and Newfoundland Oceanic Industries Association, 1998: 1-85.
- [8] EPA (1997) *Ground Transportation Industry*, United States Environmental Protection Agency, EPA/310-R-97-002. USA.

To whom correspondence should be addressed: Dr. Kevin C. Igwilo, School of Petroleum Engineering, Covenant University Ota, Ogun State, Nigeria

SYNERGISTIC EFFECT BETWEEN ETHOXYLATED SURFACTANTS AND COMMERCIAL ADDITIVE ON THE DECREASE POUR POINT FOR DISTILLATE FUEL OIL

T. T. Khidr, and O. A. A. El-Shamy*

Egyptian Petroleum Research Institute, Nasr City Cairo, Egypt

Received December 12, 2017; Accepted February 10, 2018

Abstract

Two non-ionic ethoxylated surfactants were synthesized and confirmed by infrared spectral analysis and used individually as decrease of pour point for fuel oil then mixed with commercial flow additive. The critical micelle concentration (CMC), the surface excess concentration, Γ_{\max} , the minimum area per molecule, A_{\min} , and the effectiveness of surface tension reduction, π_{CMC} , were calculated using surface tension data. The effectiveness of these molecules as pour point depressant for fuel oil with respect to concentration and alkyl chain length of the prepared additives were discussed. Correlation between pour point depression and wax modification appeared to be merely qualitative in such heterogeneous fuel system. From these measurements, Photomicrographic analysis showed that a clear effect of the additives on the wax crystal modification which is in agreement with above results.

Keywords: Nonionic surfactants; Distillate fuel oil; Pour point depressant; Surface activity; Photo micrographic analysis.

1. Introduction

The sedimentation of paraffin wax at low temperatures during the transportation of heavy oil difficult distillates reduces the flow rate of these fluids. The lamellar wax sedimented forming cage-like structures which impede liquid flow and tend to plug fuel lines, screens and filters [1-3]. Wax difficulty problems in distillate fuel oil can be solved partially dewaxing processes and a linear polymer with long site chains of specific length and nature is one of the general characteristic of decrement of pour point and wax dispersion for distillate fuel oil [4-6]. Generally, pour point depressants change size of wax crystals that precipitate from the oil and diminish their tendency to interlock and set into gel [7-8]. Polymeric molecules that are constituted of hydrophobic chain are used as wax deposition inhibitors which facilitate the interaction between additive, paraffin and a polar part that is in charge of for the wax crystal, morphology modulation causing aggregation inhibition. For this reason, such wax inhibitors are known as wax crystal modifiers. For evaluation of the improved operability of the treated fuel oil, determination by cloud point and pour point tests are the most widely adopted photo analysis is used also as a screening tool confirming other laboratory tests for appraisal the flow properties of attended/unattended distillate fuel oil.

The surface active agents are assessed by their adsorption behavior, which are controlled by different factors. The effect of some of these factors was dealt with by some researchers [9-10]. Nonionic ethoxylated compounds are applied in several applications as petroleum industry, corrosion, Detergents, and others [11-13].

In this manuscript, preparation and appraisal of two nonionic surfactants have been carried out. The efficiency of these surfactants as additives to improve pour point are estimated. Effect of additive kind and mixed with other commercial additive on wax modification studied. Interpenetration of synthetic and commercial additive is a helpful trend from the economic point of view.

2. Experimental

2.1. Materials and synthesis

The fatty acids, dodecyl and octadecyl acids were purchase from Aldrich Chemicals. The fatty acids were esterified by stirring with polyethylene glycol (Merck Chemicals) according to the methods that was mention before [14]. The chemical structures of the synthesized molecules (I and II) are listed in Table 1. Commercial additive (III) was purchased from Merck.

Table 1. The HLB values and surface properties of the investigated surfactants

Surfactants	Chemical Formula	HLB	T °C	CMC (mmol/L)	π_{CMC} (mNm ⁻¹)	$\Gamma_{max} \times 10^{10}$ (mol cm ⁻²)	A_{min} (Å ² /molecule)
I	C ₁₁ H ₂₃ COO(CH ₂ CH ₂ O) ₂₃ H	16.67	35	2.00	38.00	0.83	2.01
			45	1.26	37.50	0.95	1.75
			55	1.07	37.00	1.25	1.32
II	C ₁₇ H ₃₃ COO(CH ₂ CH ₂ O) ₂₃ H	15.60	35	2.51	34.50	1.15	1.44
			45	1.35	34.00	1.06	1.57
			55	1.58	33.00	1.08	1.54

2.2. Middle distillate fuel oil formation

Fuel oil sample sourced from Alexandria Company derived from the waxy western desert crude oil was used in appraisal of the performance of the synthesized additives. The physico-chemical preferential of the fuel oil are given in Table (2). In addition, the n-paraffin content of the used fuel oil tested to be specified by urea adduction [15]. Gas liquid chromatographic analysis (GLC) was applied to specify the average and distribution carbon number of the fuel oil.

Table 2. Physical characteristics of fuel oil

Properties	Methods	Result
Specific gravity at 60/60°F	IP 160/87	0.8512
Kinematics viscosity at 40°C (cst)	IP 71/80	4.7
Cloud point (cp), °C	IP 219/82	24
Pour point (pp), °C	IP 15/67(80)	15
Sulfur content (wt%)	IP 266/87	0.231
Flash point, °C	IP 34/82 (87)	123
Total paraffins content (wt%)	Urea adduct	21.3
n-paraffin (wt%)	GLC	20.9
Iso-paraffins (wt%)	GLC	0.40

2.3. Characterization of additives

The infrared spectra of sample (I) was recorded according to ATI Mattson Genesis series FTIR.

2.4. Evaluation tests

2.4.1. Pour point test (ASTM D 97 -96)

Sample of the investigated crude oil was doped individually at concentrations 200, 400, 600, 1000 and 2000ppm with each of the prepared flow additives I, II, III, (I+II) at ratio (1:1) and (I+II+III) at ratio (1:1:1) successively according to IP 15/67 procedure, results are given in Table (3).

2.4.2. Surface tension measurements

The surface tensions of the synthesized surfactants were measured in aqueous solution by DeNouy Tensiometer (Kruss K6 type) at different temperature ranged from 35, 45 and 55°C for concentration range 0.04-8 mmol/L. The ring was washed by ethanol after each reading then by distilled water. The critical micelle concentration (CMC) of the synthesized molecules were evaluated from the semi logarithmic plot of surface tension versus concentration.

Table 3. The effect of additives on the pour point of fuel oil

Additives designation	Additives	Additive concentration, ppm	PP, °C	ΔPP, °C
I	$C_{11}H_{23}COO(CH_2CH_2O)_{23}H$	0	15	0
		200	-3	18
		400	-3	18
		600	0	15
		1000	0	15
		2000	3	12
II	$C_{17}H_{33}COO(CH_2CH_2O)_{23}H$	0	15	0
		200	3	12
		400	3	12
		600	6	9
		1000	6	9
		2000	6	9
III	Commercial additive	0	15	0
		200	0	15
		400	3	12
		600	3	12
		1000	3	9
		2000	9	6
PPD4	I+II	0	15	0
		200	-3	18
		400	3	12
		600	3	12
		1000	6	9
		2000	6	9
PPD5	I+II+III	0	15	0
		200	-9	24
		400	-3	18
		600	0	15
		1000	0	15
		2000	3	12

PP = pour point, ΔPP = pour point depression

2.4.3. Photo micrographic analysis

Photomicrographs declare the independent action for wax crystallization of the attended and unattended fuel oil (FO) sample with the prepared additives at different ratios.

3. Results and discussion

3.1. Surfactant structure and characterization of the prepared additives

The chemical structure of the synthesized monoester was confirmed by the FTIR (Figure 1). Concerning the FTIR spectrum of the compounds, it is declared the following absorption bands at 2868.59 cm^{-1} (CH_2 str.), 1459.85 cm^{-1} (CH_2 bend.), 1108.87 cm^{-1} (C-O str.) and 1732.73 cm^{-1} (C=O) [16].

3.2. Evaluation of fuel oil additives

3.2.1. As pour point depressant

Results illustrated in Table 3 showed that the pour point diminishes with increasing the additive ratio. This is due to the oil solvation power. It is well known that the decrease the temperature, the decrease the solvation power of any solvent and vice versa. This depression in solvation power becomes clear when the ratio increases. Sufficient surface coverage is obtained additive (I) pour point depressant $\Delta PP = 18^\circ C$ is better in reducing the pour point than (II) $\Delta PP = 12^\circ C$. The combination of (I) and (II) at ratio (1:1) leads to reduction pour

point $\Delta PP = 18^\circ\text{C}$. This reduction may be attributed to entire solubility in hydrocarbon phase and due to interaction, that occurred between the two additives of the same class. I, II and commercial additive III in ratios (1:1:1) was added to the fuel oil, very nice result in reducing the pour point (PP) is observed. The pour point reducing effect of the mixture I, II and III is better than I and II and (I+II) additives $\Delta PP = 24^\circ\text{C}$. These results indicated that synergistic effect occurred between the pour point depressants and commercial additive in the fuel oil.

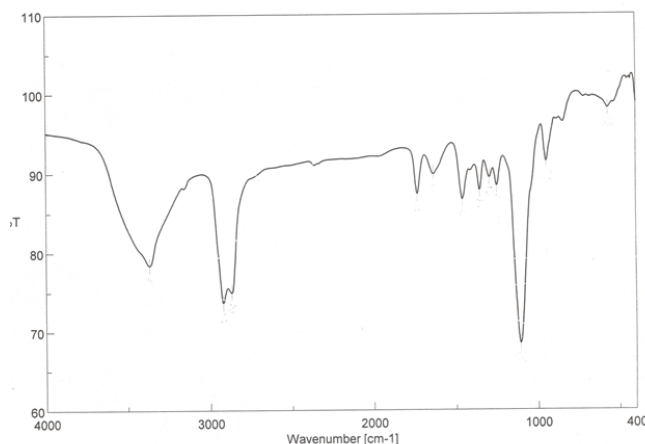


Figure 1. FTIR spectrum of an additive (I)

3.2.2. Surface properties

The CMC of the investigated surfactants at 35, 45, 55°C were calculated and listed in Table 1. By careful inspection to CMC values at 35°C, it is cleared that as the hydrophobicity decreased the CMC decreased. These linear behaviors agree with the expected trend by some investigators [17]. Also, from Table 1, it is noted that rising the temperature leads to decrease the CMC values that may be attributed to the desolvation of the surface active molecules with rising temperature [18].

The surface excess concentration Γ_{\max} in mol/cm² by applying Gibbs equation:

$$\Gamma_{\max} = -\frac{1}{2.303RT} \frac{d\gamma}{d\log C} \quad (1)$$

A_{\min} in Å²/molecule were calculated using the following relationship:

$$A_{\min} = \frac{10^{14}}{N_A \Gamma_{\max}} \quad (2)$$

Concerning the data listed in Table 1, slight increase in Γ_{\max} and decrease in A_{\min} upon raising the temperature [19]. This was expined by the priority of surfactant molecules to orientation rather than dehydration [20]. The effectiveness values (π_{CMC}), which determines their surface activity at CMCs [21] were decreased. Studies of the effectiveness of the synthesized molecules at 35°C (Table 1) decreased with increasing the hydrophobicity. The decrease in the π_{CMC} may be attributed to the increase in the area occupied at the interface. It was found that for all surfactants under investigation, π_{CMC} decreased with increasing the temperature [22].

The hydrophobic hydrophilic balance (HLB)

For an ethoxylated non-ionic surfactant, the hydrophobic hydrophilic balance were calculated from the ethylene oxide percentage of the surfactant molecules using Griffin's equation [23].

$$\text{HLB} = \frac{\text{mas\%EO}}{5} \quad (3)$$

As the HLB increase the tendency of surfactant to partition between lyophilic and lyophobic media increase (9). The data listed in Table (1) revealed that the nonionic molecules can be considered as very good wetting and detergent according to Griffin's scale (23).

3.3. Kind of additive and wax inhibition

Photomicrographs assisted in Figure 2(a-d) has showed different wax morphology changes according to the kind of surfactant. Figure 4(a) showed-like crystals of approximate size of 100µm for the untreated fuel oil which on mixed with the additive (II) at 200ppm (Figure 4c) the wax crystals were impeded into the shot pointers but still of some conglomeration degree to size of 100 µm. On using the surfactants (2000ppm from I and 2000 ppm from I+II) higher wax inhibition degree was observed and fine disband wax crystals started to appear in (Figure 2b and 2d) respectively and creation of many number of fine disbanded crystals particularly by action of additive (2000 ppm from I+II+III) Plate 1e. Concerning the correspondent flow parameter measurement, was revealed that with the increments of additive activity in term of ΔPP, the induced wax inhibition efficiency increased according to the order: I+II+III>I+II=I >II, i.e. there is good correlation between measured flow parameters and wax.

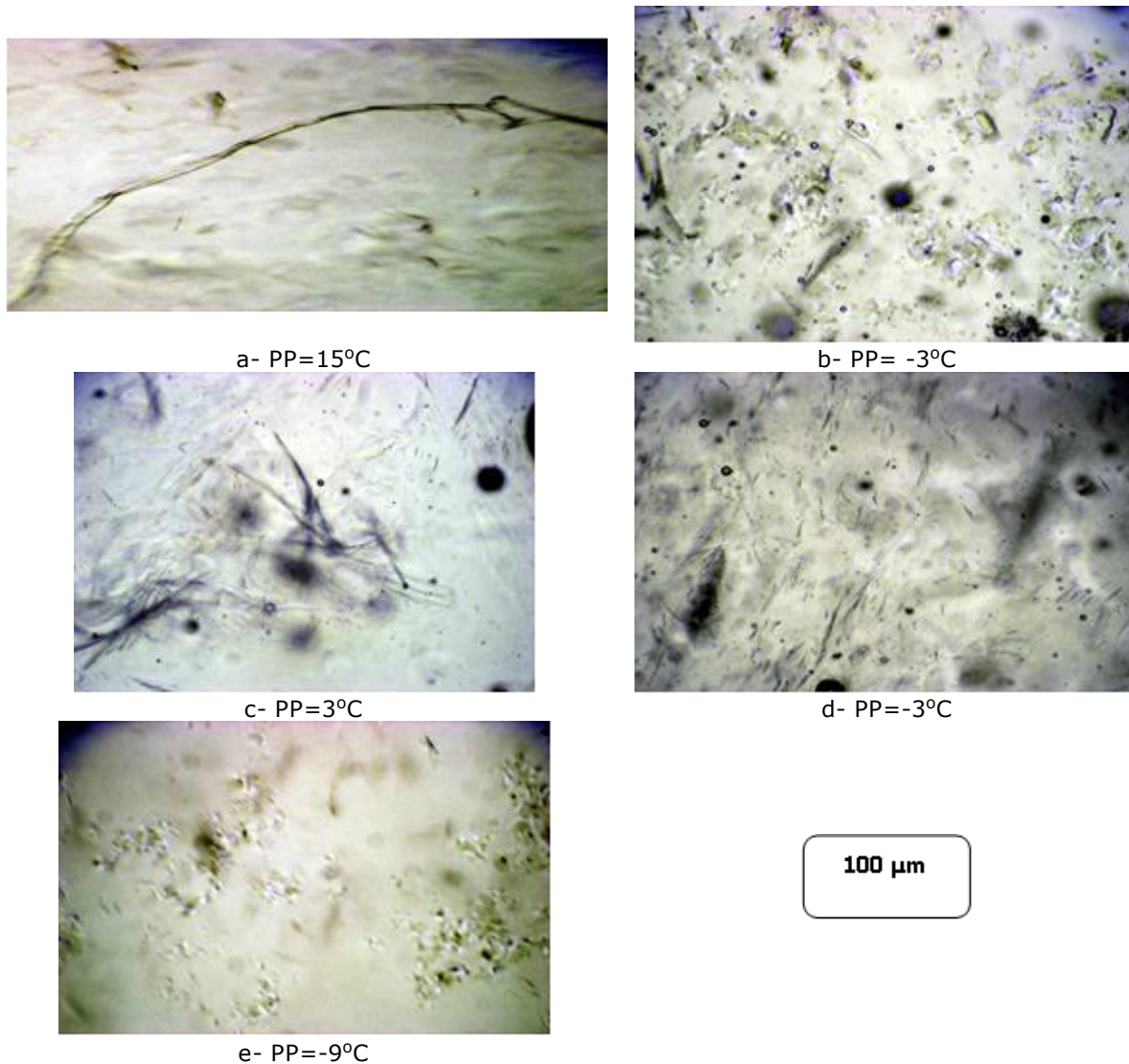


Figure 2. Photomicrographs of a: Fuel oil (FO) untreated, b: FO +200ppm (I), c: FO +200ppm (II), d: FO +200ppm (I+II) and e: FO +200ppm (I+II+III)

4. Conclusions

CMC and Γ_{\max} of the investigated surfactants were increased with increasing the hydrophobic chain length. Γ_{\max} increased while CMC decrease with increasing the temperature. Combination of commercial additive (III) with prepared additive (I+II) enhances the pour point depressant of the distillate fuel oil.

The effective of the prepared surfactants as pour point depressant diminishes by increasing the dosages and by grow thing the alkyl chain of the surfactants.

Compatibility of the combined additives in addition to bifunctionally in the one or more compound and commercial additive could be detected through photo micrographic analysis. A commit our self between the decrease of pour point for surfactant and grade of wax inhibitor has verified.

References

- [1] Khidr TT, and Omar AMA. Anionic/Nonionic Mixture of Surfactants for Pour Point Depression of Gas Oil Egyptian J. Pet., 2003; 13: 21–26.
- [2] Khidr TT, .Doheim MM and El-Shamy OAA. Effect of Ethoxylate on Pour Point Depressant of Fuel Oil. Energy Sources, Part A Recovery, Utilization and Environmental Effects, 2015; 37:1697-1703.
- [3] Al-Sabagh AM, Sabaa MW, Saad GR, Khidr TT and Khalil TM. Synthesis of Polymeric Additives Based on Itaconic Acid and Their Evaluation as Pour Point in Relation to Depressants for Lube Oil in Rheological Flow Properties., Egyptian Journal of Petroleum, 2012; 21(1): 19 -30.
- [4] Al-Sabagh, AH, El-Hamouly SH, Khidr TT, El-Ghazawy A, and Higazy SA. Synthesis of phthalimide and succinimide copolymers and their evaluation as flow improvers for an Egyptian waxy crude oil. Egyptian J. Pet., 2013; 22:381–393.
- [5] Al-Sabagh AH, El-Hamouly SH, Khidr T, El-Ghazawy A, and Higazy SA. Preparation the Esters of Oleic Acid-Maleic Anhydride Copolymer and their Evaluation as Flow Improvers of waxy Crude Oil. J. Dispers. Sci. Technol., 2013; 34:1585–1596.
- [6] Al-Sabagh AM, Khalil TM, Sabaa MW, Khidr TT, and Saad GR. Poly(n-Alkyl Itaconate-Co-Vinyl Acetate) as Pour Point Depressants for Lube Oil in Relation to Rheological Flow Properties. J. Dispers. Sci. Technol., 2012; 33:1649–1660.
- [7] Khidr TT, and Ahmed SM. The effect of Cationic Surfactant Additives on Flow Properties of Crude Oil. Petroleum Science and Technology, 2016; 34 (14): 1219-1225.
- [8] Al-Sabagh AM, Khidr TT, Moustafa HY, Mishrif MR, and Al-Damasy MH. Synergistic Effect between Surfactants and Polyacrylates-maleicanhydride copolymers to improve the Flow properties of Waxy crude oil. J. Dispers. Sci. Technol., 2017; 38:1055–1062.
- [9] Osman MM, El-Ghazawy RA, and Al-Sabagh AM. Corrosion inhibitor of some surfactants derived from maleic-oleic acid adduct on mild steel in 1 M H₂SO₄, Mat. Chem. Phys., 2003; 80: 55.
- [10] Alexandridis P, Holzwarth JF, and Hatton TA. Micellization of poly(ethylene oxide)-poly(propylene oxide)-oly(ethylene oxide) triblockcopolymers in aqueous solutions: Thermodynamics of copolymer association. Macromolecule, 1994; 27: 2414.
- [11] El-Ghazawy RA. Surface and thermodynamic properties for some polyoxyalkylenated trimethylolpropane monoester surfactants. Colloidand Surf. A: Physicochem. Eng. Asp., 2005; 260: 1
- [12] Hegazy MA, and Zaky MF. (2011) Inhibition effect of novel nonionic surfactants on the corrosion of carbon steel in acidic medium. Corr. Sci., 2011; 52: 1333.
- [13] El-Shamy OAA, Khidr TT, and Doheim MM. Effect of Ethoxylate chain length on the pour point depressant of .middle distillate fuel oil J Disp. Sci Technol., 2011; 32: 654.
- [14] Shalaby SW, McCormick CL, Butter GB. Water-soluble polymers synthesis, solution properties and application. ACS Symposium Series, Am. Chem. Soc., 1991; 467.
- [15] Marquat J, Dellow GB, and Freitas ER. Determination of normal paraffins in petroleum heavy distillates byurea adduction and gas chromatography. Anal. Chem., 1968; 40: 1633–1637.
- [16] Bellamy LJ. The infrared spectra of complex molecule, 3rd ed., London, Chapman & Hall, 1975.
- [17] Dai S, and Tam KC. Isothermal Titration Calorimetry Studies of binding interactions between polyethylene glycol and ionic surfactants. J. phys.Chem. B., 2001; 105: 10759.
- [18] Inoue T, Nakashima K, and Szuki M. Surface tension study on aqueous solution of nonionic surfactant with unsaturated hydrocarbon chain. J. Oleo Sci., 2002; 51: 753.

- [19] Hafiz AA, and Khidr TT. Hexa-triethanolamine oleate esters as pour point depressant for waxy crude oils. *J. of Petro. Sci. and Eng.*, 2007; 56: 296.
- [20] Hua XY, and Rosen MJ. Calculation of the coefficient in the Gibbs equation for the adsorption of ionic surfactants from aqueous binary mixtures with nonionic surfactants. *J. Colloid Interf. Sci.*, 1982; 87:469.
- [21] Rosen MJ. *Surfactants and Interfacial phenomena*. John Wiley & Sons, New York, 1978.
- [22] Flanders D, Sornoson BM, and Shen CK. *Advanced-Imaging*, 1997; 12:55.
- [23] Lissant KJ. *Surfactant Science V6 "Emulsion and Emulsion Technology, Part 1*, Marcel Dekker, IVC, New York, 1974.

To whom correspondence should be addressed: prof. O. A. A. El-Shamy, Egyptian Petroleum Research Institute, Nasr City Cairo, Egypt, omniaelshamy@yahoo.com

NON-STATIONARY MATHEMATICAL MODEL OF INDUSTRIAL DIESEL FUEL HYDROTREATING PROCESS

Anton A. Tataurshchikov, Nadezhda I. Krivtcova*

Tomsk Polytechnic University, Russia

Received December 17, 2017; Accepted February 15, 2017

Abstract

Catalytic hydrotreating is widely used in secondary petroleum refining industry. The main purpose of this process is to significantly lower sulfur content in the petroleum products. Currently, there is a lack of industrially applicable mathematical models of diesel hydrotreating, especially the models which take into account the reaction kinetics and catalyst deactivation.

In this paper, research is focused at processing of experimental data from laboratory equipment and industrial hydrotreating unit and developing mathematical model, which adequately describe industrial data of hydrotreating industrial unit with the use of current view of chemical mechanism and catalyst deactivation.

Keywords: Mathematical modeling; programming; hydrotreating process; diesel fraction; benzothiophene; dibenzothiophene; reaction rate constant; activation energy.

1. Introduction

Hydrotreating of diesel fraction is used to remove heteroatoms (including atoms of sulfur, nitrogen and oxygen), polycyclic aromatic hydrocarbons and metals [1-4]. Concentration of these compounds is rising accordingly with a boiling temperature of the fraction [5-7]. The industrial process of hydrotreating is performed in relatively mild conditions but yet should be effective – conversion rate of the diesel fraction should not be lower than 98-99% [8-10]. The most general purpose of this process is to significantly reduce a sulfur amount in a wide range of petroleum products including naphtha, diesel, gas-oil, kerosene and heavy oil fractions which consequently are used as a raw material for catalytic processes [11-12]. This prevalence of catalytic hydrotreating have such origins as, firstly, introduction of more high-sulfur crude oils extraction into petroleum refining industry all over the world in the last years [13-15], and, secondly, economically disadvantageous catalyst poisoning in consequent of refining processes, such as gasoline reforming and catalytic hydrocracking [16]. The third main reason is the introduction of strict environmental requirements to the content of heteroatom substances in fuel, as well as aromatic hydrocarbons amount [17]. All these reasons dictate the necessity not only for a wider use of hydrotreating process, but also more complex research of deep heterocatalytic mechanisms, including mathematical modeling, which could help in optimization of the process, development of new catalysts and proposal of new reactor construction concepts [18]. Use of mathematical modeling method allows researchers to predict new conditions and product quality, develop new proposals for industrial process optimization [19-21].

The aim of this research is to develop a dynamic mathematical model of diesel hydrotreating reactor with non-stationary material balance and thermal balance including calculation of coke formation.

2. Object of research

Technological scheme of the typical hydrotreating unit is shown in Figure 1. In the most general case the raw material arrives to the hydrotreating reactor "R" after being pre-heated

in the furnace "F". Reactor is the major part of the whole process, where the catalytic hydrotreating of diesel fraction is performed. A group of reactions of hydrogen sulfide formation from sulfur compounds are occurring on the surface of the hydrogenation catalyst. The hydrogen-containing gas (HCG) is separated from the vapor-liquid mixture in the separators "S-1" and "S-2" and enters the column "C-2" for recovery of pure hydrogen. Column "C-1" is used for separation of vapor-liquid mixture to a gas fraction and the main product – hydrotreated diesel fuel [22].

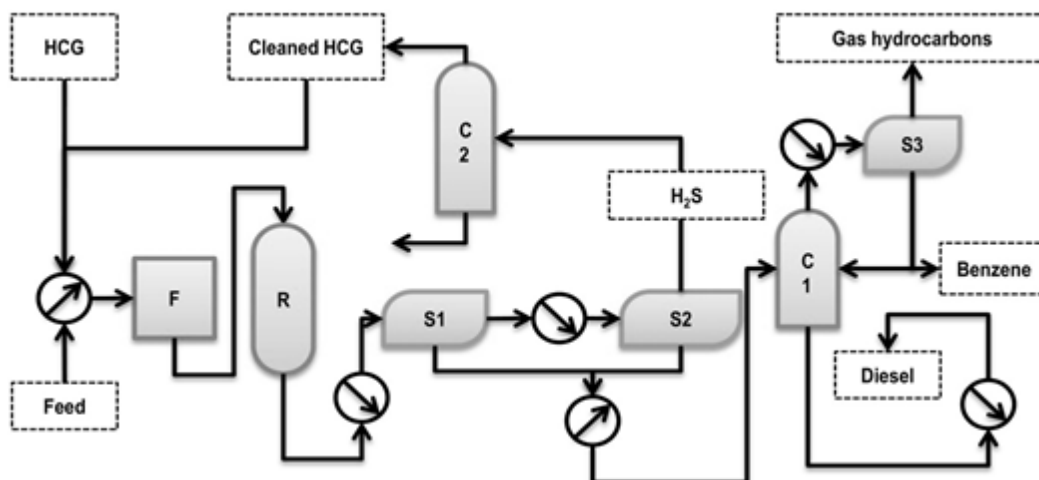


Fig. 1. Scheme of the typical hydrodesulfurization unit. Note: circles with arrow faced upwards are heaters; downwards – coolers

The plant uses catalyst HR-538 manufactured by Axens (France). Properties of the catalyst are given in Table 1. The catalyst activity towards certain sulfur-containing compounds is counted as part of the effective rate constants, which was calculated previously [23-24].

Table 1. HR-538 catalyst properties

Diameter of catalyst particles, mm	1.2; 1.6; 2.5
Composition:	
Nickel (NiO), % mass.	3.5
Molybdenum (MoO ₃), % mass.	17.0
Surface, m ² /g	210

The data which was used to calculate kinetic parameters for developed model was obtained both from laboratory equipment and from industrial hydrotreating and deparafinization unit. The laboratory experiment was performed with use of such equipment as gas-liquid chromatograph unit "Kristal-2000M" to measure sulfur-containing substances concentrations in diesel product.

The fixed-bed mini-reactor was used to simulate industrial hydrotreating process in the laboratory. Fraction of diesel fuel (boiling range is 180–320 C) with a total sulfur content of 1.4%wt. was used as the feed for the reactor. Al-Ni-Mo catalyst was used in the laboratory setup which consists of a flow system with an evaporator, reactor with a special metal grid where the catalyst was placed onto. The products of reaction were received into a condenser. The hydrotreating process was carried out with 10 mL of the Al-Ni-Mo HR-538 catalyst loaded onto a metal grid of mini-reactor in the form of granules with a diameter of 1-2 mm.

The feed and hydrogen ran through a reactor from the top to the bottom. Diesel fraction was fed to the reactor with a high pressure dosing pump. Pure hydrogen supply was controlled with automatic dispenser. The temperature in the reactor was supported on desired level by an air thermostat. Temperature controller provides heating accuracy not worse than $\pm 0.5^\circ\text{C}$. Thermocouple was used to measure the temperature in the catalyst bed. Catalyst was placed

in a pocket at the center of the reactor. The system pressure was set with a high-pressure reducer at the end of product flow.

In current laboratory setup the water-cooled condenser is used to gather products of hydrotreating from the reactor. Then, liquid products were gathered to the receiver for further analysis. Unlike liquid products, gases were released to the atmosphere through six-way valve.

Before an experiment the process of catalyst sulphidation was performed in the reactor. This process involved a straight-run diesel fraction as a sulphiding feed. Sulphur concentration in the feed was approximately 0.4% mass. Sulphidation was performed with the next steps and conditions:

1. Catalyst drying using nitrogen gas stream with the temperature of 120°C;
2. Increase of the pressure in the reactor to 3.5 MPa and start of hydrogen feed;
3. The catalyst wetting by raw diesel fraction;
4. Increase of the temperature to 240°C;
5. 2-hour sulphidation process under 240°C (phase of low temperature);
6. Increase of the temperature to 340°C;
7. 2-hour sulphidation process under 340°C (the phase of high temperature);

Feed ran through the reactor with 2 h⁻¹ volume velocity. Volume ratio of hydrogen to the diesel was: H₂/feed=300/1. After being sulphided the catalyst is ready to operate in hydrodesulphurization process under the next conditions:

Table 2. In-laboratory hydrodesulphurization conditions

Volumetric flow rate of feed	2 h ⁻¹ (relatively to catalyst's volume)
Pressure	3.5 MPa
Hydrogen/Diesel volume ratio	300/1
Temperatures	340°C, 360°C, 380°C

Spectral photometer "Spectroscan-S" was used to determine and measure the initial containment of sulfur in diesel fuel.

The method of gas-liquid chromatography was used to measure concentrations of sulfur in the products according to their homologue groups. Method of GLC was performed using a "Crystal-2000M" chromatograph. It has a quartz column with 25 m × 0,22 mm dimensions. Helium is used as a carrier gas. Under a temperature increase in the column of "Crystal-2000M" with a 4 degree/minute rate the flame photometric detector was used for analysis of sulfur compounds in products of desulfurization.

3. Experimental

3.1. Thermodynamics and chemical mechanism

Sulfur compounds are present in diesel fractions mainly in the form sulfides, homologues of thiophenes and, in lesser amounts, by mercaptanes and disulfides. In general, the initial stage of mathematical model development is the thermodynamic calculation. This stage is based on the physical and chemical laws and ensures a high degree of model's accordance to the real hydrotreating process.

In the frame of current research the thermodynamic parameters were calculated including Gibbs energy and enthalpy for each individual reaction of hydrodesulfurization of sulfur-containing-compounds [25]. In this work, the thermodynamic parameters of the hydrotreating process, including enthalpy, entropy, Gibbs energy were calculated using a computer program packages "GaussianView" and "Gaussian 09". The calculation method of DFT (Density Functional Study) was used. B3LYP model was chosen as a theoretical approach, as well as density functional theory (B3) and the electronic correlation (LYP). Basis is the set 6-311G. There were also the hydrotreating process conditions under which the calculation was performed, including a temperature of 340°C and a pressure of 3 MPa. Results of thermodynamic calculations of hydrogenation and hydrocracking reactions of several sulfur-containing compounds representatives are presented in Table 3.

Table 3. Values of enthalpy and Gibbs energy of sulfur compounds' hydrogenation reactions

Sulfur compounds group	Reaction	ΔH , kJ/mole	ΔG , kJ/mole
Sulfides	$C_5H_{11}SC_5H_{11} + H_2 \rightarrow C_5H_{11}SH + C_5H_{12}$	-65.60	-81.32
	$C_5H_{11}SH + H_2 \rightarrow C_5H_{15} + H_2S$	-67.66	-77.45
	$C_5H_{12}SC_5H_{12} + 2H_2 \rightarrow 2C_5H_{12} + H_2S$	-133.26	-158.77
Mercaptan	$C_2H_5SH + H_2 \rightarrow C_2H_6 + H_2S$	-67.29	-78.35
Disulphides	$CH_3SSC_4H_9 + H_2 \rightarrow CH_3SH + C_4H_9S$	-38.39	-57.74
	$CH_3SH + H_2 \rightarrow CH_4 + H_2S$	-78.46	-76.61
	$C_4H_9SH + H_2 \rightarrow C_4H_{10} + H_2S$	-55.41	-70.00
	$CH_3SSC_4H_9 + 3H_2 \rightarrow CH_4 + C_4H_{10} + 2H_2S$	-172.25	-204.35
Thiophenes	$C_4H_4S + 2H_2 \rightarrow C_4H_6 + H_2S$	-78.56	-52.47
	$C_4H_6 + H_2 \rightarrow C_4H_8$	-121.06	-62.89
	$C_4H_8 + H_2 \rightarrow C_4H_{10}$	-111.04	-46.92
	$C_4H_4S + 4H_2 \rightarrow C_4H_{10} + H_2S$	-310.66	-162.29
Benzothiophenes (BT)	$C_8H_6S + H_2 \rightarrow C_8H_8S$	-78.97	-17.96
	$C_8H_8S + H_2 \rightarrow C_8H_{10}S$	-50.61	-13.21
	$C_8H_{10}S + H_2 \rightarrow C_8H_{10} + H_2S$	-72.00	-84.16
	$C_8H_6S + 3H_2 \rightarrow C_8H_{10} + H_2S$	-201.58	-115.33
Dibenzothiophenes (DBT)	$C_{12}H_8S + H_2 \rightarrow C_{12}H_8 + H_2S$	-94.79	-64.99

On the basis of the data presented in Table 3 the next law is predicted: the rate of hydrogenation of sulfur compounds decreased in the series: sulfides > benzothiophenes > dibenzothiophenes, which is also confirmed by related data in the literature [26-28].

Like any process of secondary refining, hydrotreating of diesel fuel involves a large amount of chemical reactions which occur simultaneously. The so-called aggregation of different sulfur-containing components to the homologue groups is made to reduce the number of individual reaction components and, thus, reduce the amount of calculations. Any mathematical model must keep predictive power [29]. In addition, it must to remain being sensitive to the feed composition changes through hydrotreating unit's operational cycle.

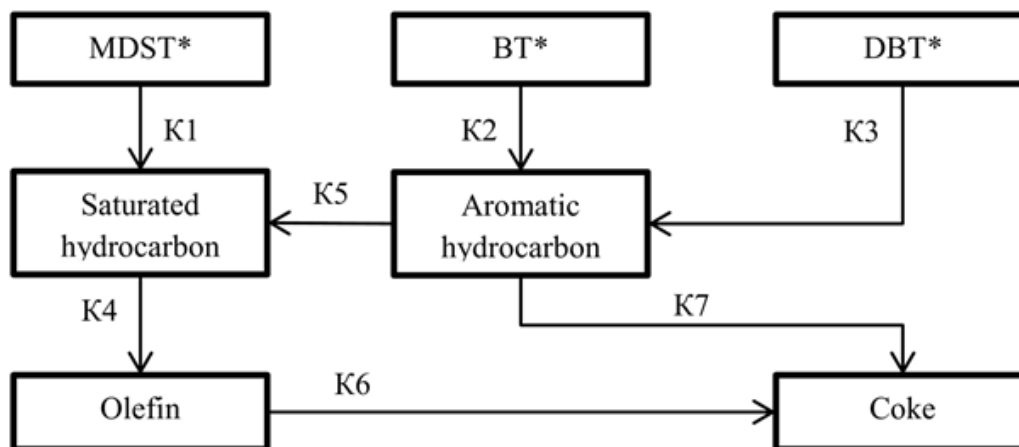


Fig. 2. Formalized kinetic scheme of hydrodesulfurization reactions* MDST –mercaptan, sulfide, disulfide, thiophene; BT – benzothiophene; DBT – dibenzothiophene

On the basis of thermodynamic parameters calculations a formalized kinetic scheme of substances transformations had been created (Fig. 2.).

All sulfur-containing substances (including mercaptanes, sulfides, disulfides, thiophenes, benzothiophene and dibenzothiophene) were joined together into separate groups (or "pseudo-components"). The rule of isobaric-isothermal potential of hydrogenation was used. Additional data on the role and kinetic parameters of saturated hydrocarbons, arenes and olefins in the process of hydrogenation was gathered from literature [30-34].

3.2. Mathematical model

The basis of the developed mathematical model is built on the hydrotreating reaction of individual groups of organic sulfur compounds such as sulfides, benzothiophene, dibenzothiophene. Also, the model takes into account hydrogenolysis reaction products: saturated and aromatic hydrocarbons.

The developed mathematical model based on the law of mass action and is a system of differential equations, which reflect changes in the concentrations of the reactants. Thus, the mathematical model performs a material balance calculation of sulfur compounds during hydro-treating.

Table 4. Material and thermal balance

Reaction rate equations	Differential equations
	$G * \frac{\partial C_{MDST}}{\partial Z} + G * \frac{\partial C_{MDST}}{\partial V} = -A_1 * W_1$
	$G * \frac{\partial C_{BT}}{\partial Z} + G * \frac{\partial C_{BT}}{\partial V} = -A_2 * W_2$
	$G * \frac{\partial C_{DBT}}{\partial Z} + G * \frac{\partial C_{DBT}}{\partial V} = -A_3 * W_3$
	$G * \frac{\partial C_{SHC}}{\partial Z} + G * \frac{\partial C_{SHC}}{\partial V} = A_1 * W_1 + A_5 * W_5 - A_4 * W_4$
	$G * \frac{\partial C_{Arom}}{\partial Z} + G * \frac{\partial C_{Arom}}{\partial V} = A_2 * W_2 + A_3 * W_3 - A_5 * W_5 - A_7 * W_7$
	$G * \frac{\partial C_{Olefins}}{\partial Z} + G * \frac{\partial C_{Olefins}}{\partial V} = A_4 * W_4 - A_6 * W_6$
	$G * \frac{\partial C_{Coke}}{\partial Z} + G * \frac{\partial C_{Coke}}{\partial V} = A_6 * W_6 + A_7 * W_7$
	(there: <i>Arom</i> – aromatic hydrocarbons)
	Thermal balance
	Initial conditions
	$Z = 0; t = 0$ $V = 0; C_i = C_{i,0}$ $T = T_0$

there: Z – the volume of total refined feed, m^3 ; V – volume of catalyst, m^3 ; k_i – chemical rate constant, h^{-1} ; C_i – the current concentration of the substance i , mole/ m^3 ; ν – the stoichiometric ratio; A_i – relative catalyst activity towards certain route i ; t – reaction time, h ; ρ – amount of pseudo-components; W_i – chemical reaction rate on the route i ; Q_i – thermal effect of chemical reaction on the route i , $kJ/mole$; G – feed flow rate, m^3/h .

3.3. Experimental data

Experimental data was obtained both from laboratory equipment and industrial hydro-treating unit monitoring database. The excerpt of laboratory data is shown in the Table 5

Table 5. Laboratory experiment results: initial and final concentrations of sulfur-containing compounds in diesel fraction

Component	Initial	Temperature, °C		
		340	360	380
Mass concentration, % mass. · 10 ⁻³				
MDST	218.00	17.46	17.52	14.74
C1-BT	35.00	1.87	1.72	2.07
C2-BT	200.00	12.47	12.70	15.16
C3-BT	351.00	21.95	22.34	22.90
(C4+C5)-BT	372.00	22.01	23.50	18.72
DBT	40.00	3.00	3.56	2.77
C1-DBT	87.00	7.05	9.52	6.49
C2-DBT	82.00	7.77	10.32	7.29
C3-DBT	19.00	4.72	4.72	3.87
Total sulphur	1404.00	98.30	105.93	94.01

The industrial data includes operational conditions for each day of unit operation. These conditions include diesel fraction feed flow rate, initial sulfur content, pressure, temperature of the feed and products, as shown in the Table 6.

Table 6. Excerpt from "LG-24/7" hydrodesulphurization unit's monitoring data

Date	Day	Feed flow rate m ³ /h	Density of diesel fraction t/m ³	Sulphur in diesel fraction, %m	Initial temperature, °C	Product temperature, °C	Sulfur in product, ppm
26.01.2014	153	110.138	0.796	0.40	330.146	338.216	4.0
24.04.2014	241	115.339	0.798	0.38	325.107	332.149	11.0
12.05.2014	259	109.835	0.797	0.42	328.085	335.097	9.0
20.08.2014	359	100.073	0.798	0.50	341.712	349.556	2.0
02.02.2015	525	84.810	0.790	0.35	320.069	327.103	1.9
24.04.2015	606	90.853	0.791	0.30	313.942	319.845	12.0

Experimental data was used in the calculation of the rate constants (Table 6) for the conversion of individual sulphur components in the industrial unit. The process of finding the kinetic parameters was performed by comparing the calculated sulfur content with the experimental total yield of sulfur using the method of least squares.

 Table 7. Effective reaction rate constants and relative error based on laboratory experiment data, h⁻¹

Identified component	340°C	360°C	380°C	Relative error, %
S	1.907	1.971	2.036	0.002
C1BT	2.191	2.153	2.114	0.006
C2BT	2.104	2.030	1.956	0.006
C3BT	2.094	2.080	2.065	0.006
(C4+C5)BT	2.140	2.201	2.262	0.007
DBT	1.877	1.907	1.937	0.007
C1DBT	1.907	1.938	1.969	0.006
C2DBT	1.761	1.786	1.810	0.006
C3DBT	0.968	1.043	1.118	0.007

4. Results discussion

Table 8 shows the results of calculations used the developed model.

Table 8. Product temperatures and sulfur concentrations

Day	Calculated sulfur in product, ppm	Calculated temperature of product, °C
153	4.0	341.4
241	11.9	336.2
259	9.4	339.8
359	2.1	354.8
525	2.0	327.5
606	11.1	320.6

Activity of the catalyst in the beginning and the end of examined period (3 years) of unit functionality, linear functional relation between total productivity and the activity of the catalyst are calculated and introduced in the mathematical model. Thus, the model takes the catalyst's activity loss into account. The regression functional equation (1) was formed to adequately predict the catalyst activity due to coke formation after specified time period of hydrotreating unit functioning:

$$A = 0.1 \cdot 10^{-7} \cdot Z + 0.8948 \quad (1)$$

where: A – relative catalyst activity; Z – tons of refined feed.

5. Conclusion

General calculation of the main process parameters is satisfyingly accurate. Relative error of ending temperature calculation does not exceed 1.5%. Thermal effect of the hydrotreating process varies between 60–80 kJ/mole. The results of the sulphur-containing compounds material balance calculation with use of developed mathematical model are demonstrating high accuracy in accordance to the data which was obtained from industrial hydrotreating unit. The relative difference between monitored and calculated total sulfur concentrations in hydrotreated products does not exceed 4–8%.

HR-538 Al-Ni-Mo catalyst shows high activity with removal of sulfur up to 98–99% mass. from diesel fraction when performing diesel hydrotreating. Chemical activity of sulfur-containing compounds increases in the row from dibenzothiophenes, benzothiophenes to sulfides. Rate of hydrotreating decreases when the number of alkyl substituents in BT and DBT homologues is increasing, consequently, hydrogenation rate of DBT is much lower than that of BT.

The conclusions made based on calculated data. Thus, the catalyst's activity loss by nearly 1/3 of its beginning activity is observed. This could be caused by imperfections in diesel fuel fraction composition and in technological parameters at hydrotreating reactors of industrial unit.

Developed mathematical model allows making conclusions on initial reasons which influence the overall process quality and helps in making a decisions in the questions of process optimization.

Acknowledgements

The research is carried out at National Research Tomsk Polytechnic University and within the framework of National Research Tomsk Polytechnic University Competitiveness Enhancement Program grant.

References

- [1] Kholod N, Evans M. Reducing black carbon emissions from diesel vehicles in Russia: An assessment and policy recommendations. *Environ. Sci. Policy*. 2016; 56: 1-8.
- [2] Barla P, Gilbert-Gonthier M, Kuela JT. The demand for road diesel in Canada. *Energy Economics*. 2014; 43: 316-322.
- [3] Melikoglu M. Demand forecast for road transportation fuels including gasoline, diesel, LPG, bioethanol and biodiesel for Turkey between 2013 and 2023. *Renewable Energy*. 2014; 64: 164-171.

- [4] Grudanova AI, Gulyaeva LA, Krasil'nikova LA, Chernysheva EA. A catalyst for producing diesel fuels with improved cold flow characteristics. *Catal. Ind.* 2016; 8(1): 40-47.
- [5] Zhang M, Fan J, Chi K, Duan A, Zhao Z, Meng X, Zhang H. Synthesis, characterization, and catalytic performance of NiMo catalysts supported on different crystal alumina materials in the hydrodesulfurization of diesel. *Fuel Process. Technol.* 2017; 156: 446-453.
- [6] Méndez FJ, Franco-López OE., Bokhimi X, Solís-Casados DA., Escobar-Alarcón L, Klimova TE. Dibenzothiophene hydrodesulfurization with NiMo and CoMo catalysts supported on niobium-modified MCM-41. *Appl. Catal., B.* 2017; 219: 479-491.
- [7] Liu H, Yin C, Li X, Chai Y, Li Y, Liu C. Effect of NiMo phases on the hydrodesulfurization activities of dibenzothiophene. *Catal. Today.* 2017; 282(2): 222-229.
- [8] Palmer E, Polcar S, Wong A. Clean diesel hydrotreating. Design considerations for clean diesel hydrotreating. *Digital Refining.* 2009.
- [9] Mochida I, Choi K. An overview of hydrodesulfurization and hydrogenation, *J. Jpn. Pet. Inst.* 2004; 47(3): 145-163.
- [10] Stanislaus A, Marafi A, Rana MS. Recent advances in the science and technology of ultra low sulfur diesel (ULSD) production. *Catal. Today.* 2010; 153(1-2): 1-68.
- [11] Schuit GCA, Gates BC, Chemistry and Engineering of Catalytic Hydrodesulphurization. *AIChE Journal.* 1973; 19(3): 417-438.
- [12] Marafi M, Stanislaus A, Furimsky E. Chapter 3 – Hydroprocessing Technology. *Handbook of Spent Hydroprocessing Catalysts*, 2nd ed.; Elsevier, 2017; p. 27-66.
- [13] Davudov D, Moghanloo RG. A systematic comparison of various upgrading techniques for heavy oil. *J. Pet. Sci. Eng.* 2017; 156: 623-632.
- [14] Fedyaeva ON, Vostrikov AA. The products of heavy sulfur-rich oil conversion in a counter supercritical water flow and their desulfurization by ZnO nanoparticles. *J. Supercrit. Fluids.* 2016; 111: 121-128.
- [15] Yin C., Lia H, Liu H, Zhao L, Bai Z, Wang Y, Zhang S, Liu C. Study on the formation, determination, and removal of elemental sulfur in ultra-low sulfur gas oil. *Fuel Process. Technol.* 2014; 120: 16-21.
- [16] Schuman SC, Shalit H, Hydrodesulfurization. *Catal. Rev.* 1970; 4: 245-270.
- [17] Control of Air Pollution From New Motor Vehicles: Heavy-Duty Engine and Vehicle Standards and Highway Diesel Fuel Sulfur Control Requirements: Final Rule, in 40 CFR Parts. 2001.
- [18] Rana MS, Samano V, Ancheyta J, Diaz JIA. A review of recent advances of hydroprocessing of heavy oils and residua. *Fuel.* 2007; 86(9): 1216-1231.
- [19] Belinskaya NS, Frantsina EV, Ivanchina ED, Popova NV, Belozertseva NE. Determination of optimal temperature of catalytic dewaxing process for diesel fuel production. *Pet. Coal.* 2016; 58(7): 695-699.
- [20] Frantsina EV, Belinskaya NS, Ivanchina ED. Intensification of the processes of dehydrogenation and dewaxing of middle distillate fractions by redistribution of hydrogen between the units. *Korean J. Chem. Eng.* 2018; 35(2): 337-347.
- [21] Zagoruiko AN, Belyi AS, Smolikov MD, Noskov AS. Unsteady-state kinetic simulation of naphtha reforming and coke combustion processes in the fixed and moving catalyst beds. *Catal. Today.* 2014; 220-222: 168-177.
- [22] Harwell L., Thakkar S, Polcar S, Palmer RE, Desai PH. Study outlines optimum ULSD hydrotreater design. *Oil Gas J.* 2003; 101: 50-57.
- [23] Krivtcova N, Tataurshikov A, Kotkova E. Modelling of the Kinetics of Sulfure Compounds in Desulfurisation Processes Based on Industry Data of Plant. *MATEC Web of Conferences.* 2016; 85. Article number 01028.
- [24] Krivtcova NI, Tataurshikov AA, Ivanchina ED, Krivtsov EB, Golovko AK. Calculation of the Kinetic Parameters of the Hydrofining Process of Diesel Fraction Using Mathematical Modeling. *Procedia Eng.* 2015; 113: 73-78.
- [25] Krivtcova N, Baklashkina K, Sabiev Sh, Krivtsov E, Syskina A. Changing the composition of the group hydrocarbons of diesel fractions in the process of hydrotreating. *IOP Conference Series: Earth and Environmental Science.* 2016; 43(1). Article number 012061.
- [26] Wang FC, Robbins WK, Di Sanzo FP, McElroy FC. Speciation of Sulfur-Containing Compounds in Diesel by Comprehensive Two-Dimensional Gas Chromatography. *J. Chromatogr. Sci.* 2003; 41: 519-523.
- [27] Luna N, Zelong L, Songbai T. Identification and Characterization of Sulfur Compounds in Straight-Run Diesel Using Comprehensive Two-Dimensional GC Coupled with TOF MS. *China Pet. Process. Petrochem. Technol.* 2014; 16(3): 10-18.

- [28] Sun F, Wu W, Wu Z, Guo J, Wei Z, Yang Y, Jiang Z, Tian F, Li C. Dibenzothiophene hydrodesulfurization activity and surface sites of silica-supported MoP, Ni₂P, and Ni-Mo-P catalysts. *J. Catal.* 2004; 228(2): 298-310.
- [29] Ancheyta J. *Modeling and Simulation of Catalytic Reactors for Petroleum Refining*, John Wiley & Sons, 2011; p. 528.
- [30] Satterfield CN, Modell M, Wilkens JA. Simultaneous Catalytic Hydrodenitrogenation of Pyridine and Hydrodesulfurization of Thiophene. *Ind. Eng. Chem. Process Des. Dev.* 1980; 19: 154-160.
- [31] Hou G, Klein MT, *Molecular Modeling Of Gas Oil Hydrodesulfurization*. Paper presented at 2nd International Conference on Refinery Process Proceedings. AIChE, Houston, TX, 1999.
- [32] Rodriguez MA, Ancheyta J. Modeling of hydrodesulfurization, hydrodenitrogenation, and the hydrogenation of aromatics in a vacuum gas oil hydrotreater. *Energy Fuels.* 2004; 18: 789-794.
- [33] Korsten H, Hoffmann U. Three-phase reactor model for hydrotreating in pilot trickle-bed reactors. *AIChE J.* 1996; 42(5): 1350-1357.
- [34] Bhaskar M, Valavarasu G, Sairam B, Balaraman KS, Balu K. Three-phase reactor model to simulate the performance of pilot-plant and industrial trickle-bed reactors sustaining hydrotreating reactors. *Ind. Eng. Chem. Res.* 2004; 43: 6654-6669.

To whom correspondence should be addressed: Dr. Anton A. Tataurshchikov, Department of Fuel Engineering and Chemical Cybernetics, Tomsk Polytechnic University, 30, Lenin Avenue, Tomsk, 6340, krivtcovani@mail.ru

PREPARATION OF OXIDIZED COAL

D. V. Miroshnichenko^{1*}, *N. Saienko*², *Y. Popov*², *D. Demidov*³, *Yu. V. Nikolaichuk*⁴

¹ National Technical University «Kharkov Polytechnic Institute», 61002, Kharkov, Ukraine

² Kharkiv National University of Civil Engineering and Architecture, 61002, Kharkov, Ukraine

³ Kharkiv State Auto-transport College, 61003, Kharkov, Ukraine

⁴ Donbass State Pedagogical University, 84166, Slavyansk, Ukraine

Received December 20, 2017; Accepted February 15, 2018

Abstract

The oxidation index is an important supplementary characteristic of coal and coal blends, indicating the change in coking properties during oxidation. The coke obtained from coal blend containing poorly coking oxidized coal has a higher content of isotropic carbon and a lower content of anisotropic carbon. That explains its increased reactivity and impaired mechanical and strength after reaction. The oxidation throughout storage is the greatest for small coal classes (<0.5 mm). Preliminary removal of <0.5 mm oxidized coal markedly improves the reactivity and also the mechanical and coke strength after reaction. A method of preparing oxidized coal for coking is proposed: finer grinding (until the content of the ≤1 mm class is 100%). That considerably reduces the influence of the oxidized coal on the quality of the blast-furnace coke produced.

Keywords: coal; oxidation; coal preparation; coke; isotropic carbon.

1. Introduction

The intensification of blast-furnace operation calls for stable high quality of the coke employed. Fluctuation in the coke quality disrupts blast-furnace operation, with loss of productivity and overconsumption of the coke. In such conditions, the composition and properties of the coal blends must be corrected so as to reduce these effects.

Accordingly, one of the best means of improving the stability of blast-furnace operation today is to ensure uniform coke quality [1]. We know that one of the main factors responsible for constant coke quality is constant quality of the coal from which it is produced [2-3].

Recently, marked decline in coke quality in particular, in mechanical and strength of after reaction the coke has been observed with unchanged composition of the coal blends. This may be attributed to the introduction of domestic and imported oxidized coal in the blends.

Accordingly, we need to correct the storage, preparation, and use of oxidized coal at coke plants. In the present work, we investigate means of preventing the impact of oxidized coal on the coke produced, by optimizing its preparation.

2. Experimental

The determination of oxidation and degree of oxidation was carried out accordingly DSTU 7611:2014 Method for determination of the oxidation and degree of the oxidation. The determination of proximate analysis was carried out accordingly ISO 17246:2010 Coal – Proximate analysis. The determination of ultimate analysis was carried out accordingly ISO 17247:2013 Coal – Ultimate analysis.

The determination of petrographic analysis was carried out accordingly ISO 7403-3:2009 Methods for the petrographic analysis of coals – Part 3: Method of determining maceral group composition; ISO 7404-5:2009 Methods for the petrographic analysis of coals – Part 5: Methods of Determining microscopically the reflectance of vitrinite.

The determination of coke reactivity index (CRI) and coke strength after reaction (CSR) was carried out accordingly ISO 18894:2006 Coke-Determination of coke reactivity index (CRI) and coke strength after reaction (CSR). The determination of expansion pressure was carried out accordingly DSTU 8724:2017 Coal and charge based on it. Method for determination of expansion pressure that occurs during coking.

The determination of size analysis of coals was carried out accordingly ISO 1953:2015 Hard coal. Size analysis by sieving. The determination of plastometric indices was carried out accordingly GOST 1186–2014 Hard Coals. Method for determination of plastometric indices.

Microstructure of laboratory coke was determined by optical microscopy. Previously prepared 10 mm coke sample was used for analysis. The sample preparation included grinding and polishing. The sample was ground and polished under top water using automatic sample preparation unit. The 600 grit size sand paper was used for grinding and microcloth containing alumina aqueous suspension of 0,3 φm granulation was used in the polishing phase. After polishing, the sample was rinsed with water and alcohol and dried by hot air.

Microstructure was analyzed by the «Olympus GX S1» with digital camera DP 70. Microstructure was observed at different magnifications under polarized light.

The structural characteristics of the coal were calculated from formulas given in [12]. The aromatic content of the structure f_a is

$$f_a = 1.007 - 0.3857(H/C) - 0.3725(O/C) \quad (1)$$

The degree of molecular association of the coal cA is

$$cA = 1 - \frac{H + 0.125(O + N + S)}{0.333C} \quad (2)$$

3. Results and discussions

Table 1 presents the proximate analysis and oxidation characteristics of Pokrovskoe coal of different size classes after open storage for four months [4-5]. Coal of the <0.5 mm class is the most oxidized throughout storage, as we see in Table 1. This corresponds to elevated oxidation index Δt and degree of oxidation d_0 , which are more than double those for coal of other size classes. In our view, the <0.5 mm class is effectively an additive to the blend.

Table 1. Proximate analysis and oxidation characteristics of Pokrovskoe coal of different size classes after open storage

Size analysis		Proximate analysis, %			Oxidation characteristics	
class, mm	yield, %	A ^d	S ^{d_t}	V ^{daf}	Δt, °C	d ₀ , %
>25	8.1	8.0	0.75	29.5	3	6.7
25–13	10.8	8.8	0.77	29.8	3	6.8
13–6	18.0	8.1	0.85	29.6	3	7.3
6–3	14.5	8.0	0.80	29.4	3	6.7
3–1	17.1	8.2	0.79	29.0	3	6.8
1.0–0.5	6.3	8.2	0.81	28.8	3	7.2
<0.5	25.2	10.3	0.75	27.5	8	17.5

The ultimate composition and structural characteristics of the coal in Table 2 show that the oxidation of <0.5 mm coal sharply reduces the carbon and hydrogen content and leads to extreme increase in the oxygen content. Accordingly, the degree of aromatic structure and molecular association of the coal's organic mass are significantly less for the <0.5 mm class than for the other coal.

We now determine the change in coke quality when using both oxidized and unoxidized Pokrovskoe coal in the blend and assess the possibility of reducing the influence of the oxidized coal by removing the <0.5 mm class.

Table 3 presents the properties and petrographic characteristic of the coals in the experimental blends and the characteristics of Pokrovskoe coal in three states: (1) initial unoxidized coal; (2) partially oxidized coal; (3) partially oxidized coal after the removal of the <0.5 mm class.

Table 2. Ultimate composition and structural characteristics of the coal's organic mass

Size class, mm	Ultimate composition, %					Degree of aromatic structure f_a	Molecular association cA
	C^{daf}	H^{daf}	N^{daf}	S^{d_t}	O^{daf_d}		
>25	90.05	5.55	1.85	0.75	1.80	0.716	0.716
25–13	89.76	5.38	1.86	0.77	2.23	0.742	0.742
13–6	89.27	5.31	1.87	0.85	2.70	0.743	0.743
6–3	89.45	5.29	1.88	0.80	2.58	0.744	0.744
3–1	88.45	5.13	1.88	0.79	3.75	0.746	0.746
1.0–0.5	88.34	5.08	1.89	0.81	3.88	0.747	0.747
<0.5	78.04	4.65	1.85	0.75	14.71	0.698	0.698

Table 3. Properties and petrographic characteristics of coal blends

Supplier	Proximate analysis, %			Plastometric characteristics, mm		Mean vitrinite reflection coefficient R_0 , %
	A^d	S^{d_t}	V^{daf}	x	y	
Sentyanovskaya mine	5.6	0.95	31.1	22	18	1.06
Kuzbassrazrezugol' enrichment facility	7.4	0.41	25.1	38	10	1.05
Pokrovskoe facility, initial state	8.9	0.78	29.0	11	15	1.13
Pokrovskoe facility, partially oxidized	8.8	0.81	29.1	12	12	1.11
Pokrovskoe facility, partially oxidized, <0.5 mm class removed	8.2	0.80	29.4	12	14	1.12

Analysis of Table 3 indicates that partial oxidation markedly impairs the coking properties. Thus, the plastic-layer thickness y falls from 15 to 12 mm. The other properties are unchanged. After removing the < 0.5 mm class, y is restored practically to its initial value. Some reduction in ash content is observed but is unrelated to oxidation.

Table 4 presents the composition of the experimental blends. They differ only in the degree of oxidation and blends size composition of the Pokrovskoe coal, with constant of the other components.

Table 4. Composition of experimental blends

Supplier	Content (%) in blend		
	1	2	3
Sentyanovskaya mine	5	5	5
Kuzbassrazrezugol' enrichment facility	15	15	15
Pokrovskoe facility, initial state	80	0	0
Pokrovskoe facility, partially oxidized	0	80	0
Pokrovskoe facility, partially oxidized, <0.5 mm class removed	0	0	80
Total	100	100	100

Table 5 summarizes the properties of the experimental blends, while Table 6 presents their vitrinite reflection coefficients. Analysis of these data indicates that the addition of partially oxidized Pokrovskoe coal to the blend mainly affects its coking power, with decrease in plastic-layer thickness y from 15 to 10 mm. Note that removing the <0.5 mm class reduces the oxidation characteristics Δt and d_0 somewhat.

The presence of the partially oxidized coal in the blend markedly affects the expansion pressure, which falls sharply from 16.8 to 2.7 kPa. Removal of the <0.5 mm class increases the expansion pressure to 15.6 kPa, which is close to its initial value. As we see in Table 6, the presence of partially oxidized coal considerably increases the oxygen content in the blend,

while reducing the carbon and hydrogen content. Removal of the <0.5 mm class somewhat restores the initial ultimate composition.

Table 5. Properties of experimental blends

Blend	Proximate analysis, %			Plastometric characteristics, mm		Expansion pressure $P_{h_{max}}$, kPa
	A^d	$S_t^{d_t}$	V^{daf}	x	y	
1	8.5	0.73	28.5	11	15	16.8
2	8.4	0.76	28.6	19	10	2.7
3	8.0	0.75	28.8	16	13	15.6

Table 6. Vitrinite reflection coefficient and ultimate composition of experimental blends

Blend	Mean vitrinite reflection coefficient $R_0, \%$	Ultimate composition, %				
		C^{daf}	H^{daf}	N^{daf}	$S_t^{d_t}$	O^{daf_d}
1	1.12	87.28	5.82	5.82	0.70	4.30
2	1.10	86.21	5.74	5.74	0.74	5.42
3	1.11	87.07	5.80	5.80	0.75	4.47

We conclude from the coking of the experimental blends in a 5-kg laboratory furnace (designed by the Ukrainian Coal-Research Institute) that the presence of partially oxidized coal reduces the mechanical strength of the coke by 1.7% in terms of the crushability M_{25} , with 1.0% increase in the wear index M_{10} (Table 7). The total content of anisotropic carbon in the coke is reduced from 80 to 73%, while the content of isotropic carbon rises from 4 to 12%. In other words, the coke becomes less ordered (Table 8). Note that our results confirm the simultaneous change in mechanical strength and expansion pressure of the experimental blends reported in [6-8].

Table 7. Quality of coke from experimental blends

Blend	Proximate analysis, %			Mechanical strength, %		Reactivity and strength after reaction, %	
	A^d	$S_t^{d_t}$	V^{daf}	M_{25}	M_{10}	CRI	CSR
1	11.1	0.65	0.7	90.0	8.1	38.6	49.1
2	11.2	0.62	0.8	88.3	9.1	40.5	44.9
3	10.4	0.63	0.7	89.8	8.3	34.4	53.6

Table 8. Microstructure of coke

Blend	Inertinite	Isotropic carbon (I)	Anisotropic carbon (A)			ΣA
			mosaic (M)	striated (S)	plate (P)	
1	16	4	78	2	0	80
2	15	12	73	0	0	73
3	17	6	75	2	0	77

Along with the loss of mechanical strength and decrease in the content of anisotropic carbon, we note deterioration in the reactivity CRI and strength after reaction CSR of the coke.

Specifically, CRI increases from 38.6 to 40.5%, while CSR decreases from 49.1 to 44.9%. For coke from blend 3, CRI and CSR are better than for the initial blend, thanks to the removal of the <0.5 mm Pokrovskoe coal.

After removal of the <0.5 mm class, the M_{25} and M_{10} values of the coke are practically the same as for coke from blend containing unoxidized Pokrovskoe coal. After removal of the <0.5 mm class, the CRI and CSR values are better than for blend 1.

Our results indicate that it is advisable to use oxidized coals separately from the other flotation concentrate for example, as a fuel in thermal power stations or as an additive to coal blend in the production of the special types of coke.

We now consider the influence of the degree of grinding of oxidized coal in coking blend on the coke quality.

Other researchers have reached a conclusion stated as follows by Gryaznov [9]: "Since the coking of coal grains is a surface process, the best coking will be observed when poorly coking components are ground more finely, while satisfactorily coking components are ground more coarsely. This will also reduce the internal stress in the coke."

Currently, Ukraine is importing large quantities of poorly coking coal and petrographically nonuniform coals, which is often oxidized. Accordingly, it is of interest to assess the prospects for reducing the negative influence of such coal on coke quality by grinding it more finely.

Tables 9 and 10 present the properties and petrographic characteristics of the coals in the experimental blend. As we see, the properties of the coal samples correspond to their rank assignments.

Table 9. Properties of coal in blends

Supplier	Proximate analysis, %			Plastometric characteristics, mm		Oxidation index Δt , °C
	A ^d	S _t ^d	V ^{daf}	x	y	
Taldinskii mine	8.7	0.62	38.2	39	10	1.0
Shchedrukhiinskaya enrichment facility, sample 1	8.0	0.63	38.9	33	11	4.0
Shchedrukhiinskaya enrichment facility, sample 2	7.6	0.42	39.4	32	10	10.0
Duvanskaya enrichment facility	7.1	1.23	33.4	13	21	1.0
Wellmore	7.0	1.08	33.7	23	19	1.0
Pokrovskoe facility	8.6	0.75	27.7	13	13	1.0
Bochatskii mine, sample 1	8.0	0.31	24.8	32	10	2.0
Bochatskii mine, sample 2	8.0	0.36	26.3	33	9	11.4
Pocahontas	7.7	0.82	17.9	8	12	2.0

Table 10 Petrographic characteristics of coal in blend

Supplier	Petrographic composition, %					Mean vitrinite reflection coefficient R ₀ , %
	Vt	Sv	I	L	ΣFC	
Taldinskii mine	73	2	2	2	25	0.67
Shchedrukhiinskaya enrichment facility, sample 1	81	0	0	2	17	0.66
Shchedrukhiinskaya enrichment facility, sample 2	82	0	0	2	16	0.61
Duvanskaya enrichment facility	88	0	0	3	9	1.00
Wellmore	78	0	0	4	18	0.96
Pokrovskoe facility	87	1	1	2	10	1.19
Bochatskii mine, sample 1	48	1	1	1	51	1.08
Bochatskii mine, sample 2	55	1	1	1	44	1.07
Pocahontas	74	0	0	0	26	1.58

Supplier	Vitrinite reflection, %					
	0.50–0.64	0.65–0.89	0.90–1.19	1.20–1.39	1.40–1.69	1.70–2.59
Taldinskii mine	73	2	2	2	25	
Shchedrukhiinskaya enrichment facility, sample 1	81	0	0	2	17	
Shchedrukhiinskaya enrichment facility, sample 2	82	0	0	2	16	
Duvanskaya enrichment facility	88	0	0	3	9	
Wellmore	78	0	0	4	18	
Pokrovskoe facility	87	1	1	2	10	
Bochatskii mine, sample 1	48	1	1	1	51	
Bochatskii mine, sample 2	55	1	1	1	44	
Pocahontas	74	0	0	0	26	

Marked oxidation of the petrographically uniform coal from Shchedrukhinskaya mine and the petrographically nonuniform coal from Bochatskii mine changes many of their properties. For example, volatile matter is higher in the oxidized coal, while the plastic-layer thickness is less. That significantly affects the coking properties, as will be shown later. The petrographic characteristics are partially unchanged, as noted in [10].

Table 11 presents the composition of the experimental blends containing oxidized coal. Blend preparation is as follows. Blend 1 is average coking blend used at Zaporozhcoke, produced by grinding until the content of the ≤ 3 mm class is 80%. In blend 2, 10% of the unoxidized Shchedrukhinskaya coal (sample 1) is replaced by oxidized coal of the same type (sample 2). Otherwise, blend preparation is unchanged. In blend 3, the oxidized Shchedruk-hinskaya coal is ground until the content of the ≤ 1 mm class is 100%. As before, the remainder of the blend is ground until the content of the ≤ 3 mm class is 80%.

Table 11. Composition of experimental blends

Supplier	Content (%) in blend					
	1	2	3	4	5	6
Taldinskii mine	20	20	20	30	30	30
Shchedrukhinskaya enrichment facility, sample 1	10	0	0	0	0	0
Shchedrukhinskaya enrichment facility, sample 2	0	10	10	0	0	0
Duvanskaya enrichment facility	10	10	10	10	10	10
Wellmore	18	18	18	18	18	18
Pokrovskoe facility	35	35	35	25	25	25
Bochatskii mine, sample 1	0	0	0	10	0	0
Bochatskii mine, sample 2	0	0	0	0	10	10
Pocahontas	7	7	7	7	7	7

Blends 4–6 are produced analogously but with petrographically nonuniform Bochatskii coal (samples 1 and 2), instead of the Shchedrukhinskaya coal.

Analysis of Table 12 indicates that, in the experimental blends, which have a relatively low content of oxidized coal, the ash content, total sulfur content, volatile matter, plastic-layer thickness, and vitrinite reflection coefficient are practically the same. Consequently, we may assess the influence of the blend preparation on the coke quality.

Table 12. Properties of experimental blends

Blend	Proximate analysis, %			Plastometric characteristics, mm		Mean vitrinite reflection coefficient $R_{0,}$, %
	A^d	$S^{d,t}$	V^{daf}	x	y	
1	8.1	0.82	31.9	22	14	1.00
2	8.0	0.80	31.9	22	14	0.99
3	8.0	0.80	31.9	21	14	0.99
4	8.1	0.78	31.5	24	14	0.99
5	8.1	0.78	31.7	24	13	0.99
6	8.1	0.78	31.7	24	13	0.99

We conclude from the coking of the experimental blends in a 5-kg laboratory furnace (designed by the Ukrainian Coal-Research Institute) that the presence of partially oxidized coal Shchedrukhinskaya enrichment facility, sample 2 and petrographically nonuniform coal impairs the crushability reactivity, and coke strength after reaction (Table 13).

As already noted, the introduction of oxidized coals has practically no influence on the blend-in particular, on the volatile matter and plastic-layer thickness, which are generally used to assess the blend properties. However, as is evident from the coking results, these characteristics are insufficient to assess the change in coking properties of the blend on introducing oxidized coal.

Table 13. Quality of coke from experimental blends

Blend	Proximate analysis, %			Mechanical strength, %		Reactivity and strength after reaction, %	
	A ^d	S ^d _t	V ^{daf}	M ₂₅	M ₁₀	CRI	CSR
1	10.7	0.74	0.3	92.9	5.8	32.6	52.7
2	10.8	0.72	0.2	91.7	6.3	33.5	51.2
3	10.9	0.72	0.3	92.5	6.1	32.7	52.6
4	10.6	0.70	0.4	92.8	5.9	32.8	52.4
5	10.8	0.71	0.2	91.4	6.2	34.0	50.3
6	10.7	0.71	0.3	92.7	6.0	32.9	51.9

The volatile matter and plastic-layer thickness are also practically unchanged during oxidation (Table 9). Accordingly, we may suppose that the oxidation index Δt is an important supplementary characteristic of coal and coal blends, reflecting the change in coking properties on oxidation.

Finer crushing of poorly coking oxidized coal practically eliminates its effect on coal quality specifically on M₂₅, M₁₀, CRI, and CSR.

4. Conclusions

The oxidation index is an important supplementary characteristic of coal and coal blends, indicating the change in coking properties during oxidation. The coke obtained from coal blend containing poorly coking oxidized coal has a higher content of isotropic carbon and a lower content of anisotropic carbon. That explains its increased reactivity and impaired mechanical and strength after reaction.

The oxidation throughout storage is the most for small coal classes (<0.5 mm). Preliminary removal of <0.5 mm oxidized coal markedly improves the reactivity and also the mechanical and coke strength after reaction.

A method of preparing oxidized coal for coking is proposed: finer grinding (until the content of the ≤1 mm class is 100%). That considerably reduces the influence of the oxidized coal on the quality of the blast-furnace coke produced.

Symbols

A ^d	ash content of coal in the dry state, %;	Δt	oxidation index, °C;
V ^{daf}	volatile matter in the dry ash-free state, %;	do	degree of oxidation, %;
S ^d _t	sulphur of coal in the dry state, %;	y	thickness of the plastic layer, mm;
cA	the degree of molecular association;	P ^h _{max}	expansion pressure of coal (blend), kPa;
f _a	the aromatic content of the structure;	CRI	coke reactivity index, %;
R _o	mean vitrinite reflection coefficient, %;	CSR	coke strength after reaction, %;
V _t	vitrinite, %;	I	isotropic texture of carbon in coke, %;
S _v	semivitrinite, %;	M	mosaic texture of carbon in coke, %;
I	inertinite, %;	S	striated texture of carbon in coke, %;
L	liptinite, %;	P	plate texture of carbon in coke, %;
ΣFC	sum of fusinized components, %;		
ΣA	sum of anisotropic texture of carbon in coke, %;		
C ^{daf} , H ^{daf} , N ^{daf} , O ^{daf}	carbon, hydrogen, nitrogen and oxygen in the dry, ash-free state, %;		
M ₁₀ , M ₂₅	indices of resistance of coke abrasion and fragmentation, respectively, %.		

References

- [1] Bepler E and Gropich KH. Influence of coke quality on blast-furnace operation, Chern. Met., 1999; 10: 10–18.
- [2] Podlubnyi AV, Rubchevskii VN, Chernyshov YuA, Ermak YuV, Toryanik EI, Zhuravskii AA, and Belikov DV. Ensuring uniform operation of the coal- preparation shop at Zap`orozhkoks, Coke and Chemistry, 2008; 51(3): 79–82.
- [3] Toryanik EI, Zhuravskii AA, Podlubnyi AV. Automated evaluation of the regular operation of the coal preparation shop of Zaporozhkoks Company, Uglekhim. Zh., 2009; (1–2): 26–31.

- [4] Miroshnichenko DV, Drozdniuk ID, Kaftan YuS, and Desna NA. Oxidation of Pokrovskoe coal in laboratory and natural conditions. 1. Kinetics of oxidation and technological properties. *Coke and Chemistry*, 2015; 58(3): 79–87.
- [5] Miroshnichenko DV, Drozdniuk ID, Kaftan YuS, Desna NA, and Golovko MB. Oxidation of pokrovskoe coal in laboratory and natural conditions. 2. Laboratory coking of experimental batch. *Coke and Chemistry*, 2015; 58(5): 156–161.
- [6] Sytni, AV, Kaftan YuS, and Miroshnichenko DV. Expansion pressure of coal with different genetic and technological properties. *Coke and Chemistry*, 2011; 54(1): 1–3.
- [7] Miroshnichenko DV, Kaftan YuS, Desna NA, and Sytnik AV. Oxidation of bituminous coal. 1. Expansion pressure. *Coke and Chemistry*, 2015; 58(10): 376–381.
- [8] Zubkova V, Strojwas A, and Joswiak M. The influence of long-term storage on thermal behavior of lower rank coal on the example of Polish coal. Part 1. The influence of long-term storage (LTS) of a lower rank coal on changes in volume in carbonized charge and changes in structural chemical parameters of pyrolysis products. *Fuel*, 2017; 188: 79–89.
- [9] Gryaznov NS. *Osnovy teorii koksovaniya (Basic Theory of Coking)*, Moscow: Metallurgiya, 1976.
- [10] Miroshnichenko DV. Influence of oxidation on the packing density of coal. *Coke and Chemistry*, 2014; 57(5): 183–191.

To whom correspondence should be addressed: Dr. D. V Miroshnichenko, National Technical University «Kharkov Polytechnic Institute», 61002, Kharkov, 2 Kirpichova Str., Ukraine, dvmir79@gmail.com

PROMOTION OF NANO STRUCTURE IRON CATALYST WITH ZIRCONIUM FOR FISCHER-TROPSCH SYNTHESIS

Yahya Zamani^{1*}, Mohammad Irani¹, Sohrab Taghipoor¹, Rahman Shakibaei Lalehloo², Amir Sepehrianazar³

¹ Research Institute of Petroleum Industry (RIPI), National Iranian Oil Company; West Blvd., Near Azadi Sports Complex P.O. BOX 14665-137, Tehran, Iran

² Department of Chemistry, Karaj Branch, Islamic Azad University, Karaj, Iran

³ Polymer Engineering Group, Ahar Branch, Islamic Azad University, Ahar, Iran

Received December 19, 2017; Accepted February 15, 2017

Abstract

The effect of zirconium on nano-structure iron catalysts were compared to the unpromoted nano-structure iron catalyst for Fischer-Tropsch Synthesis. The catalysts were prepared by micro-emulsion method. The composition of the final nano-sized iron catalysts, in term of the atomic ratio contain as: 100Fe/5Cu, 100Fe/5Cu/2Zr. XRD, BET, H₂-TPR and TEM techniques were utilized to assess the catalysts phase, structure and morphology. The promoted catalyst compare to the unpromoted catalyst, has higher FT rate and CO₂ production. Zr promoter has the best performance than unpromoted iron catalyst.

Keywords: Nanoparticles iron catalyst; Microemulsion; Fischer-Tropsch Synthesis; Zr Promoter.

1. Introduction

The Fischer-Tropsch Synthesis (FTS) is a heterogeneous surface catalyzed polymerization process. During this process, CH_x monomers formed via hydrogenation of adsorbed CO on transition metals produce hydrocarbons and oxygenates with a broad range of chain lengths and functional groups. FTS is an important step in the manufacture of hydrocarbon fuels from coal or syngas. Although several metals are active for the FTS, only iron and cobalt catalysts are economically feasible on an industrial scale. The use of iron-based catalysts is suitable not only for their low cost and availability, but also their high water-gas shift activity makes it possible to use these catalysts with low H₂/CO ratios [1-7].

Among promoters, potassium has been used as a promoter for iron catalysts. Potassium can also increase the catalytic activity for FTS and WGS reactions. Copper is normally added to Fe-based FTS catalysts as a chemical promoter. It is added to enhance hematite reducibility [8-10]. A positive effect of other transition metals, such as Mo, Ta, V, and La, on the iron based catalyst activity for both CO hydrogenation and WGS activity also has been reported [11-14]. Although the studies on the Fe-based FT catalysts are extensive, the investigations on the effect of Zr on the catalyst is scarce. In this study, a micro-emulsion method has been developed to prepare two nano-sized iron catalysts by preparing nano-size iron with copper and zirconium oxide separately from their solutions. Effect of Zr promoter was investigated on catalyst morphology, activity and product selectivity in FTS. The catalysts were tested in a fixed-bed reactor at FTS conditions.

2. Experimental

2.1. Catalyst preparation

Nano-structure iron catalysts were prepared by water-in-oil microemulsion method. A water solution of metal precursors, FeCl₃·6H₂O and Cu(NO₃)₂·4H₂O were added to a mixture of an oil

phase containing 1-propanol and chloroform and sodium dodecyl sulfate (SDS) as a surfactant. Hydrazine in the aqueous phase was added as precipitating agent and stirred for 3 hour. The obtained mixture was left to decant overnight. The solid was recovered by centrifugation and washed thoroughly with distilled water, ethanol and acetone. Finally, the samples were dried overnight at 120°C, and subsequently calcined in air at 390°C for 3 h. Nanostructured zirconium oxide was prepared like nanostructured iron and copper. At the next step, they were mixed together. The promoted catalysts were dried at 120°C for 20 h and calcined at 390°C for 3 h in air [12]. The catalyst compositions were designated in terms of the atomic ratios as: 100Fe/5Cu, 100Fe/5Cu/2Zr. All samples were pressed into pellets, crushed and sieved to obtain particles with 16-30 mesh.

2.2. Catalyst characterization

BET surface area, pore volume and average pore size distribution of the catalysts were determined by N₂ physisorption using a Micromeritics ASAP 3020 automated system. A 0.2 g catalyst sample was degassed in the system at 100°C for 1 h and then at 300°C for 2 h prior to analysis. The analysis was done using N₂ adsorption at -196°C. XRD spectra of fresh catalyst were conducted with a Philips PW1840 X-ray diffractometer with monochromatized Cu (K α) radiation for determining of iron phases. Temperature programmed reduction (TPR) profiles of the calcined catalysts were recorded using a Micromeritics TPD-TPR 290 system. The TPR of 50 mg of each sample was performed in 5% hydrogen/argon gas mixture. The H₂ reduction process illustrated three stages in the temperature range between 200-800°C. Average particle size of the calcined powders was measured by LEO 912AB TEM. The composition of catalysts was determined using atomic absorption instrument (Perkin-Elmer model 2380).

2.3. Cata-test system and operation procedure

The catalytic experiments were conducted in a fixed-bed stainless steel reactor. The reactor was loaded by 1.5g catalyst. The catalyst was reduced in a %10 H₂/N₂ flow at 400°C for 2h. The catalyst activation was followed in a stream of synthesis gas with H₂/CO=1 and SV= 2NL.h⁻¹.gCat⁻¹ for 24 h in atmospheric pressure and temperature of 270°C. Following the activation process, the reactor pressure and temperature raised to 20 bar and 290°C, respectively and the reaction initiated in synthesis gas stream with H₂/CO =1 and GHSV= 2.8 NL.h⁻¹.gCat⁻¹.

The products were analyzed by a gas chromatograph (Varian CP 3800), equipped with three subsequent connected columns: Two packed columns connected to two thermal conductivity detectors (TCD) which used for analyzing H₂, CO, CO₂, CH₄ and other non-condensable gases. A petrocol Tm DH100 fused silica capillary column attached to a flame ionization detector (FID) for analyzing organic liquid products [9,15]. The activities and product selectivities were assessed after 60 h from initial time.

3. Results and discussion

Transition elements are used as promoters because they can modify the adsorption pattern of the reactants (H₂ and CO) on the active sites. The effect of Zr promoter on the behavior of the iron-based FTS catalysts; namely, CO chemisorptions enhancement has been justified as a consequence of the iron tendency to withdraw electronic density from zirconium. Therefore the strength of the Fe-CO bond was enhanced [12]. Elemental analysis was performed to determine the composition of elements in the nano-sized iron catalysts. Table.1 shows results of catalysts surface area.

Table 1. Textural properties of the catalysts

Catalyst	BET surface area (m ² /g)	Pore volume, (cm ³ /g)	Average pore size (nm)
100Fe/5Cu	46.3	0.25	15.2
100Fe/5Cu/2Zr	43.2	0.23	13.4

By adding of zirconium, the BET surface area, pore volume and average pore size in the catalysts decrease as it promotes the aggregation of the catalyst crystallites and blocks up the pore volume of the catalyst.

Nanostructured iron catalysts were characterized by X-ray diffraction (XRD) after calcinations. Fig. 1 shows the XRD patterns of the catalysts prepared by the microemulsion method. The addition of Zr did not cause any obvious change, and no phase containing metals above were detected. All the catalysts showed the Fe_2O_3 crystalline phase. The characteristic peak at $2\theta = 33.3^\circ$ corresponds to the hematite 104 plane .

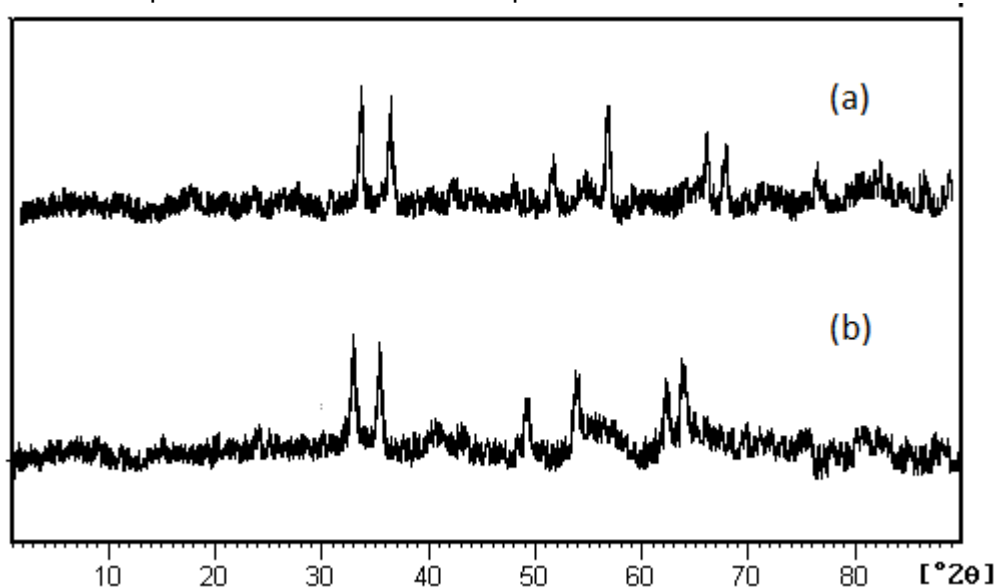


Fig. 1. XRD spectra of the fresh catalysts; (a) 100Fe/5Cu (b) 100Fe/5Cu/2Zr

The morphology of the catalyst was illustrated by TEM images as shown in Fig. 2. TEM revealed that the nanoparticles diameter was in the range of 10–30 nm.

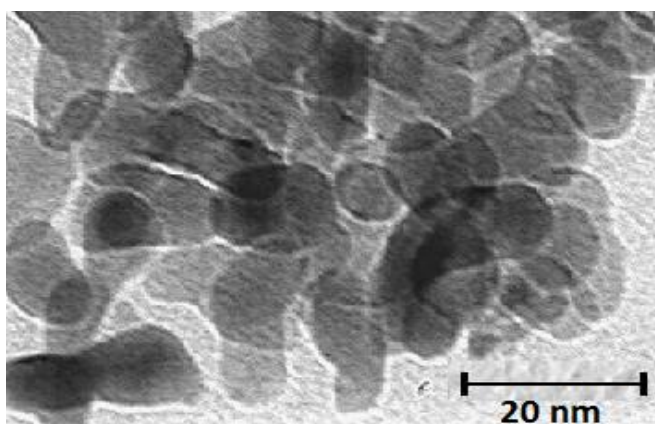


Fig 2. TEM micrograph of 100Fe/5Cu/2Zr catalyst

Fig. 3 shows the H_2 -TPR profiles of the nano-sized iron catalysts. H_2 -TPR determined reduction behavior of the catalysts. The first stage is ascribed to the transformations of CuO to Cu , the second stage is attributed to the transformation of Fe_2O_3 to Fe_3O_4 whereas the third stage represents the transformation of Fe_3O_4 to Fe .

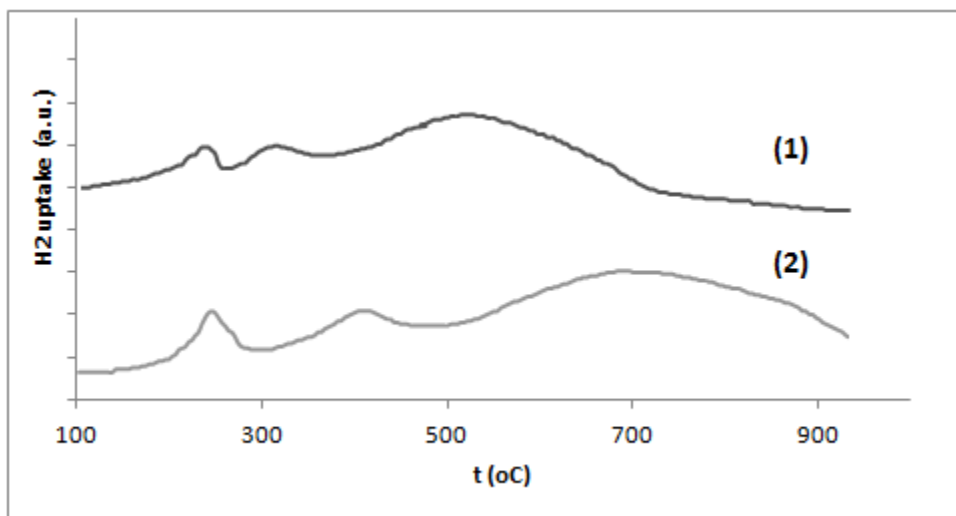


Fig.3. H₂-TPR profiles of the catalysts; (1) 100Fe/5Cu (2) 100Fe/5Cu/2Zr

Addition of promoter increased reduction temperature and reaction time. The promoter increases the catalyst activity. The addition of copper accelerates the deactivation of the catalyst, whereas the addition of Zr improve the FTS activity of iron-based catalysts. Fig.4 shows FTS rate and Water Gas Shift (WGS) rate. During FTS process, one part of H₂O produced by FTS reaction is a by WGS reaction.

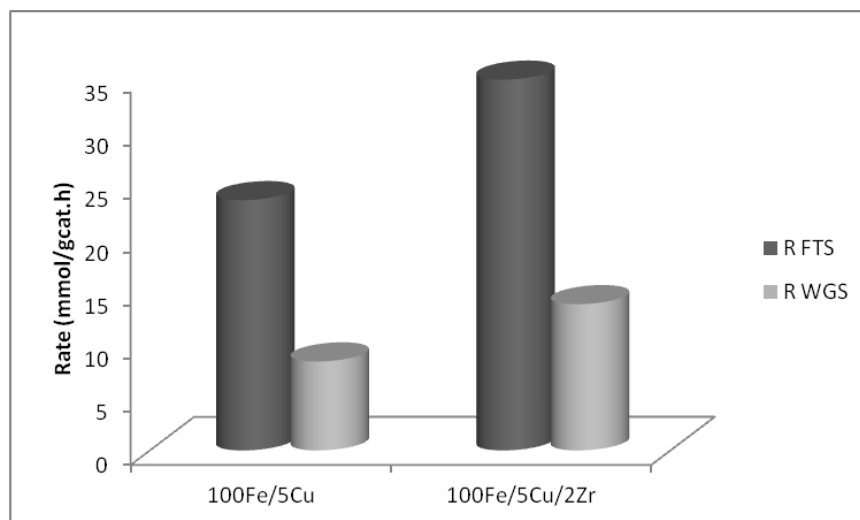


Fig. 4. R_{FTS} and R_{WGS} of the catalysts

Zr promoter into iron-based catalyst can promote CO adsorption, increases the concentration of CO species, shifts WGS reaction to right and thus improves WGS activity (Equation.1).



The high WGS activity decreases the H₂O pressure and stabilizes the iron carbides. Zr promoted iron catalyst has higher CO conversion than unpromoted catalyst. Products selectivity of the catalysts shows in fig.5. It shows selectivities to gaseous and light hydrocarbons (methane and C₂-C₄) and heavy hydrocarbons (C₅⁺). All of these results imply that the chain growth reaction is increased and the hydrogenation reaction is decreased while Zr was added in the catalyst. Both the amount of the promoters and the reaction conditions influence the product selectivity.

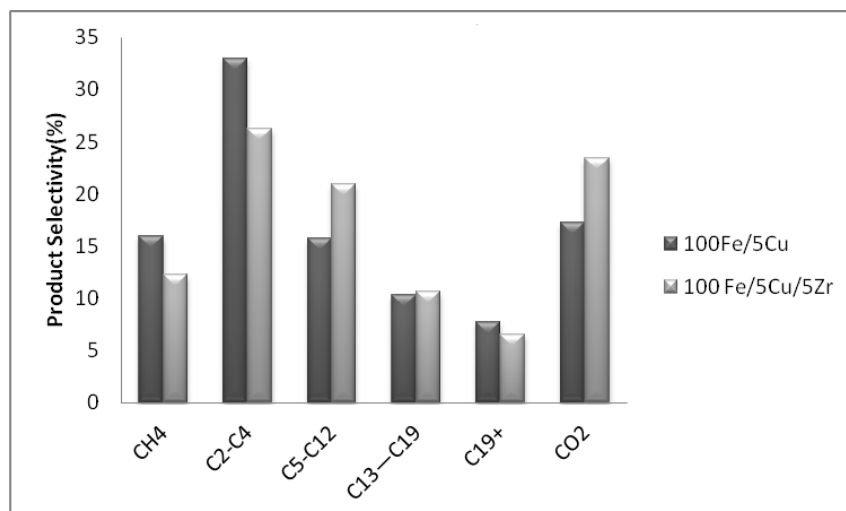


Fig 5. Products selectivity of the catalysts; Reaction condition: Time on Stream 60 h, 290 °C, 20MPa, H₂/CO = 1 and SV= 2.8nl.gCat⁻¹. h⁻¹.^a Selectivity to oxygenates was negligible (<3%) in all cases

In this work, addition of Zr promoter facilitates the CO dissociative adsorption, leading to a higher coverage of carbon species on the surface and thus promotes the chain growth reaction.

4. Conclusions

Nano-structured iron catalysts were prepared by microemulsion method. Effect of the zirconium into nanoparticles iron catalyst was investigated on the performance of the CO hydrogenation. Zr promoter into nano-sized iron catalyst has significant influences on the catalytic performances during Fischer-Tropsch synthesis. The changes in the catalytic performances can be attributed to the effect of promoter on H₂ and CO adsorption, which further significantly affects the FTS performances of the catalysts. Zr promoter significantly improve the FTS and WGS activities.

Acknowledgements

We are grateful to the Research Institute of Petroleum Industry (RIPI) for financial support. We also express our thanks to Central laboratory of Ferdowsi University of Mashhad for recording TEM micrographs.

References

- [1] Abdulbaset A, Mclroy DN, Armando GM. Effect of synthesis and activation methods on the catalytic properties of silica nanospring (NS)-supported iron catalyst for Fischer-Tropsch synthesis, *Fuel Proces. Technol.*, 2018; 169: 132-141.
- Lisheng G, Jian S, Jian W, Zhiyong W. Fischer-Tropsch synthesis over iron catalysts with corncob-derived promoters. *J. Energy Chem.*, 2017; 26(4): 632-638.
- [3] Steen EV, Claeys M, Möller KP, Nabaho D. Comparing a cobalt-based catalyst with iron-based catalysts for the Fischer-Tropsch XTL-process operating at high conversion, *Appl. Catal. A: Gen.*, 2018; 549: 51-59.
- [4] Mingyue D, Yong Y, Baoshan W, Yongwang L, Longlong M. Study on reduction and carburization behaviors of iron phases for iron-based Fischer-Tropsch synthesis catalyst. *Appl. Energy*, 2015; 160: 982-989.
- [5] van der Laan GP, Beenackers AAC. Kinetics and selectivity of the Fischer-Tropsch synthesis: A literature review. *Catal. Rev. Sci. Eng.*, 1999; 41 : 255-318.
- [6] Bukur DB, Mukesh D, Patal SA. Promoter effects on precipitated iron catalysts for Fischer-Tropsch synthesis. *Ind. Eng. Chem. Res.*, 1990; 29: 194-204.
- [7] Zamani Y, Bakavoli M, Rahimizadeh M, Mohajeri A, Seyed, SM. Study of Ce Promoter on Nano Structure Iron Catalyst in Fischer-Tropsch Synthesis. *Chem. Eng. Trans.*, 2012; 29:847-852.

- [8] Sarkari M, Fazlollahi F, Ajamein H, Atashi H, Larry LB. Catalytic performance of an iron-based catalyst in Fischer-Tropsch synthesis. *Fuel Proces. Technol.*, 2014; 127: 163-170.
- [9] Zamani Y. Fischer-Tropsch synthesis over nano-sized iron-based catalysts : Investigation of promoter and temperature effects on products distribution. *Pet Coal*, 2015; 57(1): 71-75.
- [10] Cheng K, Ordonsky VV, Virginie M, Legras B, Chernavskii PA, Kazak VO, Cordier C, Paul S, Wang Ye, Khodakov AY. Support effects in high temperature Fischer-Tropsch synthesis on iron catalysts. *Appl. Catal. A: Gen.*, 2014; 488:66-77.
- [11] Zamani Y. Effect of Mn promoter on nano-sized iron catalyst for Fischer-Tropsch Synthesis. *Pet Coal*, 2016; 58(4): 444-449.
- [12] Zamani Y, Bakavoli M, Rahimizadeh M, Mohajeri A, Seyedi SM. Synergetic Effect of La and Ba Promoters on Nanostructured Iron Catalyst in Fischer-Tropsch Synthesis. *Chin. J. Catal.*, 2012; 33: 1119-1124.
- [13] Pour AN, Kamali S SM, Bozorgzadeh HR, Zamani Y, Tavasoli A, Ahmadi MM. Effect of Mg, La and Ca promoters on the structure and catalytic behavior of iron-based catalysts in Fischer-Tropsch synthesis. *Appl Catal A: Gen*, 2008; 348: 201-208.
- [14] Feyzi M, Jafari F. Study on iron-manganese catalysts for Fischer-Tropsch synthesis. *J. Fuel Chem. Technol.*, 2012; 40(5): 550-557.
- [15] Bakavoli M, Zamani Y, Akbar ZM. Study on the carbon dioxide hydrogenation to hydrocarbons over nanoparticles iron-based catalyst. *Pet Coal*, 2014; 56(5): 480-486.

To whom correspondence should be addressed: Dr. Yahya Zamani, Research Institute of Petroleum Industry (RIPI), National Iranian Oil Company; West Blvd., Near Azadi Sports Complex P.O.BOX 14665-137, Tehran, Iran,

ENERGY SAVING TECHNOLOGIES IN THE PETROLEUM REFINING PROCESSES

Yurii Danilov, Irina Sinkevich, Inna Lavrova, Aleksey Mardupenko, Alena Tulskaaya*

National technical university “Kharkiv polytechnic institute”, Kharkiv, Ukraine

Received October 12, 2017; Accepted December 23, 2017

Abstract

This article describes the compounds of energetic material costs of the oil refining at the refineries and some tendencies of energy – saving technologies. It also shows the possibility of applying heat pumps, refrigeration machines, heat pipes for refining plants modernization and reduction in energy consumption.

Keywords: : temperature; pressure; energy-saving; heat pumps; refrigeration machines; heat pipes; heat recovery; screw compressor.

1. Introduction

Oil refining industry has defined the direction of development which stipulates deeper oil processing and increase of light products output, the requirements for motor oils quality increase as well. All these obstacles lead to considerable complication of the technological schemes and sharp increase of the refining expenses. Decrease of the energy costs is one of the most relevant problems, and its solving is connected with upgrade of equipment, integration of heat flux by using Pinch analysis. Also of interest is implementation of the modern hi-tech designs such as the absorbing heat inverter (AHI), compressor heat pump and heat pipes, which found a wide application in the nuclear and many others branches of industry [1].

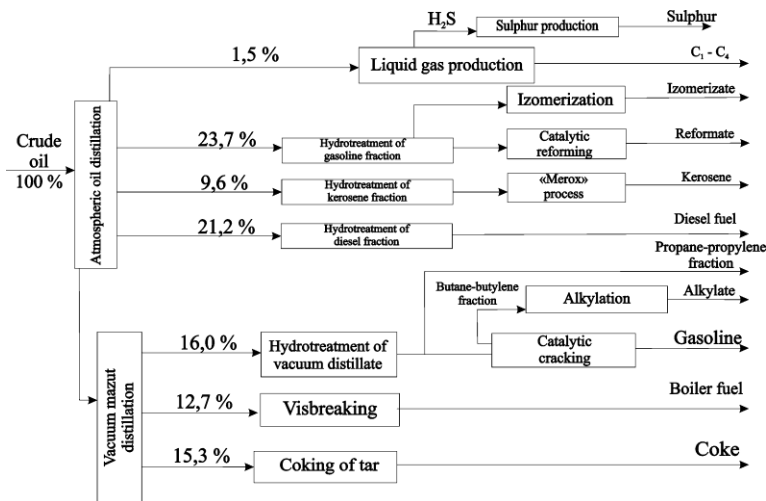


Fig. 1 presents typical structure of oil processing according to the fuel scheme.

Analysis of this scheme has shown that summary energy costs of oil processing reach from 15 to 17 % of extracted oil (fig. 2). That means not only immense material expenses but also a large amount of atmospheric emissions.

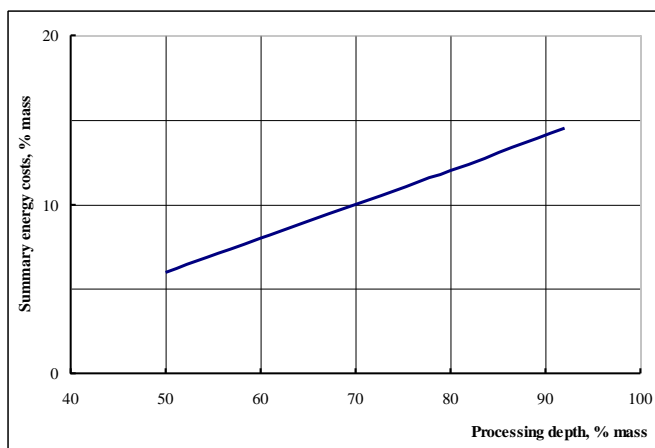


Fig. 2. Summary energy costs of oil processing

The primary oil processing facility is very energy-intensive due to the large amount of raw products. It is followed by hydrotreating and reforming facility, then – catalytic cracking and hydrocracking. The distinctive feature of these processes is the comparative low temperatures for their implementation (about 423 – 473 K). The raw is heated, as usual, by water vapour or high-temperature coolant, that has been heated previously in a furnace. The low temperature of output products does not allow to achieve high level of heat level of heat recuperation. The specific energy consumption is 70- 100 kg of fuel per 1000 kg of refining materials.

One of the most perspective hi-tech designs are the absorbing heat inverter (AHI), compressor heat pump and heat pipes, how it was already mentioned before.

The AHI has these following advantages: ability to work in coolness production mode and heat production mode at the same time, herewith secondary products may be used as the sources of energy. The secondary products are water vapour under pressure 0,15 – 0,17 MPa, hot water with the temperature about 360-370 K etc.

The most popular among the AHI's are absorbing lithium bromide refrigeration machines (ABRM). The production cost of the cold, produced by these machines is 2-3 times lower than the production cost of the cold, produced in compressing cold machines. Applying the ABRM allows to reduce energy consumption and the capital expenditures pay off in less than 2 years [2].

Domestic and foreign manufacturers propose the wide range of screw compressors for compressing the hydrocarbon gases, including oil gas, torch gases etc. Screw compressors do not become fouled because compressed vapour takes the impurities out.

Heat pump is the advice, which is able to transfer a large amount of power at the low temperature gradient. It has encapsulated design which is partly filled with liquid coolant [2-3].

In the heating zone liquid coolant evaporates with absorption of heat. The movement of vapour from the evaporation zone to the condensation zone occurs due to the gradient of pressure of saturated steam in these zones. The liquid moves back to the evaporation zone through the capillary structure (wick), which is located inside the heating tube, mainly on its walls, by the gravity force or capillary pressure gradient. The effective thermal conductivity of heat pipe is 10 times more than thermal conductivity of copper, silver or aluminum and reaches 10^7 W/m·K.

The wick heat pipes, in which the transfer of liquid phase occurs due to the capillary forces, have wide application in nuclear, space and electronic industry, in the environment where the gravity is low or absent. The most perspective for applying in petroleum industry are smooth gravity tubes with phase transition – they are also called thermosiphon. The wick-fed structures of inner surface of the pipe produce additional hydraulic resistance for the condensate flow. As a results, the heat flux in wick pipes is less than in thermosiphons.

The heat pipes may be also applied for utilization of heat of exhausted gases, cooling of the liquid flux, warming of the thermolabile liquids at the constant temperature etc.

Several ways of application of the AHI, compressing heat pumps, screw compressors and heat pipes in the oil processing are given below.

2. Primary oil processing

As it was mentioned above, the primary oil processing equipment is the most energy-intensive. There is two possible ways of cost reduction: increase of the recuperation level of waste products and optimization of the technological schemes and parameters of the oil distillation.

The first way deals with the optimization of heat-exchange scheme and decrease of temperature of oil that comes to the heating furnace. In the modern equipment this temperature reaches 540-550 K. At the same time, waste products with the temperature lower than 420 K may transfer its heat to the air in numerous air-cooling units (ACU), but they're not practically applied at all. Therefore, we have great possibility to decrease the amount of ACU and reduce the energy consumption [4].

The second way deals with the optimization of the separation scheme, decrease the pressure level in atmospheric and vacuum columns. All these obstacles allow to reduce the heat load in furnace and reduce the heating temperature in atmospheric and vacuum columns to 630 and 650 K respectively, reduce the raw decomposition level and coking of furnace coil. Due to the decrease of pressure the conditions of steam condensation at the top of the column get worse. The screw compressor may be used to support the pressure to supply the gas to the hydrotreating unit and the liquid gas emission unit [5-6].

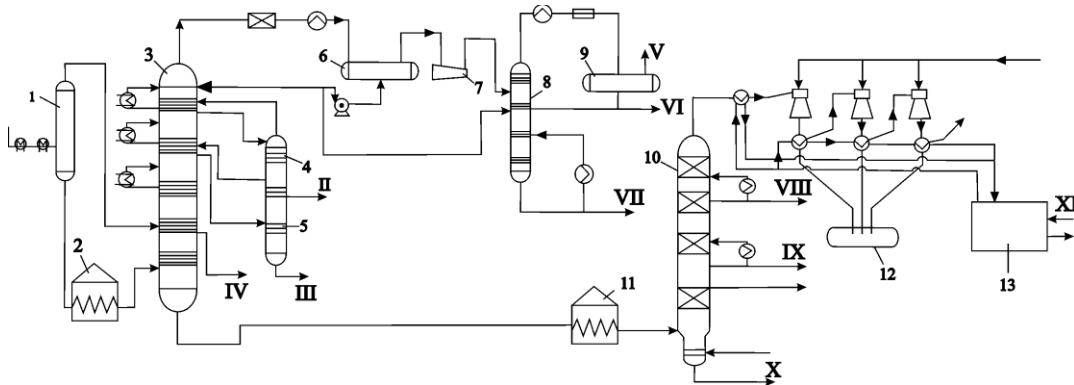


Fig.3 - The principal scheme of atmospheric distillation unit: 1 - preliminary separator; 2,11 - heating furnaces; 3 - atmospheric column; 4,5 - stripping-sections; 6,9 - reflux vessels; 7 - screw compressor; 8 - stabilizer; 10 -vacuum column; 12 - barometric vessel; 13 - ACU; I - oil; II - kerosene fraction; III - light diesel fraction; IV - heavy diesel fraction; V - fuel gas; VI - liquid gas; VII - stable gasoline fraction; VIII - diesel fuel compound; IX - vacuum gasoil; X - tar; XI - low-pressure water vapour

Fig. 3 presents the technological scheme of the primary oil processing with applying the power saving technologies. It has the following features:

- The temperature of oil after the desalter unit rises up to 550 K due to the effective heat-exchange scheme
- The furnace has a separator to decrease the pressure drop 1
- The excessive pressure on the top of the atmospheric column 3 is about 0,14 MPa
- The temperature of oil at the furnace exit is 630 K
- The screw compressor 7 has been installed to feed the stabilizer 8 with the steam.

Pressure in the compressor raises up to 0,9 MPa

The calculations have shown that due to the decrease of pressure in atmospheric column by 0,8 MPa, specific energy costs decrease by more than 10 %.

In vacuum unit due to the low pressure drop at the top of the vacuum column (3,99 kPa) and low pressure drop inside the column and transfer pipeline it is possible to decrease the temperature of fuel oil heating at the furnace exit to 650 K. To support the required pressure

of 3,99 kPa in vacuum column, the water steam is injected into the cube and it is also necessary to keep the temperature at 293 K. These conditions are provided by ABRM 13, in which the circulating water is cooled down to 288 K. Pressured steam (0,15 MPa) may be used in ABRM as a coolant.

In general, application of energy-saving technologies in the primary oil processing may provide the decrease of effective energy costs, the recoument of capital expenditures is approximately 1,5 years [51].

3. Hydrotreatment of medium distillates

The hydrotreatment of medium distillates is widely used in modern technology of oil processing and takes the second place by the energy expenditures (after the primary processing). The main ways of the energy expenditures reduction are:

- Improving of the catalysts' system
- Decrease of the hydrogen concentration (integration of the concentrated hydrogen unit into the plants)
- Combination of the cold and hot separation for more effective hydrogen emission and maximal extraction of the liquefied gas
- Optimization of the heat-exchange scheme, exclusion of the air-cooling units, which use refrigeration machines

4. Izomerization, production of Methyl tert-butyl ether (MTBE) and fractioning of gases

These processes are performed at relatively low temperatures with clear rectification of fractions, at are required high energy expenditures. For reduction of these expenditures it is reasonable to use the heat pump and ABRM

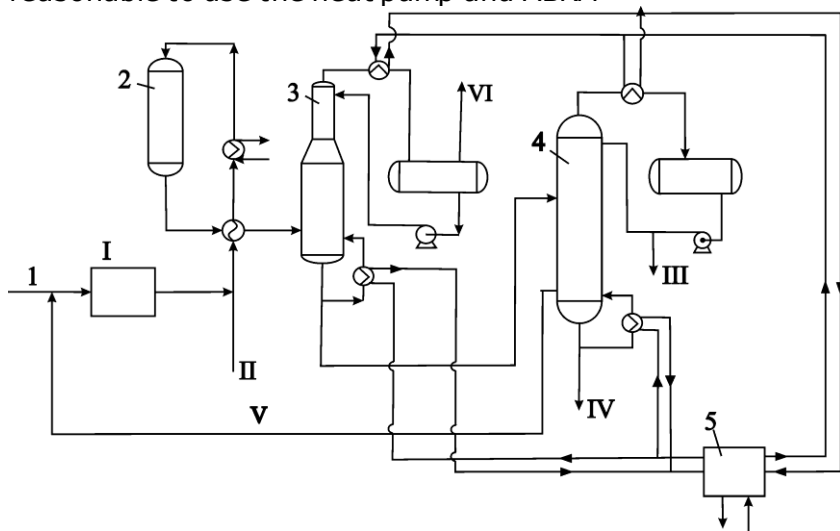


Fig. 4 – Principal scheme of isomerisation unit: 1 – dryer; 2 – reactor of isomerisation; 3 – stabilization column; 4 – deisohexanizer; 5 – ACU; I – raw material, II – hydrogen; III – isomerizate; IV – C₇₊ fraction; V – recycled material; VI – fuel gas.

Fig. 4 presents the principal technological scheme of isomerization unit with ABRM, which is able to produce cold and hot water at the same time. Cold water is used for reduction the temperature of recycling water and in rectification columns and hot water is used for heating of the columns' cubes. The water steam of fuel gas may be used as coolants.

The application of AHI provides the reduction of energy expenditures in more than 1,5 times.

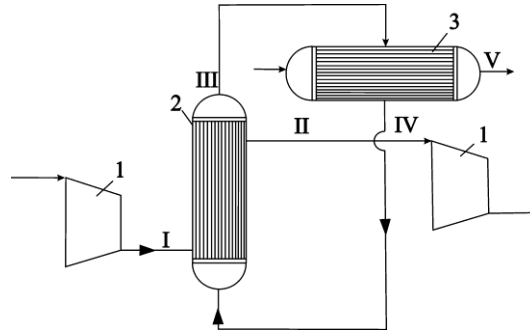


Fig. 5 – Principal scheme of gas cooling with the heat pipe: 1 – compressor; 2 – evaporator of heat pipe; 3 – condenser of heat pipe; I – hot gas; II – cold gas; III – vapour; IV – condensate; V – water

Fig. 5 presents the principal scheme of gas cooling between the compressor stages with application of heat tube. The hot steam after the first compressor's stage goes to the tubular or plate evaporator 2 where it transfers the heat to the intermediate coolant, that boils in the tubes. Then, steam goes to the condenser 3 through the heat pipe, and the condensate goes back to the evaporator by the gravity. As a result the heat-transfer process is closed.

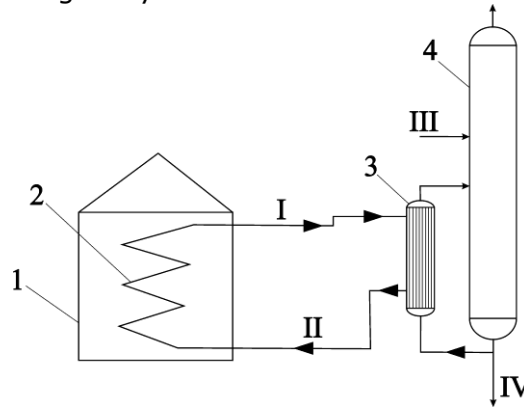


Fig. 6 Principal scheme of heating of the column cube with the heating pipe: 1 – heating furnace; 2 – evaporator of heat pipe; 3 – condenser of heat pipe; 4 – rectification column; I – coolant vapour; II – coolant condensate; III – raw material; IV – bottom stream

Fig. 6 presents the principal scheme of heating of the column cube with application of heat pipe. The evaporator of heat pipe (2) is placed into the heating furnace 1, and the condenser 3 is used for heating of the column cube (4). The heating tube can be up to tens meters long and requires the relevant support. And it is also necessary to calculate the hydraulic resistance of the whole system.

The choice of coolant depends on temperature level of heat transfer, physical and chemical properties and other. Therefore, as a coolants we may use alcohols, freons, distilled water, metals etc.

The heat pipe provides effective heat transfer with the minimal temperature drop and maximal heat transfer coefficients due to the phase transitions. And due to the absence of pumps the operation and capital costs are reduced to a minimum.

Symbols

AHI	absorbing heat inverter
ABRM	absorbing lithium bromide refrigeration machines
ACU	air-cooling units
MTBE	methyl tert-butyl ether

References

- [1] Klochkov IN, Chekmenev VG, Karmanov YeV. Nizkonapornye raspredeliteli dlya nasadochnykh kolonn. *Khimiya i tekhnologiya topliv i masel*, 2004; 1:60-62.
- [2] Lebedev YuN, Sumina AN, Chekmenev VG, Danilov DYu. Eksperimentalnaya baza osnova modernizatsii tekhnologicheskogo oborudovaniya. *Khimiya i tekhnologiya topliv i masel*, 2000, № 5:38-41.
- [3] Lisienko VG, Shchelokov YaM, Ladygichev MG. *Khrestomatiya energosberezheniya: Spravochnoe izdanie V 2 kn. Kn.1/pod red. V.G. Lisienko*, Moscow, Teplotekhnika, 2005.
- [4] Gnedoy N. *Energoeffektivnost i opredelenie potentsiala energosberezheniya v neftepererabotke*, Kiev:Naukova dumka, 2008.
- [5] Burdygina YeV. *Povyshenie energoeffektivnosti teplotekhnicheskogo oborudovaniya pervichnoy pererabotki nefiti. Avtoreferat na soiskanie uchenoy stepeni kandidata tekhnicheskikh nauk*. Ufa: Ufimskiy gosudarstvennyy neftyanoy tekhnicheskiiy universitet, 2003:23.
- [6] Burenin VV. *Teploobmennyye apparaty dlya neftepererabatyvayushchikh i neftekhimicheskikh proizvodstv. Neftepererabotka i neftekhiymiya. Nauchno-tekhnicheskiiy dostizheniya i perezodovoy opyt*, 2006, №7:41-44.

To whom correspondence should be addressed: prof. Alena Tulskaaya, National technical university "Kharkiv polytechnic institute", Kharkiv, Ukraine, fuel.khpi@gmail.com

THE FRACTAL DIMENSION OF THE CARBON DEPOSITS FROM COKE OVEN CHAMBERS

Vladimir M. Shmalko, Oleg I. Zelenskii, Alexey V. Sytnik

Ukrainian State Coal-Chemistry Institute, 61023, Kharkiv, 7 Vesnina Str., Ukraine

Received November 15, 2017; Accepted December 23, 2017

Abstract

In this paper, the fractal dimension of carbon deposits from coke oven chamber is defined. The surface of the carbon deposit has been examined using a scanning electron microscopy. The images of surfaces of the carbon deposit are given. The analysis and measurements of fractal clusters images have been presented. The data on the actual density of the deposit and its electrical resistance is given. The sphere-like clusters of the fractal structures are layered bodies. The fractal dimension D of the carbon deposit that is formed in the cells of coke ovens is 2.925.

Keywords: *fractals; carbon deposits; clusters; layered structures; scanning electron microscopy.*

1. Introduction

Fractal solid bodies are formed under conditions of energy dissipation in the open self-organizing systems. The driving force of self-organization in dissipative systems is the tendency of the substance to decrease the entropy [1]. The typical features of the fractal structures are a self-similarity, scale invariance, a structural hierarchy, nanoscale porosity and a fractal dimension.

Fractal structures are formed from atoms, molecules, nanoscale particles, and clusters. Substance clusters form three-dimensional structures with the characteristics of fractality. The typical examples of fractal structures are carbon deposits (cathode deposit) at graphite sputtering in the plasma of electric arc during the process of fullerenes obtaining [2-7]. Besides that, carbon films deposited in fusion devices are also fractal structures [8].

The above mentioned characteristic features of fractal structures were most clearly obvious in carbon deposit, obtained by plasma sputtering of graphite in an electric arc [2-3]. In the initial stage of carbon deposits, formation spherical carbon cluster size of 6-8 nm are formed, from which spherical aggregates of size 0.3-0.6 microns are formed. Carbon deposit has micro-hardness, vastly greater than graphite, the density of 1.32 g / cm^3 , while the density of graphite is 2.3 g / cm^3 . The low density of the carbon deposit is the evidence of its porosity.

It is well known that during the carbonization the growth of carbon deposits in the coke oven chambers is observed. The presence of carbon deposits can cause a number of serious problems in the coke oven operation. They may inhibit the gas flow from the furnace, and their removal can cause damage to the refractories and the coke pusher equipment. Some plants burn carbon deposits in the empty furnace, and this obviously leads to the loss of efficiency and damage of the brickwork, which can also lead to the environmental problems [9-10].

Carbon deposits from the coke oven chambers are heterogeneous materials, but most of them are composed of spherical formations, similar in structure to the carbon deposit, obtained by plasma sputtering of graphite in an electric arc. As the carbon deposits from the coke oven chambers have not considered as fractal structures yet, in this paper, we make an attempt to identify and assess their fractal characteristics.

2. Experimental

2.1. Samples preparation

The samples of the carbon deposits, selected from the existing coke oven chamber were examined. Sampling was conducted during the period between the chamber loadings. The outer layer of the carbon deposits parallel to masonry furnace was used for analysis. The parts for research (block sizes of 20 x 20 mm) were cut with a diamond cutter. The carbon deposits from the coke oven chambers, which are on the surface from the side of coking coal charge, have globular clusters that are apparent to the naked eye.

2.2. Electronic scanning microscopy

The depositing surface of the coking chamber has been examined using a scanning electron microscopy (SEM) with an electron microscope Jeol JSM 5800LV. The accelerating voltage was 20 kV. To conduct the research, we have prepared carbon deposit cleavages of size 3 x 3 mm, on which we have deposited a graphite layer in a vacuum, and then we have deposited a layer of gold. Thereafter, the samples have been placed under a microscope and examined. The analysis and measurements of the images have been presented using Altami Studio 2.1 software.

2.3. Characterization

For carbon deposits samples we have determined the yield of volatile substance on the dry and ashless dry mass, ash content, the actual density (pyknometric method) and resistivity (a two-probe method). Electrode graphite has been used as a comparison sample. We have also determined the density and electric resistance of graphite.

3. Results and discussion

Devolatilization for carbon deposit dry weight V^d constituted 1.63 % for dry ashless weight V^{daf} it constituted – 1.69 %. Ash deposit – A^d – was 3.42 %. Table 1 shows the results of determining the actual density and the electric resistance of the samples of carbon deposits and the graphite electrode.

Table 1. The characteristics of the examined samples

The name of the sample	Actual density, g/cm^3	Electrical resistance, 10^{-4} Ohm/m
Carbon deposit	1.982	9.7
Graphite	2.250	3.8

Our experiments have shown that the density of the carbon deposit is less by 12 % than graphite, and its resistivity is about 2.6 times as much as graphite. The differences in the density of graphite and deposit are probably due to the deposit porosity. A higher value of the deposit electrical resistance can occur due to special features of electron transfer in the fractal bodies as well as the deposit porosity.

There is every reason to determine the carbon deposit of the coking chamber as a fractal structure in the following ways: self-similarity, scale invariance, and a structural hierarchy. The results of the electron microscopic research confirm the fractality of the examined carbon deposit samples from the coke oven chamber, Fig. 1(a-c). Fig. 1c shows that the spherical clusters, in turn, are superficial and contain the surface clusters.

The surface clusters sizes are within 0.5-2.8 μm . It is difficult to determine the exact dimensions since the surface clusters are not the planar shapes and they present bulges of different height on the spherical surface. The surface appearance of the carbon deposit clusters resembles foam, though globular clusters are not hollow, they are a multi-layer formation of the bulbous carbon type. The layering of clusters is clearly visible in places of clusters separation from each other (Fig. 2).

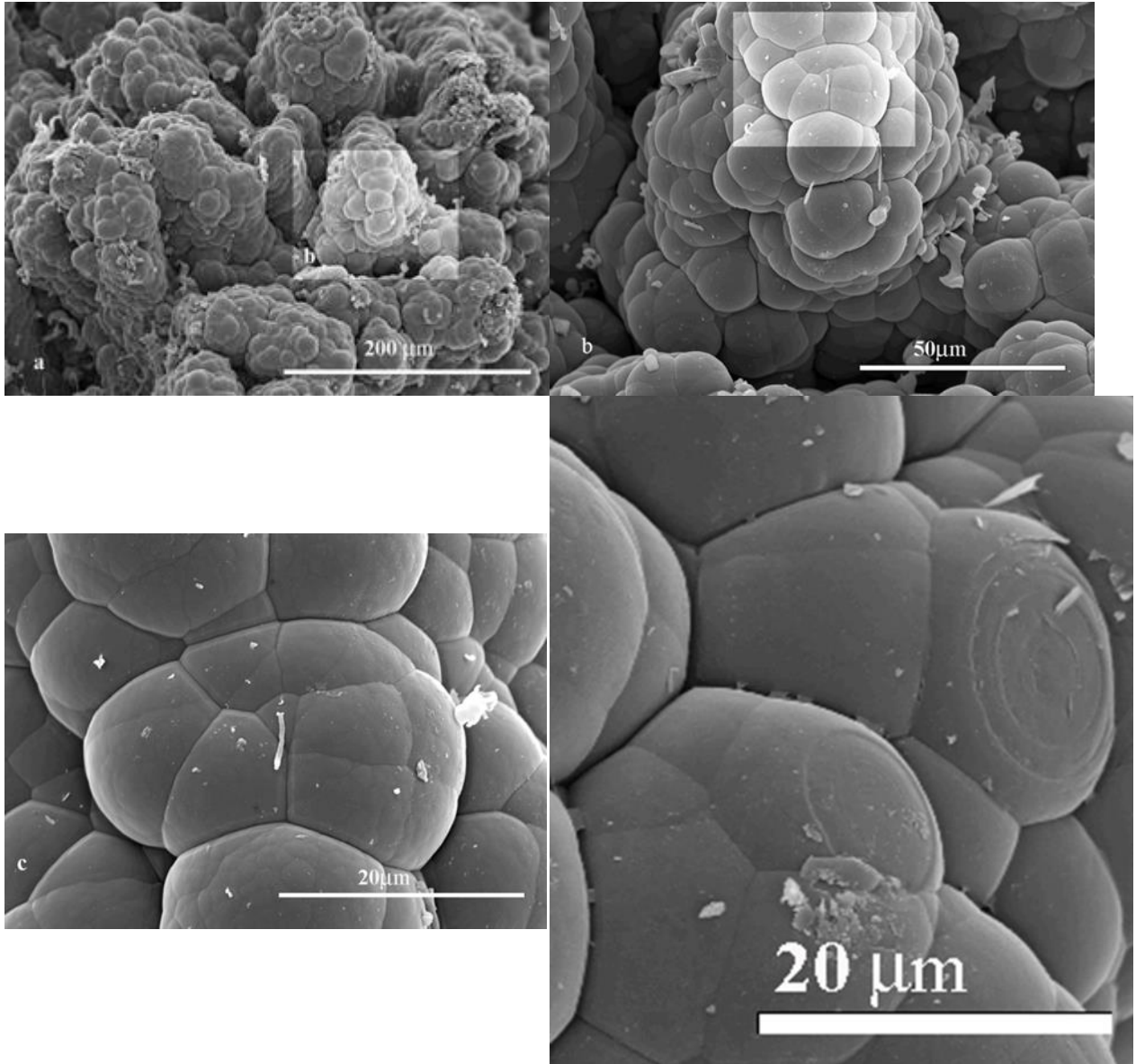


Fig. 1 (a,b,c). The fractal structure of the carbon deposits from the coke oven at different magnifications

Fig. 2. Multi-layer structure of the cluster from the coke oven deposit

The average diameter of the carbon deposit clusters is 18.5 μm . But there are opened or "destroyed" clusters with a diameter of 100-200 μm . One of such carbon deposit clusters from the chamber coke oven is shown in Fig. 3.

In the center of this cluster, we can see the embryonic structure, whose dimensions do not differ significantly from the mean size of the fractal clusters. The layered structure of the carbon cluster is visible. The layer thickness is 0.5-1.0 microns. Part of the layers is "fused."

The texture of layers resembles a cabbage leaf. Each such "cabbage leaf" has a fractal structure of the same type as the spherical surface of the clusters in Fig. 1c.

The layer thickness of the carbon clusters deposit is not apparently associated with coking periods as during the coking period of coal loading a layer carbon deposit from 200 μm or more can be formed on the surface of refractories.

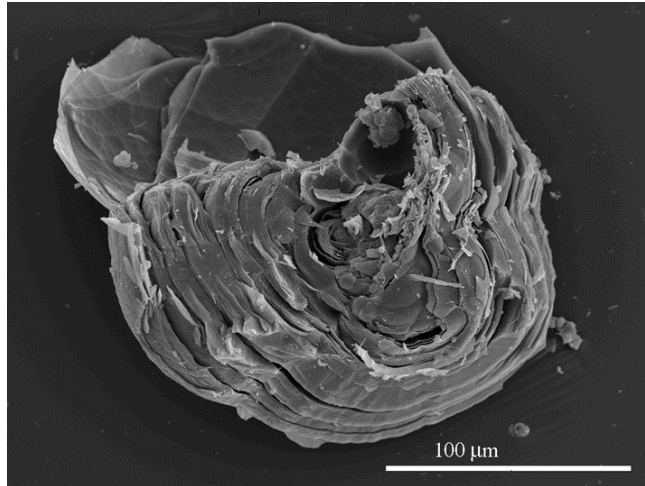


Fig. 3. Destroyed cluster of the carbon deposit from the coke oven chamber

To calculate the fractal dimension, we should use the model of fractal aggregates composing of clusters with radius r_0 and having a density of graphite ρ_0 . With a radius of a fractal aggregate $R \gg r_0$, the number of clusters is defined as [11]

$$N(r) = (R/r_0)^D, \quad 1 < D < 3, \quad (1)$$

where D is a fractal dimension.

From (1) it is followed the expression that determines the density of substance in the sphere of radius R

$$\rho = \rho_0 (r_0/R)^{3-D}, \quad (2)$$

where ρ is the density of the carbon deposit.

With an average value of $r_0 = 9.25 \cdot 10^{-3} \text{ g/cm}^3$ and $\rho = 1.982 \text{ g/cm}^3$, $\rho_0 = 2.250 \text{ g/cm}^3$, and $R = 50 \cdot 10^{-3} \text{ cm}$ we obtain the fractal dimension $D = 2.925$.

The fractal structure of the carbon deposit from the coke oven chambers are not spherical bodies in the pure form, and therefore the value of R is estimated. Nevertheless, in our opinion, the obtained value of the fractal dimension is very close to reality.

In order to "get rid" of the specific sizes of fractals and clusters, we have calculated the fractal dimension of the deposit for a fairly wide range of radii ratio of clusters and fractal structures (Fig.4).

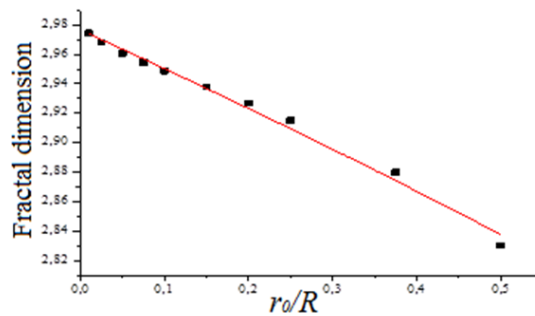


Fig. 4. The dependence of the fractal dimension D on the ratio r_0/R

We have shown the calculated dependence on the fractal dimension D of the ratio r_0/R . This dependence is well described (the determination coefficient $R^2 = 0.99$) with the equation of the following type:

$$D = \ln(a - bx), \quad (3)$$

Spherical clusters have a fairly narrow size distribution. Virtually small spherical clusters with a diameter of 10-12 μm are almost absent. Furthermore, we note almost a total absence of the separate spheres carbon deposit in micrographs. The lack of small spherical clusters suggests

that small clusters on the surface of a sphere with the accumulation of masses of carbon deposits increase in size and become spherical clusters. Carbon deposit clusters "grow" one from another, forming a conical fractal structure.

Perhaps this is due to the temperature difference between the coke gas in the furnace containing carbon aggregates, such as the ones that are described in work [11], and the chamber wall, resulting in their precipitation and an intensive growth mainly of existing "embryonic" cluster structures. Their growth speed is expected to be maximum in the direction, coinciding with the direction of the maximum gradient of "concentration," i.e., it is perpendicular to the chamber wall, which also explains the "relief angle" formations.

Obviously, the presence of attractive forces between the complexes of carbon atoms leads, as in the case with liquids, to the formation of sphere-like structures, as evidenced by a number of experimental studies [10].

4. Conclusions

Our research of the carbon deposits samples taken from the operating coke oven chamber has been carried out with the help of electron microscopy. The study has discovered that the carbon deposits samples have an evident fractal structure.

The analysis of the obtained results suggests that the fractal dimension of the carbon deposit D , which is formed in the coke oven chambers is very high and has the value $D = 2,925$. We can also assume that the spherical clusters are also fractal bodies and they "grow" from the surface of clusters, increasing in volume during the accumulation of carbon in the sediments of the coke oven chambers.

Acknowledgement

The authors express their sincere gratitude to Valentina Zubkova, Professor of the Institute of Chemistry attached to the University of Jan Kochanowski in Kielce (Poland) for invaluable assistance in the organization of electron microscopy studies of the carbon deposit.

References

- [1] Family F, Vicsek T. Dynamics of Fractal Surfaces, World Scientific: Singapore, 1991; p. 492.
- [2] Charlse ML, Chia-Chun C. Preparation of fullerenes and fullerene-based materials. Solid State Phys. 1994; 48: 109–148.
- [3] Churilov GN. Synthesis of fullerenes and other nanomaterials in arc discharge. Fuller. Nanotub. Carbon Nanostruct. 2013; 16: 395–403.
- [4] Murr LE, Brown DK, Esquivel EV et al. Carbon nanotubes and other fullerenes produced from tire powder injected into an electric arc. Materials Characterization. 2005; 55: 371–377.
- [5] Pang LSK, Vassallo AM, Wilson MA. Fullerenes from coal: A self – consistent preparation and purification process. Energy and Fuels. 1992; 2: 176–179.
- [6] Patney HK, Nordlund C, Moy A, Rose H, Young B, Wilson MA. Fullerenes, and nanotubes from coal. Fullerene Science Technology. 1999; 7(6): 941–971.
- [7] Zelenskii OI, Shmalko VM, Udovitskii VG et al. Production of carbon nanostructures by the atomization of solid coking products within an electric arc. Coke Chem. 2012; 55(2): 76–81.
- [8] Budaev VP, Khimchenko LN. Fractal nano- and microstructure of the deposited films in thermonuclear machines. Journal of Experimental and Theoretical Physics. 2007; 131(4): 711–728.
- [9] Barranco R, Patrick JW., Snape C, Poultney RM., Diez MA., Barriocanal C. Deposition and characterization of pyrolytic carbon in industrial coke ovens by optical microscopy and SEM. The Society for Organic Petrology. TSOP / ICCP 2008, Oviedo, Spain.
- [10] Zymła V, Honnart F. Coke oven carbon deposits growth and their burning off. ISIJ International. 2007; 47(10): 1422–1431.
- [11] Piechaczek M, Mianowski A. Coke optical texture as the fractal object. Fuel. 2017; 196: 59–68.

To whom correspondence should be addressed: Dr. Vladimir M. Shmalko, Ukrainian State Coal-Chemistry Institute, 61023, Kharkiv, 7 Vesnina Str., Ukraine, v.shmalko@gmail.com

EFFECTIVE CATALYST TO PRODUCE NAPHTHA FROM VACUUM GASOIL HYDROCRACKING AND DISCRETE LUMP MODELING

Ehsan Taghizadeh Yusefabad¹, Ahmad Tavasoli¹, Yahya Zamani²

¹ School of Chemistry, College of Science, University of Tehran, Tehran, Iran

² Research Institute of Petroleum Industry, Tehran, Iran

Received November 4, 2017; Accepted December 23, 2017

Abstract

A multi performance characteristics optimization based on Taguchi approach is proposed for Vacuum Gas Oil (VGO) hydrocracking process. Experimental runs have been planned as per Taguchi's principle with three important input parameters such as reaction time, temperature, and kind of catalyst. Results show that the kind of catalyst is the predominant variable for the desired performance characteristics. Discrete lumping model is developed to predict pseudo-components (gas, naphtha, kerosene, and diesel) produced during the process. Finally, a production model for the produced pseudo-components in the presence of the selected catalyst was formulated.

Keywords: : Vacuum gas oil; Hydrocracking, Catalyst; Naphtha; discrete lumping model.

1. Introduction

To improve the quality of petroleum fuels, the environmental regulations have led to the development of hydrocracking process as the second important refining process. Hydrocracking is a catalytic cracking process for conversion of complex feedstocks, such as vacuum gas oils (VGO), into lighter and valuable products such as LPG, naphtha, kerosene, and diesel [1]. As the demand for light fuels is going to increase rapidly, the quality and yield of hydrocracking products have to be further improved to meet the future demands [2].

To understand more about hydrocracking of unconventional crude oils, information about the effect of reaction conditions on selectivity, conversion, and type of feedstock is essential. This information can be obtained either from experiments or by simulation. It should be considered that experiments are highly desired, but they are costly and time consuming. Simulations are usually very rapid and cheap to conduct. However, modeling hydrocracking of heavy oils is not an easy task, since it requires detailed characterization of products and feed, in contrast to other lighter petroleum streams, is more complex to perform due to the huge amount of heavy hydrocarbons present on its composition. An accurate kinetic model must be employed during the simulation of hydrocracking reactor. There are different approaches for modeling hydrocracking kinetics which have been recently reviewed by Ancheyta *et al.* [3]. Modeling kinetics of the reactions which are occurring during hydrocracking of petroleum feedstocks has been traditionally studied by discrete approximation, specifically by lumping compounds of feed and produced products into a few cuts which are characterized by ranges of normal boiling points (e.g. naphtha, middle distillates, residue, etc.), which undergo different series and parallel reactions [3]. The important advantages of the lumping technique are its easy computational implementation and a small amount of data required for parameter estimation. The more lumps, the better description, but increasing the number of lumps increases the number of parameters to be estimated [3]. In the lump modeling, compounds have been classified based on certain factors. These pseudo-components have a same molecular structure and classified based on different properties such as boiling point,

molecular mass, a number of carbon atoms and so on [4]. Some examples of research done in this field are given as follows.

In 2013, Al-Humaidan *et al.* have investigated the effect of operating conditions (i.e., residence time and reaction temperature) on the quality of the products and yield. They also determined the kinetic parameters from the experimental data and compared them with each other [5]. Browning *et al.* based on analyzing results which are obtained from two-dimensional gas chromatography have developed a kinetic model for hydrocracking of a real VGO in a semi-batch reactor [6]. In 2014, Ignacio Elizalde and Jorge Ancheyta studied the kinetics of the hydrocracking of residue and catalyst deactivation by using the continuous kinetic lumping approach [7].

To simulate and design the behavior of heavy oil upgrading processes at commercial scale, adequate reactor modeling tools are required. The objective of this work is the development of a kinetic model based on experimental data, to account major VGO hydrocracking reactions capable of describing the behavior of both pilot and industrial scale reactors. The experiments were designed by Taguchi method to produce naphtha from VGO hydrocracking, and then the discrete lumping model of the selected catalyst is studied.

2. Reaction systems

2.1. Testing procedure of the catalysts in hydrocracking of VGO

Hydrocracking of n-hexadecane was conducted on a steel tubular fixed-bed down-flow reactor. The experimental setup was depicted in figure 1.

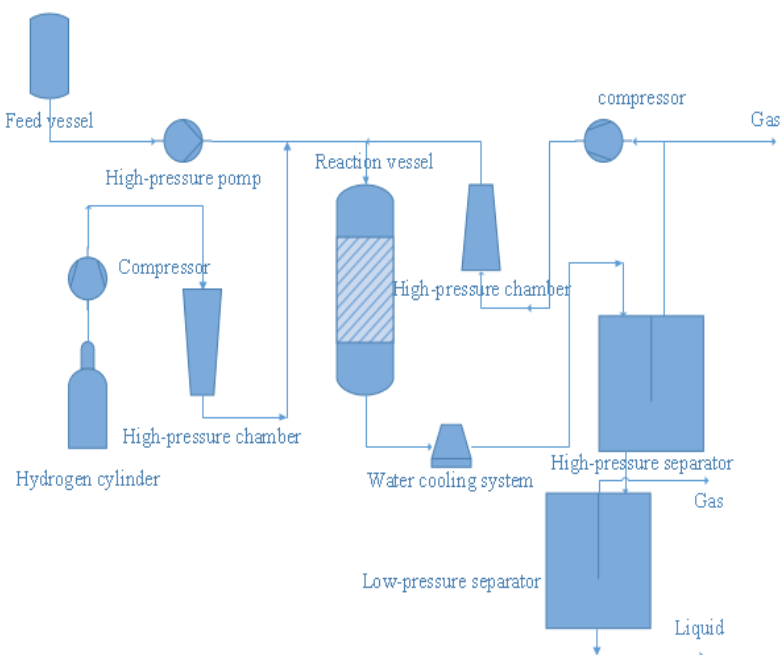


Figure 1. Schematic of the experimental setup

For each test, 1 gr catalyst was filled in the reactor and reduced by H₂ gas at 30 bar pressure and space velocity of 200 h⁻¹ with constant heating rate from ambient to 453 K and maintained at this temperature for 1 h. for pre-paring Ni-Mo-S phases, the catalysts were sulfided by a stream of 1wt% of dimethyl disulfide in hexane. Conditions of sulfidation were as follows: hydrogen atmosphere with an H₂/Oil volumetric ratio of 80 nL/L at 30 bar and a space velocity of 200 h⁻¹. Then, the samples were heated from 453 to 583 K with a constant heating rate of 0.5 K/min and kept at this temperature for 10 h. After the activation step, the performances of catalysts were evaluated using n-C₁₆ hydrocarbons. Conditions of the reaction are as

follows: Feed injection rate of 30 cm³/h and H₂/Oil = 175 nL/L, 30 bar, WHSV = 3 kg/ (L·h), LHSV = 4.2 h⁻¹. Physical and chemical properties of the feedstock are presented in table 1.

Table 1. Physical and chemical properties of the feedstock

Property	Feedstock	Property	Feedstock
Sp. Gr.	0.893	10 Vol%, °C	380
Viscosity @ 100°C	4.8	30 Vol%, °C	407
S, wt%	1.57	50 Vol%, °C	426
C7 insoluble wt%	0.12	70 Vol%, °C	443
Distillation	ASTM D-86	90 Vol%, °C	473
IBP, °C	250	95 Vol%, °C	489
5 Vol%, °C	356	100 Vol%, °C	506
Lumps of feed comp. (wt%)	Diesel	%10	
	VGO	%90	

2.2. Experimental Design method

The Taguchi method has been usually selected to optimize the design parameters [8] because this approach can strikingly minimize the overall experimental costs and the testing time. The optimum experimental conditions, using the orthogonal array can be determined by the Taguchi method, [9]. In this study, Taguchi model with L₁₆(4³) orthogonal array was based on three controllable factors with four levels (Table 2).

Table 2. Factors and levels of each factor

Factor	Description	Level 1	Level 2	Level 3	Level 4
A	Catalyst	USY-ASA/Ni-Mo	USY-ASA/Ni-W	β-ASA/Ni-W	β-ASA/Ni-Mo
B	Temperature, (°C)	380	395	400	410
C	Reaction time, (hr.)	1	2	4	6

The analysis of the signal-to-noise (S/N) ratio is an important parameter in this model. Three usual types of S/N ratio analysis are as follows: (1) higher is better (HB), (2) nominal is best (NB), and (3) lower is better (LB) [9]. Since the target of this study is to maximize the naphtha cut produced from VGO hydrocracking using co-impregnated catalysts, the S/N ratio with HB characteristics is required, which is calculated by:

$$\frac{S}{N} = -10 \log \left(\frac{1}{n} \sum_{i=1}^n \frac{1}{Y_i^2} \right) \quad (1)$$

where: n is the number of repetitions which are under the same experimental conditions and Y is the measurement result.

The analysis of mean (ANOM) statistical approach is adopted herein to determine the optimal conditions. Initially, the mean of the S/N ratio of each controllable factor must be calculated at a certain level. For example, $(M)_{Factor=I}^{Level=i}$, the mean of the S/N ratio of factor I in level i, is given by:

$$(M)_{Factor=I}^{Level=i} = \frac{1}{n_{li}} \sum_{j=1}^{n_{ji}} \left[\left(\frac{S}{N} \right)_{Factor=I}^{Level=i} \right]_j \quad (2)$$

In Eq. (2), n_{li} is the number of appearances of factor I in the level i, $\left[\left(\frac{S}{N} \right)_{Factor=I}^{Level=i} \right]_j$ is the S/N ratio of factor I in level i and j^{th} is its appearance sequence in Table 2. The analysis of variance (ANOVA) statistical method is also used to analyze the influence of each controllable factor under discussion process of VGO hydrocracking. The percentage contribution of each factor, ρ_F , is given by:

$$\rho_F = \frac{SS_F - (DOF_F V_{Er})}{SS_T} \times 100 \tag{3}$$

In Eq. (3), DOF_F is the degree of freedom of each factor, which is obtained by subtracting one from the number of the level of each factor (L). In equation (3) SST is the total sum of squares and given by:

$$SS_T = \sum_{(j=1)}^m (\sum_{(i=1)}^n Y_i^2) j - mn(\bar{Y}_T) \tag{4}$$

In equation (4), \bar{Y}_T is:

$$\bar{Y}_T = (\sum_{(j=1)}^m (\sum_{(i=1)}^n Y_i) j) \div mn \tag{5}$$

In equation (5), m represents the number of experiments carried out in this study, and n is the number of repetitions under the same experimental conditions. In equation (3) SSF is the factorial sum of squares and given by:

$$SS_F = \frac{mn}{L} \sum_{(k=1)}^L (\bar{Y}_K - \bar{Y}_T)^2 \tag{6}$$

Here \bar{Y}_K is the average value of the measurement results of each factor in the k_{th} level.

Furthermore, the variance of error, V_{Er} , is given by

$$V_{Er} = \frac{(SS_T - \sum_{(F=A)}^E SS_F)}{(m(n-1))} \tag{7}$$

In this research, the minimum applied temperature was set at 380°C, and the maximum temperature was set at 410°C. In temperatures above 500°C, all of the liquid feedstock can be converted into gas [10], on the other hand, at temperatures below 350°C; hydrocracking of VGO to the liquid product is ineffective. Reaction time is also an important factor in effectively designing catalytic process of hydrocracking [12], so it considered in this model investigation. The reason could be explained by the fact that when the reaction time exceeds the optimum time, the majority of the liquid feed will be converted into other products such as naphtha and gas [10]. Experiments designed using Taguchi method is listed in Table 3.

Table 3. Experiments design by Design-Expert software and Taguchi method

Test number	Factor A: catalyst	Factor B: Temperature, (°C)	Factor C: reaction time (hr.)
1	USY-ASA/Ni-Mo	380	1
2	USY-ASA/Ni-Mo	395	2
3	USY-ASA/Ni-Mo	400	4
4	USY-ASA/Ni-Mo	410	6
5	USY-ASA/Ni-W	380	2
6	USY-ASA/Ni-W	395	1
7	USY-ASA/Ni-W	400	6
8	USY-ASA/Ni-W	410	4
9	β-ASA/Ni-W	380	4
10	β-ASA/Ni-W	395	6
11	β-ASA/Ni-W	400	1
12	β-ASA/Ni-W	410	2
13	β-ASA/Ni-Mo	380	6
14	β-ASA/Ni-Mo	395	4
15	β-ASA/Ni-Mo	400	2
16	β-ASA/Ni-Mo	410	1

3. Kinetic model development

Hydrocracking models have significantly been developed over the last few decades [13]. A number of kinetic models have been suggested to hydrocracking process which has been composed of a limited number lumps (generally less than 10) [13-16]. These models can be used to simulate a small number of quantities which are important to the designer and/or operator of an HCK unit, such as naphtha yield [13]. Two different kinetic lumping models have been used to VGO hydrocracking reaction, (1) continuous and (2) discrete lumping models [17]. The kinetics of gas oil hydrocracking in a continuous fixed-bed tubular flow reactor was studied by Qader and Hill [4]. They found that rate of hydrocracking is of first order with respect to feed concentration [4]. The hydrocarbon mixture is studied in terms of a continuous assignment (i.e., in terms of boiling point) rather than being made up of discrete entities. Then, the reactivity of the hydrocarbon mixture is defined as a continuous function. This subject without an exponential increase in the number of parameters let a fine resolution of the distillation curve. Besides, it is possible to combine the continuous and discrete lumping approaches by defining more than one continuous distribution [18]. The Increase of computational capabilities and the availability of sophisticated analytical techniques (e.g. [19] and [20]) are caused to develop of microkinetic models for HCK of heavy petroleum fractions. In order to reduce the size of the reaction networks, computational algorithms have been made. The single event microkinetic modeling method was originally developed by Froment *et al.* [21]. Before a rigorous lumping model is performed, the single events coefficients [22-23] are calculated for each individual reaction in order to reduce the size of the network without loss in information.

3.1. Discrete lumping model

3.1.1. Models based on wide distillation range fractions

The kinetics of VGO hydrocracking was studied by Hill and Qader in a continuous fixed-bed tubular flow reactor [4, 14, 17]. They found that the rate of hydrocracking is followed by first order with respect to the concentration of feed [17] and activity energy of this reaction is about 21.1 kcal/mol. In this investigation, the kinetic data were obtained at 80 bar pressure, temperatures between [380-410°C], a constant H₂/oil ratio of 5900 scfb. Then based on boiling point range of product, it was classified into LPG (0-39°C), naphtha (IBP- 150 °C), kerosene (IBP- 150-250°C) and diesel (IBP- 250-380 °C). In this investigation, it was observed that depend on temperature, hydrocracking of VGO using a catalyst has been followed by different models. In this letter, a discrete lumping model of the selected catalyst, β -ASA/Ni-W, is considered and changing procedure of their products during the hydrocracking process of VGO was formulated.

3.1.1.1. Discrete lumping model of VGO hydrocracking in presence with β -ASA/Ni-W catalyst

After conducting research on catalyst β -ASA/Ni-W, it was found that in temperatures 380°C this catalyst follows the model listed in Fig. 2. In this model, the four produced cut oils followed by parallel reactions.

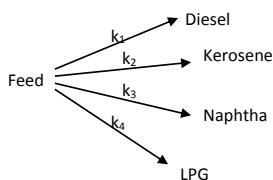


Fig. 2 Schematic of model 1 of hydrocracking process in parallel reactions

Attentive to one-degree kinetic of VGO hydrocracking, kinetic equations of this process in presence with the β -ASA/Ni-W catalyst are as follows. In this process, VGO was converted as equation 3:

$$-r_F = (k_1 + k_2 + k_3 + k_4)F \rightarrow \frac{dF}{dt} = -(k_1 + k_2 + k_3 + k_4)F \xrightarrow{t=0 \Rightarrow F=1} F = e^{-(k_1+k_2+k_3+k_4)t} \quad (3)$$

In mentioned process, the differential kinetic equation of the produced diesel cut follow of equation 4:

$$\frac{dD}{dt} = k_1F = k_1e^{-(k_1+k_2+k_3+k_4)t} \quad (4)$$

Kerosene was changing follows of equation 5:

$$\frac{dK}{dt} = k_2F = k_2e^{-(k_1+k_2+k_3+k_4)t} \quad (5)$$

The differential kinetic equation of produced naphtha follows of as equation 6:

$$\frac{dN}{dt} = k_3F = k_3e^{-(k_1+k_2+k_3+k_4)t} \quad (6)$$

The differential kinetic equation of the produced gas is followed of equation 7:

$$\frac{dG}{dt} = k_4F = k_4e^{-(k_1+k_2+k_3+k_4)t} \quad (7)$$

By this suppose that amount of gas, naphtha, kerosene and diesel were zero at first, solving above equations are as follows:

$$D = \frac{-k_1}{(k_1 + k_2 + k_3 + k_4)} e^{-(k_1+k_2+k_3+k_4)t} + \frac{k_1}{(k_1 + k_2 + k_3 + k_4)} \quad (8)$$

$$K = \frac{-k_2}{(k_1 + k_2 + k_3 + k_4)} e^{-(k_1+k_2+k_3+k_4)t} + \frac{k_2}{(k_1 + k_2 + k_3 + k_4)} \quad (9)$$

$$N = \frac{-k_3}{(k_1 + k_2 + k_3 + k_4)} e^{-(k_1+k_2+k_3+k_4)t} + \frac{k_3}{(k_1 + k_2 + k_3 + k_4)} \quad (10)$$

$$G = \frac{-k_4}{(k_1 + k_2 + k_3 + k_4)} e^{-(k_1+k_2+k_3+k_4)t} + \frac{k_4}{(k_1 + k_2 + k_3 + k_4)} \quad (11)$$

In above equations, kinetic constants, k_1 , k_2 , k_3 , and k_4 , was calculated by fitting between experiment data and the equations [8-11] by Levenberg-Marquart algorithm. After considering experimental data in temperatures between 395-410°C, it could be found this catalyst don't follow the model depicted in Fig. 1. So, another model (Fig. 3) was proposed to explain the performance of the catalyst and changing procedure of different oil cuts.

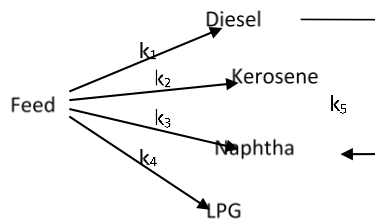


Fig. 3 Schematic of model 2 of hydrocracking process

Kinetic equations of oil cuts during VGO hydrocracking are as follows:

$$-r_F = (k_1 + k_2 + k_3 + k_4)F \xrightarrow{t=0 \Rightarrow F=1} F = e^{-(k_1+k_2+k_3+k_4)t} \quad (12)$$

Diesel is changed during two steps. In step (1) diesel is produced from VGO conversion and (2) converted into naphtha. Differential kinetic equation of diesel is as follows:

$$\frac{dD}{dt} = k_1 F - k_5 D \quad (13)$$

At this model, Kinetic equation of kerosene is as follows:

$$\frac{dK}{dt} = k_2 F \quad (14)$$

Kinetic equation of naphtha is:

$$\frac{dN}{dt} = k_3 F + k_5 D \quad (15)$$

Kinetic equation of gas is:

$$\frac{dG}{dt} = k_4 F \quad (16)$$

By this suppose that initial amount of gas, naphtha, kerosene, and diesel were zero, solving above equations are:

$$D = \left(\frac{k_1}{(k_5 - (k_1 + k_2 + k_3 + k_4))} \right) \left(e^{-(k_1 + k_2 + k_3 + k_4)t} - e^{-k_5 t} \right) \quad (17)$$

$$K = \frac{-k_2}{(k_1 + k_2 + k_3 + k_4)} e^{-(k_1 + k_2 + k_3 + k_4)t} + \frac{k_2}{(k_1 + k_2 + k_3 + k_4)} \quad (18)$$

$$N = \left(\frac{-k_3}{(k_1 + k_2 + k_3 + k_4)} \right) e^{-(k_1 + k_2 + k_3 + k_4)t} + \quad (19)$$

$$\left(\frac{k_1 k_5}{(k_5 - (k_1 + k_2 + k_3 + k_4))} \right) \left(\left(\frac{e^{-k_5 t}}{k_5} \right) - \left(\frac{e^{-(k_1 + k_2 + k_3 + k_4)t}}{(k_1 + k_2 + k_3 + k_4)} \right) \right) + \left(\frac{k_3}{(k_1 + k_2 + k_3 + k_4)} \right) -$$

$$\left(\frac{k_1 k_5}{(k_5 - (k_1 + k_2 + k_3 + k_4))} \right) \left(\left(\frac{1}{k_5} \right) - \left(\frac{1}{(k_1 + k_2 + k_3 + k_4)} \right) \right) \quad (20)$$

$$G = \frac{-k_4}{(k_1 + k_2 + k_3 + k_4)} e^{-(k_1 + k_2 + k_3 + k_4)t} + \frac{k_4}{(k_1 + k_2 + k_3 + k_4)}$$

4. Results and discussion

4.1. Results from Taguchi method

Using Taguchi method in this research, 16 experiments (Table 2) were chosen to consider a suitable catalyst from among four catalysts, β -ASA/Ni-Mo, β -ASA/Ni-W, USY-ASA/Ni-Mo, and USY-ASA/Ni-W, to grow conversion of VGO and naphtha cut produced during the process. Results of these experiments and S/N of them were calculated using equation (1) and listed in Table 4.

To choose an appropriated choice for each factor in conversion in Taguchi method, the amount of $(M)_{Factor=1}^{level=i}$ (equation 2) was calculated, and the optimum condition for enhancing conversion of VGO hydrocracking is achieved. Using Minitab software, yield and S/N of VGO conversion were calculated in optimum condition and listed in Table 5.

Table 4 Results of experiments designed and S/N of them calculated using equation 20

Test number	Conversion %	S/N	naphtha %	S/N
1	3.936	11.9369	0.44	-7.05799
2	11.3066	20.6455	1.6666	3.83324
3	26.4279	28.8168	4.6096	13.9044
4	51.7	34.2796	12.2	21.6265
5	7.42	17.4549	0.8	-1.64193
6	5.376	14.9477	0.783	-1.89061
7	35.8901	31.2487	6.52452	16.8119
8	40.75	31.6680	9.4	18.4112
9	38.76	31.9946	15.3	24.1038
10	74.7	37.6170	40.4	32.4866
11	24.599	27.1801	13.733	21.6413
12	59.3486	35.7290	37.7	31.8719
13	53.6	34.2737	23.4	26.6051
14	55.722	34.8526	27.716	28.8649
15	41.84	32.5453	21.6	26.6511
16	30.25	29.8785	17.65	25.7418

Table 5. Optimum condition for conversion of VGO hydrocracking

Optimum condition	catalyst	Temperature (°C)	Reaction time (hr.)	Yield (%wt.)	S/N
Conversion	β -ASA/Ni-W	410	6	78.6333	43.4901

S/N curve of conversion of VGO hydrocracking is depicted based on reaction factors by Taguchi method. This figure comes in Fig. 4:

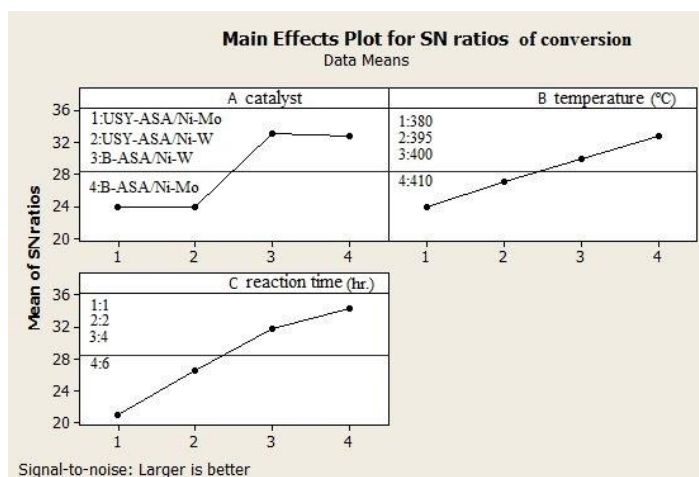


Fig. 3. Conversion of VGO during hydrocracking in different reaction time and temperature

Based on Fig. 4, as time and temperature of reaction are increased, the amount of VGO conversion is increased. This could be because the hydrocracking reaction is done more with increasing temperature and reaction time. This subject is in accordance with references [10] and [24]. In comparison with two catalysts, USY-ASA/Ni-W and USY-ASA/Ni-Mo, the amount of VGO conversion was very much when β -ASA/Ni-W and β -ASA/Ni-Mo catalysts were used in this process. Since USY and β are two different zeolites which have two different crystallites and since crystallite of the catalyst is much important factor affected the performance of catalyst, and this is in accordance with reference [25], it could be said that crystallite of two both catalysts could be caused by the difference between amount conversion of VGO. By comparing the performance of two catalysts, β -ASA/Ni-W and β -ASA/Ni-Mo, in VGO hydrocracking, it could be said that capability of W metal in VGO hydrocracking is more amount than that of Mo metal. This should be by reason of the difference of electron properties of W

and Mo. To choose a suitable choice for each factor in producing naphtha, the amount of $(M)_{Factor=1}^{level=i}$ (equation 21) is calculated. optimum conditions for producing naphtha is listed in Table 6. Using Minitab software, yield and S/N of naphtha in this condition were calculated.

Table 6 the optimum condition for producing naphtha during VGO hydrocracking

Optimum condition	catalyst	Temperature (°C)	Reaction time (hr.)	Yield (%wt.)	S/N
Conversion	B-ASA/Ni-W	410	6	41.0759	37.4115

S/N Produced naphtha is depicted in different factors. This is depicted in Fig. 5:

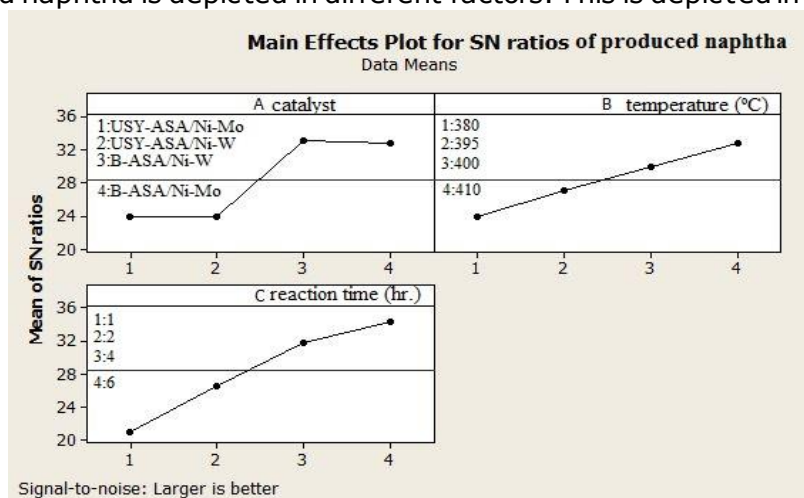


Fig. 4. Produced naphtha during VGO hydrocracking in different reaction time and temperature

According to above, as reaction time and temperature were increased, the amount of produced naphtha was increased. This subject could be approved that when the temperature is increased, production of light products is increased [26], in other hand; kerosene and diesel produced are decreased. This subject could be approved that hydrocracking of VGO is thermally controlled [24]. In VGO hydrocracking, the amount of produced naphtha was increased when β -ASA/Ni-W or β -ASA/Ni-Mo were used as a catalyst; this subject could be due to crystallite of β zeolite because crystallite of the catalyst has an effective impact on the performance of catalyst [25]. These observations showed that effect of W metal should be more than Mo in producing naphtha from VGO hydrocracking. This could be because of different electronic properties of these two metals. Obtained results approved that although temperature and resistance times are very important parameters an effective parameter to produce a certain cut from VGO hydrocracking should be kind of catalyst.

4.2. Results from modeling VGO hydrocracking

Obtained experimental data from VGO hydrocracking in temperature 380°C, when β -ASA/Ni-W catalyst was used, have been listed in Table 7:

Table 7 Experimental data obtained from VGO hydrocracking using β -ASA/Ni-W catalyst in temperature 380°C

Time(hr.)	Temperature (°C)	Gas (%wt.)	Naphtha (%wt.)	Kerosene (%wt.)	Gas oil (%wt.)
1	380	0.19	1.32	2.16	3.66
2	380	0.39	2.47	4.18	6.9
4	380	0.82	4.76	7.77	12.83
6	380	1.098	6.5	10.6	17.864

It was observed, in 380°C temperature, the production model pseudo-components (gas, naphtha, kerosene, and diesel) during VGO hydrocracking has been followed by model 1. Based on this figure, it could be said that in this temperature diesel, kerosene, naphtha, and gas produced during VGO hydrocracking were followed by four parallel reactions and equations. This subject has also come in references [27] and [17]. Kinetic equations (3-11) describe kinetic behavior of this catalyst in 380°C. Kinetic constants, k_1 , k_2 , k_3 , and k_4 , of these equations, were calculated by fitting between experiment data and the equations using the Levenberg-Marquart algorithm. These Kinetic constants, k_1 , k_2 , k_3 , and k_4 , were listed in Table 8.

Table 8 Kinetic constants calculated by fitting experimental data obtained from VGO hydrocracking using β -ASA/Ni-W catalyst in temperature 380°C

Temperature (°C)	k_1	k_2	k_3	k_4
380	0.0281	0.0329	0.0484	0.0124

Changing procedure of each pseudo-components produced during VGO hydrocracking in the presence of the β -ASA/Ni-W catalyst in 380°C were shown in Fig. 6:

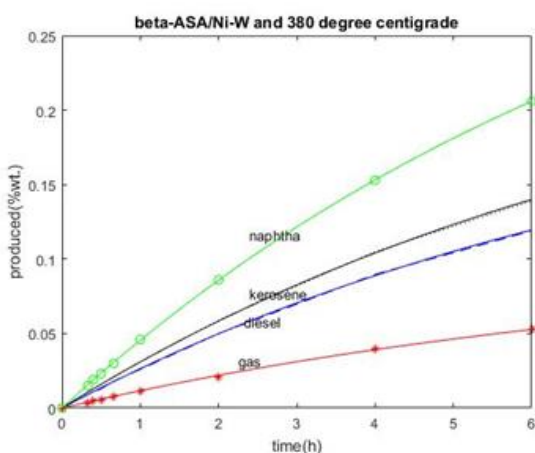


Fig. 5 Procedure of changing of products produced during VGO hydrocracking using β -ASA/Ni-W catalyst at 380°C

Fig. 6 shows that produced naphtha during the process is more amount than other products, in other words, it could be said that this catalyst is selective to produce naphtha and this result is in accordance with what is reported previously [28].

The amount of gas, kerosene, and diesel produced in the process was less than naphtha. In temperature range 395-410°C, it was found that behavior of this catalyst wasn't followed by parallel reactions, in other words, diesel produced from VGO hydrocracking could be converted into naphtha. This model could approve that the catalyst, β -ASA/Ni-W, is selective to produce naphtha. Experimental data in this temperature range are listed in Table 9:

Table 9 Experimental data obtained from VGO hydrocracking using β -ASA/Ni-W catalyst in temperature range 395-410°C

Time (hr.)	Temperature (°C)	Gas (%wt.)	Naphtha (%wt.)	Kerosene (%wt.)	Gas oil (%wt.)
1	395	2.3	10.733	4.75	2.3
2	395	4.3	19.466	8.6	4.2
4	395	6.8	31.85	14.07	6.7
6	395	8.2	40.4	17.7	8.4
1	400	3.3	13.733	5.2	2.366
2	400	5.9	23.966	9.0	4.132
4	400	9.2	38.08	14.1	6.03
6	400	11.1	46.5	17.4	7.6
1	410	6.116	22.35	4.9833	1.9
2	410	10.132	37.7	8.5666	2.95
4	410	14.3	54.8	11.93	2.975
6	410	16.3	62.1	13.7	3

Between temperature ranges 395-410°C, changing procedure of each pseudo-component produced during VGO hydrocracking using β -ASA/Ni-W catalyst is shown in Fig. 7:

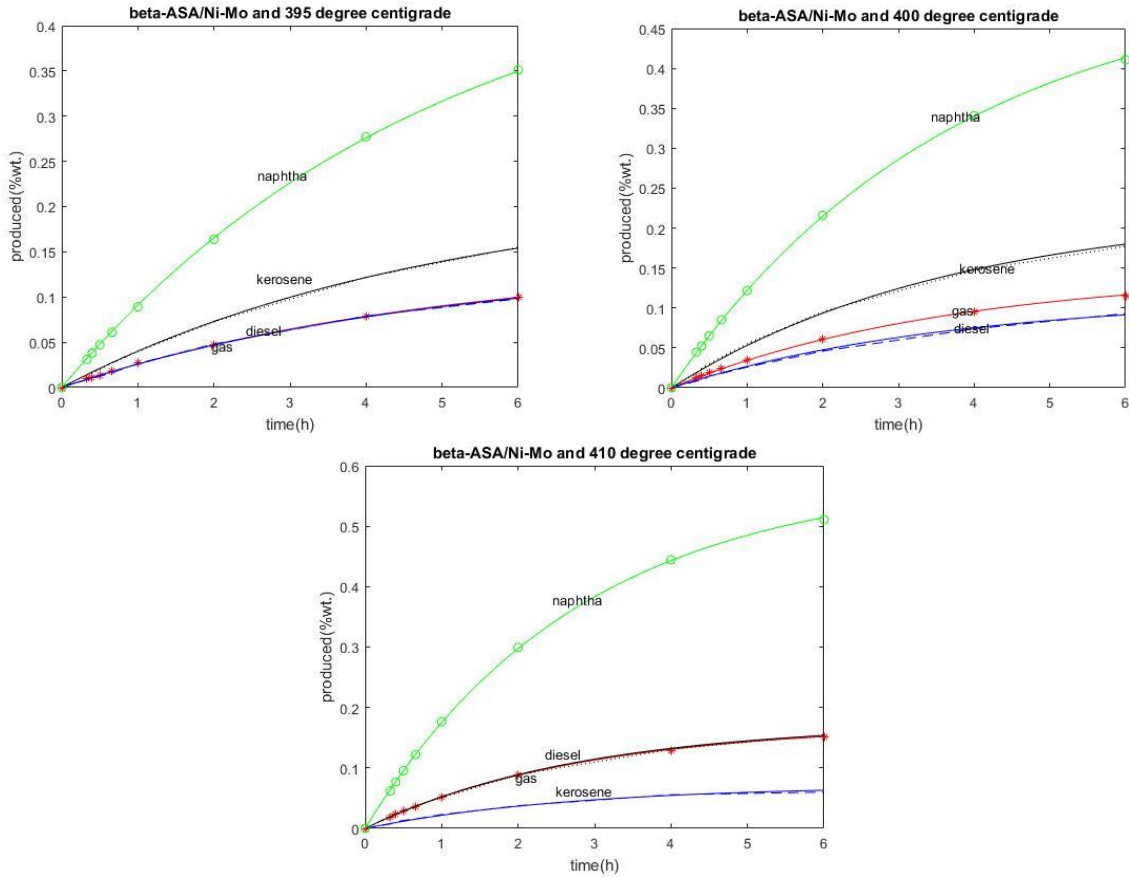


Fig. 6 Procedure of changing of products produced during VGO hydrocracking using β -ASA/Ni-W catalyst in temperature range 395-410°C

Based on data obtained in temperature range 395-410°C (Table 4-7), it could be found that VGO hydrocracking was followed by the model showed in Fig. 2 and equations (12-20). Kinetic constants, k_1 , k_2 , k_3 , k_4 , and k_5 , of these equations in the presence of this catalyst, were calculated by fitting experiment data and the equations using the Levenberg-Marquart algorithm. These Kinetic constants, k_1 , k_2 , k_3 , k_4 , and k_5 , are listed in Table 10.

Table 10. Kinetic constants calculated by fitting experimental data obtained from VGO hydrocracking using β -ASA/Ni-W catalyst in temperature range 395-410°C

Temperature (°C)	k_1	k_2	k_3	k_4	k_5
395	0.027	0.0536	0.1205	0.0254	0.0207
400	0.0282	0.0593	0.157	0.0382	0.0315
410	0.0296	0.0637	0.2781	0.0762	0.2539

According to Arrhenius equation (19), Arrhenius constants (k_0) and activation energy (E_a/R) of VGO hydrocracking were calculated and listed in Table 11:

Table 11. Arrhenius constants (k_0) and activation energy (E_a/R) of VGO hydrocracking using β -ASA/Ni-W catalyst

I=lump No.	K_{0i} (1/hr)	$E_{i/R}$ (°K)
1	1.588833	2719.1
2	94.59456	4982.8
3	4.95E+15	25566
4	9.8E+19	33199
5	3.83E+49	78996

As it is shown in Fig. 6, it could be found that with increasing temperature, the amount of naphtha produced during VGO hydrocracking is increased and amount of the produced diesel is decreased when β -ASA/Ni-W catalyst is used in this process. This subject could be approved the fact that diesel could be converted into naphtha as the temperature is increased. Obtained results approved that conversion of VGO into lighter products (i.e., gas, naphtha, kerosene, and diesel) is thermally controlled [24]. It is also shown that whatever temperature is increased, naphtha is increased, in other word; diesel could more be converted into naphtha. According to the trend of changing diesel with the temperature in Fig. 6, it could be said that amount of produced gas is increased with time and temperature.

5. Validation of the model

First according to experiment data the parameters affected by the process were properly estimated and adjusted with the one-degree kinetic reaction of VGO hydrocracking. then kinetic equations of the process were written. Good agreement was observed between experimental and predicted values. Average deviation was also lower than 5% for the total set of operating conditions. An analysis of residuals was conducted, and the results are showed in Fig. 6 and 5. All these results approve that the values of the optimized model parameter, their dependence with temperature in the range 380-410°C, and in general the discrete kinetic model represent a good compatibility with experimental data curve of heavy oil distillation hydrocracking.

6. Conclusion

In this investigation, a multi performance characteristics optimization based on Taguchi approach is proposed for Vacuum Gas Oil (VGO) hydrocracking process. Experimental data obtained in presence of four catalysts, β -ASA/Ni-Mo, β -ASA/Ni-W, USY-ASA/Ni-Mo and USY-ASA/Ni-W, and different conditions; pressure 80bar, four temperatures (380°C, 395°C, 400°C, 410°C) and eight reaction times (0.33, 0.4, 0.5, 0.667, 1, 2, 4, 6 hr), were analyzed by design expert software and Taguchi method. The production model was based on temperature and time and kinetic constants of discrete lumping equations and calculated by experimental data and Levenberg-Marquardt algorithm. As a result of this investigation, it should be proposed that effect of the β -ASA/Ni-W catalyst on conversion of VGO and producing light products (i.e., gas and naphtha) during the hydrocracking process is more than those of β -ASA/Ni-Mo, USY-ASA/Ni-W, and USY-ASA/Ni-Mo.

References

- [1] Valavarasu G, Bhaskar M, Sairam B, Balaraman KS, and Balu K. A Four Lump Kinetic Model for the Simulation of the Hydrocracking Process. *Pet. Sci. Technol.*, Feb. 2007.
- [2] Rana MS, Sámano V, Ancheyta J, and Diaz JAI. A review of recent advances on process technologies for upgrading of heavy oils and residua. *Fuel*, 2007; 86(9): 1216-1231.
- [3] Elizalde I, Rodríguez MA, and Ancheyta J. Application of continuous kinetic lumping modeling to moderate hydrocracking of heavy oil. *Appl. Catal. A Gen.*, 2009; 365(2): 237-242.
- [4] Ancheyta J, Sánchez S, and Rodríguez MA. Kinetic modeling of hydrocracking of heavy oil fractions: A review. *Catal. Today*, v2005; 109(1-4): 76-92, 2005.
- [5] AlHumaidan F, Hauser A, Al-Rabiah H, Lababidi H, and Bouresli R. Studies on thermal cracking behavior of vacuum residues in Eureka process. *Fuel*, 2013; 109: 635-646.
- [6] Browning B, Afanasiev P, Pitault I, Couenne F, and Tayakout-Fayolle M. Detailed kinetic modelling of vacuum gas oil hydrocracking using bifunctional catalyst: A distribution approach. *Chem. Eng. J.*, 2016; 284: 270-284.
- [7] Elizalde I and Ancheyta J. Modeling catalyst deactivation during hydrocracking of atmospheric residue by using the continuous kinetic lumping model. *Fuel Process. Technol.*, 2014; 123: 114-121.
- [8] Chou C-S, Lin S-H, Peng C-C, and Lu W-C. The optimum conditions for preparing solid fuel briquette of rice straw by a piston-mold process using the Taguchi method. *Fuel Process. Technol.*, 2009; 90(7-8): 1041-1046.

- [9] Chou C-S, Yang R-Y, Chen, J-H, and Chou S-W. The optimum conditions for preparing the lead-free piezoelectric ceramic of $\text{Bi}_0.5\text{Na}_0.5\text{TiO}_3$ using the Taguchi method. *Powder Technol.*, 2010; 199(3): 264–271.
- [10] Hew KL, Tamidi AM, Yusup S, Lee KT, and Ahmad MM. Catalytic cracking of bio-oil to organic liquid product (OLP). *Bioresour. Technol.*, 2010; 101(22): 8855–8858.
- [11] Tamunaidu P and Bhatia S. Catalytic cracking of palm oil for the production of biofuels: Optimization studies. *Bioresour. Technol.*, 2007; 98(18): 3593–3601.
- [12] Zhang S, Yan Y, Li T, and Ren Z. Upgrading of liquid fuel from the pyrolysis of biomass. *Bioresour. Technol.*, 2005; 96(5): 545–550.
- [13] Becker PJ, Serrand N, Celse B, Guillaume D, and Dulot H. Comparing hydrocracking models: Continuous lumping vs. single events. *Fuel*, 2016; 165: 306–315.
- [14] Qader SA and Hill GR. Hydrocracking of Petroleum and Coal Oils. *Ind. Eng. Chem. Process Des. Dev.*, 1969; 8(4): 462–469.
- [15] S Sánchez, M A. Rodríguez, and J. Ancheyta Kinetic Model for Moderate Hydrocracking of Heavy Oils. *Ind. Eng. Chem. Res.*, 2005; 44(25): 9409–9413.
- [16] Lababidi HMS, Chedadeh D, Riazi MR., Al-Qattan A, and Al-Adwani HA. Prediction of product quality for catalytic hydrocracking of vacuum gas oil. *Fuel*, 2011; 90(2): 719–727.
- [17] Barkhordari A, Fatemi S, Daneshpayeh M, and Zamani H. Development of a Kinetic Model for Modeling the Industrial VGO Hydrocracker Accompanied By Deactivation. *Int. J. Chem. React. Eng.*, 2010; 8(1) 1542-6580.
- [18] Becker PJ, Celse B, Guillaume D, Dulot H, and Costa V. Hydrotreatment modeling for a variety of VGO feedstocks: A continuous lumping approach. *Fuel*, 2015; 139: 133–143.
- [19] Dutriez T, Thiébaud D, Courtiade M, Dulot H, Bertoncini F, and Hennion M-C. Application to SFC-GC × GC to heavy petroleum fractions analysis. *Fuel*, 2013; 104: 583–592.
- [20] Dutriez T, Courtiade M, Thiébaud D, Dulot H, and Hennion M-C. Improved hydrocarbons analysis of heavy petroleum fractions by high temperature comprehensive two-dimensional gas chromatography. *Fuel*, 2010; 89(9): 2338–2345.
- [21] Baltanas MA, van Raemdonck KK, Froment GF, and Mohedas SR. Fundamental kinetic modeling of hydroisomerization and hydrocracking on noble metal-loaded zeolites. II. The elementary cracking steps. *Ind. Eng. Chem. Res.*, 1989; 28(7): 899–910.
- [22] Guillaume D, Valéry E, Verstraete JJ., Surla K, Galtier P, and Schweich D. Single Event Kinetic Modelling without Explicit Generation of Large Networks: Application to Hydrocracking of Long Paraffins. *Oil Gas Sci. Technol. – Rev. d'IFP Energies Nouv.*, 2011; 66(3): 399–422.
- [23] Froment GF. Single Event Kinetic Modeling of Complex Catalytic Processes. *Catal. Rev.*, 2005; 47(1): 83–124 2005.
- [24] Panariti N, Del Bianco A, del Piero G, Marchionna M, and Carniti P. Petroleum residue upgrading with dispersed catalysts. Part 2. Effect of operating conditions. *Appl. Catal. A Gen.*, 2000; 204(2): 215–222.
- [25] Raseev S. Thermal and catalytic processes in petroleum refining, vol. 2004. 2003.
- [26] Gutiérrez A, JM Arandes, P Castaño, M Olazar, A Barona, and J. Bilbao Effect of Temperature in Hydrocracking of Light Cycle Oil on a Noble Metal-Supported Catalyst for Fuel Production. *Chem. Eng. Technol.*, 2012; 35(4): 653–660.
- [27] Ancheyta J, Sánchez S, and Rodríguez MA. Kinetic modeling of hydrocracking of heavy oil fractions: A review. *Catal. Today*, 2005; 109(1–4): 76–92
- [28] Ali MA, Tatsumi T, and Masuda T. Development of heavy oil hydrocracking catalysts using amorphous silica-alumina and zeolites as catalyst supports. *Appl. Catal. A Gen.*, 2002; 233(1-2): 77–90

To whom correspondence should be addressed: prof. Dr. Ahmad Tawasoli, School of Chemistry, College of Science, University of Tehran, Tehran, Iran, tavassolia@khayam.ut.ac.ir

SYNTHESIS OF AN AUTOMATIC CONTROL METHOD FOR MAJOR OIL PIPELINES BASED ON INVERSE DYNAMICS PROBLEM CONCEPT

A. E. Karelin¹, A. V. Maystrenko¹, A. A. Svetlakov¹, V.M. Dmitriev¹, T.V. Gandzha¹,
Natalia V. Aksenova²

¹Tomsk State University of Control Systems and Radio-electronics (Tomsk, Russia)

²National Research Tomsk Polytechnic University (Tomsk, Russia)

Received December 12, 2017; Accepted February 28, 2018

Abstract

A new approach to synthesis of automatic control of objects is proposed, based on application of the inverse dynamics concept. A nature of PID control of objects is studied as well as causes that stipulate search for automatic control methods alternative to PID control; the above-mentioned approach to synthesis of automatic control methods is developed. A new generation PID controller is synthesized, featuring higher control quality, simplicity of adjustment and high accuracy. Such results were obtained thanks to application of a new method of digital differentiation of signals. Currently Russian oil pipelines use controllers from the different manufacturers, international, such as ABB, Foxboro, Honeywell, Yokogawa, Toshiba, Siemens, Omron, and Russian, such as Kontravt, Oven, Tekon, NIL AP; they all have a common disadvantage that they use a finite difference algorithm for differentiation, thus leading to lower quality of control and increased complexity of adjustments.

Keywords: automatic controller; PID control; inverse dynamics; derivative.

1. Introduction

The purpose of this paper is to lay out a new approach to synthesis of automatic control, based on application of the inverse dynamics concept. In this concept, just like in reality, any changes in behavior of the controlled object are considered consequence of some change in control action, which is formed by the automatic controller and delivered to the controlled object. At that, the task to form the control action u_t in any moment of time t (at the t th cycle of object control) is formulated as an inverse problem, that is, as a problem to find an unknown value (in this case a value of u_t), whose inputs are predefined (desirable) value of $y_{t+1,z}$ of the control variable Y of the controlled object in the following moment of time $t+1$ and a difference equation linking its values $y_{t+1}, y_t, y_{t-1}, \dots$, to values $u_t, u_{t-1}, u_{t-2}, \dots$.

A nature of PID control of objects is studied as well as causes that stipulate search for automatic control methods alternative to PID control; the above-mentioned approach to synthesis of automatic control methods for objects is developed below.

2. The essence of PID control

As it is known from multiple sources [1-3], one of the types of automatic controllers finding the widest range of application in automatic and automated control systems for different process parameters (APCSs), are so-called PID controllers. The main idea, determining the name and essence of this type of controllers is that the value u_t of the control action U exerted onto the process variable Y of the controlled process (CP) in any given moment of time t is formed in accordance with the following equation (law of control):

$$u_t = c_1 \Delta y_t + c_2 \int_{t_0}^t \Delta y_\tau d\tau + c_3 d(\Delta y_t) dt. \quad (1)$$

Here Δy_t is a deviation (error value) of an actual value y_t of the process variable Y in the moment t from a predefined value y_{zt} of the variable (setpoint of the controller), which is calculated with the equation in the form of

$$\Delta y_t = y_t - y_{zt} \quad (2)$$

where: c_1 , c_2 and c_3 are adjusted parameters (coefficients) of the PID controller; t_0 is the initial moment of CP control; τ is the integration variable all the values of which satisfy the condition $\tau \in I_t$, where I_t is the time interval, described by the equation

$$I_t = [t_0, t]. \quad (3)$$

The most important advantage of PID controllers, which has determined and is still determining their popularity and wide application in automation of diverse processes, is that the law of control (1) has tuning parameters c_1 , c_2 and c_3 . Having such parameters in (1) allows selecting their numeric values in each concrete case (adjusting the PID controller) in such a way that the values of u_t , $t=1, 2, 3, \dots$, calculated from the equation (1), provide satisfaction of a sequence of equations in the form of

$$y_t = y_{zt}, t=1, 2, 3, \dots \quad (4)$$

Here, just like in equation (2), y_{zt} is a predefined (desirable) value of Y in moment t . Taken together the equations (1) and (4), evidently, mean, that the control actions u_t exerted onto the process variable Y shall provide change of its values in time and in accordance with a preset (desirable) law of change.

3. Two problems arising from practical application of PID controllers

The vast number of theoretical and experimental studies of PID controllers [1-3], as well as over a hundred years of practical application in automation of diverse processes [1-4] revealed two topical issues, which significantly complicate and limit practical use of such controllers. The first one is the PID controller tuning problem, which comes down to determination and setting of numeric values of parameters c_1 , c_2 and c_3 in the law of control (1) such, that their implementation allows for calculation of controlling actions u_t , providing satisfaction to the equation (4). Finding such parameters is a non-trivial task and its solution is available only to high quality specialists with expertise not in process automation, in specific domain knowledge of the controlled process itself.

The second problem that limits practical application of PID controllers is due to the fact that the law of control (1) includes the derivative $d(\Delta y_t)/dt$ of Δy_t deviation. As it is known [5-6], calculation of a derivative of any signal (signal differentiation) is one of a classical examples of ill-posed problems. The characteristic feature of such problems is that their solutions are extremely sensitive to even the slightest changes in input data. As for the error value Δy_t differentiation problem, whose solution and inputs are, respectively, a derivative $d(\Delta y_t)/dt$ and a error value Δy_t , the above noted feature of ill-posed problems means, that in case where the values y_t , $t=1, 2, 3, \dots$ are not exact, the value of the derivative that is calculated and then applied in (1), may be indefinitely different from its actual value. As evident from (1), in any such cases, the value of u_t will be indefinitely far from its actual value as well. Taking this into account, as well as the fact that in real life the values of y_t are the results of measurement of the process variable Y with some kind of a transmitter or other measurement instrument, thus introducing the measurement errors, it is evident, that, first, the process of adjustment

of the variable Y with the help of the PID controller is unstable as a whole. Second, the cause of this instability is the fact that PID controllers use a derivative of error value Δy_t with respect to the deviation time.

4. Two possible solutions for the problem of practical implementation of PID controllers

If we set our goal as to remove PID controller instability thus extending their practical applicability, and consider the facts set out before, it is evident, that to achieve this goal we may either regularize the differentiation of the error value Δy_t , using some regularization method applied to ill-posed problems [6-7], or withdraw from application of PID controllers and replace them with an analogue which does not use the derivative of the process variable. The first way was implemented by the authors in [8]. At that, regularization of differentiation of the process variable is provided by the use of moving quadratic approximation of change in the variable and analytical differentiation of algebraic second order polynomials. The results of the work show that the PID controller proposed there has a higher interference immunity and provides a higher control accuracy.

The second possibility to improve the automatic control methods and their efficiency is shown in this paper. From the above-mentioned concept of inverse dynamics problems we propose a method of process automatic control, alternative to the PID control and other automatic control methods based on process variable differentiation. At that, second order difference equations are used as a mathematical model to describe the connection between the values $y_t, t=1,2,3\dots$ of the process variable Y and the values u_t of the controlling action U . For this case a numerical algorithm is synthesized for calculation of controlling actions $u_t, t = 1,2,3\dots$

5. Synthesis of an automatic control method based on difference equations and inverse problem concept

Taking into account the features of the inverse dynamics problems noted above, we synthesize the automatic control method. To simplify the following, we will hold that:

1. Values $y_{t+1}, y_t, y_{t-1}, y_{t-2}$ of the process variable Y of the controlled object (CO) in moments of time $t+1, t, t-1, t-2$ are linked among themselves and with the values u_t, u_{t-1} of its input U (control actions) by a difference equation in the form of

$$y_{t+1} = \alpha_1 y_t + \alpha_2 y_{t-1} + \alpha_3 y_{t-2} + \alpha_4 u_t + \alpha_5 u_{t-1} \quad (5)$$

coefficients $\alpha_1 - \alpha_5$, are some constants independent of values u_t, u_{t-1} of the input U of the CO and of the values y_t, y_{t-1} and y_{t-2} of its input Y .

2. A desired (necessary) law of changes in values y_{zt} of the process variable Y through time is determined by the equations

$$y_{zt} = \varphi(t), t = 1,2,3\dots, \quad (6)$$

where $\varphi(t)$ is a certain function of time t .

3. Values u_t of the control actions shall be selected in such a way that values y_t of the controlled object output Y in any moment t satisfy the equations

$$y_t = y_{zt}, t=1,2,3\dots, \quad (7)$$

and the equation (5) holds true.

The initial data, represented by the equations (5) – (7), are necessary and sufficient conditions for synthesis of an automatic control method, which is of our interest. Indeed, the equation (5) links values y_{t+1}, y_t, y_{t-1} of the process variable Y in each moment t to the values u_t and u_{t-1} of the control action U and thus, using this equation and equation (5), to calculate the desirable values $u_{zt}, t = 1,2,3\dots$, we may compose an equation in unknown value u_t

$$\alpha_1 y_t + \alpha_2 y_{t-1} + \alpha_3 y_{t-2} + \alpha_4 u_t + \alpha_5 u_{t-1} = y_{zt} \quad (8)$$

Values y_t , y_{t-1} , y_{t-2} and y_{zt} , in this equation are known, as well as those of u_{t-1} , and as evident from (8), only the value u_t , which is of interest to us, is unknown. Having moved

the known summands $\alpha_1 y_t, \alpha_2 y_{t-1}, \alpha_3 y_{t-2}$ and $\alpha_5 u_{t-1}$ to the right part of the equation, let us represent it in a form, which is more compact and traditional in linear algebra:

$$\alpha_4 u_t = \Delta z_t, \quad t = 1, 2, 3, \dots \quad (9)$$

here $\Delta z_t = y_{zt+1} - \alpha_1 y_t - \alpha_2 y_{t-1} - \alpha_3 y_{t-2} - \alpha_5 u_{t-1}$. The resulting equation is the simplest linear algebraic equation in u_t . Its solution is determined by the following evident equation:

$$u_t = \Delta z_t / \alpha_4, \quad t = 1, 2, 3, \dots \quad (10)$$

4. Let us check the correspondence of the calculated value u_t to the conditions of its physical realizability which appear as a formula

$$u_t \in I_t \equiv [u_t^{min}, u_t^{max}] \quad (11)$$

where u_t^{min} and u_t^{max} are some given numbers, selected with respect for physical limitations applicable in a moment of time t to the values of the control action u_t .

If the calculated value u_t satisfies this formula, we suppose that it is the desirable control action u_{zt} , and, correspondingly assume

$$u_{zt} = u_t \quad (12)$$

Otherwise, that is, if the calculated value u_t does not satisfy the given formulas, we use it to calculate the desirable value u_{zt} , which is obtained from the equation

$$u_{zt} = \begin{cases} u_t^{min}, & \text{если } u_t \leq u_t^{min}; \\ u_t^{max}, & \text{если } u_t \geq u_t^{max}. \end{cases} \quad (13)$$

Here u_t^{min} and u_t^{max} are some given functions of time t , such, that $u_t^{min} < u_t^{max}$. In the simplest case these functions are defined by the equations $u_t^{min} = u^{min}$ and $u_t^{max} = u^{max}$, where u^{min} and u^{max} are some given constants, satisfying the inequality $u^{min} < u^{max}$.

To finalize the synthesis of the proposed automatic control method let us produce the following comments that provide more insight into its nature, features and possibility of practical implementation.

1. As directly seen from equations (5)–(10), none of them includes derivative $d(\Delta y_t)/dt$ of the error value Δy_t , defined by the equation (2), and thus, the method lacks the main cause determining instability of PID controller and other control types that employ such derivative.
2. The synthesis of a proposed automatic control method given above is performed for a particular case of a controlled object, where the link between the process variable values and those of the control action are described by a difference equation (5). However, it is evident, that similar reasoning and actions may lead to synthesis of such method for other, both simpler and more complex controlled objects where the link between the process variables and control actions is described by a difference equation [9-10]. Such methods will differ from the controller synthesis given above only in their respective difference equations used, primarily by the number of summands with the value of process variable and control actions in the difference equation. General scheme of calculations that implement the control method being synthesized stays the same in all cases.

3. Currently, a number of methods is known for transformation of the ordinary differential equations commonly used in theory and practice of automatic control into difference equations.

Thus, as it was undertaken above, when synthesizing a certain automatic control method it is always possible to hold that the link between a process variable and control actions is described by a difference equation of some sort.

6. Conclusion

Summarizing the above, let us note the following main results.

1. The nature of inverse dynamics problems is explained as applied to the automatic control tasks.
2. PID control, being one of the most popular methods of control, is discussed and problems in its practical application are noted; those problems are new to instability of calculated control actions when there are measurement errors prominent in the process variable of the controlled object.
3. An automatic control method was synthesized on the basis of inverse dynamics problem and difference equations linking process variable values to the controller's control actions.
4. It is shown, that the proposed method of automatic controller synthesis is quite universal and allows synthesizing regulators for any controlled objects whose functioning may be described with either ordinary differential equations or difference equations of any order.

Acknowledgement

This paper was prepared within the framework of Federal Targeted Program for Research and Development in Priority Areas of Advancement for Russian Science and Technology Complex for 2014-2020, project no. 14.577.21.0266

References

- [1] Yurevich EI. Automatic Control Theory. 4th Ed., revised and enlarged – Saint Petersburg: BHV-Peterburg, 2016; 560 p.
- [2] Rotach VYa. Calculation of adjustments for actual PID controllers. Teploenergetika, 1993; 10: 31-35.
- [3] Maystrenko AV, Svetlakov AA, Starovoytov NV. Digital Signal Differentiation in Automatic Process Control Systems with Multi-Point Methods. Doklady TUSURa, 2009; 2(20): 86-89.
- [4] Maystrenko AV, Svetlakov AA. Indirect Pumped Liquid Flow Measurement in Pump Units. Doklady TUSURa, 2014; 4 (34): 215-220.
- [5] Tikhonov AN, Arsenin VYa. Solution Methods for Ill-Posed Problems. 2nd ed. Moscow: Nauka Publishing, 1979; 286 p.
- [6] Vasin VV. On Stable Calculation of Derivative. Computational Mathematics and Mathematical Physics, 1973; 13(6): 1383 -1389.
- [7] Tikhonov AN. On Ill-Posed Problems of Linear Algebra and Their Stable Solution Methods. Proceedings of the USSR Academy of Sciences, 1965; 163(3): 591-594.
- [8] Maystrenko AV, Svetlakov AA, Starovoytov NV. Real-Time Digital Signal Differentiation with Moving Quadratic Approximation. Omsk Scientific Bulletin. Series: Instruments, Machines and Technologies. 2006; 7(43): 106-108.
- [9] Maystrenko AV, Svetlakov AA, Gandzha TV, Dmitriev VM, Aksenova NV. Application of numeric signal differentiation methods to determine stationarity of a process. Pet Coal, 2017; 59(3): 311-318.
- [10] Maystrenko AV, Svetlakov AA, Gandzha TV, Aksenova NV. Indirect measurement of flow of liquid pumped with pump packages. Pet Coal, 2017; 59(2): 244 - 249.

To whom correspondence should be addressed: Dr. Natalia V. Aksenova, Division for foreign languages of the School of Core Engineering Education, Tomsk Polytechnic University, 30, Lenin Avenue, Tomsk,

KINETIC STUDY OF TRANSESTERIFICATION OF WASTE FRYING OIL TO BIODIESEL USING AN THILL-EGGSHELL-Ni-Co MIXED OXIDE COMPOSITE CATALYST

A. S. Yusuff^{1,2*}, O. D. Adeniyi², M. A. Olutoye², U. G. Akpan²

¹ Department of Chemical and Petroleum Engineering, Afe Babalola University, Ado-Ekiti, Nigeria

² Department of Chemical Engineering, School of Engineering and Engineering Technology, Federal University of Technology, Minna, Nigeria

Received November 6, 2017; Accepted February 28, 2018

Abstract

In this present study, the transesterification of waste frying oil with methanol over anthill-eggshell-Ni-Co mixed oxide catalyst was investigated. The composite catalyst was prepared via co-precipitation method and characterized by Brunauer-Emmett-Teller (BET), basicity, X-ray diffraction (XRD) and Fourier transform infrared (FTIR) techniques prior to its activity study. The effects of reaction temperature and reaction time on the catalytic reaction were investigated. The reaction order, activation energy and reaction mechanism based on Eley-Rideal principle were evaluated. From the BET analysis, it was revealed that calcination process has a positive effect on the textural properties of the catalyst. The high basicity exhibited by the catalyst implied that Lewis base sites are active centers for the catalytic reaction. From the XRD analysis, the active phases in the catalyst were determined to be calcium oxide (CaO), silica (SiO₂), nickel oxide (NiO) and cobalt oxide (CoO). From the FTIR studies, the peak changes of the spectra obtained before and after calcination process corresponded to temperature effect. The obtained results showed that both reaction temperature and reaction time had significant influence on transesterification reaction. The reaction was first order with respect to triglyceride and second order with respect to methanol. The activation energy and collision factor were 23.99 kJ/mol and $1.62 \times 10^6 \text{ M}^{-1} \text{ min}^{-1}$ respectively. The reaction mechanism agreed reasonably well with Eley-Rideal kinetic.

Keywords: Biodiesel; composite catalyst; kinetics; transesterification; waste frying oil.

1. Introduction

The global realization of the finite nature of fossil hydrocarbon and the deleterious effect arising from its consumption has triggered a worldwide search for alternative fuels. The utilization of diesel fuel from petroleum source continues to rise due to increase in population, energy consumption and rapid industrialization [1]. These have triggered a worldwide search for alternative fuels which include biodiesel, bio-alcohol, biogases and other biomass sources. Among the aforementioned renewable fuels, biodiesel has received considerable attention mainly because it provides a solution to problems associated with fossil fuel which include its depletion and environmental degradation [2]. Besides, it could be obtained from biomass [3]. Generally, biodiesel is prepared from plant oils or animal fat [4]. Biodiesel is an alternative and biogenic fuel which comprises of different esters of fatty acid and has been attracted worldwide because of the problems associated with the petroleum derived fuel [5].

There are four major techniques, which are usually used for biodiesel synthesis. They include pyrolysis (thermal cracking), micro-emulsification, blending, and transesterification or esterification. Transesterification is a commonly used method whereby triglyceride contained in the vegetable oil or animal fat reacts with primary alcohol (methanol, ethanol, and propanol) to produce alkyl esters and glycerol in the presence of catalyst [7-8]. The required catalyst can either be homogeneous, enzyme or heterogeneous. However, homogeneous catalyzed trans-

esterification process has some disadvantages, which include the formation of the unwanted product, corrosion problems, generation of wastewater, and difficult to recycle [3]. Although, enzymatic transesterification has the advantage to provide high yields, but cannot be employed industrially as a result of the exorbitant cost of the enzyme. Another problem is that of deactivation usually caused by impurities present in reaction feed. Therefore, heterogeneous catalysts are very important for biodiesel production as they possess many advantages over homogeneous catalysts and enzymes [5]. They are noncorrosive, environmentally benign and do not form soaps through free fatty acid neutralization or saponification of triglyceride. Besides, product purity and regeneration of the catalyst are achievable in heterogeneous catalysis [9-10].

Many types of heterogeneous catalysts for biodiesel production have been reported ranging from the use of strong acid catalysts to strong base catalysts [11]. Findings have proven that rare earth metals are the most suitable heterogeneous catalyst in biodiesel production [12], but unfortunately, these catalysts are expensive, and their preparation is quite complex. Therefore, to make biodiesel production sustainable, the use of low cost solid heterogeneous catalysts from waste and naturally occurring materials is suggested [13]. These are being investigated to replace the homogeneous catalysts and enzymes, and this research constitutes part of that investigation. These low cost materials include chicken eggshell [14], ostrich eggshell [15], quail eggshell [16], waste shells of mollusk [17], waste animal bone [18], solid waste coral fragment [19], alum [20], montmorillonite clay [21], modified- peanut husk ash [22], just to mention, but few.

Although there is an increasing interest in deriving solid catalysts from naturally occurring and waste materials, but locally sourced anthill has not been explored as a catalyst to transesterify vegetable oil to fatty acid methyl esters. This also includes its modification by any of the metal oxides. Moreover, previous research has not provided detailed work on the catalytic performance of two or more of these materials in a combined form (composite) to synthesize fatty acid methyl esters. Furthermore, to the best of our knowledge no literature on the kinetic studies for the transesterification of waste frying oil over mixed metal oxides promoted anthill-eggshell is reported. It has been widely reported that transesterification reaction occurs much faster when uses basic catalyst compared to acidic [23]. Thus, the technique involving the use of the heterogeneous base catalyst in converting waste oil to biodiesel is adopted for this present study.

This research work, however, considers the development of anthill-eggshell-Ni-Co mixed oxides (AENiCo) composite catalyst for biodiesel production from waste frying oil. Waste frying oil is selected for this study because it offers advantages which include a reduction in environmental pollution and the production cost [24]. Following this, the prepared catalyst was characterized to gather information about its properties. The effects of reaction temperature and time on the catalytic reaction process were investigated. Moreover, kinetic of transesterification of waste frying oil (WFO) over AENiCo catalyst was studied in details and all the parameters contained in derived models were evaluated.

2. Materials and methods

2.1. Materials

Chicken eggshells and waste frying oil (WFO) were collected from students' Cafeteria 1, Afe Babalola University, Ado-Ekiti, Nigeria. The specific gravity, acid value, free fatty acid and saponification value of the oil are 0.9147, 3.824 mg KOH/g, 1.412 wt% and 183.1 mg KOH/g, respectively. The anthill employed in this study is situated in Ado-Ekiti, Nigeria on an elevation of 1165 ft above sea level, having latitude (N007°36.409') and longitude (E005°18.627') with height and base of 2.59 m and 4.60 m. The anthill was sprayed with insecticide before it was harvested. Cobalt nitrate hexahydrate [$\text{Co}(\text{NO}_3)_2 \cdot 6\text{H}_2\text{O}$] and nickel nitrate hexahydrate [$\text{Zn}(\text{NO}_3)_2 \cdot 6\text{H}_2\text{O}$] used as precursors in this current study were procured from Topjay Chemical Enterprise, Ado-Ekiti, Nigeria. The methanol (JHD, AR China) used was of analytical-grade and was used as received.

2.2. Preparation and characterization of AENiCo composite catalyst

The procedure employed in preparing AENiCo catalyst was referred to our previous study [25]. The nickel nitrate hexahydrate, cobalt nitrate hexahydrate, anthill powder and eggshell powder were mixed in the proportion of 4.3, 8.6, 17.4 and 69.7%, respectively. The rationale behind this adopted mixing proportion was based on preliminary studies. The mixtures were dissolved in 150 mL of deionized water under continuous stirring for 5 h at 80°C. The pH of the resulting slurry was adjusted to 8.0 by adding 0.1 M Na₂CO₃ and then age in a fume hood at 80°C for 2 h with stirring. The solution was then filtered with filter paper and residue collected was dried in an oven at 110°C for 12 h. Thereafter, the raw catalyst was calcined at 1000°C for 4 h. The basicity of the calcined catalysts was determined by colorimetric titration method reported by Abdoulmoumine [27]. The physical properties of the catalysts were obtained by BET method using a Quantachrome Instrument (Nova station-A model No: 11.03). The catalyst samples were degassed at 200°C for 5 h before taking adsorption data. The functional groups present on the catalyst surface were examined by Fourier transform infrared (FTIR) spectrophotometer (IR Affinity-1S, Shimadzu, Japan). The crystalline phases in the as-synthesized catalyst were identified using a GBC eMMA XRD analyzer. A Cu- α radiation (1.54051 Å) was employed to generate diffraction patterns at ambient temperature in the scanning angle 2θ of 5-70°

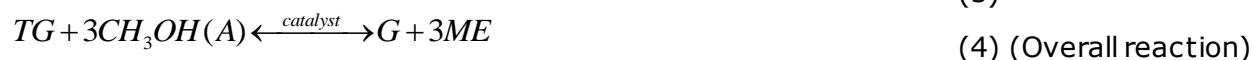
2.3. Transesterification reaction process

The activity of the as-synthesized AENiCo catalyst was tested by subjecting it to transesterification reaction. The reaction was conducted in a batch reactor made up of a 250 mL one way round bottom flask. The inlet mouth of the flask was connected with a condenser, while a thermometer was inserted through the side neck of the flask in order to monitor the temperature of the reaction mixture and was placed on temperature and speed controlled orbital shaker. The WFO was reacted with methanol under the operating conditions; different reaction temperature of 60, 70 and 80°C, the reaction time of 2 h, catalyst loading of 3 wt% and methanol to oil ratio of 12:1 [25]. The stirring speed was kept constant for all experiments.

After the completion of the transesterification reaction, the resulting mixture comprising of unreacted methanol, crude methyl ester (biodiesel), glycerol, and used catalyst was left for 2 h to settle, after which, it was poured into the separating funnel without catalyst. After settling in the separating funnel, the two layers of liquid were observed, the top layer is methyl ester (biodiesel), while the bottom liquid layer is glycerol. The synthesized biodiesel was characterized by FTIR analysis, and its physicochemical and fuel properties were determined in order to ascertain its quality.

2.4. Kinetics of waste frying oil transesterification

The transesterification kinetics of waste frying oil (WFO) on AENiCo catalyst was studied at 60°C, 70°C, and 80°C. In the reaction process, three consecutive reactions were involved as illustrated in Eqs. 1-3. The first reaction is the one between triglycerides (TG) molecules present in WFO and excess methanol (A) which gave diglyceride (DG) (intermediate) and methyl ester (ME). The diglyceride (DG) then reacted with part of the remaining methanol leading to the formation of another intermediate (monoglyceride [MG]) and more methyl ester (ME). The monoglyceride then also combined with remaining methanol to give more methyl ester (ME) and glycerol (G).



(a) Equations (1) - (3) are transesterification reaction steps (b) Equation (4) is the overall transesterification with methanol.

The reaction order, activation energy, and mechanism were determined as explained in details below.

2.4.1. Determination of reaction order and activation energy

The method adopted to investigate the reaction order of WFO conversion was previously documented by Singh *et al.* [26] and Abdoulmoumine [27]. As widely reported in the literature, the transesterification reaction is a reversible type. Thus, the rate expression for the overall reaction equation presented in Eq. (4) could be written as:

$$\frac{-dC_{TG}}{dt} = kC_{TG}^n C_A^m \quad (5)$$

$$C_{TG} = C_{TG_0} (1 - X) \quad (6)$$

$$C_A = C_{TG_0} (\theta - 3X) \quad (7)$$

$$\theta = \frac{C_{A_0}}{C_{TG_0}} \quad (8)$$

Bringing Eqs. (5), (6), (7) and (8) together and also express left hand side of the Eq. (5) in term of fractional conversion (X) to obtain Eq. (9)

$$\frac{dX}{dt} = kC_{TG_0}^{(n+m-1)} (1 - X)^n (\theta - 3X)^m \quad (9)$$

where X = fractional conversion; t = reaction time (min); C_{TG} = concentration of triglyceride (M); C_A = concentration of methanol (M); C_{A_0} = initial concentration of methanol (M); C_{TG_0} = initial concentration of triglyceride (M); θ = molar ratio of methanol to triglyceride; n and m represent the reaction order with respect to triglyceride and methanol; k = reaction rate constant ($\text{mol}^{-1} \cdot \text{min}^{-1} \cdot \text{g}^{-1} \cdot \text{cat}$).

In most of the researches conducted on transesterification kinetics of vegetable oils, the overall reaction order was obtained to be equal to or less than three [26-29]. This implies that the reaction order of triglyceride and methanol could be zero, first or second. In this study, Eq. (9) was solved by integration by partial fraction coupled with excel solver and it was assumed that the reaction order of triglyceride (n) and methanol (m) was either zero, first or second order. Meanwhile, the activation energy and collision factor were both determined using Arrhenius expression given in Eq. (10). Eq. (10) was linearized to obtain Eq. (11) and a plot of $\ln k$ against $1/T$ yields slope equal to $-E/R$ and $\ln k_0$ as intercept.

$$k = k_0 \exp\left(-\frac{E}{RT}\right) \quad (10)$$

$$\ln k = \ln k_0 - (E/R) \frac{1}{T} \quad (11)$$

where: k ($\text{mol}^{-1} \cdot \text{min}^{-1} \cdot \text{g}^{-1} \cdot \text{cat}$), is the reaction rate constant of the rate determining step; k_0 ($\text{M}^{-1} \cdot \text{min}^{-1}$), is the collision factor; E (kJ/mol) is the activation energy; R ($\text{J} \cdot \text{mol}^{-1} \cdot \text{K}^{-1}$) is the gas constant and T (K) is the reaction temperature.

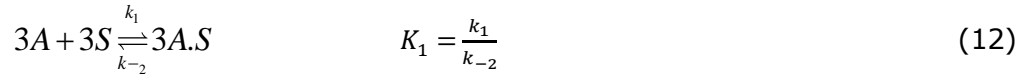
2.4.2. Investigation of the reaction mechanism

In order to develop a kinetic model able to represent adsorption, desorption and surface reaction steps (mass transfer phenomena), the following probable assumptions are made:

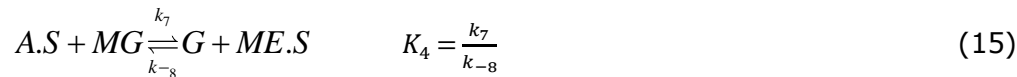
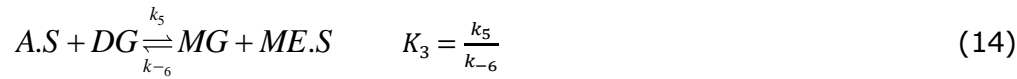
- (1) The catalyst behaviour is a single site, Eley-Rideal (ER), that is, only methanol is adsorbed on the catalyst surface.
- (2) The reaction takes place at the active site of the catalyst.
- (3) The surface reaction step is the rate-controlling step (RCS), and the adsorption and desorption are quasi-equilibrated steps, which are used to eliminate the intermediates (DG and MG) that could not be taken into account.
- (4) The rate of reaction is not influenced by internal and external diffusion.

However, the following mechanistic scheme can then be written for the overall transesterification reaction (Eq. 4).

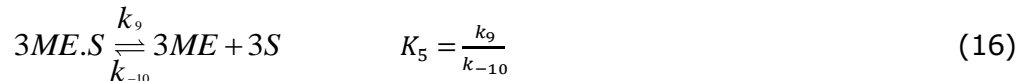
Adsorption step:



Surface reaction step:



Desorption step:



The total concentration of catalyst active sites is:

$$C_T = C_S + C_{A.S} + C_{ME.S} \quad (17)$$

Thus, based on those aforementioned assumptions and reaction mechanisms, the global/overall rate equation was derived and given in Eq. (18).

$$R = \frac{C_T k_3 K_1 \left(C_{TG} C_A - \frac{C_{ME}^3 C_G}{K K_1^2 K_2^2 C_A^2} \right)}{1 + K_1 C_A + \frac{C_{ME}}{K_5}} \quad (18)$$

where A.S = adsorbed methanol on catalyst surface, S = vacant site, ME.S = methyl esters on catalyst surface, C_T = total concentration of catalyst active sites (M); $C_{A.S}$ = concentration of adsorbed methanol on catalyst surface (M); $C_{ME.S}$ = concentration of adsorbed methyl ester on catalyst surface (M); K_i = equilibrium rate constant; k_i = forward reaction rate constant, $\text{mol}^{-1} \text{min}^{-1} \text{g}^{-1} \text{cat}$ and k_{-i} = backward reaction rate constant, $\text{mol}^{-1} \text{min}^{-1} \text{g}^{-1} \text{cat}$.

3. Results and discussions

3.1. Catalyst characterization

The textural properties and basic sites of raw and calcined AENiCo catalysts are presented in Table 1. The result revealed that the surface area of calcined catalyst was higher than that of the raw. This implies that calcination process has a positive effect on performance of the composite catalyst [15]. According to Olutoye and Hameed [21], calcination of solid catalyst at an elevated temperature eliminates adsorbed gases, moisture content and volatile components, thus opening up the surface of the catalyst

Table 1. Summary of the textural properties and basic sites of raw and calcined AENiCo catalyst

Sample	BET surface area (m^2/g)	Total pore volume (cm^3/g)	Average pore diameter (\AA)	Basic sites ($\text{mmol}/\text{g cat}$)
Raw	8.12	0.0228	12.40	2.40
Calcined	424.9	0.1119	17.72	12.80

In addition, as can be seen in Table 1, the total pore volume and average pore diameter of the calcined AENiCo catalyst were determined to be $0.1119 \text{ cm}^3/\text{g}$ and 17.72 \AA respectively and found to be higher than those values obtained in the case of raw. Therefore, these results imply that external surface of the calcined catalyst is largely dominated by active sites and it has a tendency to eliminate the mass transfer limitation [15]. This explains the reason why calcined catalyst exhibited better performance in the transesterification reaction.

The high activity of calcined catalyst was also attributed to the large number of basic sites $12.80 \text{ mmol}/\text{g.cat}$, which exceeds that of raw catalyst. The increase in basic strength of the composite catalyst is partly attributed to the presence of oxides of calcium, nickel, and cobalt as revealed by XRD analysis (Fig. 1) [21]. According to Di Serio *et al.* [30], the high biodiesel

yield could be achieved in short period of time when stearate metal oxides are used as heterogeneous catalysts in the transesterification reaction. However, those stearate metals in their oxides form possess Lewis acidity (electron acceptor), and negative oxygen ions are thus Lewis bases (proton acceptor) [2, 31]. Therefore, the high basicity exhibited by calcined AENiCo catalyst implied that Lewis base sites are active centers for transesterification reaction.

Figure 1 shows the XRD spectrum of calcined sample of AENiCo catalyst. The main peaks observed at $2\theta = 32.34^\circ$, 54.05° , 64.33° and 67.69° were attributed to CaO, while the peak at $2\theta = 34.35^\circ$ was a characteristic of $\text{Ca}(\text{OH})_2$ and its appearance is as a result of hydroscopic nature of CaO, which may have reacted with atmospheric moisture [15]. More so, the XRD patterns in spectrum shown in Figure 1 displayed peaks at $2\theta = 20.80^\circ$ and 26.70° , which were attributed to SiO_2 . According to Hassani *et al.* [32], the two observed peaks indicate crystal phases. The peak occurred at $2\theta = 37.52^\circ$ was a characteristic of NiO, while peak at $2\theta = 42.97^\circ$ was for CoO. However, it could be noted that the calcined AENiCo catalyst is made up of CaO, $\text{Ca}(\text{OH})_2$, SiO_2 , NiO and CoO..

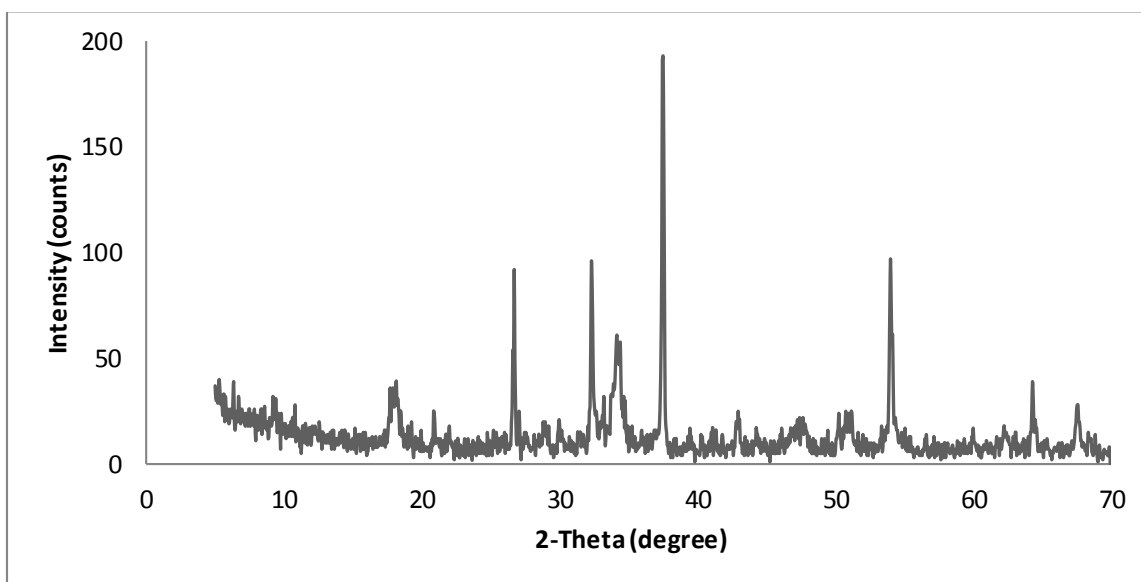


Figure 1. X-ray diffraction spectrum of the calcined AENiCo catalyst

The FTIR spectra of raw and calcined AENiCo catalysts presented in Figure 2 revealed that some peaks were shifted, changed or vanished after calcination process. However, in the raw AENiCo catalyst the absorption band occurred around 3689 cm^{-1} was attributed to O-H stretching vibration mode. The appearance of band at 2517 cm^{-1} was assigned to C-H symmetric stretching bond, while peaks around 1406 cm^{-1} , 874 cm^{-1} and 712 cm^{-1} were due to the symmetric stretch, out-of-plane bend and in-plane bend of C-O vibration modes, respectively [14]. These peaks confirmed the presence of CaCO_3 , which was decomposed into CaO upon calcination [15]. This is corroborated by XRD analysis. The observed peak around 1089 cm^{-1} could be attributed to the Si-O-Si stretching [21]. As well the band at 538 cm^{-1} was due to Al-OH stretching. For calcined catalyst, the peaks around 1647 cm^{-1} and 1001 cm^{-1} were due to C=O and C-O stretching respectively. Appearance of peak at 1055 cm^{-1} could be attributed to Al-Al-OH vibration of anthill clay [33]. The wide absorption band at 428 cm^{-1} was due to CaO vibration formed as a result of complete decomposition of CaCO_3 in eggshell [34]. Moreover, there was a new peak form around 3641 cm^{-1} which could be attributed to O-H stretching vibration and this peak is usually assigned to hydroxyl bond in calcium hydroxide, $\text{Ca}(\text{OH})_2$ [15]. However, formation of $\text{Ca}(\text{OH})_2$ was as result of adsorption of atmospheric moisture onto calcined catalyst surface during analysis. This is corroborated by XRD analysis and is attributed to why calcined AENiCo exhibited high basicity. A similar observation was reported by Margaretha *et al.* [35] in the production of biodiesel using CaO based catalyst derived from *Pomacea sp.* shell.

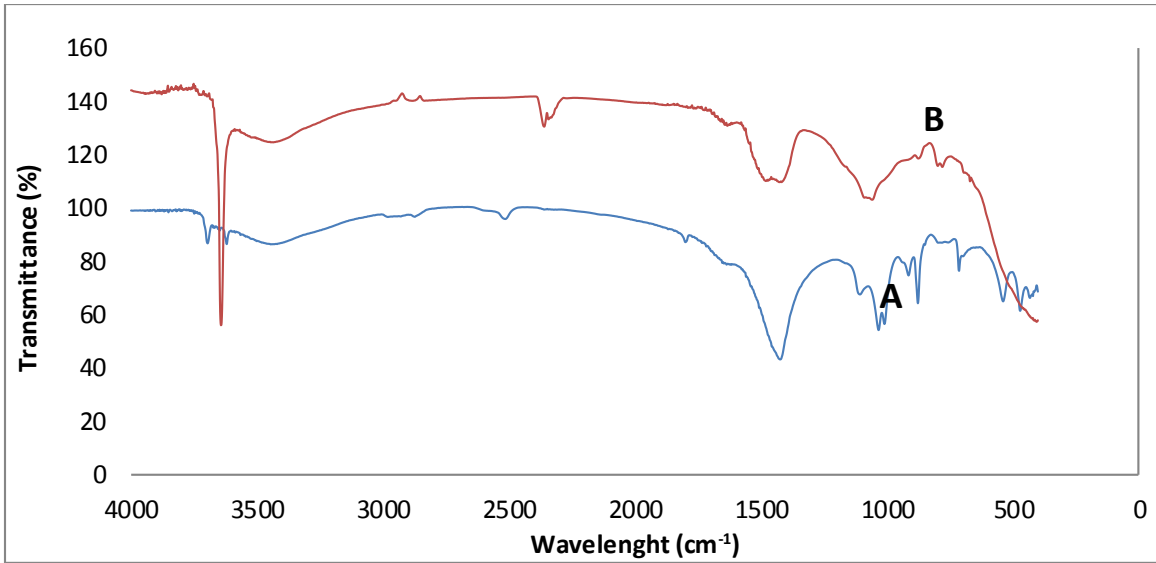


Fig. 2. FTIR spectra of A- raw and B-calcined AENiCo catalysts

3.2. Kinetics of waste frying oil transesterification

The influence of the reaction temperature on the transesterification of WFO to biodiesel using AENiCo catalyst is shown in Figure 3.

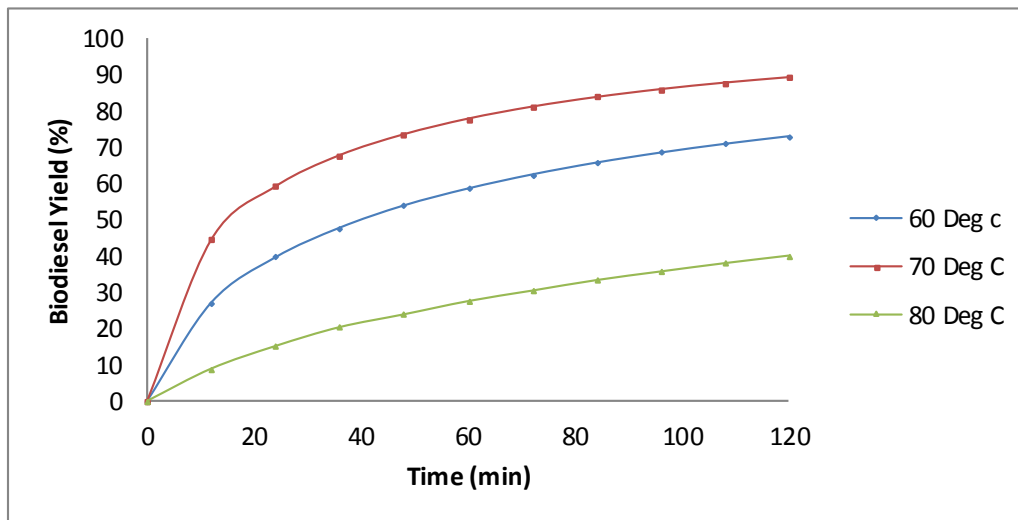


Figure 3. Effect of time and temperature on the biodiesel yield

It can be observed that considering reaction temperature from 60°C to 70°C, the biodiesel yield (%) increased with increased temperature and remained constant after the reaction attained equilibrium. As reflected in literature, higher reaction temperature enhances mass transfer of reactants and dispersion of the catalyst particles [15]. High temperature also favours high reaction rate, which eventually results to high conversion to biodiesel [36]. Meanwhile, at lower reaction temperature, there would be poor interaction between methanol and catalyst particles, thus leading to slower reaction rate [37]. Relatively, either high reaction temperature or reaction time is needed to achieve a maximum yield of biodiesel in most of the heterogeneous catalyzed transesterification reactions [37]. This is attributed to why maximum biodiesel yield of 89.22% was attained at reaction temperature of 70°C. However, with reaction temperature above 70°C, that is 80°C, lower yield was recorded. This is due to liquid

methanol in the reaction medium that had been totally gasified, therefore favouring the formation of glycerol over biodiesel [15].

3.2.1. Determination of reaction order and activation energy

In an attempt to determine the order of the overall reaction with respect to triglyceride and methanol (n and m) at temperatures 60, 70 and 80°C, eight cases were examined. The best overall reaction order was chosen based on the values of correlation coefficient (R^2). The closer the R^2 value to unity, the more accurate the order for the overall reaction could give the best fit with the experimental results [27]. The R^2 values for all the three temperatures considered were highest when reaction is first order with respect to triglyceride and a second order with respect to methanol. The values of R^2 were obtained to be 0.835, 0.914 and 0.948 for 60°C, 70°C and 80°C respectively. Thus, a third overall order ($n = 1$ and $m = 2$) indicates better agreement with the experimental data. This confirms that rate of reaction is sensitive to change in temperature. As reported by Nouredini and Zhu [38], transesterification process being a multiple and reversible reaction often exhibits an optimal temperature with respect to the biodiesel yield. Thus, these findings show that an optimal reaction temperature favours reaction rate.

The activation energy (E) and collision factor (k_o) were determined from the plot of $\ln k$ against $1/T$ (the plot is not given) to be 23.99 kJ/mol and $1.62 \times 10^6 \text{ M}^{-1}\text{min}^{-1}$ respectively.

3.2.2. Reaction mechanism

In order to evaluate the kinetic parameters contained in overall reaction rate expression (Eq. 18), it was assumed that the concentration of glycerol was extremely low and eliminated. The reduced model derived based on Eley-Rideal kinetic was solved by using least mean square analysis. The estimated kinetic parameters are presented in Table 2.

Table 2. Estimated kinetic parameters based on Eley-Rideal principle

Reaction temperature	$\beta \times 10^{-5}$	K_1	$K_5 \times 10^{-6} (\text{mol}^{-1})$
60°C	8.35	5.19	1.12
70°C	14.03	5.60	3.84
80°C	2.23	3.10	0.96

where β is $C_T K_5$

Based on the results obtained, it could be concluded that the transesterification of waste frying oil over AENiCo composite catalyst obeyed Eley-Rideal mechanism. The result obtained herein is in trend with the work reported by Abdoulmoumine [27].

3.3. Analysis of synthesized biodiesel

3.3.1. FTIR analysis

The functional groups of biodiesel prepared at reaction temperature of 70°C, catalyst loading of 3 wt%, reaction time of 2 h and methanol to WFO ratio of 12:1 was confirmed by FTIR analysis. As shown in Figure 4, the broad absorption band at 3439 cm^{-1} was attributed to O-H stretching vibration. Those sharp peaks around 2926 cm^{-1} and 2854 cm^{-1} were due to C-H stretching vibrations of methylene groups. The strong peak at 1745 cm^{-1} (C=O ester) and at 1165 cm^{-1} (C-O ester) which are obviously present in the spectrum were assigned to carbonyl functional groups. These two functional groups confirm the presence of esters and are only attributed to biodiesel [39]. While the band at 1466 cm^{-1} could be attributed to the CH_3 group in the methyl ester mixtures [40]. As well the peak at 721 cm^{-1} was attributed to C-H_2 methylene rock. The presence of these functional groups confirmed the quality of the synthesized biodiesel and this observation is in trend with the experimental data reported by Yadav *et al.* [41].

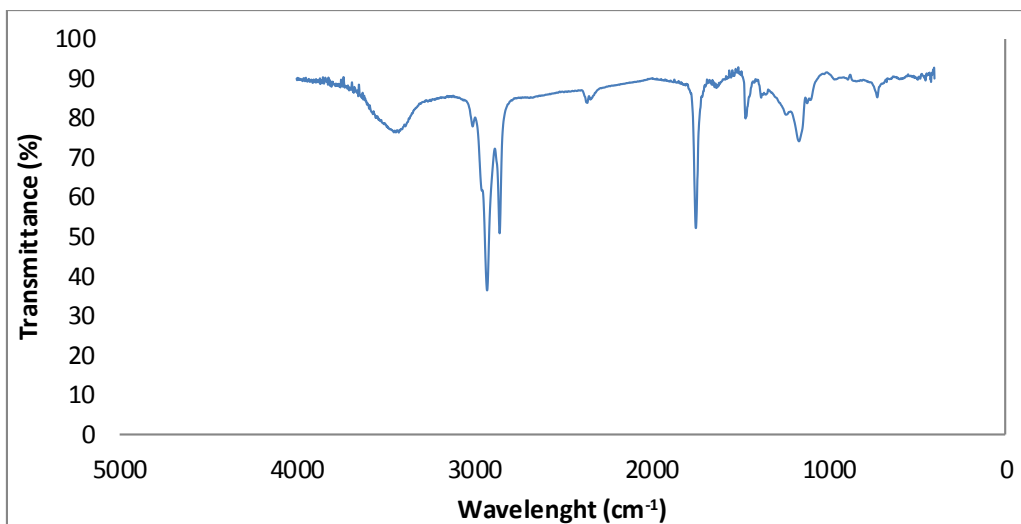


Figure 4. FTIR spectrum of synthesized biodiesel at reaction temperature of 70°C

3.3.2. Determination of physicochemical properties

The biodiesel prepared under the reaction temperature of 70°C, catalyst loading of 3 wt%, the reaction time of 2 h and methanol to WFO molar ratio of 12 was characterized based on its physicochemical and fuel properties. Table 3 shows the properties of the WFO-biodiesel. However, these properties were compared with those of commercial biodiesel [23] and ASTM/EN standard for biodiesel. Some of these properties were found to be comparable and in reasonable agreement with ASTM/EN standard for biodiesel.

Table 3. WFO-biodiesel physicochemical and fuel properties

Parameter	WFO-biodiesel	Commercial biodiesel	Biodiesel standard ASTM/EN
Specific gravity	0.886	0.844	0.86-0.90
Kinematic viscosity at 40°C (mm ² /s)	3.58	-	1.9-6.0
Acid value (mgKOH/g)	0.92	0.34	>0.8
Flash point (°C)	148	70	100-170
Cloud point (°C)	-9	-	-
Pour point (°C)	-12	-10	-15-10
Lower heating value (MJ/kg)	37.49	40.9	40.13

4. Conclusion

The activity of anthill-eggshell-Ni-Co mixed oxide composite catalyst in transesterification of WFO to biodiesel was investigated. The results of BET and basicity analyses revealed that the surface area and basic sites of as-synthesized catalyst increased upon calcination. XRD analysis showed that the calcined AENiCo catalyst contains a mixture of CaO, Ca(OH)₂, SiO₂, NiO and CoO, thus indicating a composite catalyst. Various surface functional groups of the catalyst were identified from the FTIR results. A detail study on the kinetics of WFO transesterification at 60°C, 70°C and 80°C showed that the reaction was first order with respect to triglyceride and second order with respect to methanol. The activation energy and collision factor were found to be 23.99 kJ/mol and $1.62 \times 10^6 \text{ M}^{-1} \text{ min}^{-1}$ respectively. After evaluation of model parameters, it was found that the transesterification reaction obeyed Eley-Rideal kinetic.

References

- [1] Lin L, Cunshan Z, Vittayapadung S, Xiangqian S, Mingdong D. Opportunities and challenges for Biodiesel fuel. *Applied Energy*, 2011; 88: 1020-1031.
- [2] Refaat AA. Biodiesel production using solid metal oxide catalysts. *International Journal of Environmental Science and Technology*, 2011; 8(1): 203-221.
- [3] Zabeti M, wan Daud WMA, Aroua K. Activity of solid catalysts for biodiesel production: A Review. *Fuel Processing Technology*, 2009; 90(6): 770-777.
- [4] Refaat AA. Different techniques for the production of biodiesel from waste vegetable oil. *International Journal of Environmental. Science and Technology*, 2010; 7(1): 183-213.
- [5] Basumatary S. Transesterification with heterogeneous catalyst in production of biodiesel. A Review. *Journal of Chemical and Pharmaceutical Research*, 2013; 5(1): 1-7.
- [6] Aijaz B, Flora TTN. A single step solid acid-catalyzed process for the production of biodiesel from high free fatty acid feedstock. *Energy & Fuels*, 2010; 24(9): 4712-4720.
- [7] Shah B, Sulaimana S, Jamal P, Alam MZ. Production of heterogeneous catalyst for biodiesel synthesis. *International Journal of Chemical and Environmental Engineering*, 2014; 5(2): 73-75.
- [8] Serio MD, Cozzolino M, Tesser R, Patrono P, Pinzarij Bonelli B, Santacesaria E (2007). Vanadyl phosphate catalysts in biodiesel production. *Applied Catalysis A: General*, 2007; 320: 1-7.
- [9] Alonso DM, Mariscal R, Granados ML, Maireles-Torres P. Biodiesel preparation using Li/CaO catalysts: Activation process and homogeneous contribution. *Catalysis Today*, 2009; 143(1-2): 167-171.
- [10] Olutoye MA, Hameed BH. A highly active clay-based catalyst for the synthesis of fatty acid methyl ester from waste cooking palm oil. *Applied Catalysis A: General*, 2013; 450: 57-62
- [11] Kondamudi N, Mohapatra S, Misra M. (2011). Quintinite as a bifunctional heterogeneous catalyst for biodiesel synthesis. *Applied Catalysis A, General*, 2011; 393(1-2): 36-43.
- [12] Pinzi S, Gandia LM, Arzamendi G, Ruiz JJ, Dorado MP. Influence of vegetable oils fatty acid composition on reaction temperature and glycerides conversion to biodiesel during transesterification. *Bioresource Technology*, 2011; 102: 1044-1050.
- [13] Boey PL, Mariam GP, Hamid SA, Ali DMH. Utilization of waste cockle shell (*Anadara granosa*) in biodiesel production from palm olein optimization using response surface methodology. *Fuel*, 2011; 90: 2353-2358.
- [14] Sharma YC, Singh B, Korstad J. Application of an efficient nonconventional heterogeneous catalyst for biodiesel synthesis from *Pongamia pinnata* oil. *Energy Fuels*, 2010; 24: 3223-3231.
- [15] Tan YH, Abdullah MO, Hipolito CN, Taufiq-Yap YH. Waste ostrich and chicken-eggshells as heterogeneous base catalyst for biodiesel production from used cooking oil: catalyst characterization and biodiesel yield performance. *Applied Energy*, 2015; 2: 1-13.
- [16] Cho YB, Seo G. High activity of acid treated of quail eggshell catalysts in the transesterification of palm oil with methanol. *Bioresource Technology*, 2010; 101: 8515 -8524.
- [17] Viriya-Empikul N, Krasae P, Nualpaeng W, Yoosuk B, Faungnawakij K. Biodiesel production over Ca-based solid catalysts derived from industrial wastes. *Fuel*, 2012; 92: 239-344.
- [18] Obadiah A, Swaroopa GA, Kumar SV, Jeganathan KR, Ramasubbu A. Biodiesel production from Palm oil using calcined waste animal bone as catalyst. *Bioresource Technology*, 2012; 116: 512-516.
- [19] Roschat W, Kacha M, Yoosuk B, Sudyo duk T, Promarak V. Biodiesel production based on heterogeneous process catalyzed by solid waste coral fragment. *Fuel*, 2012; 2: 194-202.
- [20] Aderemi BO, and Hameed BH. Alum as a heterogeneous catalyst for the transesterification of palm oil. *Applied Catalysis: A Gen.*, 2009; 370: 54-58.
- [21] Olutoye MA, Hameed BH. Synthesis of fatty acid methyl ester from used vegetable cooking oil by solid reusable $Mg_{1-x}Zn_{1+x}O_2$ catalyst. *Bioresource Technology*, 2011; 102: 3819-3826.
- [22] Dai Y, Chen K, Wang Y, and Chen C. Application of peanut husk ash as a low-cost solid catalyst for biodiesel production. *International Journal of Chemical Engineering and Applications*, 2014; 5 (3): 1-8.
- [23] Pratap SR, Shamshuddin SZM, Thimmaraju N, Shyumsundar M, Reena SS. Kinetic of transesterification of *Madhuca Indica* oil over modified zeolites: biodiesel synthesis. *Bangladesh Journal of Scientific and Industrial Research*, 2015; 50(4): 271-278.
- [24] Talebian-Kiakalaieh A, Amin NAS, Mazaheri H. A review on novel processes of biodiesel production from waste cooking oil. *Applied Energy*, 2013; 104: 683-710.

- [25] Yusuff AS, Adeniyi OD, Olutoye MA, Akpan UG. (2017). Performance and emission characteristics of diesel engine fuelled with waste frying oil derived biodiesel-petroleum diesel blend. *International Journal of Engineering in Africa*, 2017; 32: 100-111.
- [26] Singh AK, Fernando SD. Reaction kinetics of soybean oil transesterification using heterogeneous metal oxide catalysts. *Chemical Engineering & Technology*, 2007; 30(12): 1716-1720.
- [27] Abdoulmoumine N. Sulphated and hydroxide supported on zirconium oxide catalyst for biodiesel production. Published M.Sc Thesis. (2010), Faculty of the Virginia Polytechnic Institute and State University, USA.
- [28] Liu X, He H, Wang Y, Zhu S, Piao X. Transesterification of soybean oil to biodiesel using CaO as a solid base catalyst. *Fuel*, 2008; 87: 216-221.
- [29] Marjanovic AV, Stamentovic OS, Todorovic ZB, Lazic ML, Veljkovic VB. Kinetics of the base-catalyzed sunflower oil ethanolysis. *Journal of Energy and Fuel*, 2010; 88(3): 665-667.
- [30] di Serio M, Dimiccoli M, Cammarota F, Nastasi M, Santacesaria E. Synthesis of biodiesel via homogeneous Lewis acid catalyst. *Journal of Molecular Catalysis A: Chemical*, 2005; 239(1): 111-115.
- [31] Chorkendorff I, Niemantsverdriet JW. *Concepts of modern catalysis and kinetics*: Weinheim, Germany: Wiley-VCH press, (2001).
- [32] Hassani M, Najafpour GD, Mohammadi M, Rabiee M. Preparation, characterization and application of zeolite-based catalyst for production of biodiesel from waste cooking oil. *Journal of Scientific & Industrial Research*, 2014; 73: 129-133.
- [33] Yusuff AS, Preparation and characterization of composite anthill-chicken eggshell adsorbent: Optimization study on heavy metals adsorption using response surface methodology. *Journal of Environmental Science and Technology*, 2017; 10(3): 120-130.
- [34] Li H, Niu S, Lu C, Cheng S. The stability evaluation of lime mud as transesterification catalyst in resisting CO₂ and H₂O for biodiesel production. *Energy Conversion and Management*, 2015; 103: 57-65.
- [35] Margaretha YY, Prastyn HS, Ayucitra A, Ismadji S. Calcium oxide from Pomacea sp. shell as a catalyst for biodiesel production. *International Journal of Energy and Environmental Engineering*, 2012; 3: 1-9.
- [36] Olutoye MA, Wong SW, Chin LH, Asif M, Hameed BH. Synthesis of fatty acid methyl esters via transesterification of waste cooking oil by methanol with a barium-modified montmorillonite K10 catalyst. *Renewable Energy*, 2015; 86: 392-398.
- [37] Yee KF, Lee KT. Palm oil as feedstock for biodiesel production via heterogeneous transesterification: Optimization Study. *International Conference on Environment (ICENV)*, 2008; 1-5.
- [38] Nouredini H, Zhu D. (1997). Kinetic of transesterification of soybean oil. *Journal of the American Oil Chemist Society*, 1997; 74: 795-804
- [39] Taufiq-Yap YH, Abdullah NF, Basri M. Biodiesel production via transesterification of palm oil using NaOH/Al₂O₃ catalysts. *Sains Malaysiana*, 2011; 40(6): 587-594.
- [40] Siatis NG, Kimbaris AC, Pappas CS, Tarantilis PA, Polissiou MG. Improvement of biodiesel production based on the application of ultrasound: Monitoring of the procedure by FTIR spectroscopy. *Journal of the American Oil Chemists' Society*, 2006; 83(1): 1-7.
- [41] Yadav PKS, Singh O, Singh RP. Performance test of palm fatty acid biodiesel on compression ignition engine. *Journal of Petroleum Technology and Alternative Fuels*, 2010; 1(1): 1 -9.

To whom correspondence should be addressed: Dr. A. S. Yusuff, Department of Chemical and Petroleum Engineering, Afe Babalola University, Ado-Ekiti, Nigeria, yusuffas@abuad.edu.ng

Jubilant profesor Martin Bajus



Začiatkom tohto roku oslavil 75. narodeniny profesor Martin Bajus v zdraví, pokoji, pokore a spokojnosti v kruhu svojej rodiny. V septembri minulého roku rektor STU prof Ing. Robert Redhammer, PhD., ocenil jeho doterajšiu prácu na FCHPT udelením čestného titulu profesor emeritus. Na dielo, ktoré vytvoril vo vede a v pedagogike môže byť hrdý. Prof. Martin Bajus je významnou osobnosťou v oblasti rafinérskych, petrochemických, energetických a recyklačných technológií. Charakteristickým rysom bratislavskej školy pyrolýzy nie sú len získané výsledky, ale aj ich priemyselná realizácia v navrhovaných petrochemických technológiách nielen na Slovensku ale i v zahraničí (ČR).

Profesor Bajus naďalej aktívne vedecky a pedagogicky pôsobí na FCHPT. V roku 2016 sa aktívne zúčastnil na 4. ICCT, v Mikulove plenárnou prednáškou: Uhl'ovodíkové technológie, trendy a výhľady petrochémie. Prednášku mal aj na 68. Zjazde chemických spoločnosti v Prahe. Pre študentov na oddelení OTKR urobil úvod do predmetu „Petrochémia“. O tradícii vedeckej školy na FCHPT STU prednášal v „Emeritus klube“ (zima 2017). Bol predsedom komisie ŠVOČ na fakulte. Doplnil údaje do encyklopédie Beliana. Naďalej spolupracuje s firmou Dron-Industry pri inovovaní existujúcej technológie v Mliečanoch.

Začiatkom roka 2018 sa profesor Bajus tešil z vydania jeho novej knihy Hydrocarbon Technology - Petrochemistry, ktorú vydalo nakladateľstvo Slovenskej Chemickej knižnice Fakulty chemickej a potravinárskej technológie v Bratislave.

Profesor Martin Bajus napísal veľmi potrebný a pedagogicky vynikajúci text, ktorý na slovenskom trhu chýbal takmer 30 rokov. Vytvoril originálnu koncepciu petrochémie založenú na štyroch základných pilieroch.

Predložená vysokoškolská učebnica je aktuálna, napísaná moderným štýlom v angličtine. Predstavuje komplexné poňatie spracovanej tematiky. Široký a rozsiahly záber problematiky na 430 stranách zaiste znamenal pre autora veľké úsilie a trpezlivosť. Predovšetkým obrovské vedomosti z oblasti uhľovodíkových technológií. Kniha je vhodná najmä pre pedagógov a študentov vysokých škôl, v bakalárskych, inžinierskych a doktorandských študijných programoch. Zameraných na výučbu chemickej technológie, prípadne špecializovaných na petrochémiu (recenzia knihy je v ChemZi č.1 (2018)).

Sme veľmi radi, že sa pán profesor Martin Bajus dožil významného životného jubilea v pevnom zdraví a vysokom pracovnom nasadení. Želáme Martinovi do ďalších rokov veľa zdravia, úspechov a spokojnosti v pracovnom i rodinnom živote.

Viktor Milata

Professor Martin Bajus celebrates



Earlier this year, Professor Martin Bajus celebrated his 75th birthday in health, feeling peaceful satisfaction as a humble member and head of his family. In September last year the Rector of the Slovak University of Technology, prof. Ing. Robert Redhammer, PhD., praised his life-long work at the Faculty of Chemical and Food Technology by awarding Mr. Bajus the title of *honorary professor emeritus* for his considerable contribution to science and education. Prof. Martin Bajus is a proud contributor to the field of refining, as well as petrochemical, energy and recycling technologies. The characteristic features of the *Bratislava School of Pyrolysis* headed by Professor Bajus are not only the results obtained, but also their industrial applications in the newly devised petrochemical technologies, not only in Slovakia but also abroad (Czech Republic).

Professor Bajus is still active in science and is still an active supervising teacher at the Faculty. In 2016 he participated in the 4th International Chemical Technology Conference in Mikulov and contributed with the plenary lecture *Hydrocarbon Technologies - Trends and Prospects of Petrochemistry*. Mr. Bajus had a lecture at the 68th Conference of Chemical Societies in Prague. He lectured on "Introduction to Petrochemistry" for the students at the Department of Organic Technology, Catalysis and Petroleum Chemistry. His lectures on traditions of the scientific school at the Faculty were of great interest in the "Emeritus Club" (winter 2017). Still another activity of this great scholar and excellent teacher was his leading role as a chairman of the Commission for Student Scientific and Specialist Presentation at the Faculty.

Professor Bajus contributed data to the *Beliana Encyclopedia*. Presently he cooperates with the company Dron-Industry in Mliečany on innovation of already existing technology.

At the beginning of 2018, Professor Bajus was pleased to release his new book *Hydrocarbon Technology – Petrochemistry*, published by the Slovak Chemical Library at the Faculty of Chemical and Food Technology in Bratislava.

This publication, written by Professor Martin Bajus, is a necessary and pedagogically excellent text, which has been missing on the Slovak market for almost 30 years. The author has created a rather original concept of petrochemistry built on four basic pillars.

The presented college textbook is current, written in English, in a modern style. It represents a complex concept of the subject matter. The wide and extensive coverage of the topic on 430 pages has surely required a great effort and patience on the side of the author, in particular, huge knowledge of hydrocarbon technology. The book is especially suitable for college educating staff and students studying in bachelor, master or doctoral study programmes focusing on chemical technology, possibly teaching specialized petrochemistry (for review of the book see ChemZi, No. 1 (2018)).

We are very pleased that Professor Martin Bajus has experienced a significant life anniversary in good health, in the middle of intensive work endeavors. We wish Martin many happy years to come, that he would live in great health condition, satisfied at work and in family life.

Viktor Milata